

**SPECTROSCOPY AND KINETICS OF WEAKLY BOUND GAS  
PHASE ADDUCTS OF ATMOSPHERIC INTEREST**

A Dissertation  
Presented to  
The Academic Faculty

by

Venus Dookwah-Roberts

In Partial Fulfillment  
of the Requirements for the Degree  
Doctor of Philosophy in the  
School of Earth and Atmospheric Sciences

Georgia Institute of Technology  
August 2008

**SPECTROSCOPY AND KINETICS OF WEAKLY BOUND GAS  
PHASE ADDUCTS OF ATMOSPHERIC INTEREST**

Approved by:

Dr. Paul H. Wine, Advisor  
School of Chemistry & Biochemistry  
School of Earth & Atmospheric Sciences  
*Georgia Institute of Technology*

Dr. Athanasios Nenes  
School of Chemical and Biomolecular  
Engineering  
School of Earth & Atmospheric Sciences  
*Georgia Institute of Technology*

Dr. Rodney Weber  
School of Earth and Atmospheric Sciences  
*Georgia Institute of Technology*

Dr. Greg Huey  
School of Earth and Atmospheric  
Sciences  
*Georgia Institute of Technology*

Dr. Robert Whetten  
School of Chemistry & Biochemistry  
*Georgia Institute of Technology*

Date Approved:

To my dearest mother, Joyce - Your unending love, sacrifice, and dedication have made me all that I am. Your spirit lives in me forever. You inspire me.

To my wonderful husband, Dexter - Your loving support, patience, and commitment strengthened me through this journey.

To my beautiful daughter, Christin - You are truly a blessing.

## ACKNOWLEDGEMENTS

This work was supported by the National Science Foundation through grant ATM-03-50185.

I would like to sincerely thank my advisor, Dr. Paul H. Wine, for giving me the opportunity of doing this PhD. in his group and for his support, direction, and guidance on my research projects. Dr. John M. Nicovich, thank you for all your help in every aspect of my research – from plumbing to data analysis. I could not have accomplished this without help from both of you. Special thanks to my first advisor, Dr. Gregory Huey, for his advice and encouragement throughout my graduate years. My sincerest appreciation to Dr. Judith Curry for her support and for the empowering experiences provided to me.

My appreciation to all members of the Huey group for their help and support during my years here. Special thanks go to former graduate students and friends Anne Case, Carissa Howard, Lei Zhu, Darlene Slusher, Steve Sjostedt, Willis Shem, Stephanie Chow, Amy Sullivan, Kari Maxwell; to my office mates: Zhijun Zhao, Patrick Laine; to postdocs Raenell Soller and Patrice Bell; to other Wine group members Dow Huskey (III), Katie Olsen, and Rosetta Lee; and to current graduate student Arsineh Hecobian. Thank you all for making my experience here a warm and enriching one.

I wish to especially thank my sister, Rhonda, for her support and encouragement during these years; my brothers, DeVaughn and Roger for believing in me; and my father, Harry, for the universe you and my mother have created for me, for your prayers

and support. My gratitude also to my sister-in-law Cheryl and brother-in-law, Ralph, thank you for your continued prayers and well wishes.

# TABLE OF CONTENTS

	Page
ACKNOWLEDGEMENTS	iv
LIST OF TABLES	ix
LIST OF FIGURES	x
SUMMARY	xiii
<u>CHAPTER</u>	
1 INTRODUCTION	1
Role of Adducts in the Atmosphere	1
Sulfur in the Atmosphere	5
Role of Halogens in Tropospheric Chemistry	13
Bromine in the Atmosphere	19
Iodine in the Atmosphere	23
CH <sub>3</sub> I and C <sub>2</sub> H <sub>5</sub> I in the Atmosphere	27
Aims of this work	28
2 EXPERIMENTAL TECHNIQUES	32
Experimental Approach	32
Gas flow system	34
Concentrations of reagent gases	36
Chemicals	42
3 SPECTROSCOPIC AND KINETIC STUDY OF THE GAS PHASE CS <sub>2</sub> -Cl ADDUCT	44
Carbon Disulfide in the Atmosphere	44
The Reaction of Cl with CS <sub>2</sub>	45

Experimental Method	47
Results and Discussion	48
Adduct Identification	48
Adduct Absorption Spectrum	51
Radical-Radical Reaction Kinetics	61
Kinetics of the $\text{CS}_2\text{-Cl} + \text{O}_2$ reaction	62
Kinetics of $\text{CS}_2\text{-Cl}$ Reactions with NO and $\text{NO}_2$	65
Role of $\text{CS}_2\text{-Cl}$ in Atmospheric Chemistry	72
4 SPECTROSCOPIC AND KINETIC STUDY OF THE GAS PHASE $\text{CH}_3\text{I-Cl}$ AND $\text{C}_2\text{H}_5\text{I-Cl}$ ADDUCTS	74
Reaction of Cl atom with $\text{CH}_3\text{I}$ and $\text{C}_2\text{H}_5\text{I}$	74
Experimental Method	78
Results and Discussion	79
Identification of Absorbing Species	80
Adduct Absorption Spectra	81
Radical-Radical Reaction Kinetics	93
Kinetics of $\text{RI-Cl}$ Reactions with $\text{O}_2$ and RI	98
Kinetics of $\text{RI-Cl}$ Reactions with NO and $\text{NO}_2$	103
Atmospheric Implications	109
5 SPECTROSCOPIC AND KINETIC STUDY OF THE GAS PHASE $(\text{CH}_3)_2\text{S-Br}$ ADDUCT	114
Effect of Bromine on the Sulfur Cycle	114
The Reaction of Br with DMS	116
Experimental Method	118
Results and Discussion	121
Identification of Absorbing Species	121

Adduct Absorption Spectrum	125
Radical-Radical Reaction Kinetics	130
Kinetics of Br–DMS Reaction with O <sub>2</sub>	134
Kinetics of Br–DMS Reaction with NO and NO <sub>2</sub>	137
Atmospheric Fate of Br–DMS	142
6 SPECTROSCOPIC AND KINETIC STUDY OF THE GAS PHASE (CH <sub>3</sub> ) <sub>2</sub> S–I ADDUCT	145
Effect of Iodine on the Sulfur Cycle	145
The Reaction of Iodine Atoms with DMS	147
Experimental Method	148
Results and Discussion	151
Adduct Absorption Spectrum	157
Radical-Radical Reaction Kinetics	162
Kinetics of I–DMS Reaction with O <sub>2</sub>	164
Kinetics of I–DMS Reaction with NO and NO <sub>2</sub>	166
Atmospheric Fate of I–DMS	173
7 SUMMARY OF ADDUCT SPECTROSCOPIC AND KINETIC STUDIES	174
Observed Trends in Adduct Spectroscopic Data	174
Adduct Kinetics Comparisons and Future Research Recommendations	180
REFERENCES	183

## LIST OF TABLES

	Page
Table 1.1: Comparison of adduct stabilities and addition rates	6
Table 1.2: Estimated global emissions of important atmospheric sulfur gases	8
Table 1.3: Observed atmospheric mixing ratios (pptv) of important gaseous sulfides and their major sources and sinks	9
Table 1.4: Summary of CH <sub>3</sub> I measurements reported in literature	30
Table 1.5: Estimates of global annual sources and sinks for CH <sub>3</sub> I (Gg/yr)	31
Table 2.1: Table of molecular structure correction factors	39
Table 2.2: Summary of absorption cross-sections for molecules used in this work	41
Table 2.3: Minimum stated purity of chemicals used in this work	43
Table 3.1: Absorption cross sections for the CS <sub>2</sub> -Cl adduct as a function of wavelength at a spectral resolution of 5.5 nm (FWHM)	56
Table 4.1: Absorption cross sections for the RI-Cl adducts as a function of wavelength at $T = 250$ K and a spectral resolution of 5.5 nm (FWHM)	88
Table 4.2: Rate coefficients for the reactions of Cl and OH with CH <sub>3</sub> I and C <sub>2</sub> H <sub>5</sub> I used in construction of Table 4.5	110
Table 4.3: Rate of loss of CH <sub>3</sub> I and C <sub>2</sub> H <sub>5</sub> I under typical surface MBL conditions	111
Table 6.1: Literature rate coefficients at 298 K for the reaction of IO radicals with DMS	146
Table 6.2: Structural parameters used in the evaluation of absolute entropies for DMS, I atoms and I-DMS adduct	159
Table 6.3: Absorption cross sections for the I-DMS adduct as a function of wavelength at a spectral resolution of 5.5 nm (FWHM)	161
Table 7.1: Comparison of adduct $\lambda_{\max}$ , $\sigma_{\max}$ , molecular ionization potential, and radical electron affinity	172
Table 7.2: Comparison of adduct kinetics	175

## LIST OF FIGURES

	Page
Figure 1.1: A simplified representation of the CLAW Hypothesis	11
Figure 1.2: A simplified schematic of DMS cycling in the marine boundary layer	14
Figure 1.3: Graphical depiction of Bromine cycling	22
Figure 1.4: Simplified scheme of tropospheric iodine oxidation	25
Figure 2.1: Laser flash photolysis/UV-vis absorption spectroscopy apparatus	35
Figure 2.2: Vapor pressure versus temperature plot for liquid DMS	37
Figure 2.3: Vapor pressure versus temperature plot for liquid CS <sub>2</sub>	38
Figure 3.1: Typical absorbance temporal profile observed following laser flash photolysis of Cl <sub>2</sub> CO/CS <sub>2</sub> /N <sub>2</sub> mixtures	50
Figure 3.2: Plot of $k_a$ versus [CS <sub>2</sub> ] for data obtained at $T = 240$ K and $P = 100$ Torr N <sub>2</sub>	52
Figure 3.3: Absorption spectrum of the gas phase CS <sub>2</sub> -Cl adduct	55
Figure 3.4: Liquid phase spectra of CS <sub>2</sub> -Cl adduct	57
Figure 3.5: Simple schematic for the optimized geometry computed for the two most probable CS <sub>2</sub> -Cl structures	60
Figure 3.6: CS <sub>2</sub> -Cl absorbance temporal profile plotted as [CS <sub>2</sub> -Cl] <sup>-1</sup> vs. time obtained at $T = 240$ K and $P = 100$ Torr N <sub>2</sub>	63
Figure 3.7: CS <sub>2</sub> -Cl absorbance temporal profile plotted as [CS <sub>2</sub> -Cl] <sup>-1</sup> vs. time obtained at $T = 240$ K and $P = 100$ Torr O <sub>2</sub>	66
Figure 3.8: Typical absorbance temporal profile observed following 248 nm laser flash photolysis of Cl <sub>2</sub> CO/CS <sub>2</sub> /NO <sub>x</sub> /N <sub>2</sub> mixtures at $T = 240$ K and $P = 30$ Torr	68
Figure 3.9: Plots of pseudo first order CS <sub>2</sub> -Cl adduct decay rate ( $k_d$ ) versus [NO <sub>x</sub> ] under conditions of $T = 240$ K and $P = 30$ Torr of N <sub>2</sub>	70

Figure 4.1: Typical absorbance (base e) temporal profile observed following laser flash photolysis of RI/Cl <sub>2</sub> /N <sub>2</sub> mixtures at 308 nm	82
Figure 4.2: Plots of $k_a$ versus [CH <sub>3</sub> I] for data obtained at $T = 261$ K and $P = 100$ Torr N <sub>2</sub> and $k_a$ versus [C <sub>2</sub> H <sub>5</sub> I] for data obtained at $T = 258$ K and $P = 263$ Torr N <sub>2</sub>	83
Figure 4.3: Absorption spectra of CH <sub>3</sub> I–Cl and C <sub>2</sub> H <sub>5</sub> I–Cl at a spectral resolution of 5.5 nm (FWHM)	88
Figure 4.4: Structures for CH <sub>3</sub> I and CH <sub>3</sub> I–Cl derived from ab initio calculations at the B3LYP/ECP level	91
Figure 4.5: Structures for C <sub>2</sub> H <sub>5</sub> I and C <sub>2</sub> H <sub>5</sub> I–Cl derived from ab initio calculations at the B3LYP/ECP level	92
Figure 4.6: Typical RI–Cl absorbance temporal profile plotted as [RI–Cl] <sup>-1</sup> vs. time	95
Figure 4.7: Comparison of CH <sub>3</sub> I–Cl absorbance temporal profiles observed at $T = 250$ K and $P = 300$ Torr in N <sub>2</sub> vs. O <sub>2</sub> bath gas	99
Figure 4.8: CH <sub>3</sub> I–Cl absorbance temporal profile plotted as [CH <sub>3</sub> I–Cl] <sup>-1</sup> vs. time	102
Figure 4.9: Typical absorbance temporal profile observed following 308 nm laser flash photolysis of Cl <sub>2</sub> /RI/NO <sub>x</sub> /N <sub>2</sub> mixtures at $T = 250$ K and $P = 300$ Torr	105
Figure 4.10: Plots of pseudo first order CH <sub>3</sub> I–Cl decay rates ( $k_d$ ) versus [NO <sub>x</sub> ] under conditions of $T = 250$ K and $P = 300$ Torr of N <sub>2</sub>	107
Figure 4.11: Plots of pseudo first order C <sub>2</sub> H <sub>5</sub> I–Cl decay rates ( $k_d$ ) versus [NO <sub>x</sub> ] under conditions of $T = 256$ K and $P = 300$ Torr of N <sub>2</sub>	108
Figure 5.1: Typical absorbance (base e) temporal profile observed following 248 nm laser flash photolysis of DMS/CF <sub>2</sub> Br <sub>2</sub> /N <sub>2</sub> mixtures	122
Figure 5.2: Plots of $k_a$ versus [DMS] for data obtained at $T = 265$ K and $P = 200$ Torr N <sub>2</sub>	124
Figure 5.3: Absorption spectrum of Br–DMS at a spectral resolution of 5.5 nm	128
Figure 5.4: Structures for (CH <sub>3</sub> ) <sub>2</sub> S–Br derived from ab initio calculations at the B3LYP/ECP level	131
Figure 5.5: Typical Br–DMS absorbance temporal profile plotted as [Br–DMS] <sup>-1</sup> vs. time	133
Figure 5.6: Comparison of Br–DMS absorbance temporal profiles observed at $T = 265$ K and $P = 200$ Torr in N <sub>2</sub> vs. O <sub>2</sub> bath gas	136

Figure 5.7: Typical absorbance temporal profile observed following 248 nm laser flash photolysis of $\text{CF}_2\text{Br}_2/\text{DMS}/\text{NO}_x/\text{N}_2$ mixtures at $T = 265$ K and $P = 200$ Torr $\text{N}_2$	139
Figure 5.8: Plots of pseudo first order Br–DMS decay rates ( $k_d$ ) versus $[\text{NO}_x]$ under conditions of $T = 265$ K and $P = 200$ Torr of $\text{N}_2$	140
Figure 6.1: Typical absorbance (base e) temporal profile observed following 248 nm laser flash photolysis of $\text{CH}_3\text{I}/\text{DMS}/\text{O}_2/\text{N}_2$ mixtures	154
Figure 6.2: Absorption spectrum of I–DMS at a spectral resolution of 5.5 nm	155
Figure 6.3: Absorption spectrum of $\text{I}_2$	156
Figure 6.4: Structures for $(\text{CH}_3)_2\text{S-I}$ derived from ab initio calculations at the B3LYP/ECP level	163
Figure 6.5: Typical I–DMS absorbance temporal profile in 50 Torr of 2% $\text{O}_2$ in $\text{N}_2$ plotted as $[\text{I-DMS}]^{-1}$ vs. time	165
Figure 6.6: I–DMS absorbance temporal profile in 258 Torr of 2% $\text{O}_2$ in $\text{N}_2$ plotted as $[\text{I-DMS}]^{-1}$ vs. time	167
Figure 6.7: Typical absorbance temporal profile observed following 248 nm laser flash photolysis of $\text{CH}_3\text{I}/\text{DMS}/\text{NO}_x/2\%$ $\text{O}_2$ mixtures at $T = 205$ K and $P = 50$ Torr	169
Figure 6.8: Plots of pseudo first order I–DMS decay rates ( $k_d$ ) versus $[\text{NO}_x]$ under conditions of $T = 205$ K and $P = 50$ Torr of 2% $\text{O}_2$	171
Figure 7.1: Comparison of X–DMS adduct absorption spectra	173
Figure 7.2: Plot of $[\text{IP (DMS)} - \text{EA (X)}]$ ( $X = \text{I, Br, I}$ ) vs. adduct bond strength	178

## SUMMARY

A number of weakly bound adducts play important roles in atmospheric chemistry, such as DMS–OH and CS<sub>2</sub>–OH. The work comprising this dissertation involves kinetic and spectroscopic studies of adducts formed between halogen atoms and the important atmospheric trace gases CS<sub>2</sub>, CH<sub>3</sub>SCH<sub>3</sub> (DMS), CH<sub>3</sub>I, and C<sub>2</sub>H<sub>5</sub>I. The results reported in these studies are useful for developing an understanding of the reactivity of these species and for testing the ability of electronic structure theory and reaction rate theory to predict or rationalize any observed trends. Oxidative pathways of both alkyl halides and sulfur compounds, especially DMS, are of atmospheric interest based on the roles of these species in affecting the oxidizing capacity of the troposphere and in the formation of new particles which impact the Earth's radiation budget and climate variability.

The experimental approach employed laser flash photolysis (LFP) coupled with time resolved UV-visible absorption spectroscopy (TRUVVAS) to investigate the spectroscopy and kinetics of the gas phase adducts: SCS–Cl, CH<sub>3</sub>I–Cl, C<sub>2</sub>H<sub>5</sub>I–Cl, (CH<sub>3</sub>)<sub>2</sub>S–Br, and (CH<sub>3</sub>)<sub>2</sub>S–I. The SCS–Cl adduct was found to possess a strong absorption band at  $\lambda_{\text{max}} \approx 365$  nm with  $\sigma_{\text{max}} = (2.3 \pm 0.7) \times 10^{-17}$  cm<sup>2</sup> molecule<sup>-1</sup> (base e) and a weaker band at  $\lambda_{\text{max}} \approx 480$  nm. Reaction of the adduct with O<sub>2</sub> was not observed and the data obtained in this study suggest an upper limit of  $k_{3,2} < 5 \times 10^{-18}$  cm<sup>3</sup> molecule<sup>-1</sup> s<sup>-1</sup> for the SCS–Cl + O<sub>2</sub> rate coefficient at 240 K. The SCS–Cl adduct was found to react with both NO and NO<sub>2</sub>. Rate coefficients for the adduct self reaction ( $k_{3,4}$ ), reaction with

NO ( $k_{3.6}$ ), and reaction with NO<sub>2</sub> ( $k_{3.7}$ ) were measured at 240 K and, in units of  $10^{-11}$  cm<sup>3</sup> molecule<sup>-1</sup> s<sup>-1</sup>, were found to be  $2k_{3.4} = (15 \pm 6)$ ,  $k_{3.6} = (2.2 \pm 0.5)$ , and  $k_{3.7} = (1.3 \pm 0.4)$ .

The RI–Cl adducts (where R = CH<sub>3</sub>, C<sub>2</sub>H<sub>5</sub>) were found to absorb strongly over the wavelength range 310 – 500 nm. Their spectra were very similar in wavelength dependence with  $\lambda_{\max} \approx 315$  nm and with  $\sigma_{\max} = (3.5 \pm 1.2) \times 10^{-17}$  and  $(2.7 \pm 1.0) \times 10^{-17}$  cm<sup>2</sup> molecule<sup>-1</sup> (base e) for CH<sub>3</sub>I–Cl and C<sub>2</sub>H<sub>5</sub>I–Cl, respectively. Two weaker bands at  $\lambda_{\max} \approx 350$  and 420 nm were also observed. Reactions of RI–Cl with O<sub>2</sub> were not observed and the data obtained in this study suggest that upper limit rate coefficients for these reactions at 250 K are  $1.0 \times 10^{-17}$  and  $2.5 \times 10^{-17}$  cm<sup>3</sup> molecule<sup>-1</sup> s<sup>-1</sup> for R = CH<sub>3</sub> and R = C<sub>2</sub>H<sub>5</sub>, respectively. Possible reactions of these adducts with RI could not be confirmed or ruled out, although data obtained from this study suggest that upper limit rate coefficients for these reactions at 250 K are  $3 \times 10^{-13}$  cm<sup>3</sup> molecule<sup>-1</sup> s<sup>-1</sup> for R = CH<sub>3</sub> and  $5 \times 10^{-13}$  cm<sup>3</sup> molecule<sup>-1</sup> s<sup>-1</sup> for R = C<sub>2</sub>H<sub>5</sub>. Rate coefficients for CH<sub>3</sub>I–Cl reactions with CH<sub>3</sub>I–Cl ( $k_{4.22}$ ), NO ( $k_{4.24}$ ) and NO<sub>2</sub> ( $k_{4.9}$ ) and C<sub>2</sub>H<sub>5</sub>I–Cl reactions with C<sub>2</sub>H<sub>5</sub>I–Cl ( $k_{4.14}$ ), NO ( $k_{4.23}$ ), and NO<sub>2</sub> ( $k_{4.25}$ ) were measured at 250 K and were found to be, in units of  $10^{-11}$  cm<sup>3</sup> molecule<sup>-1</sup> s<sup>-1</sup>,  $2k_{4.9} = (35 \pm 12)$ ,  $k_{4.22} = (1.8 \pm 0.4)$ ,  $k_{4.24} = (3.3 \pm 0.6)$  and  $2k_{4.14} = (40 \pm 16)$ ,  $k_{4.23} = (1.8 \pm 0.3)$ ,  $k_{4.25} = (4.0 \pm 0.9)$ .

The X–DMS (X= Br, I) adducts were found to possess similar, strong, broad, unstructured absorption spectra, with  $\lambda_{\max} \approx 366$  nm and  $\sigma_{\max} = (2.7 \pm 0.9) \times 10^{-17}$  cm<sup>2</sup> molecule<sup>-1</sup> (base e) for X = Br, and with  $\lambda_{\max} \approx 395$  nm and  $\sigma_{\max} = (4.1 \pm 1.4) \times 10^{-17}$  cm<sup>2</sup> molecule<sup>-1</sup> (base e) for X = I. Reactions of X–DMS with O<sub>2</sub> were not observed and the data obtained in this study suggest upper limit rate coefficients of  $8.0 \times 10^{-18}$  and  $3.0 \times 10^{-17}$  cm<sup>3</sup> molecule<sup>-1</sup> s<sup>-1</sup> for Br–DMS + O<sub>2</sub> at 265 K and I–DMS + O<sub>2</sub> at 205 K, respectively.

Rate coefficients for Br–DMS reactions with Br–DMS( $k_{5.10}$ ), NO ( $k_{5.15}$ ) and NO<sub>2</sub> ( $k_{5.16}$ ) were measured at 265 K and were found to be, in units of  $10^{-11}$  cm<sup>3</sup> molecule<sup>-1</sup> s<sup>-1</sup>,  $2k_{5.10} = (29 \pm 10)$ ,  $k_{5.15} = (1.3 \pm 0.3)$ ,  $k_{5.16} = (2.6 \pm 0.5)$  while rate coefficients for I–DMS reactions with NO ( $k_{6.11}$ ) and NO<sub>2</sub> ( $k_{6.12}$ ) were measured at 205 K and were found to be,  $k_{6.11} = (5.9 \pm 1.6)$ ,  $k_{6.12} = (6.8 \pm 1.3)$  in units of  $10^{-11}$  cm<sup>3</sup> molecule<sup>-1</sup> s<sup>-1</sup>.

The fate of all adducts in the atmosphere is almost certainly thermal decomposition leading to regeneration of reactant molecules, however, adduct reactions with O<sub>2</sub> cannot be ruled out as in the case of C<sub>2</sub>H<sub>5</sub>I–Cl reaction with O<sub>2</sub>. This reaction could possibly play an important role in the troposphere under conditions of low temperatures found in polar environments. Also, evidence presented in the literature suggests that thermal decomposition of Br–DMS may not necessarily regenerate Br and DMS.

Kinetic data for radical-radical reactions and reactions of adducts with atmospherically relevant species such as O<sub>2</sub>, NO, and NO<sub>2</sub> are reported for the first time in all cases except for SCS–Cl and Br–DMS where upper limits for their reactions with O<sub>2</sub> have been reinvestigated and reduced. All adduct + NO<sub>x</sub> rate coefficients were found to be within the range  $(1-7) \times 10^{-11}$  cm<sup>3</sup> molecule<sup>-1</sup> s<sup>-1</sup> and reactivity of these adducts with O<sub>2</sub> was not observed. Upon examination of the X–DMS spectra, where X = Cl, Br, or I, we observe an expected trend in  $\lambda_{\max}$  reflecting a red shift in peak wavelength from 340 to 395 nm as we move from Cl to I.

Spectroscopy data presented in this thesis also allows for comparison between RI–Cl adducts, where R = CH<sub>3</sub> or C<sub>2</sub>H<sub>5</sub>. In both cases three absorption bands were detected, occurring at 315, 350, and 420 nm while  $\sigma_{\max}$  observed at 315 nm was ~ 30% higher for

R = CH<sub>3</sub>. The band observed at 420 nm also represents disagreement between our experimental results and theoretical results reported by Enami et al., 2005. The gas phase spectrum of SCS-Cl is slightly blue shifted when compared to the liquid phase SCS-Cl adduct spectrum but in both cases two absorption bands are observed, a strong band at ~ 365 nm and a weak band at ~ 480 nm.

# CHAPTER 1

## INTRODUCTION

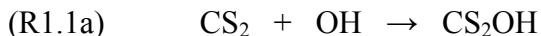
### Role of Adducts in the Atmospheric Chemistry

Short-lived adducts play key roles in atmospheric oxidation pathways. Generally, adducts provide either a barrierless or reduced energy barrier pathway for an otherwise high energy barrier reaction to occur. For reactions that do proceed via an intermediate adduct, this pathway is usually preferred under low temperature conditions (again because of energetics). One important example of such an intermediate is the Criegee intermediate (CI) formed by the addition of ozone to unsaturated compounds leading to the formation of atmospherically important species such as HO<sub>x</sub> and RO<sub>x</sub> radicals, hydrogen peroxide, and organic peroxides (Atkinson, 2000; Martinez et al., 1981; Gab et al., 1985; Paulson et al., 1999; Ariya et al., 2000; Criegee and Wenner, 1949).

The OH initiated atmospheric oxidation of toluene, a major component of total volatile organic carbon compounds (VOCs) produced largely as a by-product of vehicular combustion, proceeds via OH addition to the aromatic ring. This pathway accounts for 90% of the OH + toluene reaction and results in the formation of the adduct radical, methylhydroxycyclohexadienyl (Knispel et al., 1990). Similarly, 95% of the OH + benzene reaction proceeds through the addition channel, forming the hydroxycyclohexadienyl radical adduct (Atkinson, 1989). Other important gas phase adducts of atmospheric interest include the CS<sub>2</sub>-OH and DMS-OH adducts.

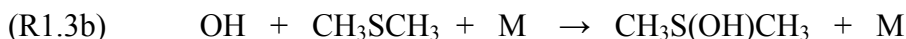
Early direct studies of the OH + CS<sub>2</sub> reaction indicated that this reaction was too slow to be of significance to the atmospheric oxidation of CS<sub>2</sub> (Kurylo, 1978b; Atkinson et al., 1978; Wine et al., 1980), however, Jones et al. (1982) found that this reaction was significantly enhanced in the presence of O<sub>2</sub> and this was later confirmed by investigators

such as Barnes et al., 1983, and Hynes et al., 1988. The findings were interpreted as evidence for the occurrence of the following mechanism:



Studies such as Stickel et al. (1993) and McKee and Wine (2001) have shown that reaction (R1.2) leads ultimately to formation of OCS, which is atmospherically important. Following the postulation of the above mechanism, reaction rates  $k_{1.1a}$ ,  $k_{1.1b}$ , and  $k_{1.2}$  have been reported by investigators such as Murrells et al., 1990, Hynes et al., 1988, and Bulatov et al., 1988.

Adduct formation also plays a key role in the OH initiated atmospheric oxidation of dimethyl sulfide (DMS). Early studies (Atkinson et al., 1978; Kurylo, 1978a; Cox and Sheppard, 1980; Wine et al., 1981) suggested that the DMS + OH reaction proceeded by H-atom abstraction, however, a combined resonance fluorescence (RF) and laser induced fluorescence (LIF) study conducted by Hynes et al. (1986) provided evidence of an OH addition mechanism together with an abstraction channel such as reactions R1.3a – R1.3c. Their findings were confirmed by investigators such as Wallington et al. (1986); Barnes et al. (1988); and Witte and Zetzsch (1986). The current interpretation of kinetic data involves two separate channels, an  $O_2$  independent, H-abstraction channel and an OH addition,  $O_2$ -dependent, adduct forming channel:

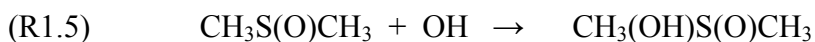


The existence of a stable DMS–OH adduct has been confirmed by investigators both experimentally (Hynes et al., 1995; Barone et al., 1996) and theoretically (McKee, 1993a; Gu and Turecek, 1992; Turecek, 1994; Turecek, 2000; Wang and Zhang, 2001; McKee, 2003; Uchimaru et al., 2005; Gross et al., 2004, Aloisio, 2006). It is now well established that the DMS–OH adduct reacts with O<sub>2</sub> under low NO<sub>x</sub> conditions, as in reaction (R1.4) to produce DMSO + HO<sub>2</sub> (Barnes et al., 1994, Turpinseed et al., 1996, Sorensen et al., 1996, Barnes et al., 1996, Patroescu et al., 1999, Arsene et al., 1999, Arsene et al., 2001). Laboratory studies have firmly established that the main fate of DMSO (CH<sub>3</sub>SOCH<sub>3</sub>) in the atmosphere is oxidation by OH. In earlier studies of Barnes et al. (1989) and Sorensen et al. (1996) significant yields of SO<sub>2</sub> and DMSO<sub>2</sub> (CH<sub>3</sub>SO<sub>2</sub>CH<sub>3</sub>) were observed, however, new studies have shown that MSIA (CH<sub>3</sub>S(O)OH) is the dominant product of DMSO oxidation (Urbanski and Wine, 1998; Arsene et al., 2002; Kukui et al., 2003). The different experimental conditions and sampling methods employed by these authors are possibly responsible for the apparent discrepancy, for example, in the studies of Sorensen et al. (1996), samples were collected at the end of the irradiation period and the identified products were SO<sub>2</sub> and DMSO<sub>2</sub>, while in the studies of Arsene et al. (2002) where samples were analyzed during the irradiation period, MSIA was found to be the dominant primary product.

The most probable atmospheric fate of MSIA can be a combination of gas phase oxidation by OH (leading to SO<sub>2</sub> and CCN formation) as well as heterogeneous reactions of MSIA involving gas phase uptake by existing aerosols and droplets (leading to MSA production – non CCN forming) (Barnes et al., 2006; Kukui et al., 2003). Both laboratory and field observations support that, under low NO<sub>x</sub> conditions typically found in the remote atmosphere, SO<sub>2</sub> is a major product of gas phase OH oxidation of DMS and that the addition (adduct forming) and abstraction channels are both important in this process. The ultimate atmospheric fate of SO<sub>2</sub> can be oxidation by OH to form H<sub>2</sub>SO<sub>4</sub> in

the gas phase (Wine et al., 1984; Atkinson et al., 1997 and references therein) or uptake into the condensed phase and oxidation by O<sub>3</sub> and H<sub>2</sub>O<sub>2</sub> to produce S(VI) (Kreidenweis et al., 2003 and references therein).

Adducts also play important roles in aqueous phase atmospheric chemistry, for example, DMSO, which is highly water soluble (Watts et al., 1987), is oxidized in the aqueous phase by OH radicals mainly via addition of OH to the sulfur atom (Veltwisch et al., 1980):



Studies have demonstrated that the dissociation of the DMSO–OH adduct proceeds via rapid fragmentation of one of the C–S bonds rather than the reverse reaction of R1.5 (Veltwisch et al., 1980; Sehested and Holcman, 1996; Flyunt et al., 2001; Bardouki et al., 2002), yielding methane sulphinic acid (MSIA) which dissociates in water to form the methanesulfinate anion (MSI<sup>-</sup>) (Babbs and Griffin, 1989; Steiner and Babbs, 1990):



Scaduto (1995) reported that MSI<sup>-</sup> is only an intermediate product of the aqueous phase DMSO/OH system because it can react further leading to MS<sup>-</sup> (CH<sub>3</sub>(O)S(O)O<sup>-</sup>) formation. This was confirmed by investigators such as Sehested and Holczman (1996) and Bardouki et al., (2002) who reported that MSI<sup>-</sup> can react rapidly with OH radicals leading to MS<sup>-</sup> and sulfate (SO<sub>4</sub><sup>2-</sup>) formation. Aqueous phase oxidation of DMSO can occur by other oxidants such as Cl, Cl<sub>2</sub><sup>-</sup>, SO<sub>4</sub><sup>-</sup>, and to a lesser extent H<sub>2</sub>O<sub>2</sub> (Zhu et al., 2005; Zhu et al., 2003; Amels et al., 1997; Bardouki et al., 2002). Oxidation of DMSO by Cl proceeds via adduct formation in both the gas and aqueous phases.

Halogens are also important oxidants and the mechanism for their reactions with important atmospheric species such as alkyl halides and DMS also involves abstraction and addition channels analogous to OH oxidation as discussed above, while CS<sub>2</sub> oxidation by Cl and OH radicals proceeds entirely by addition. Addition channels are favored at low temperatures and measured addition rate coefficients generally approach the gas kinetic limit ( $10^{-10} \text{ cm}^3 \text{ molecule}^{-1} \text{ s}^{-1}$ ) under these conditions (Wine et al., 2003; Orlando et al., 2005). The importance of adducts depends on their thermal stability relative to their bimolecular reaction with O<sub>2</sub> (mainly), as well as the products formed from thermal decomposition, their bimolecular reactions and their photochemistry. This represents the aims of the work presented in this thesis. Investigation into the spectroscopy and kinetics of the reactions of halogen adducts with atmospherically important species allows us to determine their potential importance and adds to our present understanding of these important radical species. Table 1.1 compares all available literature data on thermal stabilities of gas phase adducts of OH and halogen atoms with CS<sub>2</sub>, DMS, CH<sub>3</sub>I, and C<sub>2</sub>H<sub>5</sub>I. With the exception of SCS–OH, all of the adducts listed in Table 1.1 exhibit 2 center – 3 electron bonding. Generally, the experimentally determined adduct bond strengths are within the range 40 – 60 kJ mol<sup>-1</sup> with the exception of DMS–Cl and DMSO–Cl which have bond strengths of > 70 kJ mol<sup>-1</sup>. An expected trend in bond strengths is also observed as the difference between the ionization potential of any organic molecular reactant (such as DMS) and the respective radical electron affinity ( $\Delta\text{IP}$ ) decreases i.e., bond dissociation enthalpy decreases in the order DMS–Cl > DMS–Br > DMS–I. On average, theoretical calculations are found to be in reasonable agreement with experimental determinations.

### **Sulfur in the Atmosphere**

Sulfur is recognized as one of the critical elements for which an understanding of its biogeochemical cycle is pivotal to climate change studies (Berresheim et al., 1995).

**Table 1.1 Comparison of Adduct Stabilities**

Adduct	Dissociation Enthalpy at 298 K (kJ mol <sup>-1</sup> ) <sup>a</sup>	
	Experimental	Theoretical
SCS-Cl	40 <sup>b</sup>	33 <sup>c</sup>
SCS-OH	41 <sup>d</sup> , 46 <sup>e</sup> , 44 <sup>f</sup>	27 <sup>g</sup>
(CH <sub>3</sub> ) <sub>2</sub> S-Cl	na	53 <sup>h</sup> , 81 <sup>i</sup> , 97 <sup>j</sup> , 74 <sup>k</sup>
(CH <sub>3</sub> ) <sub>2</sub> S-Br	61 <sup>l</sup> , 51 <sup>m</sup>	59 <sup>k,m</sup>
(CH <sub>3</sub> ) <sub>2</sub> S-OH	42 <sup>n</sup> , 45 <sup>o</sup>	50 <sup>p</sup>
(CH <sub>3</sub> ) <sub>2</sub> (O)S-Cl	73 <sup>q</sup>	67 <sup>q</sup> , 73 <sup>r</sup>
CH <sub>3</sub> I-Cl	54 <sup>s</sup>	44 <sup>s</sup> , 61 <sup>s</sup> , 59 <sup>t</sup> , 52 <sup>u</sup>
C <sub>2</sub> H <sub>5</sub> I-Cl	58 <sup>v</sup>	38 <sup>v</sup> , 59 <sup>v</sup> , 62 <sup>w</sup>

<sup>a</sup>Uncertainties in theoretical values are typically ~8 kJ mol<sup>-1</sup>.

<sup>b</sup>Nicovich et al., 1990; <sup>c</sup>Wang and Phillips, 2002; <sup>d</sup>Hynes et al., 1988; <sup>e</sup>Murrels et al., 1990; <sup>f</sup>Diau and Lee, 1991; <sup>g</sup>McKee and Wine, 2001; <sup>h</sup>Resende and De Almeida, 1997; <sup>i</sup>Wilson and Hirst, 1997; <sup>j</sup>Thompson et al., 2002; <sup>k</sup>Enami et al., 2004; <sup>l</sup>Wine et al., 1993; <sup>m</sup>Nakano et al., 2001; <sup>n</sup>Hynes et al., 1995; <sup>o</sup>Barone et al., 1996; <sup>p</sup>McKee, 2003; <sup>q</sup>Nicovich et al., 2006; <sup>r</sup>Vandresen and Resende, 2004; <sup>s</sup>Ahyens et al., 1997; <sup>t</sup>Enami et al., 2005; <sup>u</sup>Lazarou et al., 1997; <sup>v</sup>Orlando et al., 2005; <sup>w</sup>Piety et al., 1998.

The atmospheric sulfur cycle begins with emission of volatile sulfur compounds into the atmosphere and ends with sulfur removal by dry or wet deposition to the Earth's surface. Sulfur in the troposphere has been the subject of intensive investigation because of its role in acid rain production, deleterious health effects, and climate modification. Sulfur bearing compounds can form aerosol particles that act to directly modulate the Earth's radiation budget by absorbing and scattering radiation (Charlson et al., 1992a, b) and to indirectly influence many aspects of climate through their interaction with clouds. By serving as cloud condensation nuclei (CCN) they influence the size and number of cloud droplets, thereby, influencing the radiative properties (Twomey, 1974), and the lifetime and precipitation properties of clouds (Albrecht, 1989). In the stratosphere, sulfur chemistry also plays a significant role in the Earth's radiation budget through its role in the formation and maintenance of stratospheric sulfate aerosols (Hofmann, 1990; Chin and Davis, 1993; Seinfeld and Pandis 1998), and affects stratospheric ozone concentrations via heterogeneous chemistry. It has been postulated that acidic aerosols in the stratosphere provide surfaces for heterogeneous chemical reactions that convert inactive halogens, for example, HCl, and HBr into HOCl and HOBr, which are photolytic precursors to Cl, ClO, Br, and BrO, which then participate in stratospheric ozone catalytic cycles (Molina et al., 1996 and references therein).

Sulfur enters the atmosphere from both natural (oceans, coastal wetlands, soils and plants, volcanoes, and biomass burning) and anthropogenic (coal refining, fossil fuel combustion, and industrial processes) sources, which are highly variable in time and space. Table 1.2 provides the estimated global emissions of the most important atmospheric sulfur gases, evaluated by Pham et al. (1995) using a global three-dimensional chemistry-transport model (IM-AGES), while Table 1.3 summarizes the observed mixing ratios of these species based on field measurements. According to Pham et al. (1995), anthropogenic emissions dominate as the source of sulfur (as SO<sub>2</sub>) to

**Table 1.2 Estimated global emissions of important atmospheric sulfur gases**

<b>Sources</b>	<b>SO<sub>2</sub></b>	<b>H<sub>2</sub>S</b>	<b>COS</b>	<b>DMS</b>	<b>CS<sub>2</sub></b>	<b>Total</b>
Volcanoes	9.2					9.2
Biosphere		0.52	0.35	0.31	0.0064	1.18
Vegetation		0.5	0.21	0.29	0.004	1
Soils		0.02	0.14	0.02	0.0024	0.18
Biomass burning	2.9		0.11			3
Ocean			0.3	19.2	0.2	19.7
Anthropogenic	92		0.07		0.3	92.4
<b>Total</b>	<b>104.1</b>	<b>0.52</b>	<b>0.83</b>	<b>19.5</b>	<b>0.5</b>	<b>125.5</b>

Emissions are in 10<sup>12</sup> grams of S per year (Pham et al., 1995)

**Table 1.3 Observed atmospheric mixing ratios of important gaseous sulfides, and their major sources and sinks (Warneck, 1999; Watts, 2000)**

GAS	MIXING RATIO <sup>a</sup>	LOCATION	MAJOR SOURCES	MAJOR SINKS
OCS	500	uniform	Soils Ocean From sulfides	Uptake by vegetation Loss to stratosphere
CS <sub>2</sub>	11 – 340 3.3 – 14 7 – 184	Continental Marine Estuaries	Industrial Saline marshes	Reaction with OH Soil uptake
H <sub>2</sub> S	1.3 – 340 0 - 110	Continental Marine	Soils Vegetation Volcanoes	Reaction with OH
DMS	2 – 440 1 - 3440	Continental marine	Oceans	Reaction with OH Reaction with NO <sub>3</sub> Reaction with Cl Reaction with BrO

<sup>a</sup>Units in pptv.

the atmosphere accounting for approximately 70% of total sulfur emissions and nearly 100% of anthropogenic emissions, while ocean emissions (as DMS) account for ~ 15% of total sulfur emissions and ~ 56% of natural emissions. The atmospheric concentration of a species depends on its source strength, transport, reactivity, and deposition velocity. Reduced sulfur gases such as H<sub>2</sub>S, DMS, and CS<sub>2</sub> react rapidly with OH radicals, and their atmospheric lifetimes are short, on the order of days. Consequently, their mixing ratios fluctuate considerably. Reactions of OCS with OH radicals and oxygen atoms are slow, leading to a tropospheric lifetime of ~ 7 years. Carbonyl sulfide (OCS) is, therefore, uniformly distributed with an average mixing ratio of ~ 500 pptv. The major sources and sinks of OCS, H<sub>2</sub>S, DMS, SO<sub>2</sub> and CS<sub>2</sub> are listed in Table 1.3. DMS is the major natural source of sulfur to the troposphere and is a steady source unlike sporadic volcanic emissions. Understanding the natural sulfur cycle, of which DMS is the main component, is critical for understanding past climate as interpreted from ice core data, and predicting future effects resulting from anthropogenic sulfur emissions. In particular, the postulation of the CLAW hypothesis by Charlson et al. (1987) has led to numerous investigations into the role of DMS in natural climate regulation as depicted in Figure 1.1.

Essentially, the CLAW hypothesis suggests that marine phytoplankton ecosystems may effectively regulate climate by a feedback associated with the production of dimethyl sulfide (DMS). Charlson et al. (1987) observed that some of the DMS produced by marine ecosystems is transferred from the ocean to the atmosphere where it can be a major source of cloud condensation nuclei (CCN) over the remote oceans. The aerosols resulting from biogenic DMS emissions can have a direct effect on the solar radiative forcing experienced by the Earth through scattering, absorption and reflection and can also lead to increased cloud formation. The CLAW hypothesis proposes that these mechanisms could regulate climate.

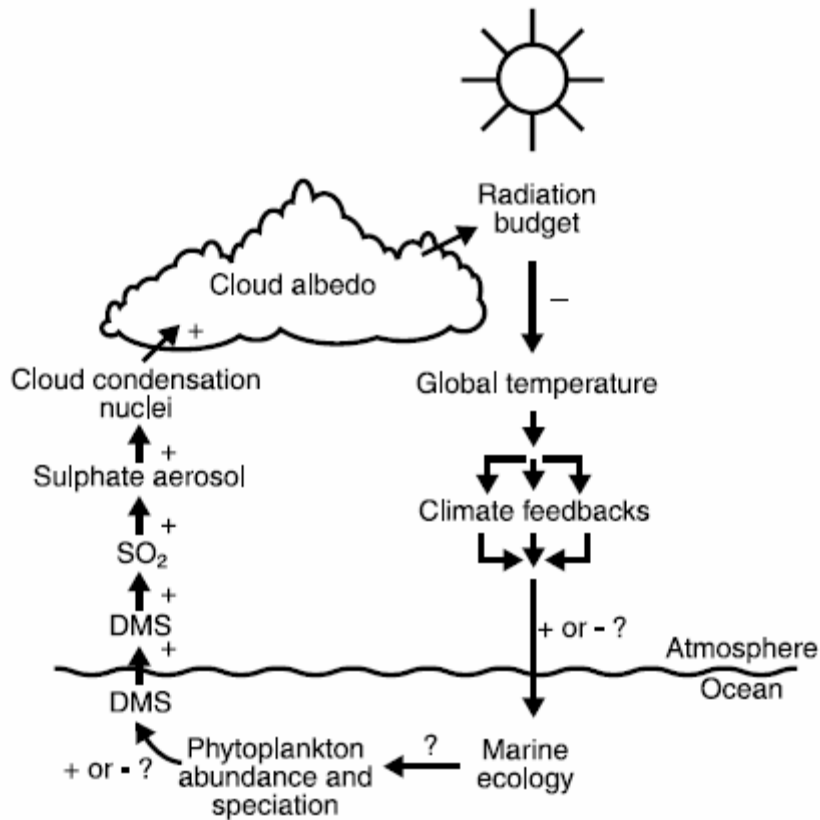


**Figure 1.1** A simplified representation of the CLAW Hypothesis (Andreae, 1990). The pluses and minuses indicate if an increase in the value of the preceding parameter in the cycle is expected to lead to an increase (+) or decrease (-) in the value of the subsequent parameter.

Charlson et al. (1987) postulated that an increase in global temperature would lead to increased biogenic DMS emissions from the ocean and result in an increase in scattering, cloud cover and cloud albedo that would increase the proportion of the incoming solar radiation reflected back into space (thus changing the global albedo), and thereby cooling the planet.

The CLAW hypothesis has, for over two decades, provided the intriguing prospect of oceanic and atmospheric coupling in a manner such as to oppose perturbations in climate. Many scientific papers have resulted which confirm details of specific links between oceanic phytoplankton and DMS emission to the atmosphere, the importance of DMS oxidation products in regulation of marine atmospheric CCN populations, and a concomitant influence on marine stratocumulus cloud properties (Ayers and Cainey, 2007 and references therein). However, many gaps remain, such as a lack of quantitative understanding of new particle formation processes in the marine boundary layer (MBL) (Ayers and Cainey, 2007). Major questions that require resolution, (Ayers and Cainey, 2007 and references therein), include: what factors control the flux of DMS to the atmosphere?; what fraction of atmospheric DMS will eventually form SO<sub>2</sub>, MSA, and sulfate aerosol and will this lead to higher particle number concentrations?; what are the relationships between particle number concentration (CN), cloud condensation nuclei (CCN), and cloud droplet number concentrations (CDN); and will changes in CDN have a significant radiative impact?

Shown in Figure 1.2 is a simplified schematic of the DMS cycling involved in the CLAW hypothesis. It represents oceanic production of DMS by phytoplanktonic activity followed by its emission into the MBL where it is oxidized. DMS oxidation products can then be further oxidized to form sulfate and CCN and/or partition into the condensed phase where heterogeneous processes occur. In spite of intensive efforts, determination of the quantitative contribution of DMS-derived non-sea-salt sulfate (nss-SO<sub>4</sub><sup>2-</sup>) to CCN

formation in the MBL is still highly uncertain and model studies of global SO<sub>2</sub>, for example, Chin et al. (1998), indicate that there may be unaccounted for oxidants involved in the DMS oxidation. In particular, based on measurements of reactive halogen species (X<sub>2</sub>, XO) and also on the behavior of non methane hydrocarbons (NMHC), it has been speculated that Cl atoms, ClO, and BrO radicals might also play a role in the chemistry of DMS oxidation (Barnes et al., 1991; Ingham et al., 1999; Maurer et al., 1999; Urbanski and Wine, 1999; Saiz-Lopez et al., 2007). Further progress in the elucidation of the DMS oxidation mechanism requires advances in field studies and detailed kinetic/product studies combined with modeling of field data.

### **Role of Halogens in Tropospheric Chemistry**

The role of reactive halogen species (e.g. Cl, Br) in the destruction of the stratospheric ozone layer is well known and largely understood (Solomon, 1990), while their role in the troposphere has only been widely investigated since their destructive effect on boundary layer ozone after polar sunrise was postulated (Barrie et al., 1988). It has been assumed that these events were confined to polar regions during springtime, however, with the advent of satellite measurements and new field measurement techniques such as differential optical absorption spectroscopy (DOAS) and chemical ionization mass spectrometry (CIMS), significant amounts of BrO (Hebestreit et al., 1999; Stutz et al., 2002; Honninger et al., 2004; Wagner et al., 2001), and Cl atoms (Wingenter et al., 2005) have been detected outside the Arctic and Antarctic boundary layer. At the levels suggested by available measurements, reactive halogen species can have a significant effect on tropospheric chemistry by contributing to ozone depletion, influencing partitioning of NO<sub>x</sub> and HO<sub>x</sub> radicals, oxidizing organic compounds, removing elemental mercury from the atmosphere, and forming new particles in coastal environments.

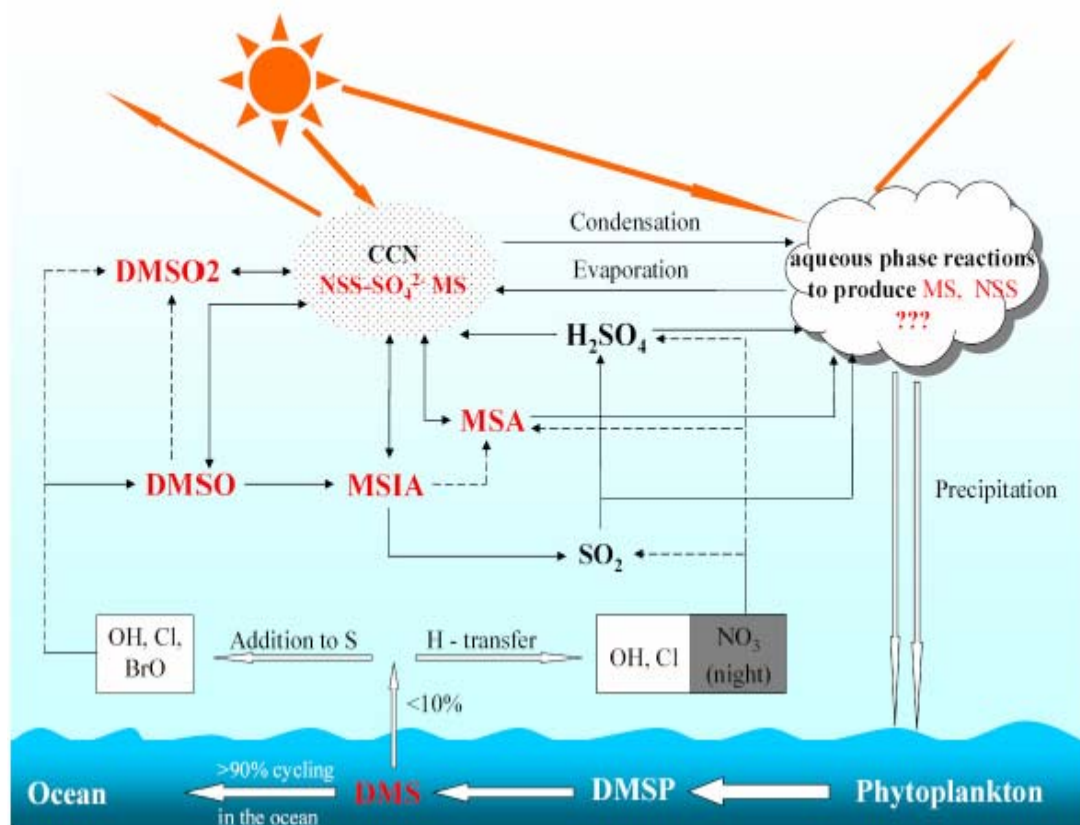
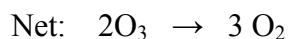
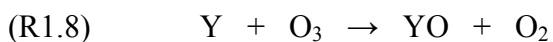
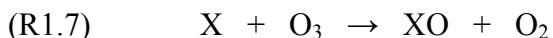


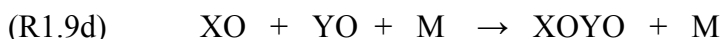
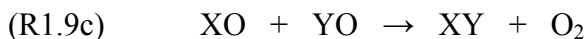
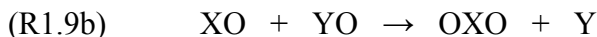
Figure 1.2 A simplified schematic of DMS cycling in the marine boundary layer

### Ozone depletion

Halogen-catalysed depletion of tropospheric ozone often occurs by the following reactions (X and Y = Cl, Br, I):

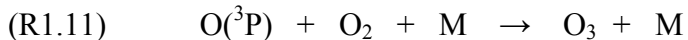
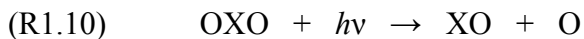


Reaction (R1.9) can occur via other channels:

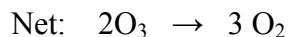
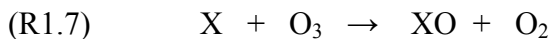
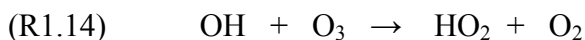
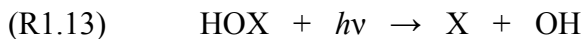


Channels (R1.9a) and (R1.9c) are equivalent since XY is readily photolysed to X and Y. The efficiency of ozone destruction by reaction (R1.9) varies depending on the halogen species involved. In the ClO self-reaction, the Cl<sub>2</sub>O<sub>2</sub> dimer is formed which thermally decomposes back to ClO (Platt and Janssen, 1995); in the BrO self reaction, the production of 2 Br atoms is favored over Br<sub>2</sub> formation; the BrO + IO reaction produces OIO and Br (80%) and I + Br (20%) (Sander et al., 2006); the IO self reaction is fast and produces mainly OIO and I<sub>2</sub>O<sub>2</sub>. I<sub>2</sub>O<sub>2</sub> is either photolysed, undergoes uptake into existing aerosol surfaces, or is involved in the nucleation of new particles (McFiggans et al., 2000; Jimenez et al., 2003a, b; O'Dowd et al., 2002). The efficiency of the ozone

depletion cycle can be reduced by photolysis of the halogen dioxide formed in reaction (R1.9b):

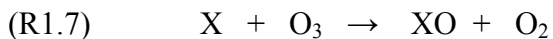
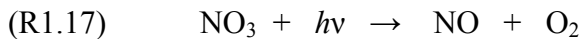
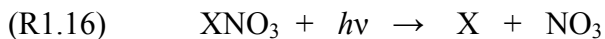
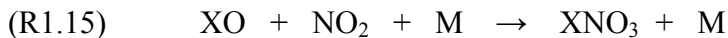


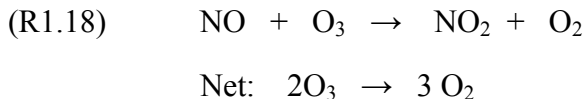
However, in the case of OIO, photodissociation probably accounts for < 10% of OIO loss (Plane et al., 2006). Reaction (R1.7) will dominate ozone destruction when relatively high mixing ratios of halogen oxides are present (> 2 ppt of IO and BrO Saiz-Lopez et al., 2004) but at lower XO concentrations, reaction with HO<sub>2</sub> radicals becomes important (Adams and Cox, 2002):



As a result of photolysis of halogen species in remote marine environments at sunrise, this cycle has been proposed to account for substantial ozone depletion events (Nagao et al., 1999; Galbally et al., 2000).

In semi-polluted environments, halogen nitrate formation can also lead to ozone depletion:

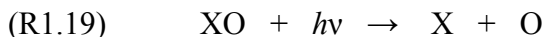
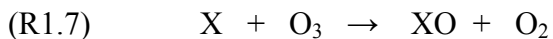




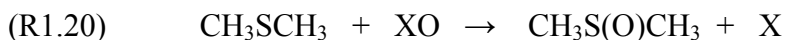
The efficiency of this cycle is reduced because  $\text{XNO}_3$  can also photolyse to  $\text{XO} + \text{NO}_2$  leading to a null cycle, also, the major photolysis pathway of  $\text{NO}_3$  produces  $\text{NO}_2 + \text{O}$ , which again leads to no net  $\text{O}_3$  depletion.

#### Oxidation of organic compounds

A photochemical steady-state is established between X and XO during the daytime, where X = Br or I:



The halogen oxide radical BrO can significantly increase the daytime oxidation of DMS in the MBL (Saiz-Lopez et al., 2004; Toumi, 1994; Bedjanian et al., 1996; James et al., 2000; Boucher et al., 2003; Saiz-Lopez et al., 2007).

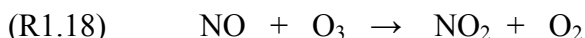
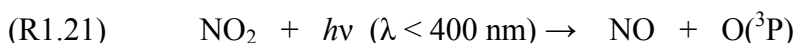


At the observed XO levels in the MBL, the rate of oxidation of DMS by BrO is now thought to be most important (Saiz-Lopez et al., 2007) although there is some uncertainty about the rate coefficient for the BrO + DMS reaction (Barnes et al., 1991; Bedjanian et al., 1996; Ingham et al., 1999; Nakano et al., 2001). It is thought that  $\text{CH}_3\text{S(O)CH}_3$  is then oxidized to methane sulphinic acid (MSIA), whose fate is dependent on whether its uptake into the condensed phase occurs, in which case MSA is probably formed, or

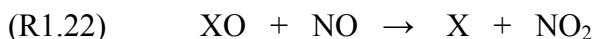
whether it remains in the gas phase, in which case SO<sub>2</sub>, a CCN precursor, appears to be the major product.

#### Changes to the NO<sub>x</sub> and HO<sub>x</sub> ratios

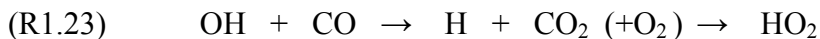
The ratio of NO<sub>2</sub> to NO is controlled principally by the reactions:



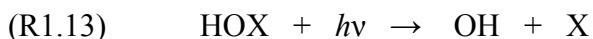
In the presence of significant halogen concentrations, the balance will be shifted towards NO<sub>2</sub> (McFiggans et al., 2000):



In the remote MBL, the HO<sub>2</sub> radical is formed from OH through the sequence:



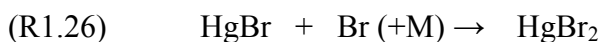
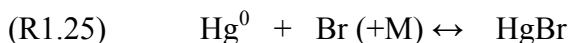
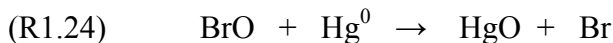
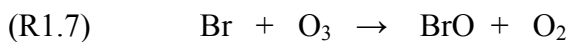
In the presence of BrO and IO, the HO<sub>2</sub>/OH ratio will be reduced (Carpenter et al., 1999; Davis et al., 1996; McFiggans et al., 2000; Jenkin et al., 1985; Cronkhite et al., 1999):



#### Removal of atmospheric Hg

The major primary source of elemental mercury (Hg<sup>0</sup>) in the atmosphere is coal combustion. The atmospheric lifetime of Hg<sup>0</sup> is ~ 1 year, except during polar spring when it is oxidized to Hg<sup>2+</sup> (probably as HgO, HgBr<sub>2</sub> or HgCl<sub>2</sub>). When this happens, Hg can enter the foodchain in the Arctic ecosystem (Lindberg et al., 2001; Goodsite et al.,

2004; Calvert and Lindberg, 2003) which can then lead to bioaccumulation with associated adverse effects such as brain damage. It has been observed that ozone depletion events correlate with  $\text{Hg}^0$  depletion and the following possible pathways for this occurrence have been postulated (Lindberg et al., 2001; Goodsite et al., 2004; Calvert and Lindberg, 2003):



#### New particle formation

It has been proposed that observed high concentrations of ultra-fine particles (diameter  $\sim$  3 nm), during the daytime around low tide in the coastal MBL, are caused by the polymerization of iodine oxides produced from photolabile compounds such as  $\text{CH}_2\text{I}_2$  and  $\text{I}_2$  (Saiz-Lopez and Plane, 2004; McFiggans et al., 2004; Jimenez et al., 2003; O'Dowd et al., 2002; Burkholder et al., 2004), however, the mechanisms whereby species such as IO, OIO, and  $\text{I}_2\text{O}_2$  are oxidized to higher oxides such as  $\text{I}_2\text{O}_3$ ,  $\text{I}_2\text{O}_4$ , and  $\text{I}_2\text{O}_5$ , which are likely condensable, are not fully understood.

### **Bromine in the Atmosphere**

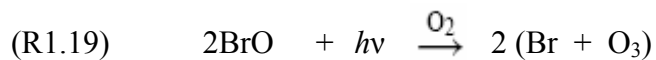
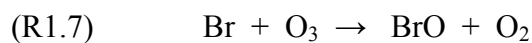
Reactive bromine species, especially Br, BrO, and HOBr, are efficient catalysts to stratospheric ozone destruction (Yung et al., 1980; McElroy et al., 1986; Solomon et al., 1995; Garcia and Solomon, 1994), and have also been linked to severe ozone depletion events (ODEs) in the surface atmosphere of polar regions (Barrie et al., 1988; Wagner and Platt, 1998; Fan and Jacob, 1992; McConnell et al., 1992; LeBras and Platt, 1995).

Jobson et al. (1994) showed that bromine atoms, rather than chlorine atoms, were responsible for most of the ozone destruction. In addition, modeling studies indicate that bromine activation could be an important factor in ozone destruction in the marine boundary layer (MBL) and in affecting the oxidizing capacity of the troposphere (Sander and Crutzen, 1996; Vogt et al., 1996; von Glasow et al., 2004; Yang et al., 2005).

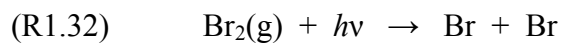
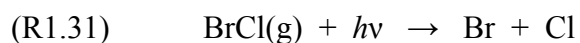
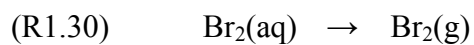
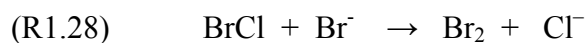
Natural sources of bromine to the atmosphere include brominated organic compounds such as  $\text{CH}_3\text{Br}$ ,  $\text{CHBr}_3$ ,  $\text{CH}_2\text{Br}_2$ ,  $\text{CH}_2\text{BrCl}$ ,  $\text{CHBr}_2\text{Cl}$ , and  $\text{CHBrCl}_2$ ; their main identified sources being macroalgae, ice algae, and phytoplankton (Carpenter and Liss, 2000; Quack and Wallace, 2003). Other than via the photochemical destruction of organobromines, reactive bromine can also be released into the atmosphere through the autocatalytic oxidation of sea salt aerosol (Sander et al., 2003); this may be the dominant source of reactive bromine in the boundary layer and lower troposphere. Anthropogenic sources of bromine to the atmosphere include industrially produced halons such as  $\text{CF}_3\text{Br}$  and  $\text{CF}_2\text{ClBr}$  (primarily used as fire extinguishers), and methyl bromide ( $\text{CH}_3\text{Br}$ ), which has a combination of natural and anthropogenic sources including industrial fumigation, burning of leaded fuel, biomass burning, terrestrial ecosystems and the ocean (Montzka and Fraser, 2003; Mano and Andreae, 1994; Penkett et al., 1994).

Bromine cycling as depicted in Figure 1.3 involves release of bromine atoms from organobromide molecules or sea salt, as discussed above. Once released, bromine atoms can abstract H atoms from  $\text{HO}_2$  or aldehydes yielding  $\text{HBr}$ , which, via condensed phase chemistry, may lead to  $\text{Br}_2$  being transferred to the atmosphere. Bromine atoms also react rapidly with ozone to produce bromine oxide ( $\text{BrO}$ ) which can then undergo (i)

photolysis to regenerate Br atoms (Platt, 1995) (ii) reaction with HO<sub>2</sub> yielding HOBr or (iii) self reaction:



Vogt et al. (1997) suggested that in the aqueous phase HOBr reacts with chloride in the presence of protons (H<sup>+</sup>) to form BrCl, which may react further with bromide to form Br<sub>2</sub>; both BrCl(aq) and Br<sub>2</sub>(aq) are then partitioned to the gas phase where they undergo photolysis, ultimately yielding Br atoms into the atmosphere:



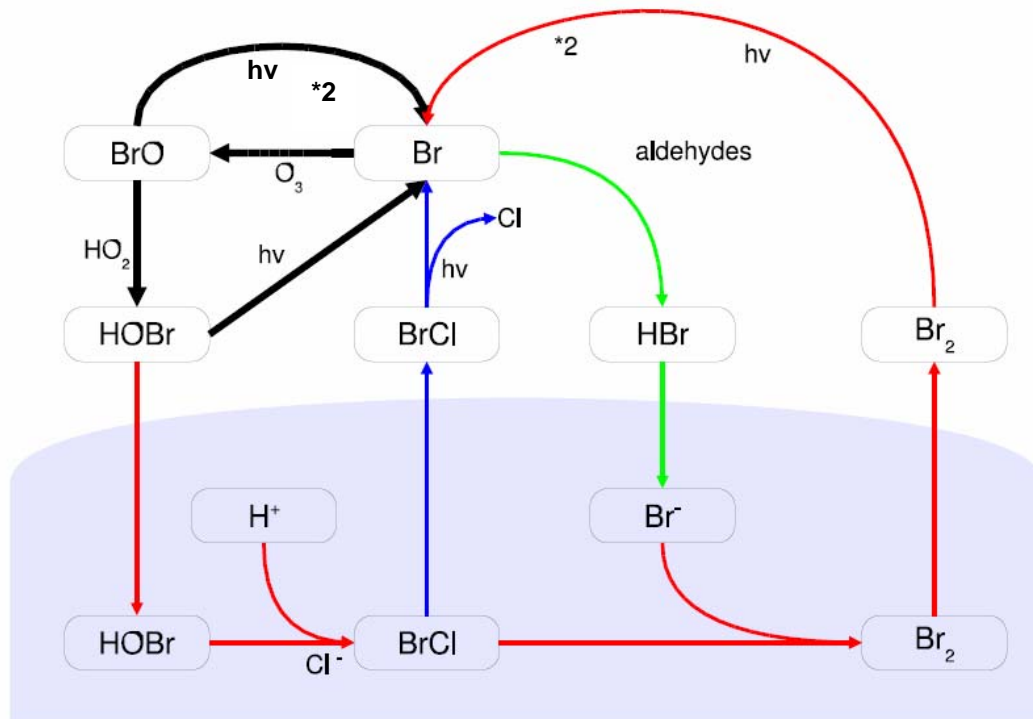


**Figure 1.3 Graphical depiction of Bromine cycling adapted from Simpson et al. (2007).** The blue area at the bottom is meant to represent the condensed phase (liquid brine or ice surface).

## **Iodine in the Atmosphere**

The role of iodine in atmospheric processes has been under investigation for over two decades. The potential significance of iodine photochemistry in tropospheric ozone destruction was first highlighted by Chameides and Davis (1980) and has been the subject of study by investigators such as Jenkin et al., 1985; Chatfield and Crutzen, 1990; Davis et al., 1996; and McFiggans et al., 2000. It has also been postulated that iodine in the atmosphere (i) contributes to lower stratospheric ozone depletion (Solomon et al., 1994; Bosch et al., 2003), (ii) plays a role in new particle formation in marine environments (O'Dowd et al., 2002a, 2002b; Makela et al., 2002), and (iii) enhances release of gaseous halogen from sea salt aerosols through its interaction with bromide and chloride (Vogt et al., 1999; McFiggans et al., 2002).

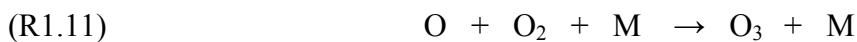
Although much progress has been made in the way of deciphering iodine chemistry in the troposphere, many uncertainties remain especially in quantifying iodine sources, sinks, and recycling. Natural sources of atmospheric iodine are thought to dominate over anthropogenic releases from industry or fossil fuel combustion. The primary natural source is postulated to be the release of iodo-carbons such as  $\text{CH}_3\text{I}$ ,  $\text{CH}_2\text{I}_2$ ,  $\text{CH}_2\text{IBr}$ , and  $\text{CH}_2\text{ICl}$ , from the sea surface (Carpenter 2003; Carpenter et al., 2003). Unlike the di- and tri-iodated compounds,  $\text{CH}_3\text{I}$  has terrestrial sources including biomass burning, rice paddies, and wetlands and a recent study has reported a large terrestrial source strength which equals the estimated oceanic source strength of methyl iodide (Sive et al., 2007). Methyl iodide was first detected in the marine boundary layer by Lovelock et al. (1973) and was thought to be the major source of atmospheric iodine,

however, other organo-iodides such as  $\text{CH}_2\text{I}_2$  are now believed to dominate as iodine sources to the atmosphere (Carpenter et al., 1999; Carpenter et al., 2000; Schall and Heumann, 1993). The following cycles are thought to be operative and are summarized in Figure 1.4:

Cycle 1



Cycle 2



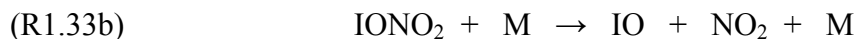
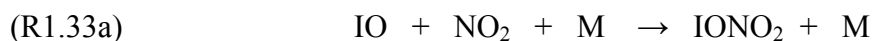
Cycle 1 is the predominant pathway for I-to-IO inter-conversion and like Cycle 2, has no net effect on I or IO (collectively called  $\text{IO}_x$ ), however, other cycles involving  $\text{IO}_x$  reactions with  $\text{HO}_2$ ,  $\text{NO}_x$ , and IO can regenerate I atoms without concomitant O atom formation leading to catalytic ozone loss, for example:



### Cycle 3



### Cycle 4



According to Davis et al., 1996,  $I_x$  levels of 7 pptv can result in  $HO_2/OH$  shifts of  $\sim -15\%$  via Cycle 3, thus this cycle is of particular importance in  $HO_x$  partitioning. Cycle 3 has also been suggested as the dominant ozone loss cycle at  $NO_x$  levels  $< 500$  pptv (Stutz et al., 1999), whereas, at higher  $NO_x$  levels Cycles 3 and 4 can be operative, with Cycle 3 being a null cycle (no net ozone loss) and Cycle 4 being ozone depleting only if photolysis of iodine nitrate (R1.34) is fast compared with its thermal dissociation (R1.33b) and reaction (R1.34a) is the dominant pathway for photolysis of  $IONO_2$ . Based

on calculations performed by Allan and Plane (2002), Cycle 4 can contribute to boundary layer ozone depletion at temperatures < 290 K.

Another important pathway of IO<sub>x</sub> cycling involves the IO self reaction:

#### Cycle 5



Only reaction (R1.36a) results in net ozone loss and quantum calculations performed by Ashworth et al. (2002) indicate that this channel dominates in the visible region.

### **CH<sub>3</sub>I and C<sub>2</sub>H<sub>5</sub>I in the Atmosphere**

Several measurements of CH<sub>3</sub>I are reported in the literature as summarized in Table 1.4, whereas few measurements of C<sub>2</sub>H<sub>5</sub>I exist (Carpenter et al., 1999; Yokouchi et al., 1997). On average, MBL levels of CH<sub>3</sub>I range between 1 and 4 pptv (Rasmussen et al., 1992; Kurylo and Rodriguez 1999; Elkins et al., 1998), but can be as high as 43 pptv at coastal sites associated with high biological activity (Oram and Penkett, 1994; Davis et al., 1996); Yokouchi et al., 1997 and Carpenter et al., 1999 reported a measured C<sub>2</sub>H<sub>5</sub>I concentration range between <0.03 to 0.31 pptv and <0.02 to 0.21 pptv respectively. Estimates of global annual sources and sinks of CH<sub>3</sub>I are listed in Table 1.5 and clearly demonstrate large uncertainties in the magnitude of the oceanic source, estimates of which vary between 214 and 1300 Gg/year. As a result, large variation also exists in estimates of the photolysis sink (Bell et al., 2002; Roehl et al., 1997), which is the

dominant loss process for the CH<sub>3</sub>I molecule (Garraway, 1981; Brown et al., 1990; Cotter et al., 2003).

As mentioned above, the dominant fate of atmospheric CH<sub>3</sub>I is thought to be photolysis and the atmospheric lifetime of CH<sub>3</sub>I toward photolysis is estimated to be a few days (Roehl et al., 1997; Rattigan et al., 1997). However, larger alkyl iodides may also react with OH and Cl at a rate that is significant compared with their photolysis (Carl and Crowley 2001; Cotter et al., 2003; Cotter et al., 2001a, b). In the MBL, where Cl atom concentrations are elevated, reactions of these alkyl iodides with Cl may be potentially important. The mechanisms for reactions of Cl with alkyl iodides appear to involve both H- abstraction and adduct-forming pathways (Cotter et al., 2001b; Ahyens et al., 1997; Bilde and Wallington, 1998; Piety et al., 1996; Bilde et al., 1997; Goliff and Rowland, 1997; Enami et al., 2005).

### **Aims of this work**

The focus of this dissertation is a series of laboratory kinetic and spectroscopic studies of adducts of halogen atoms (Cl, Br, and I) with atmospherically important species, such as CS<sub>2</sub>, CH<sub>3</sub>I, C<sub>2</sub>H<sub>5</sub>I, and DMS, using laser flash photolysis (LFP) coupled with time resolved UV-visible absorption spectroscopy (TRUVVAS). The studied gas phase spectra include: CS<sub>2</sub>-Cl (Chapter 3), CH<sub>3</sub>I-Cl (Chapter 4), C<sub>2</sub>H<sub>5</sub>I-Cl (Chapter 4), Br-DMS (Chapter 5), and I-DMS (Chapter 6) all of which are being reported for the first time except for Br-DMS for which there exists some discrepancy in the literature. The studied gas phase kinetics include: self reaction of CS<sub>2</sub>-Cl and reaction of CS<sub>2</sub>-Cl with O<sub>2</sub>, NO, and NO<sub>2</sub> (Chapter 3), self reaction of CH<sub>3</sub>I-Cl and reactions of CH<sub>3</sub>I-Cl with O<sub>2</sub>, NO, and NO<sub>2</sub> (Chapter 4), self reaction of C<sub>2</sub>H<sub>5</sub>I-Cl and reactions of C<sub>2</sub>H<sub>5</sub>I-Cl with

O<sub>2</sub>, NO, and NO<sub>2</sub> (Chapter 4), self reaction of Br–DMS and reactions of Br–DMS with O<sub>2</sub>, NO, and NO<sub>2</sub> (Chapter 5), and reactions of I–DMS with O<sub>2</sub>, NO, and NO<sub>2</sub> (Chapter 6). None of the above mentioned kinetics have been previously reported in the literature except for an upper limit on the rate constant of the Br–DMS self reaction and an SCS–Cl + O<sub>2</sub> upper limit.

The results reported in this work are useful for developing an understanding of (i) the kinetics and spectroscopy of gas-phase adducts of radicals with sulfur compounds and radicals with iodine compounds; (ii) differences (similarities) between gas- and liquid-phase adduct spectroscopy and kinetics; (iii) kinetics and spectroscopy of radical-molecule adducts that involve two-center – 3 - electron (2c-3e) bonds and (iv) the potential role of these adducts in atmospheric chemistry. As discussed above, a number of similar radical – molecule adducts are known to play important roles in atmospheric chemistry.

**Table 1.4 Summary of CH<sub>3</sub>I measurements reported in literature**

Source	Global Emission, Gg/yr	Reference
Oceanic <sup>a</sup>	270	<i>Liss and Slater</i> [1974]
	1300	<i>Rasmussen et al.</i> [1982]
	300–500	<i>Singh et al.</i> [1983]
	140	<i>Nightingale</i> [1991]
	800	<i>Reifenhauser and Heumann</i> [1992]
	150	<i>Campos et al.</i> [1996]
	130–350	<i>Moore and Groszko</i> [1999]
Terrestrial		
Biomass burning	<10	<i>Andreae et al.</i> [1996]
	3.4	<i>Blake et al.</i> [1996b]
Plant-soil systems		
Rice paddies	20	<i>Muramatsu and Yoshida</i> [1995]
	71	<i>Redeker et al.</i> [2000]
Peatland ecosystems	1.4	<i>Dimmer et al.</i> [2000]
Wetlands	7.3	<i>Dimmer et al.</i> [2000]

<sup>a</sup>Extrapolated from field measurements over limited regions

**Table 1.5 Estimates of global annual sources and sinks for CH<sub>3</sub>I (Gg/yr) (Adapted from Keene et al., 1999)**

Source/Sink	Magnitude (Gg yr <sup>-1</sup> )	References
Natural Sources		
Ocean estimate 1	240	Moore and Groszko, 1999
Ocean estimate 2	500	Singh <i>et al.</i> , 1983
Ocean estimate 3	800	Reifenhauser and Heumann, 1992
Ocean estimate 4	1300	Rasmussen <i>et al.</i> , 1982
Ocean estimate 5	214	Bell <i>et al.</i> , 2002
<i>Ocean average</i>	610	
Macroalgae	300	Manley and Dastoor, 1987; Manley and Dastoor, 1988
Wetlands	7	Dimmer <i>et al.</i> , 2001
Peatlands	1	Dimmer <i>et al.</i> , 2001
Total natural	920	
Anthropogenic		
Rice estimate 1	26	Muramatsu and Yoshida, 1995
Rice estimate 2	71	Redeker <i>et al.</i> , 2000
<i>Rice average</i>	50	
<b>Total sources</b>	<b>970</b>	
Sinks		
Photolysis estimate 1	1650	Roehl <i>et al.</i> , 1997
Photolysis estimate 2	304	Bell <i>et al.</i> , 2002
<i>Photolysis average</i>	980	
<b>Sources – Sinks</b>	<b>-10</b>	

## CHAPTER 2

### EXPERIMENTAL TECHNIQUES

#### Experimental Approach

Application of the LFP-TRUVVAS technique involves the following steps: A flowing gas mixture consisting of the molecular reactant, the photolytic precursor for the radical of interest, and buffer gases was flowed through a reaction cell. The free radical chemistry was initiated by laser flash photolysis of the photolytic precursor. The desired free radical reactant could be generated either directly from the photolysis of the precursor or through rapid secondary chemistry. The reaction mixture was then probed using UV-Visible absorption spectroscopy, and temporal absorption profiles of the transient species were monitored. A schematic diagram of the LFP-TRUVVAS apparatus is shown in Figure 2.1. It consists of a pulsed excimer laser photolysis light source, a high pressure 75 watt Xe arc lamp cw probe light source, an insulated Pyrex, jacketed reaction cell (100 cm long, 40 mm internal diameter), a pre-mixing and pre-cooling cell, a monochromator to isolate the probe wavelength of interest, a photomultiplier tube (PMT) to detect the probe radiation, an oscilloscope to record the temporal evolution of the transmitted probe radiation, a photodiode to detect the laser flash and trigger the oscilloscope, a computer to store and average the waveforms from the oscilloscope, absorption cells outfitted with appropriate band pass filters (BPF) and lamps to facilitate *in situ* photometric measurements of reactant gases, thermocouples to measure the temperature of the reaction gas mixture, and numerous optical components to manipulate and align the photolysis and probe beams.

Important features of the methodology include the following: (1) Reactive intermediates are probed in “real time”, that is, on time scales corresponding to their lifetimes under the experimental conditions employed ( $10^{-6} - 10^{-2}$  s); and (2) All experiments were conducted under “slow flow” conditions, with a linear flow rate of the reaction mixture through the reaction cell (typically  $10 \text{ cm s}^{-1}$ ) sufficient to replenish or mostly replenish the reaction mixture between photolysis laser pulses (typical laser repetition rate was 0.1 Hz) but slow enough that kinetic observations could be analyzed assuming static conditions.

The photolysis laser employed in this work was a Lambda Physik Compex 102 excimer laser. Photolysis wavelengths of 248 nm and 308 nm were achieved by using KrF and XeCl gas fill mixtures respectively. After adjustment of the height, distance and size of the laser beam (using an iris with diameter 1.27 cm) the laser was directed through the reaction cell by employing mirrors and lenses. Variations of laser power for averaged shots were typically less than 2%. As depicted in Figure 2.1, the UV-vis probe beam was directed through the reaction cell to overlap collinearly with the photolysis beam. Upon exiting the reaction cell, the probe beam was focused onto the entrance slit of a 0.22 m grating monochromator to isolate the desired probe wavelength. The monochromator entrance and exit slits were set at 1.5 mm, providing a spectral resolution of 5.5 nm (full width half maximum; FWHM). The light exiting the monochromator was converted from optical signal to electrical signal using a photomultiplier tube (PMT). The time dependent current output by the PMT was routed through a fixed resistor and the resulting DC voltage was passed through an amplifier (Data Precision model D1000). Depending on the required time resolution, the RC time constant of the circuit (PMT/coaxial cable/resistor) was varied by changing the resistor. A TDS210 two channel digital real-time oscilloscope (Tektronix) was then used to digitize and record the electrical signals. The oscilloscope was triggered by the laser pulse detected by a

photodiode, and a computer connected to the oscilloscope was employed to average and store the data using a program (SCOPE) designed in our lab.

### Gas Flow System

Gases were introduced into the reaction system from their respective containers through Teflon tubing connected to calibrated mass flow meters (MKS instruments) with a shut off valve and a needle valve used to control the flow rate. With the exception of DMS and CS<sub>2</sub>, all gases were taken either directly from their high pressure storage cylinders or from a 12 L Pyrex bulb containing a dilute mixture of the reagent gas in N<sub>2</sub>. Dimethyl sulfide (DMS) and CS<sub>2</sub> were transferred under N<sub>2</sub> into Pyrex reservoirs which were then submerged into a thermostat-regulated bath. As shown in Figures 2.2 and 2.3, the vapor pressures of these liquids at room temperature were high enough to create the required pressure drop to drive the pure gases through their calibrated flow meters (Osborne et al., 1942; Waddington et al., 1962). MKS flow meters are calibrated in N<sub>2</sub> gas. In order to correct the calibration for flow of other concentrated gases such as pure CS<sub>2</sub> a gas correction factor (GCF) was determined based on the following equation (MKS manual):

$$\text{(Eq. 2.1)} \quad C_x = 0.3098 S/p_x C_{p_x}$$

where  $C_x$  = GCF of gas X,  $p_x$  = density of gas X at 0°C, g/liter,  $C_{p_x}$  = specific heat capacity of gas X, calories/g/°C,  $0.3098 = p_{N_2} C_{p_{N_2}}$  for N<sub>2</sub> at 0°C, and S = molecular structure correction factor. A GCF of 0.62 was computed for CS<sub>2</sub>.

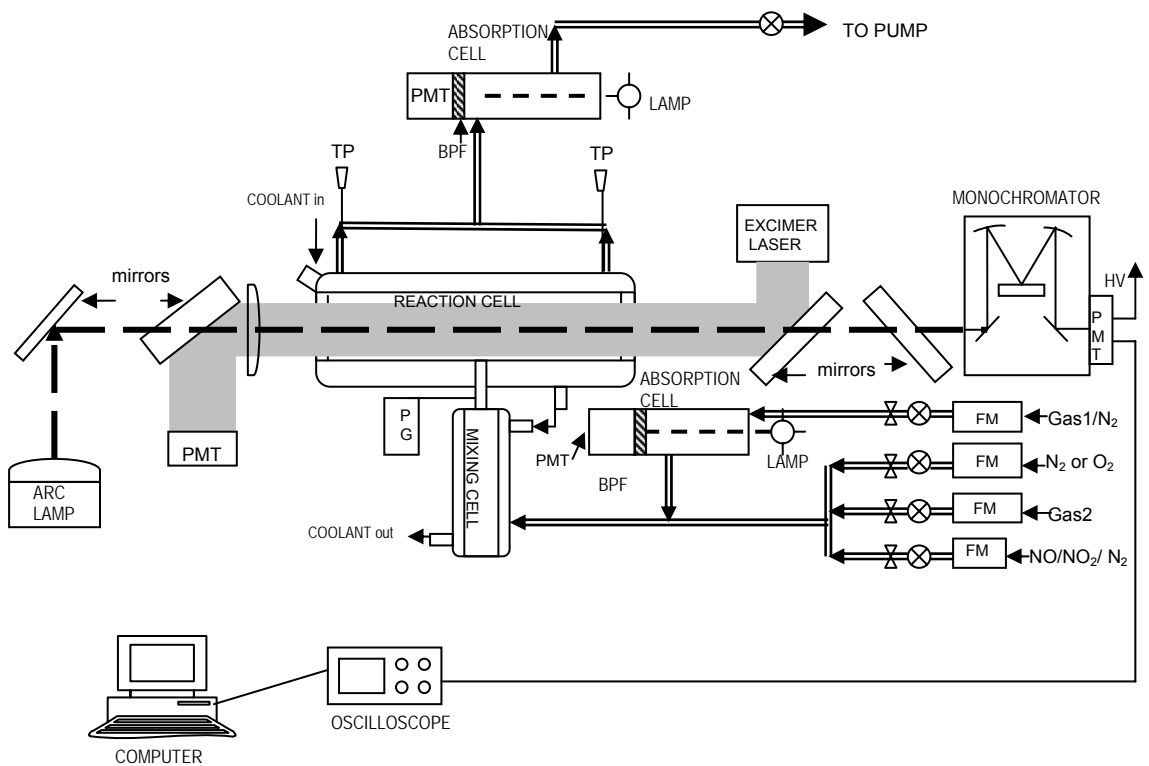


**Figure 2.1 Laser flash photolysis/UV-vis absorption spectroscopy apparatus:** PMT = photomultiplier tube, BPF = band pass filter, PM = power meter, PG = pressure gauge, FM = flow meter, TP = temperature probe.

Table 2.1 provides a list of S values for gases. These gas flows were then mixed into the buffer gas flow. Capacitance manometers were used to measure the pressures inside the reaction and photometry cells over the range of experimental conditions employed. Pressure drops between reaction cell and photometry cells were thus determined and photometrically derived concentrations were corrected accordingly. After passing through the reaction cell and photometry cells, the gas flow was exhausted through a throttle valve. The flow of gas through the reaction system was achieved using a mechanical pump. Downstream from the throttle valve, but prior to entering the mechanical pump, the gas mixture was passed through a liquid nitrogen cold trap to remove toxic and corrosive gases, and also prevent backstreaming of pump oil into the reaction and photometry cells.

### **Concentrations of Reagent Gases**

The buffer gases ( $N_2$ ,  $O_2$ ) were introduced into the reaction cell directly from their high pressure storage cylinders. The concentrations of these gases in the reaction mixture were evaluated based on gas flow rates measured using calibrated mass flow meters in conjunction with measurements of temperature and pressure in the reaction cell. The gases  $Cl_2$ ,  $NO$  and  $Cl_2CO$  were diluted with  $N_2$  and stored in 12 L Pyrex bulbs. Nitrogen dioxide ( $NO_2$ ) gas was made in our lab by diluting a  $NO/N_2$  bulb mixture with enough  $O_2$  to convert all  $NO$  to  $NO_2$ . The species  $CH_3I$ ,  $C_2H_5I$ , and  $CF_2Br_2$  are liquids at room temperature and pressure. These liquid reagents were transferred under  $N_2$  into vials fitted with high-vacuum stopcocks. After repeated degassing at 77 K, appropriate amounts were transferred into 12 L Pyrex bulbs and diluted with  $N_2$ . The mole fraction of a reagent gas in the storage bulb was determined by introducing a known pressure of the bulb mixture into a vacuum-sealed cylindrical Pyrex cell arranged for photometric measurements.

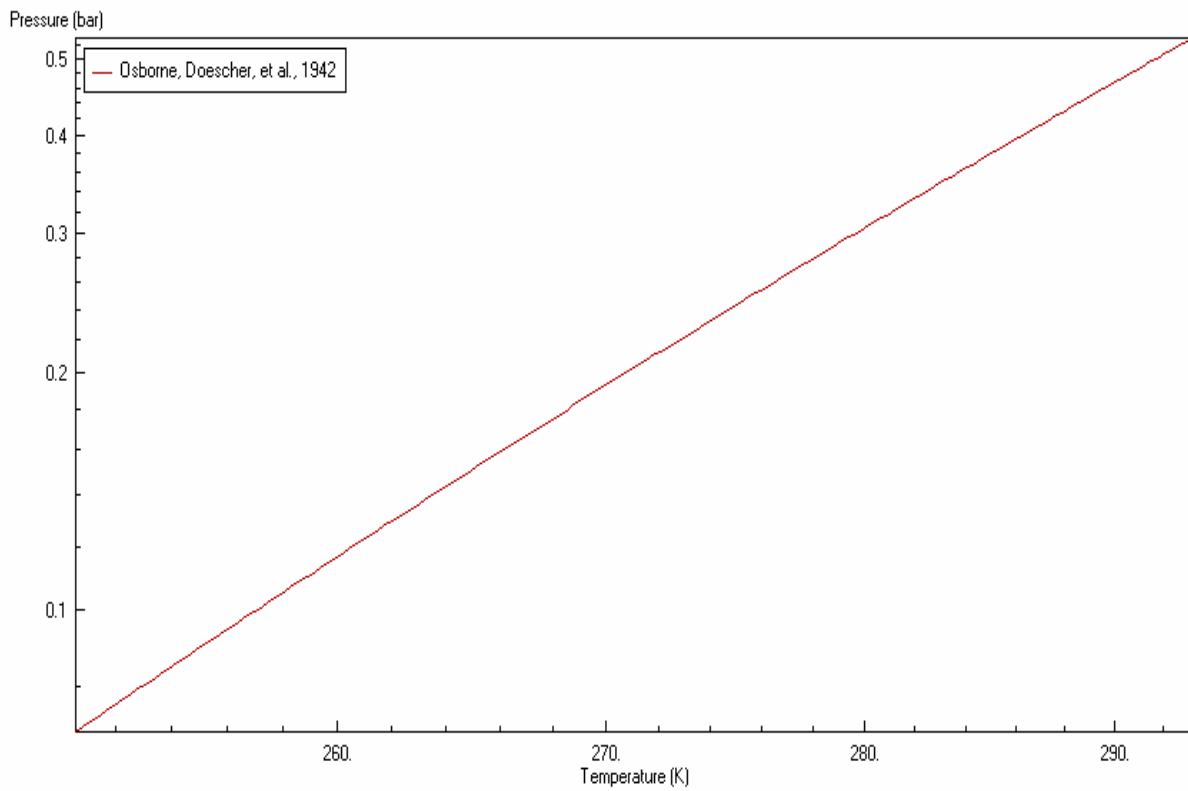


**Figure 2.2 Vapor pressure versus temperature plot for liquid dimethyl sulfide**

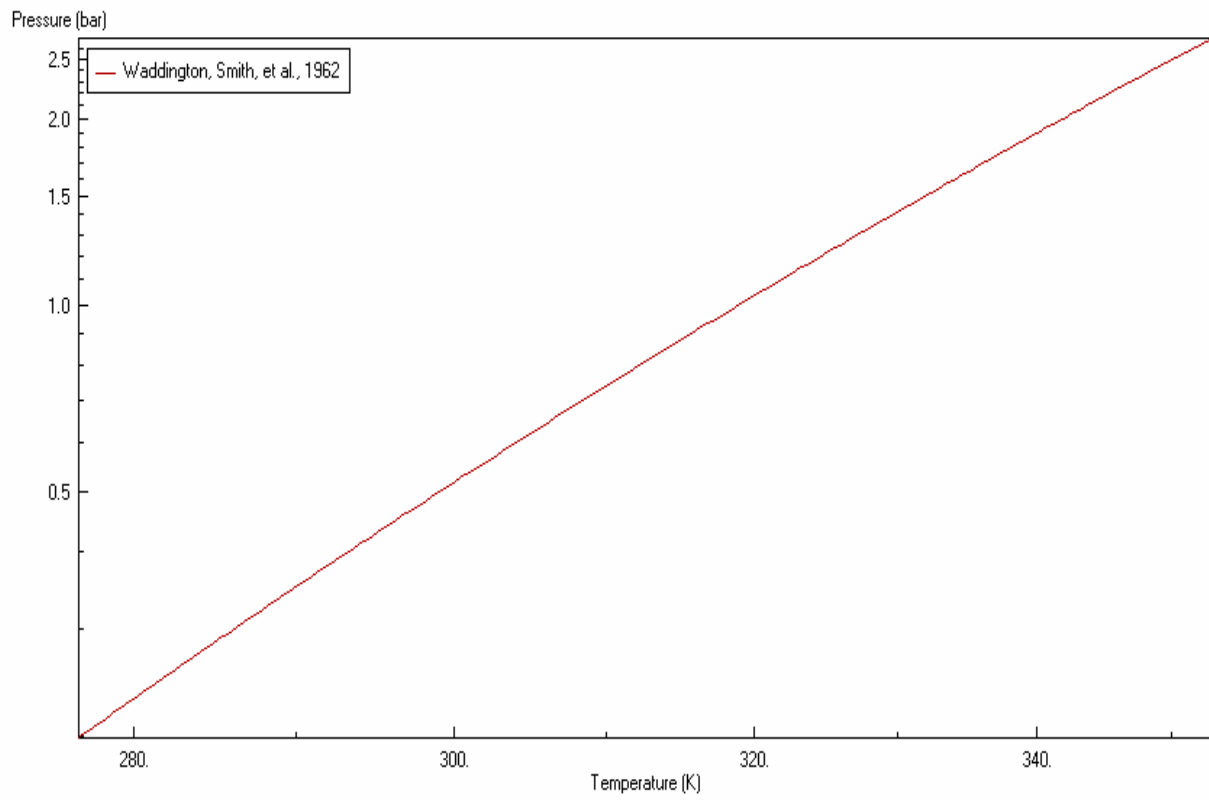


**Figure 2.3** Vapor pressure versus temperature plot for liquid carbon disulfide

**Table 2.1 Table of Molecular Structure Correction Factors (MKS manual)**

<b>Molecular Structure</b>	<b>S</b>
Monatomic Gases	1.030
Diatomic Gases	1.000
Triatomic Gases	0.941
Polyatomic Gases	0.880

The photometric measurements were taken using a side-on PMT with an interference bandpass filter mounted in front of the PMT, a photocathode as a detector, and a pen ray lamp as the light source. The PMT current output was monitored using a digital picoammeter (Keithley). The pen ray lamp and interference band pass filter were chosen based on the gas being measured. The monitoring wavelengths and cross sections used to measure the gases in this study are summarized in Table 2.2. The mole fraction of the absorbing gas was determined by recording the light intensity as a function of gas mixture pressure and applying Beer's Law:

$$(Eq. 2.2) \quad A(\lambda) = \sigma(\lambda)c l$$

$$(Eq. 2.3) \quad A_I = I_0/I_I$$

In the above equations, A is the absorbance of the gas species at wavelength  $\lambda$ ,  $\sigma$  is absorption cross section of the absorbing gas at wavelength  $\lambda$ , c is the concentration of absorbing gas measured by photometry,  $l$  is the path length of the photometry cell,  $I_0$  is the measured current in the absence of absorbing gas,  $I_I$  is measured current of absorbing gas pressure  $P_1$ . The ideal gas law is employed to convert gas pressure to molecular concentration and the bulb mole fraction is then calculated.

**Table 2.2 Summary of absorption cross-sections for molecules used in this work**

Species	Wavelength (nm)	$\sigma$ ( $10^{-20}$ cm <sup>2</sup> molec <sup>-1</sup> )	References
Cl <sub>2</sub> CO	248	8.93	a
	213.9	12.60	b
CS <sub>2</sub>	213.9	360	c
NO <sub>2</sub>	366	60.5	d
Cl <sub>2</sub>	308	17.20	e
	326	24.8	e
CH <sub>3</sub> I	248	84	e
	254	116	e
	213.9	169	e
C <sub>2</sub> H <sub>5</sub> I	248	87	e
	254	128	e
DMS	248	1.28	f
	228.8	116	g
	213.9	170	f
CF <sub>2</sub> Br <sub>2</sub>	248	72	e
	228.8	245	e
IO	427.2	1800	h,i

a. Zhao et al., 1996

b. Urbanski and Wine, 1999

c. Xu and Joens, 1993

d. Estupinan et al., 2001

e. Sander et al., 2006

f. Hearn et al., 1990

g. Wine et al., 1981

h. Daykin and Wine, 1990

i. spectral resolution is 0.74 nm

*In situ* concentration of reagent gases were measured using an appropriate length photometry cell, pen ray lamp, and PMT with an interference band pass filter appropriate for specific absorbing gas (see e.g. Figure 2.1). The PMT current output was monitored using a digital picoammeter (Keithley) and the concentration of the reagent gas in the reaction cell was determined from the following equation:

$$(Eq. 2.4) \quad [Y]_{abs} = P T_p / P_p T \ln\{ I_o / I \}$$

Where  $[Y]_{abs}$  is the concentration of reagent gas Y in the reaction cell (molecules  $\text{cm}^{-3}$ ), P and T ( $P_p$  and  $T_p$ ) are the pressure (Torr) and temperature (K) of the gas mixture in the reaction cell (photometry cell), I and  $I_o$  are the light intensity observed to pass through the photometry cell in the presence (I) and absence ( $I_o$ ) of absorber Y. The agreement between  $[Y]_{abs}$  and  $[Y]_{flow}$  was typically within 5%.

## Chemicals

The chemicals used in these experiments were either gases at room temperature and atmospheric pressure as supplied in high pressure gas cylinders or liquids at room temperature and atmospheric pressure and supplied in appropriate liquid storage vessels. The chemicals served in one or more of the following roles: buffer gas, photolytic precursor, or reagent gas. The stated minimum purities of the chemicals used in this work are tabulated in Table 2.3.

**Table 2.3 Minimum stated purity of chemicals used in this work.**

A. Gases

<b>Chemical</b>	<b>Minimum Purity (%)<sup>a</sup></b>	<b>Supplier</b>
O <sub>2</sub>	99.994	Air Products
N <sub>2</sub>	99.999	Air Products
Cl <sub>2</sub> CO	99.0	Matheson
NO <sub>2</sub>	99.5	Matheson
Cl <sub>2</sub>	99.0	Spectra Gases
NO	99.0	Spectra Gases

<sup>a</sup>Minimum purity as stated by the supplier

B. Liquids

<b>Chemical</b>	<b>Minimum Purity (%)<sup>a</sup></b>	<b>Supplier</b>
CS <sub>2</sub>	99.9	Aldrich
CH <sub>3</sub> I	99.9	Sigma-Aldrich
C <sub>2</sub> H <sub>5</sub> I	99.0	Sigma-Aldrich
DMS	99.0	Sigma-Aldrich
CH <sub>3</sub> OH	99.8	Sigma-Aldrich
CF <sub>2</sub> Br <sub>2</sub>	97	Sigma-Aldrich

<sup>a</sup>Minimum purity as stated by the supplier

**CHAPTER 3**  
**SPECTROSCOPIC AND KINETIC STUDY OF THE GAS PHASE**  
**CS<sub>2</sub>-Cl ADDUCT**

**Carbon Disulfide in the Atmosphere**

Carbon disulfide (CS<sub>2</sub>) is a trace constituent of both the troposphere and stratosphere (Sandalls et al., 1977; Maroulis and Bandy 1980; Bandy et al., 1981) and its importance stems from its role as precursor to OCS. Sulfur dioxide (SO<sub>2</sub>) produced from OCS oxidation may be oxidized to H<sub>2</sub>SO<sub>4</sub>, which can serve as cloud condensation nuclei (CCN) via condensation-evaporation equilibrium processes as it enters the tropopause-upper troposphere region, and contribute to the Junge layer. Carbonyl sulfide (OCS), due to its long atmospheric lifetime (Chin and Davis, 1993; Berresheim et al., 1995), can be transported to the stratosphere. It is thought that CS<sub>2</sub> oxidation accounts for 30% of the OCS budget (Chin and Davis, 1993). The products of oxidation and photolysis of stratospheric OCS are CO and atomic sulfur, the latter is thought to be an important source of the persistent sulfate aerosol layer in the lower stratosphere (Chin and Davis, 1993; Crutzen 1976; Junge et al., 1961; Hofmann, 1990), which in turn may significantly impact the Earth's radiation balance. Both OCS and SO<sub>2</sub> products of CS<sub>2</sub> oxidation, therefore, impact global climate and ecological balance (Sze and Ko, 1979).

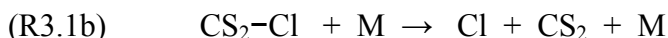
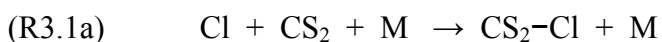
Natural sources of CS<sub>2</sub> are volcanic eruptions, ocean, marshes, and forests (Chin and Davis, 1993; Halmer et al., 2002) while anthropogenic CS<sub>2</sub> is mainly generated from industrial related processes such as viscose filaments, rayon, rubber production, cellulose film, solvents and pesticide manufacturing (Lin, 2001; Wang and Vanhoorne, 2000).

The well established atmospheric sinks for CS<sub>2</sub> are photolysis, reaction with OH (Chin and Davis, 1993) and soil uptake (Watts, 2000 and references therein).

Techniques used for measuring atmospheric CS<sub>2</sub> are long path differential optical absorption spectroscopy (Yu et al., 2004) and gas chromatography (GC) coupled with various forms of detection such as flame photometric detection (GC-FPD) (Maroulis and Bandy, 1980; Cooper and Saltzman, 1993; Sandalls and Penkett, 1977; Inomata et al., 1999), fluorination with electron capture detection (GC-F-ECD) (Johnson and Bates, 1993), electron capture sulfur detection (GC-ECD-S) (Weiss et al., 1995), and mass spectrometry (GC-MS) (Bandy et al., 1985).

### **The Reaction of Cl with CS<sub>2</sub>**

The gas phase reaction of atomic chlorine with CS<sub>2</sub> has been studied experimentally because of its potential importance in atmospheric chemistry. Martin et al., (1987), employing a competitive kinetics technique, found that in the presence of O<sub>2</sub> the apparent bimolecular rate coefficient for destruction of CS<sub>2</sub> by Cl is of order 10<sup>-13</sup> cm<sup>3</sup> molecule<sup>-1</sup> s<sup>-1</sup> and, in 1 atm N<sub>2</sub> + O<sub>2</sub> at 293 K, increases by nearly a factor of three as the O<sub>2</sub> partial pressure increases from 50 to 760 Torr. Martin et al. interpreted their results in terms of a mechanism that is analogous to the generally accepted mechanism for the OH + CS<sub>2</sub> reaction, i.e., formation of a weakly-bound CS<sub>2</sub>-Cl adduct that reacts with O<sub>2</sub> in competition with decomposition back to reactants:





Nicovich et al., (1990a) employed the laser flash photolysis – resonance fluorescence (LFP-RF) technique to directly confirm the occurrence of reactions (R3.1a) and (R3.1b). Rate coefficients for reactions (R3.1a) and (R3.1b) were determined as a function of temperature and pressure over the ranges 193-258 K and 30-600 Torr N<sub>2</sub>. From the temperature dependence of  $k_{3.1a}/k_{3.1b}$ , Nicovich et al. were able to deduce a 0 K adduct bond dissociation energy of  $40 \pm 3$  kJ mol<sup>-1</sup>, in reasonable agreement with the recently reported theoretical SCS–Cl bond dissociation energy of 33 kJ mol<sup>-1</sup> (Wang and Phillips, 2002). Based on observation of the dependence of observed Cl temporal profiles on [O<sub>2</sub>], Nicovich et al. concluded that  $k_{3.2} < 2 \times 10^{-15}$  cm<sup>3</sup> molecule<sup>-1</sup> s<sup>-1</sup> at T = 230 K and P = 30 Torr N<sub>2</sub> + O<sub>2</sub>. Wallington et al., (1991) studied the gas phase Cl + CS<sub>2</sub> reaction using an experimental approach similar to the one employed by Martin et al., (1987). These investigators concluded that the overall reaction was much slower than reported by Martin et al. ( $k < 4 \times 10^{-15}$  cm<sup>3</sup> molecule<sup>-1</sup> s<sup>-1</sup>) and suggested that the loss of CS<sub>2</sub> observed in the Martin et al. study was not the result of the Cl + CS<sub>2</sub> + O<sub>2</sub> reaction, but rather the result of the OH + CS<sub>2</sub> + O<sub>2</sub> reaction, with OH generated primarily by the secondary reaction of Cl with CH<sub>3</sub>OOH.

In this work we report the results of an experimental study of the gas phase Cl + CS<sub>2</sub> reaction that couples laser flash photolysis (LFP) with time-resolved UV-visible absorption spectroscopy (TRUVVAS). The gas phase absorption spectrum of the CS<sub>2</sub>–Cl adduct is reported for the first time, and the TRUVVAS technique is used as a probe to investigate the kinetics of CS<sub>2</sub>–Cl reactions with O<sub>2</sub>, NO, NO<sub>2</sub>, and CS<sub>2</sub>–Cl.

## Experimental Method

The LFP–TRUVVAS apparatus was employed in all studies of the CS<sub>2</sub>–Cl adduct and is discussed in detail in Chapter 2. Only aspects of the apparatus not discussed in Chapter 2 are covered in the current section.

Concentrations of both CS<sub>2</sub> and Cl<sub>2</sub>CO were measured *in situ* in the slow flow system by UV photometry as well as by mass flow measurements. The *in situ* photometry measurements were conducted using a Zn pen ray lamp, a 214 nm band-pass filter, and a side-on PMT. The cross-sections used to convert 214 nm absorbances to concentrations were  $3.6 \times 10^{-18} \text{ cm}^2 \text{ molecule}^{-1}$  (Xu and Joens, 1993) and  $1.26 \times 10^{-19} \text{ cm}^2 \text{ molecule}^{-1}$  (Urbanski and Wine, 1999) for CS<sub>2</sub> and Cl<sub>2</sub>CO, respectively. In the kinetics experiments, the concentrations of NO and NO<sub>2</sub> were determined from mass flow measurements.

Photolysis of Cl<sub>2</sub>CO at 248 nm results in the production of Cl atoms:



The photolysis of Cl<sub>2</sub>CO was used as the source of Cl, and concentration of Cl produced right after the laser flash was estimated using the following equation:

$$\text{(Eq. 3.1)} \quad [\text{Cl}] = \Phi \sigma F [\text{Cl}_2\text{CO}]$$

where  $\Phi = 2$  is the yield of Cl from Cl<sub>2</sub>CO photolysis .i.e., R3.3;  $\sigma = 8.93 \times 10^{-20} \text{ cm}^2 \text{ molecule}^{-1}$  (Zhao et al., 1996) is the absorption cross section of Cl<sub>2</sub>CO at 248 nm;  $F$  is the

laser fluence at the reaction cell, typically  $2.5 \times 10^{16}$  photons/cm<sup>2</sup>/pulse. Under the above experimental conditions, typical Cl concentrations produced right after the laser flash were  $(0.05 - 2) \times 10^{13}$  atoms cm<sup>-3</sup>.

## Results and Discussion

When Cl<sub>2</sub>CO was photolyzed in the presence of CS<sub>2</sub> and N<sub>2</sub> buffer gas, absorption of the UV-visible probe beam was observed throughout the 320 to 550 nm spectral region. Absorption of the UV-visible probe beam was observed only when both CS<sub>2</sub> and Cl<sub>2</sub>CO were simultaneously subjected to LFP. When the photolyzed mixture contained only Cl<sub>2</sub>CO, CS<sub>2</sub>, and N<sub>2</sub>, the observed absorbance (A) decayed slowly with time according to second order kinetics. Under the experimental conditions employed, the appearance of absorbance was very fast compared to the decay of absorbance. Hence, the peak absorbance for each experiment could be determined with good accuracy by plotting A<sup>-1</sup> versus time and extrapolating back to  $t = 0$  using a linear fit to the A<sup>-1</sup> versus time data.

### Adduct Identification

Evidence verifying the identity of the absorbing species was obtained by measuring its appearance rate. Absorbance temporal profiles were recorded and analyzed using a nonlinear least squares fit to the sum of an exponential rise and an exponential decay (Figure 3.1). In this set of experiments, absorbance disappearance resulted primarily from radical-radical reactions and was not a first-order process. The first-order absorbance disappearance rate,  $k_d$ , is thus a parameterized rate coefficient rather than the

sum of actual loss processes which are quantitatively attributable to specific first order processes. However, because the observed absorbance loss rates are slow compared to the rapid rate of absorbance appearance, the parameterization of the absorbance disappearance as a first order process does not seriously impact the reliability of the analysis to determine the pseudo-first order rate coefficient for absorbance appearance. As shown by the example in Figure 3.1, the quality of the double exponential fits is quite good. Pseudo-first-order appearance rate coefficients ( $k_a$ ) were measured at 365 nm in  $N_2$  buffer gas. As shown in Figure 3.2, a plot of  $k_a$  vs.  $[CS_2]$  is linear over the range of  $CS_2$  concentrations employed. The linearity of the  $k_a$  vs.  $[CS_2]$  plot up to the fastest appearance rate measured (ca.  $300\,000\ s^{-1}$ ) demonstrates that the rate-limiting step in production of the absorbing species is the  $Cl + CS_2$  reaction under the conditions investigated. The slope of the  $k_a$  vs.  $[CS_2]$  plot yields the second order rate coefficient  $k_{3.1} = (5.2 \pm 0.8) \times 10^{-12}\ cm^3\ molecule^{-1}\ s^{-1}$  at 240 K and 100 Torr total pressure, where the uncertainty is  $2\sigma$  and represents precision only. The value measured here for  $k_1(P,T)$  is in good agreement with the value  $(4.8 \pm 0.3) \times 10^{-12}\ cm^3\ molecule^{-1}\ s^{-1}$  reported by Nicovich et al. (1990) based on measurements of Cl atom decay using atomic resonance fluorescence spectroscopy as the detection technique. This represents strong evidence that the species being observed is indeed the  $CS_2$ -Cl adduct formed from the reaction of Cl with  $CS_2$ .

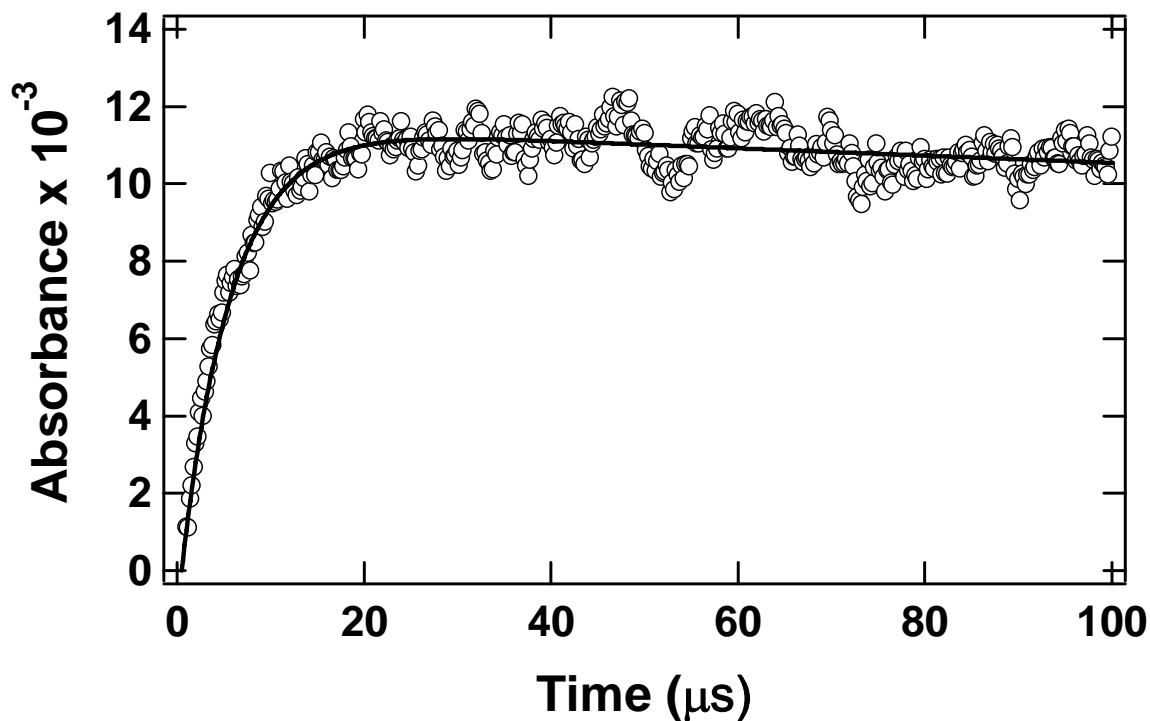


**Figure 3.1 Typical absorbance temporal profile observed following laser flash photolysis of  $\text{Cl}_2\text{CO}/\text{CS}_2/\text{N}_2$  mixtures.** Experimental conditions:  $T = 240 \text{ K}$ ;  $P = 100 \text{ Torr}$ ; Concentrations in units of  $10^{13} \text{ molecules cm}^{-3}$  are  $[\text{CS}_2] = 1870$ ,  $[\text{Cl}_2\text{CO}] = 900$ , and  $[\text{Cl}]_0 \approx 0.5$ . The solid line is obtained from a nonlinear least squares fit of the data to the sum of an exponential rise and an exponential decay. Best fit appearance ( $k_a$ ) and disappearance ( $k_d$ ) rate coefficients in units of  $\text{s}^{-1}$  are  $k_a = 1.30 \times 10^5$  and  $k_d = 804$ .

The liquid phase Cl + CS<sub>2</sub> rate coefficient of  $1.7 \times 10^{10} \text{ M}^{-1} \text{ s}^{-1}$  reported by Chateaufneuf (1993) is very near the diffusion-controlled limit, while the rate coefficient obtained in this work is about a factor of 50 below the gas kinetic limit. Although solvent effects undoubtedly play some role in the liquid phase kinetics, the most important factor accounting for the difference in observed rate coefficients is probably that liquid-phase conditions are equivalent to the gas-phase high pressure limit, which is not approached at pressures where gas-phase kinetic data for reactions (R3.1) are available. In fact, the pressure dependence results reported by Nicovich et al. (1990a) suggest that  $k_{3,1}(P,T)$  is much closer to the low pressure limit than it is to the high pressure limit at  $T = 240 \text{ K}$  and  $P = 100 \text{ Torr N}_2$ .

#### Adduct absorption spectrum

The absorption spectrum of the CS<sub>2</sub>-Cl adduct was measured at 100 Torr total pressure (N<sub>2</sub> buffer) and 240 K. A reference wavelength of 365 nm was selected. Absorption measurements were made at this reference wavelength after every 5 measurements at other wavelengths. This was done in order to account for systematic drifts in experimental parameters such as laser power, [Cl<sub>2</sub>CO], optical alignment, etc. over time. Absorbance measurements at wavelengths other than 365 nm were normalized to the average of the “before” and “after” 365 nm absorbances. The adduct absorption cross section was carefully measured at 365 nm and all cross-sections were then determined by applying the normalization factor to the carefully measured reference cross-section.

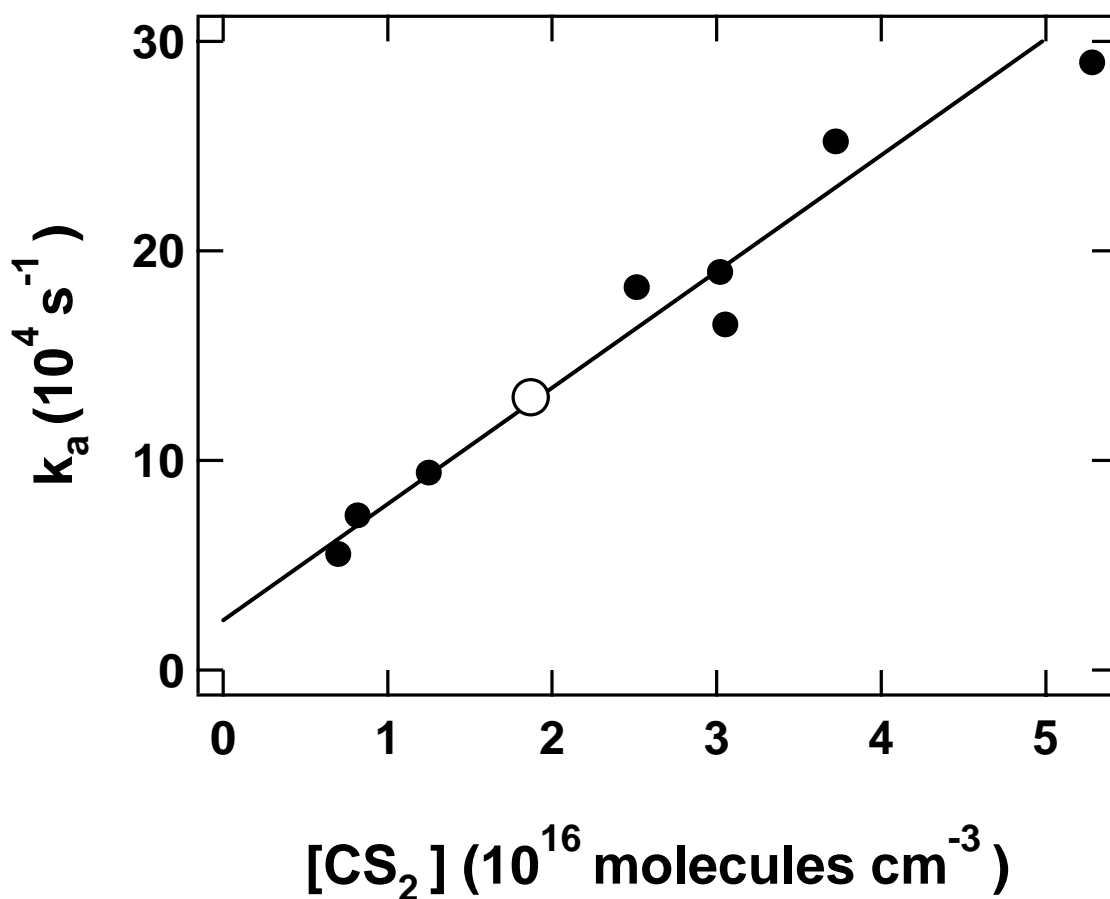


**Figure 3.2** Plot of  $k_a$  versus  $[\text{CS}_2]$  for data obtained at  $T = 240 \text{ K}$  and  $P = 100 \text{ Torr N}_2$ . The solid line is obtained from a linear least squares analysis; its slope gives the second order rate coefficient  $(5.20 \pm 0.84) \times 10^{-12} \text{ cm}^3 \text{ molecule}^{-1} \text{ s}^{-1}$ . The open data point is the one obtained from the data shown in Figure 3.1.

Reagent concentrations employed in the 365 nm cross-section measurements at 240 K were (in units of  $10^{13}$  molecules  $\text{cm}^{-3}$ ):  $[\text{CS}_2] \approx 7000$ ;  $[\text{Cl}_2\text{CO}] = 5\text{-}200$ ;  $[\text{Cl}]_0 = 0.05\text{-}2$ . Values for  $A_0$  (defined below) were obtained by extrapolation of  $A^{-1}$  versus time ( $t$ ) data to  $t = 0$ . High  $\text{CS}_2$  concentrations were employed in order to obtain  $\sim 95\%$  conversion of Cl to  $\text{CS}_2\text{-Cl}$  at equilibrium (based on the equilibrium constants reported by Nicovich et al., 1990a). Each cross section measurement involved averaging  $\sim 50$  photolysis laser pulses. To verify reproducibility, multiple absolute cross section measurements at 365 nm and relative cross section measurements at other wavelengths were made over a period of several days. The adduct cross section at 365 nm ( $\sigma_{365}$ ) was determined from the data using the following relationship:

$$\text{(Eq. 3.2)} \quad \sigma_{365} = A_0 / (l [\text{Cl}]_0 F)$$

In Eq. 3.2,  $A_0$  is the absorbance at a time shortly after the laser flash when Cl and adduct have reached equilibrium but negligible radical decay has occurred,  $l$  is the absorption path length (100 cm),  $[\text{Cl}]_0$  is the concentration of chlorine atoms produced by the laser flash, and  $F$  is the fraction of Cl atoms converted to adduct (taken to be the adduct equilibrium fraction). As typical for gas-phase spectroscopic data, the absorbance is defined as  $A = \ln(I_0/I)$ , that is, it is a base e value. Cross-sections obtained from Eq. 3.2 were found to be independent of  $[\text{Cl}]_0$  over the range specified above, i.e., Beer's law was obeyed. Evaluation of  $[\text{Cl}]_0$  required (i) careful measurements of  $[\text{Cl}_2\text{CO}]$  and laser power, (ii) assumption of a quantum yield of 2.0 for production of Cl from 248 nm photolysis of  $\text{Cl}_2\text{CO}$ , and (iii) careful measurements of the photolysis laser beam cross-sectional area and its divergence down the length of the cell.

Maul et al., (1995) have studied the photo-dissociation dynamics of  $\text{Cl}_2\text{CO}$  using 235 nm pulsed laser excitation and resonance enhanced multiphoton ionization (REMPI)-time of flight mass spectrometry (TOFMS) detection. Based on the analysis of kinetic energy release in the photolysis products, Maul et al., (1995) conclude that photo-dissociation of  $\text{Cl}_2\text{CO}$  occurs by concerted release of the three photofragments  $\text{Cl} + \text{Cl} + \text{CO}$ . Temperature- and pressure-dependent rate coefficients for  $\text{ClCO}$  unimolecular dissociation are reported in literature (Nicovich et al., 1990a). Based on these rate coefficients, we expect to see evidence for slow Cl atom production after the photoflash in studies of low temperature chlorine atom kinetics carried out in our laboratory that employed 266 nm photolysis of  $\text{Cl}_2\text{CO}$  as the Cl source (Nicovich et al., 1995; Piety et al., 1998) if thermalized  $\text{ClCO}$  was produced as a photolysis product. Observed Cl atom temporal profiles following laser flash photolysis of  $\text{Cl}_2\text{CO}/\text{N}_2$  mixtures showed no evidence for Cl atom production by post-flash chemistry. As mentioned above, transient absorption was observed only when both  $\text{Cl}_2\text{CO}$  and  $\text{CS}_2$  were present in the reaction mixture. Hence, if  $\text{ClCO}$  was produced, it was not detected as an interfering absorber in this study.

The adduct spectrum measured in this study at  $T = 240$  K and  $P = 100$  Torr  $\text{N}_2$  is shown in Figure 3.3, and is given in digitized form in Table 3.1. The  $\text{CS}_2$ -Cl absorption spectrum was also measured at 298 K, and was found to be identical to the spectrum obtained at 240 K within the precision and accuracy of the measurements. The similarity between the gas phase absorption spectrum reported in this study and the published liquid

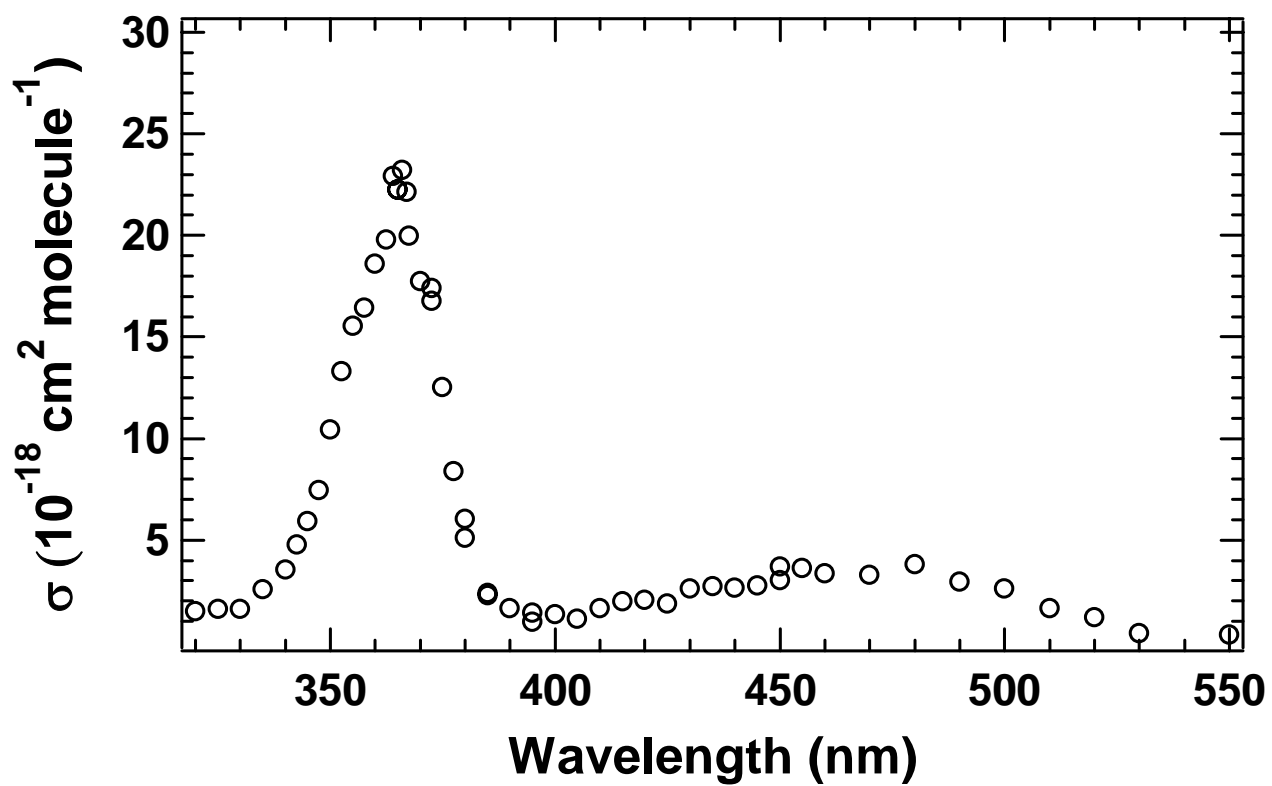
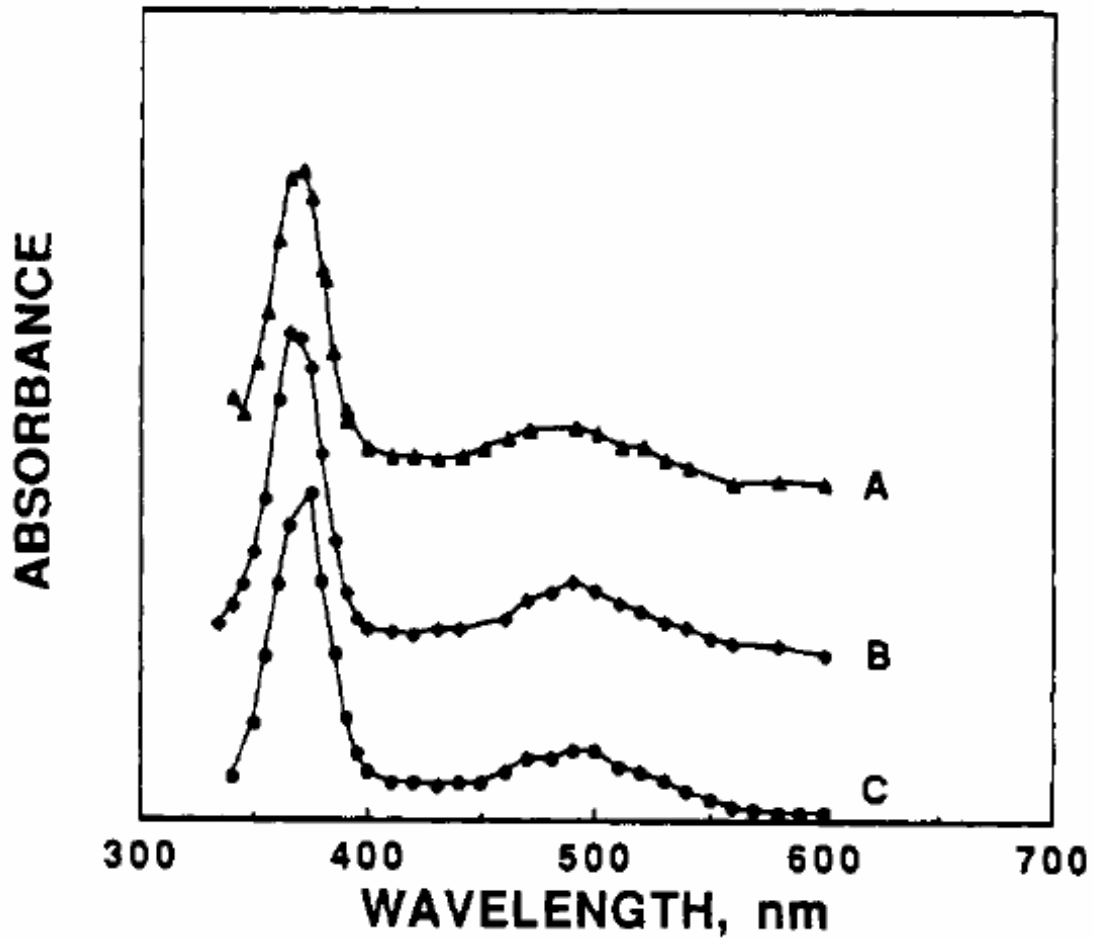


Figure 3.3 Absorption spectrum of the gas phase  $\text{CS}_2\text{-Cl}$  adduct

**Table 3.1 Absorption cross sections for the CS<sub>2</sub>-Cl adduct as a function of wavelength at a spectral resolution of 5.5 nm (fwhm).**

wavelength (nm)	cross section (10 <sup>-18</sup> cm <sup>2</sup> molec <sup>-1</sup> )	wavelength (nm)	cross section (10 <sup>-18</sup> cm <sup>2</sup> molec <sup>-1</sup> )	wavelength (nm)	cross section (10 <sup>-18</sup> cm <sup>2</sup> molec <sup>-1</sup> )
310	1.53	375	13.1	440	2.77
315	4.09	380	6.29	445	2.86
320	1.56	385	2.35	450	3.13
325	1.67	390	1.72	455	3.76
330	1.66	395	1.47	460	3.49
335	2.68	400	1.41	470	3.42
340	3.68	405	1.18	480	3.94
345	6.17	410	1.70	490	3.07
350	10.9	415	2.07	500	2.73
355	16.2	420	2.12	510	1.71
360	19.4	425	1.95	520	1.26
365	23.2	430	2.73	530	0.44
370	18.5	435	2.83	550	0.33
				600	0.19



**Figure 3.4** Liquid phase spectra of  $\text{CS}_2\text{-Cl}$  observed following: (A)  $\text{Cl}_2$  LFP in  $\text{CCl}_4$ ; (B) 266 nm  $\text{CCl}_4$  LFP; and (C) pulse radiolysis of  $\text{CCl}_4$ , each containing 0.25 M  $\text{CS}_2$ . (Chateaufneuf, 1993).

phase spectrum (Chateaufeuf, 1993) shown in Figure 3.4 lends further support to our conclusion that the species observed in this study is in fact the CS<sub>2</sub>-Cl adduct; the liquid phase spectra shown in Figure 3.4 were obtained in the non-polar solvent CCl<sub>4</sub>. Consideration of uncertainties in the parameters that must be known to obtain the adduct cross section (see above), leads to an estimate of ±30% for the accuracy of the measured cross section at 365 nm (95% confidence level). We report this cross-section to be  $\sigma_{365} \approx \sigma_{\max} = (2.3 \pm 0.7) \times 10^{-17} \text{ cm}^2 \text{ molecule}^{-1}$ .

Comparison of observed vibrational frequencies with those obtained from electronic structure calculations (Wang et al., 2002; Wang and Phillips, 2002) suggest that the complex formed by addition of Cl to CS<sub>2</sub> is SCS-Cl, not S<sub>2</sub>C-Cl as had been suggested by earlier theoretical studies (Marshall, 1991; McKee, 1993; Wilson and Hirst, 1997). Similar conclusions have been reached concerning the structure of CS<sub>2</sub>-OH, which has been studied extensively in the gas phase because of its importance in atmospheric chemistry (Jones et al., 1982; Jones et al., 1983; Barnes et al., 1983; Hynes et al., 1988; Bulatov et al., 1988; Lovejoy et al., 1990; Murrells et al., 1990; Lunell et al., 1990; Becker et al., 1990; Diau and Lee, 1991; McKee, 1993; Stickel et al., 1993; Lovejoy et al., 1994; Zhang and Qin, 2000; McKee and Wine, 2001). Wang and Phillips (2002) reported that (i) formation of SCS-Cl is essentially a barrierless process whereas formation of S<sub>2</sub>C-Cl has a barrier of 74 kJ mol<sup>-1</sup>; (ii) the 0 K bond dissociation energies for SCS-Cl and S<sub>2</sub>C-Cl are 33 kJ mol<sup>-1</sup> and 28 kJ mol<sup>-1</sup>, respectively; (iii) the barrier for isomerization of SCS-Cl to S<sub>2</sub>C-Cl is 55 kJ mol<sup>-1</sup>; and (iv) the isomerization barrier is

reduced to 11 kJ mol<sup>-1</sup> in the presence of Cl atoms via formation of a low-energy transition state with Cl atoms weakly attached to both the carbon atom and one of the sulfur atoms. Figure 3.5 shows a schematic of the most probable structures for the CS<sub>2</sub>-Cl adduct. An important question that remains to be answered concerns the origin of the weak band observed at longer wavelength. Does this band result from promotion of ground state SCS-Cl to a lower energy excited electronic state or is it an absorption band of the S<sub>2</sub>C-Cl isomer? Further experimental and theoretical research appears to be needed to answer this question. We have employed the theoretical energetics, structures, and vibrational frequencies reported by Phillips and coworkers (Wang et al., 2002; Wang and Phillips, 2002) to evaluate the equilibrium constant for SCS-Cl ↔ S<sub>2</sub>C-Cl. It appears that even if the initially generated SCS-Cl equilibrates rapidly with S<sub>2</sub>C-Cl, only a few percent of the adduct molecules would exist as S<sub>2</sub>C-Cl at the temperatures employed in our study. Hence, if the theoretical information is accurate, and if the weak long-wavelength band originates from S<sub>2</sub>C-Cl, the peak absorption cross-section for this band, defined as  $\sigma(480 \text{ nm}) \approx \sigma_{\text{peak}} = A_0(I[\text{S}_2\text{C-Cl}])^{-1}$  must be extremely large, i.e., approaching 10<sup>-16</sup> cm<sup>2</sup> molecule<sup>-1</sup>.

### Adduct Kinetics

The kinetics of the CS<sub>2</sub>-Cl adduct have been investigated in an attempt to determine the fate of the adduct under atmospheric conditions. In the atmosphere, O<sub>2</sub> is the most abundant reactive species and is the most likely candidate for reactive adduct removal.

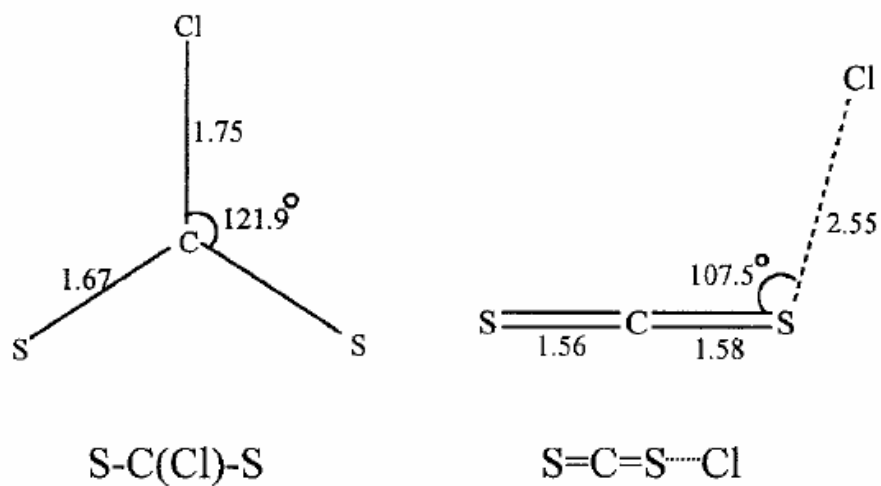
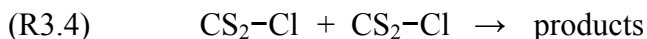


**Figure 3.5** Simple schematic for the optimized geometry computed for the two most probable CS<sub>2</sub>-Cl structures (S-C(Cl)-S and S=C=S $\cdots$ Cl) computed from UB3LYP/cc-PVDZ density functional theory calculations (Wang et al., 2002). Bond lengths given in Å units.

If the adduct is unreactive towards O<sub>2</sub>, other atmospheric species with which it may react include NO and NO<sub>2</sub>. The kinetics of the adduct reactions with O<sub>2</sub>, NO, and NO<sub>2</sub> have, therefore, been investigated as part of this study.

### Radical–Radical Reaction Kinetics

When reaction mixtures containing only Cl<sub>2</sub>CO, CS<sub>2</sub>, and N<sub>2</sub> are subjected to 248 nm laser flash photolysis and detectable levels of CS<sub>2</sub>–Cl are generated, we expect that CS<sub>2</sub>–Cl loss will be dominated by the following radical-radical reactions:



In the limit of very high [CS<sub>2</sub>], the ratio [CS<sub>2</sub>–Cl]/[Cl] becomes large and reaction (R3.4) is expected to dominate adduct removal. As the CS<sub>2</sub> concentration is reduced, reaction (R3.5) is expected to become an important adduct loss pathway.

To experimentally determine  $k_{3,4}$  at  $T = 240$  K and  $P = 100$  Torr, experiments were carried out using [CS<sub>2</sub>]  $\sim 1 \times 10^{17}$  molecules cm<sup>-3</sup>; at this temperature and [CS<sub>2</sub>], the ratio [CS<sub>2</sub>–Cl]/[Cl] is approximately 24 (Nicovich et al., 1990). The concentrations of Cl<sub>2</sub>CO employed in these experiments were in the range (1.5-26)  $\times 10^{15}$  molecules cm<sup>-3</sup>, and values for [Cl]<sub>0</sub> were in the range (6-90)  $\times 10^{12}$  atoms cm<sup>-3</sup>. A typical absorbance temporal profile, plotted as [CS<sub>2</sub>–Cl]<sup>-1</sup> versus time, is shown in Figure 3.5. The linearity

of  $[\text{CS}_2\text{-Cl}]^{-1}$  versus time plot is consistent with the hypothesis that adduct loss is dominated by reaction (R3.4), and the self-reaction rate coefficient  $2k_{3.4}$ , is obtained from the slope of the plot. The average of 17 experiments like the one depicted in Figure 3.5 gives  $2k_{3.4} = (1.5 \pm 0.3) \times 10^{-10} \text{ cm}^3 \text{ molecule}^{-1} \text{ s}^{-1}$ , where the uncertainty is  $2\sigma$  and represents precision only. The accuracy of the derived value for  $2k_{3.4}$  is limited by the accuracy of  $[\text{CS}_2\text{-Cl}]$ , which in turn is limited by the accuracy of the  $\text{CS}_2\text{-Cl}$  absorption cross section at the monitoring wavelength (365 nm), i.e.,  $\pm 30\%$  (see above). Taking the  $\text{CS}_2\text{-Cl}$  absorption cross section and imprecision to be the two main sources of uncertainty, we report  $2k_{3.4} = (1.5 \pm 0.6) \times 10^{-10} \text{ cm}^3 \text{ molecule}^{-1} \text{ s}^{-1}$ , where the uncertainty represents accuracy at the 95% confidence level.

In order to obtain information about  $k_{3.5}$ , it is necessary to employ experimental conditions where absorption signals are very low. Hence, it has not proven possible to obtain a quantitative value for  $k_{3.5}$ . Examination of the dependence of the  $\text{CS}_2\text{-Cl}$  disappearance rate on  $[\text{CS}_2]$  while keeping  $[\text{Cl}]_0$  approximately constant does, however, suggest that  $k_{3.5} > k_{3.4}$ .

### Kinetics of the $\text{CS}_2\text{-Cl} + \text{O}_2$ Reaction

To investigate the kinetics of the reaction of  $\text{CS}_2\text{-Cl}$  with  $\text{O}_2$ ,



$\text{CS}_2\text{-Cl}$  absorbance temporal profiles were measured in 200 Torr of  $\text{O}_2$  with experimental conditions adjusted to relatively high  $[\text{CS}_2]$  and low  $[\text{Cl}]_0$  in order to minimize the

contribution of radical-radical reactions to CS<sub>2</sub>-Cl removal. Temporal profiles observed in 200 Torr O<sub>2</sub> were indistinguishable from those observed in N<sub>2</sub> bath gas; a plot of

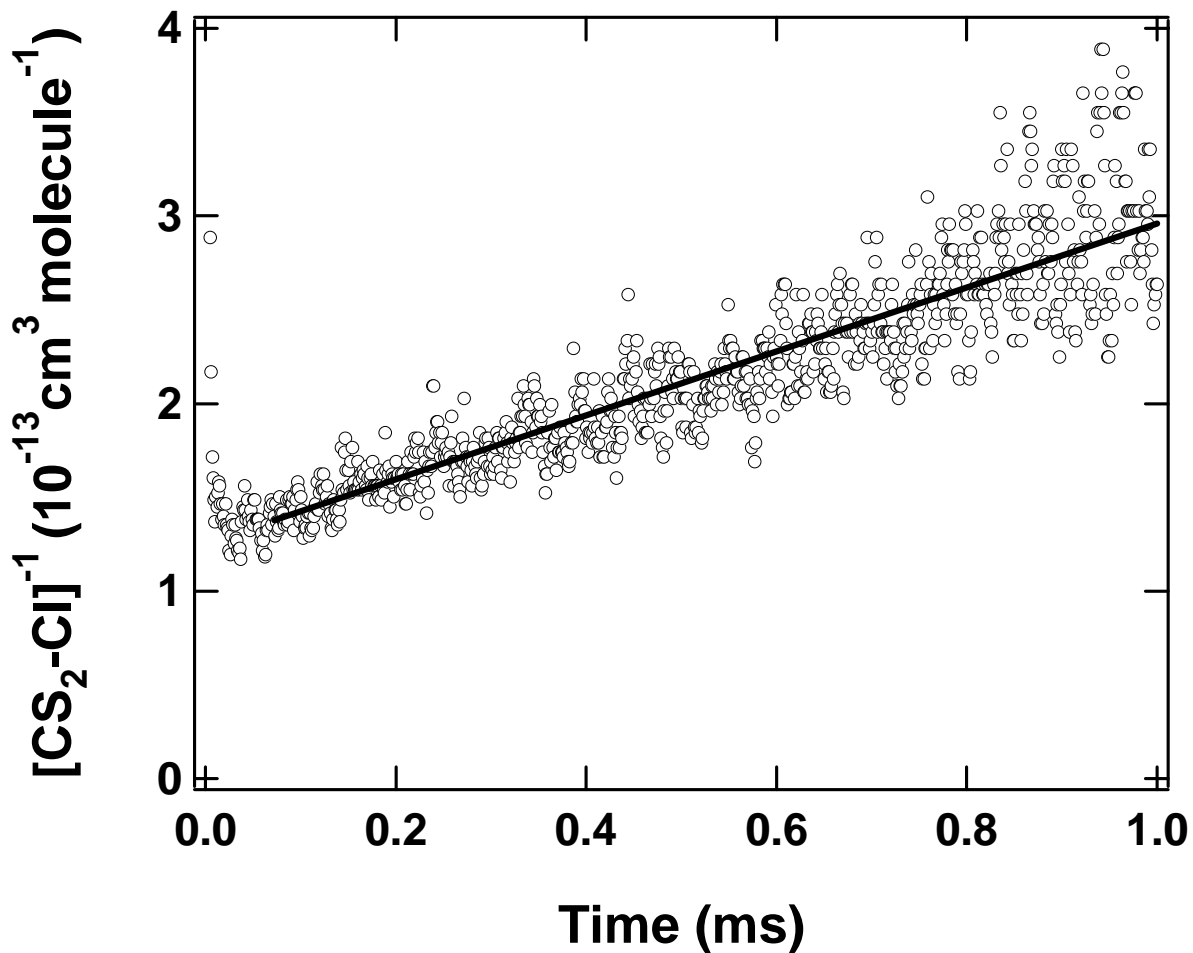


**Figure 3.6 CS<sub>2</sub>-Cl absorbance temporal profile plotted as  $[\text{CS}_2\text{-Cl}]^{-1}$  vs. time.** Experimental conditions:  $T = 240$  K;  $P = 100$  Torr N<sub>2</sub>;  $[\text{CS}_2] = 1.0 \times 10^{17}$  molecules cm<sup>-3</sup>. The solid line is obtained from a linear least squares analysis; its slope gives  $2k_{3,4} = (1.70 \pm 0.04) \times 10^{-10}$  cm<sup>3</sup> molecule<sup>-1</sup> s<sup>-1</sup> where the uncertainty is  $2\sigma$  and represents precision only.

$[\text{CS}_2\text{-Cl}]^{-1}$  versus time for a typical experiment is shown in Figure 3.6. The data are well described by a straight line, and the second-order rate coefficient obtained from the slope is equal within experimental uncertainty to the value of  $2k_{3,4}$  obtained from the data with  $\text{N}_2$  as the bath gas (see above).

We conclude that our data show no evidence for a reaction between  $\text{CS}_2\text{-Cl}$  and  $\text{O}_2$ . In order to put a reasonable upper limit on  $k_{3,2}$ , kinetic simulations were carried out for a simple two-reaction scheme, i.e., reactions (R3.2) and (R3.4), with  $2k_{3,4}$  fixed at the value obtained from the slope of  $[\text{CS}_2\text{-Cl}]^{-1}$  in  $\text{N}_2$  versus time plot and  $k_{3,2}$  varied. Shown in Figure 3.7 are plots of simulated temporal profiles for  $k_{3,2} = 0.5, 1.0,$  and  $2.0 \times 10^{-17} \text{ cm}^3 \text{ molecule}^{-1} \text{ s}^{-1}$ . We conclude that upward curvature in  $[\text{CS}_2\text{-Cl}]^{-1}$  versus time plot would have been observed if  $k_{3,2} > 5.0 \times 10^{-18} \text{ cm}^3 \text{ molecule}^{-1} \text{ s}^{-1}$ , and we adopt this value as the upper limit for  $k_{3,2}$  that is consistent with our data.

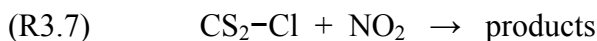
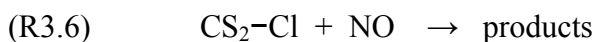
As discussed previously, little or no ClCO is thought to be generated from 248 nm photolysis of  $\text{Cl}_2\text{CO}$ . In the presence of 200 Torr  $\text{O}_2$  at 240 K, any thermalized ClCO that was produced would rapidly react with  $\text{O}_2$  to generate ClC(O)OO (Hewitt et al., 1996). The UV absorption spectrum of ClC(O)OO has recently been observed in cryogenic matrices (Pernice et al., 2004); this species absorbs only very weakly to the red of 300 nm and would not interfere with the detection of  $\text{CS}_2\text{-Cl}$  in this study even if it was generated with significant yield. In back-to-back experiments where we interchange  $\text{N}_2$  and  $\text{O}_2$  as the bath gas but experimental conditions otherwise remain constant, the observed peak transient absorbance remains unchanged within experimental uncertainty.

This observation is consistent with other evidence that supports prompt production of Cl with a quantum yield of 2.0 from Cl<sub>2</sub>CO photolysis.

Nicovich et al. (1990a) studied the effect of added O<sub>2</sub> on Cl + CS<sub>2</sub> ↔ CS<sub>2</sub>-Cl equilibrium kinetics and concluded that  $k_{3,2} < 2 \times 10^{-15} \text{ cm}^3 \text{ molecule}^{-1} \text{ s}^{-1}$  at  $T = 230 \text{ K}$  and  $P = 30 \text{ Torr O}_2$ . Wallington et al. (1991) used their measured upper limit “effective” rate coefficient of  $4 \times 10^{-15} \text{ cm}^3 \text{ molecule}^{-1} \text{ s}^{-1}$  for CS<sub>2</sub> reaction with Cl at 298 K in 700 Torr air in conjunction with values for  $k_{3,1a}$  and  $k_{3,1b}$  reported by Nicovich et al. (1990a) to deduce the upper limit rate coefficient  $k_{3,2} (298 \text{ K}) < 8 \times 10^{-17} \text{ cm}^3 \text{ molecule}^{-1} \text{ s}^{-1}$ . Hence, the observations reported in this paper reduce the upper limit value for  $k_{3,2}$  by a factor of 16 compared to the previously reported limits, although it is worth noting that our data were obtained at 240 K, while the upper limit reported by Wallington et al. (1991) is based on data at 298 K, but requires extrapolation of Nicovich et al. (1990) results to higher temperature and pressure in order to obtain estimates for  $k_{3,1a}$  and  $k_{3,1b}$  at  $P = 700 \text{ Torr air}$  and  $T = 298 \text{ K}$ .

#### Kinetics of CS<sub>2</sub>-Cl Reactions with NO and NO<sub>2</sub>

The reactions of CS<sub>2</sub>-Cl with NO and NO<sub>2</sub> were studied at  $T = 240 \text{ K}$  and  $P = 30 \text{ Torr}$  (N<sub>2</sub> bath gas) under pseudo-first order conditions with  $[\text{NO}_x] \gg [\text{CS}_2\text{-Cl}]$ .



The reagent concentrations (in units of molecules cm<sup>-3</sup>) used in these experiments were as follows:  $[\text{Cl}_2\text{CO}] = 1.5 \times 10^{15}$ ;  $[\text{Cl}]_0 = (2\text{-}4) \times 10^{12}$ ;  $[\text{CS}_2] \approx 3 \times 10^{17}$ ;

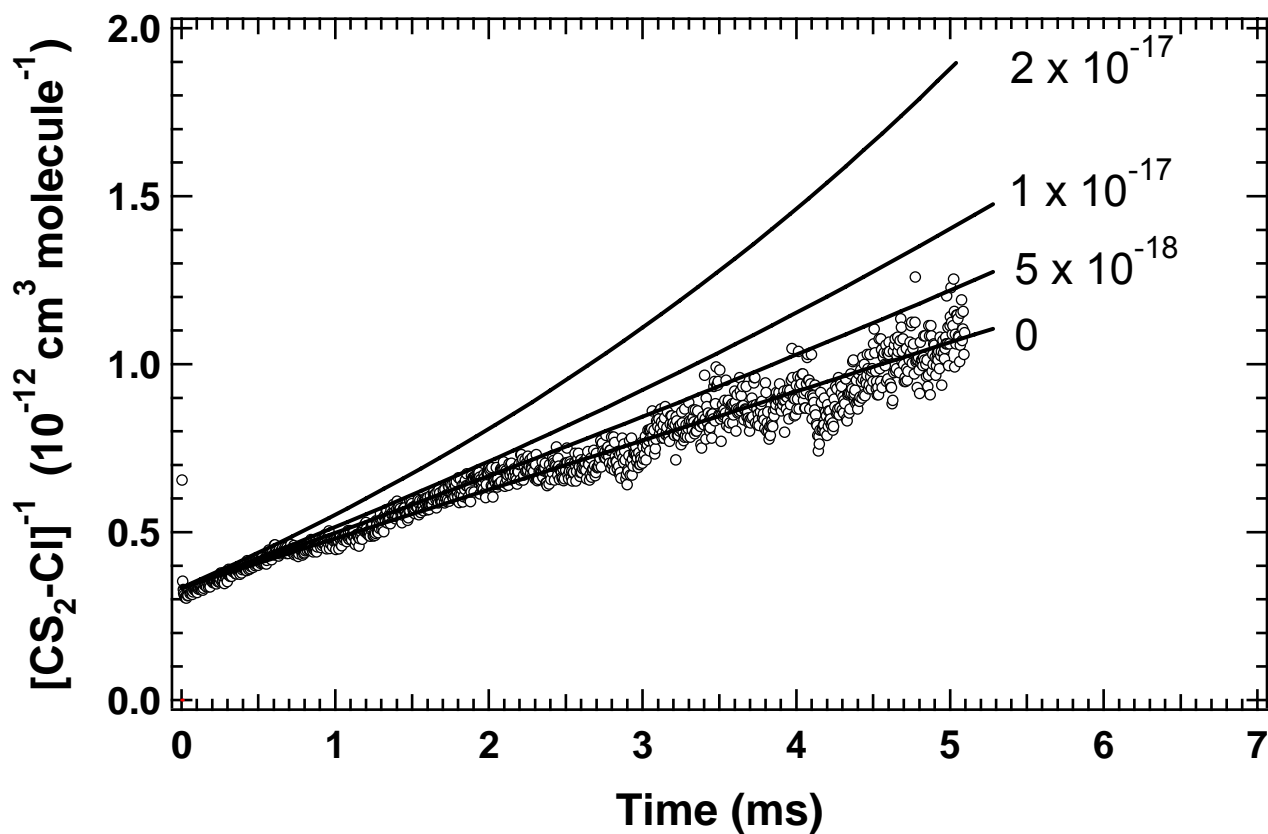
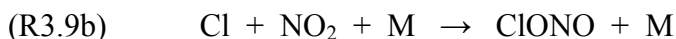
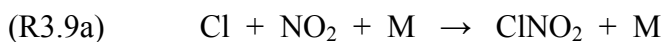
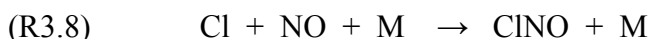


**Figure 3.7** CS<sub>2</sub>-Cl absorbance temporal profile plotted as [CS<sub>2</sub>-Cl]<sup>-1</sup> vs. time. Experimental conditions:  $T = 240$  K;  $P = 200$  Torr O<sub>2</sub>; [CS<sub>2</sub>] =  $6.1 \times 10^{16}$  molecules cm<sup>-3</sup>; and [Cl<sub>2</sub>CO] =  $7.4 \times 10^{14}$  molecules cm<sup>-3</sup>. The straight line is obtained from a linear least squares analysis; its slope gives  $2k_{3,4} = (1.46 \pm 0.02) \times 10^{-10}$  cm<sup>3</sup> molecule<sup>-1</sup>s<sup>-1</sup> where the uncertainty is  $2\sigma$  and represents precision only. The curved lines are simulations of the [CS<sub>2</sub>-Cl]<sup>-1</sup> vs. time plots expected if  $k_{3,2}$  had the values shown in the figure (in units of cm<sup>3</sup> molecule<sup>-1</sup>s<sup>-1</sup>).

$[\text{NO}] = (2-26) \times 10^{14}$ ;  $[\text{NO}_2] = 1-25 \times 10^{14}$ . Relatively low radical concentrations were employed in order to minimize the effect of radical-radical side reactions, i.e., reactions R3.4 and R3.5, on the observed absorbance temporal profiles. Experimental conditions of high  $[\text{CS}_2]$ , low temperature, and low pressure minimized the contribution of Cl reactions with NO and  $\text{NO}_2$  to observed  $\text{CS}_2$ -Cl kinetics.



For  $[\text{CS}_2] \approx 3 \times 10^{17}$  molecules  $\text{cm}^{-3}$  and  $T = 240$  K, the equilibrium concentration of  $\text{CS}_2$ -Cl exceeds that of Cl by more than a factor of 30 (Nicovich et al., 1990).

As typified by the data shown in Figure 3.8, absorbance decays were exponential, i.e., plots of  $\ln A$  vs. time were linear, as would be expected under the experimental conditions employed (see above). Measured pseudo-first order decay rates ( $k_d$ ), obtained from the slopes of plots like the one shown in Figure 3.8, are plotted as a function of  $[\text{CS}_2]$  in Figure 3.9. The slopes of the  $k_d$  vs.  $[\text{CS}_2]$  plots give the following second order rate coefficients in units of  $10^{-11}$   $\text{cm}^3$  molecule $^{-1}$  s $^{-1}$ :  $k_{3.6} = 2.17 \pm 0.07$  and  $k_{3.7} = 1.33 \pm 0.09$ ; uncertainties are  $2\sigma$  and represent precision only. The  $\text{NO}_2$  concentration data plotted in Figure 3.9 are corrected for dimer formation assuming a 240 K equilibrium constant of  $6.2 \times 10^{-17}$   $\text{cm}^3$  molecule $^{-1}$  for  $\text{NO}_2 + \text{NO}_2 \leftrightarrow \text{N}_2\text{O}_4$  (Sander et al., 2006); the magnitude of the correction ranged from 0.6% to 14% for the range of  $\text{NO}_2$  concentrations employed to measure  $k_{3.7}$ .

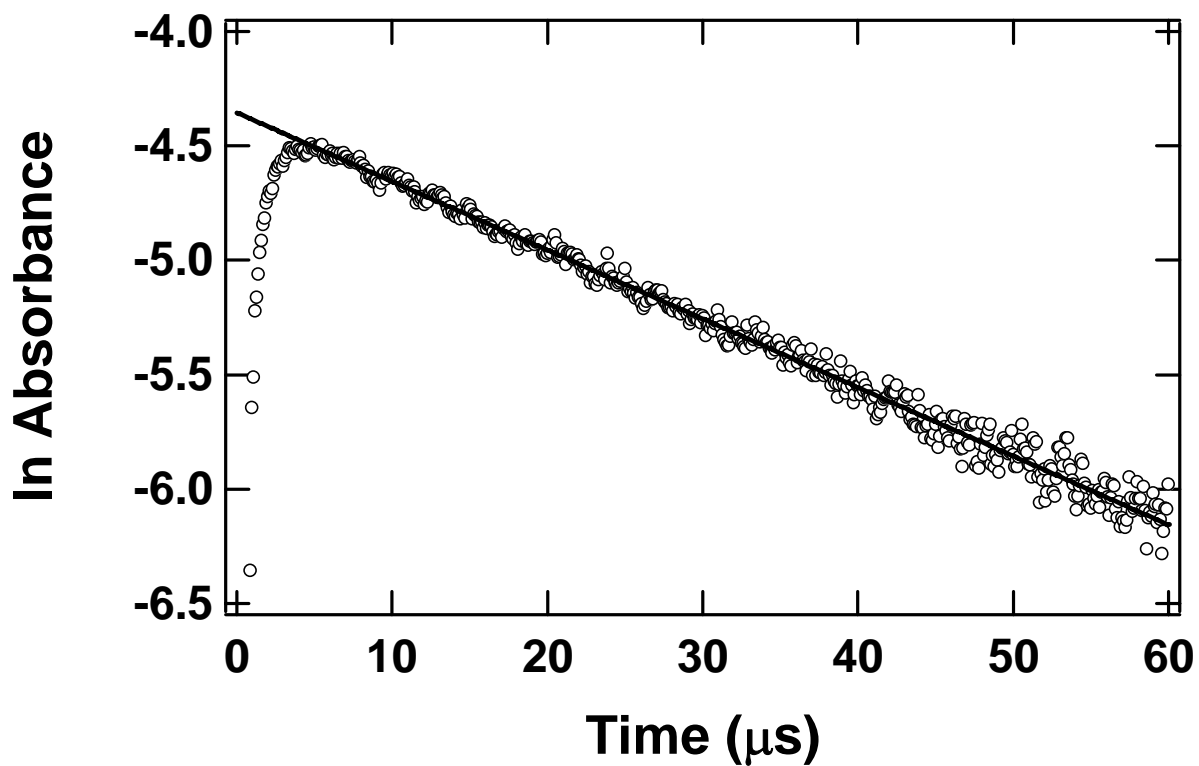


**Figure 3.8** Typical absorbance temporal profile observed following 248 nm laser flash photolysis of  $\text{Cl}_2\text{CO}/\text{CS}_2/\text{NO}_x/\text{N}_2$  mixtures at  $T = 240 \text{ K}$  and  $P = 30 \text{ Torr}$ . The data shown were obtained with  $\text{NO}_x = \text{NO}_2$ . Concentrations in units of  $10^{13} \text{ molecules cm}^{-3}$  are  $[\text{CS}_2] = 19000$ ,  $[\text{NO}_2] = 259$ ,  $[\text{Cl}_2\text{CO}] = 150$ , and  $[\text{Cl}]_0 \approx 0.36$ . The solid line is obtained from a linear least squares analysis of the  $\ln$  absorbance vs. time ( $t$ ) data at  $t > 5 \mu\text{s}$ ; its slope gives the pseudo-first order decay rate  $29,900\text{s}^{-1}$ .

The value for  $k_{3.7}$  reported above is derived under the (certainly valid) assumption that  $\text{CS}_2\text{-Cl}$  is much more reactive toward the open shell species  $\text{NO}_2$  than toward the closed shell species  $\text{N}_2\text{O}_4$ .

For  $[\text{Cl}]_0 \leq 4 \times 10^{12}$  per  $\text{cm}^3$  (see above), reactions (R3.8) and (R3.9a, R3.9b) contribute  $<600 \text{ s}^{-1}$  to the early time part of observed decays and even less at longer times after the flash. Since most measured decay rates exceeded  $10,000 \text{ s}^{-1}$  as shown in Figure 3.9, we conclude that the occurrence of radical-radical side reactions does not compromise the accuracy of the reported values for  $k_{3.6}$  and  $k_{3.7}$ . At  $T = 240 \text{ K}$  and  $P = 30 \text{ Torr N}_2$ ,  $k_{3.8} \sim 1.5 \times 10^{-13} \text{ cm}^3 \text{ molecule}^{-1} \text{ s}^{-1}$  (Lee et al., 1978) and  $k_{3.9a} + k_{3.9b} \equiv k_9 \sim 2 \times 10^{-12} \text{ cm}^3 \text{ molecule}^{-1} \text{ s}^{-1}$  (Ravishankara et al., 1988). In our experiments, about 30% of the bath gas was  $\text{CS}_2$ , which is more efficient than  $\text{N}_2$  as a third body. Hence,  $k_{3.8}$  and  $k_{3.9}$  were a little faster under our experimental conditions than the literature values given above. Nonetheless, it is clear that the values for  $k_{3.6}$  and  $k_{3.7}$  reported in this study are much faster than the known values for  $k_{3.8}$  and  $k_{3.9}$ ; this observation, along with the establishment of experimental conditions where the equilibrium concentration of  $\text{CS}_2\text{-Cl}$  was much greater than the equilibrium concentration of  $\text{Cl}$ , leads to the conclusion that reactions (R3.8) and (R3.9) made negligible contributions to  $\text{CS}_2\text{-Cl}$  kinetics in this study.

To our knowledge, no kinetic data are reported in the literature for the reaction of  $\text{Cl}$  atoms with  $\text{N}_2\text{O}_4$ . However, given that (i) a relatively small fraction of  $\text{NO}_2$  existed in the dimer form under the experimental conditions employed (see above); and (ii)  $\text{Cl}$  is

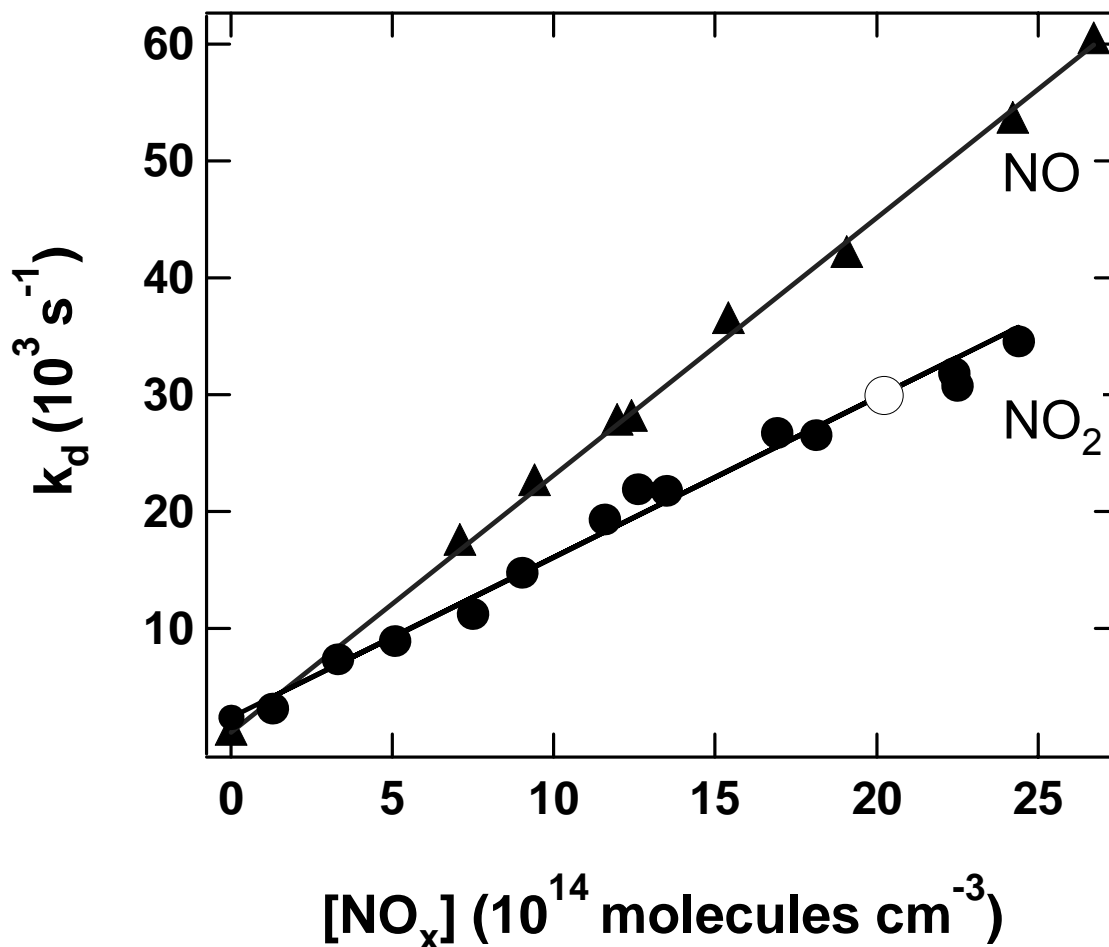


**Figure 3.9** Plots of pseudo-first-order adduct decay rate ( $k_d$ ) versus for data obtained at  $T = 240 \text{ K}$  and  $30 \text{ Torr}$  of  $\text{N}_2$ . The solid lines are obtained from linear least-squares analyses; their slopes give rate coefficients (in units of  $10^{-11} \text{ cm}^3 \text{ molecule}^{-1} \text{ s}^{-1}$ ) of  $2.17 \pm 0.07$  and  $1.33 \pm 0.09$  for the reactions of  $\text{CS}_2\text{-Cl}$  with  $\text{NO}$  and  $\text{NO}_2$ , respectively (uncertainties are  $2\sigma$  and represent precision only).

almost certainly much more reactive with NO<sub>2</sub> than with N<sub>2</sub>O<sub>4</sub>, it seems safe to assume that the Cl + N<sub>2</sub>O<sub>4</sub> reaction had a negligible influence on CS<sub>2</sub>-Cl kinetics in this study.

Since side reactions have little or no impact on the accuracy of the reported rate coefficients, it appears that accuracy is limited by precision and by the accuracy with which the concentrations of NO and NO<sub>2</sub> were known (estimated to be ± 5% for each). Hence, we report the rate coefficients  $k_{3,6} = (2.2 \pm 0.5) \times 10^{-11} \text{ cm}^3 \text{ molecule}^{-1} \text{ s}^{-1}$  and  $k_{3,7} = (1.3 \pm 0.4) \times 10^{-11} \text{ cm}^3 \text{ molecule}^{-1} \text{ s}^{-1}$ , where the uncertainties represent accuracy at the 95% confidence level.

Although there are no other reported measurements of  $k_{3,6}$  and  $k_{3,7}$  with which to compare our results, it is of interest to note that the rate coefficients reported in this study are very similar in magnitude to rate coefficients for the reactions of (CH<sub>3</sub>)<sub>2</sub>S-Cl with NO and NO<sub>2</sub> ( $1.2 \times 10^{-11}$  and  $2.7 \times 10^{-11} \text{ cm}^3 \text{ molecule}^{-1} \text{ s}^{-1}$ , respectively) that were measured by Urbanski and Wine (1999) using an analogous technique to the one employed in this study. Urbanski and Wine also observed no reactivity of (CH<sub>3</sub>)<sub>2</sub>S-Cl with O<sub>2</sub>. Similar results have also been reported for reactions of (CH<sub>3</sub>)<sub>2</sub>(O)S-Cl with NO, NO<sub>2</sub>, and O<sub>2</sub>, i.e., in units of  $10^{-11} \text{ cm}^3 \text{ molecule}^{-1} \text{ s}^{-1}$  rate coefficients are 1.5, 1.9, and  $<1 \times 10^{-7}$ , respectively (Kleissas et al., 2007). It appears that Cl adducts to sulfur compounds react rapidly with compounds like NO and NO<sub>2</sub>, where transfer of the chlorine atom to generate ClNO, ClNO<sub>2</sub>, or ClONO is energetically favorable. Because Cl-OO is bound by only ~20 kJ mol<sup>-1</sup> (Nicovich et al., 1990b), the chlorine transfer reaction between the sulfur adducts and O<sub>2</sub> cannot occur at T < 300 K. While thermochemistry can explain why NO and NO<sub>2</sub> are highly reactive and O<sub>2</sub> is unreactive

toward chlorine adducts with sulfur compounds, there appears to be little correlation between the rate coefficients and adduct bond strength for the energetically favorable  $\text{NO}_x$  reactions. All the adduct +  $\text{NO}_x$  rate coefficients summarized above are similar in magnitude even though the S–Cl bond strengths (at 0 K) are quite different ( $37 \pm 6 \text{ kJ mol}^{-1}$ ) for SCS–Cl (Wang and Phillips, 2002; Nicovich et al., 1990),  $72 \pm 4 \text{ kJ mol}^{-1}$  for  $(\text{CH}_3)_2(\text{O})\text{S–Cl}$  (Wine et al., 2006; Vandresen and Resende, 2004), and  $85 \pm 12 \text{ kJ mol}^{-1}$  for  $(\text{CH}_3)_2\text{S–Cl}$  (Wilson and Hirst, 1997; Thompson et al., 2002; Enami et al., 2004). Diau and Lee, (1991) have deduced rate coefficients for the reactions of  $\text{CS}_2\text{–OH}$  with  $\text{NO}$  and  $\text{NO}_2$  by examining the effect of added  $\text{NO}_x$  on  $\text{OH} + \text{CS}_2 \leftrightarrow \text{CS}_2\text{–OH}$  equilibration kinetics. They obtain a very fast rate coefficient ( $4.2 \times 10^{-11} \text{ cm}^3 \text{ molecule}^{-1} \text{ s}^{-1}$ ) for the  $\text{CS}_2\text{–OH} + \text{NO}_2$  reaction, but a much slower rate coefficient ( $7.3 \times 10^{-13} \text{ cm}^3 \text{ molecule}^{-1} \text{ s}^{-1}$ ) for the  $\text{CS}_2\text{–OH} + \text{NO}$  reaction. A mechanistic understanding of the differences in reactivity of  $\text{NO}$  and  $\text{NO}_2$  toward  $\text{CS}_2\text{–OH}$  remains to be developed.

### Role of $\text{CS}_2\text{–Cl}$ in Atmospheric Chemistry

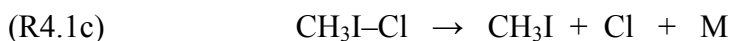
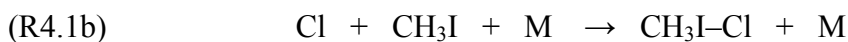
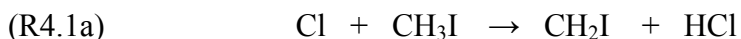
In the marine boundary layer (MBL), Cl concentrations are typically  $5 \times 10^4$  atoms  $\text{cm}^{-3}$  (Wingenter et al., 2005) and have been reported to be as high as  $10^5$  atoms  $\text{cm}^{-3}$  in some locations (Spicer et al., 1998); these concentrations are 10-100 times lower than typical OH levels, but are higher than Cl concentrations in other regions of the troposphere (Wingenter et al., 1999). On the other hand, the rate coefficient for Cl addition to  $\text{CS}_2$  is a factor of 5-10 faster than the rate coefficient for OH addition to  $\text{CS}_2$  under typical MBL conditions ( $P \sim 1 \text{ atm}$ ;  $250 \text{ K} < T < 310 \text{ K}$ ) (Hynes et al., 1988; Nicovich et al., 1990). Removal of  $\text{CS}_2$  by OH is a relatively efficient process in the

atmosphere because the  $\text{CS}_2\text{-OH} + \text{O}_2$  reaction competes favorably with adduct thermal decomposition under atmospheric conditions (Jones et al., 1982; Jones et al., 1983; Barnes et al., 1983; Hynes et al., 1988; Bulatov et al., 1988; Lovejoy et al., 1990; Murrells et al., 1990; Lunell et al., 1990; Becker et al., 1990; Diau and Lee, 1991; McKee, 1993; Stickel et al., 1993; Lovejoy et al., 1994; Zhang and Qin, 2000; McKee and Wine, 2001). The results reported in this paper suggest that under MBL conditions the lifetime of  $\text{CS}_2\text{-Cl}$  toward reaction with  $\text{O}_2$  is  $> 0.025$  seconds and the lifetime of  $\text{CS}_2\text{-Cl}$  toward photo-dissociation is several seconds (even under the assumptions of unit photo-dissociation quantum yield and  $0^\circ$  zenith angle). Since the  $\text{CS}_2\text{-Cl}$  lifetime toward thermal decomposition back to  $\text{CS}_2 + \text{Cl}$  is  $< 10^{-5}$  s under MBL conditions (Nicovich et al., 1990a), it is clear that the  $\text{Cl} + \text{CS}_2$  association reaction will be of little importance as a destruction pathway for  $\text{CS}_2$  in the atmosphere.

**CHAPTER 4**  
**SPECTROSCOPIC AND KINETIC STUDY OF THE GAS PHASE**  
**CH<sub>3</sub>I–Cl AND C<sub>2</sub>H<sub>5</sub>I–Cl ADDUCTS**

**The Reaction of Cl with CH<sub>3</sub>I and C<sub>2</sub>H<sub>5</sub>I**

The first indication that Cl reactions with iodoalkanes may involve a complex mechanism came from product angular distributions observed in molecular beam studies by Hoffmann et al. (1984a, b). Evidence for production of a thermalized CH<sub>3</sub>I–Cl adduct was first reported by Ayhens et al. (1997). These investigators followed Cl kinetics over a wide range of temperature and pressure, and demonstrated that both addition and H-abstraction pathways were operative:



At  $364 \text{ K} \leq T \leq 694 \text{ K}$  the rate coefficient  $k_{4.1a} = 5.4 \times 10^{-11} \exp(-1250/T) \text{ cm}^3 \text{ molecule}^{-1} \text{ s}^{-1}$  was reported and a significant H/D kinetic isotopic effect was observed at 373 K ( $k_1^{\text{H}}/k_1^{\text{D}} = 4.3$ ), providing evidence that H-abstraction was dominant under these conditions. At  $T \leq 250 \text{ K}$ , reaction occurred via formation of a stable adduct with a reported rate coefficient  $k_{4.1b} \approx 2 \times 10^{-11} \text{ cm}^3 \text{ molecule}^{-1} \text{ s}^{-1}$  at  $P = 500 \text{ Torr N}_2$ . Rate coefficients for reactions (R4.1b) and (R4.1c) were determined as a function of temperature and pressure over the ranges 263–309 K and 25–500 Torr N<sub>2</sub>, respectively.

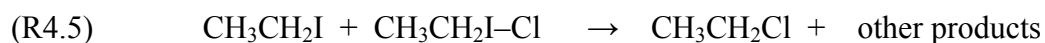
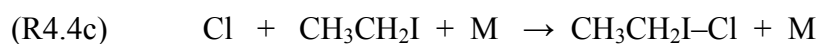
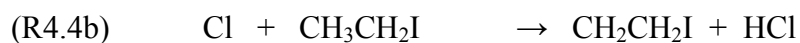
From a combination of second- and third-law analyses, Ayhens et al. (1997) deduced a 0 K adduct bond dissociation energy of  $52.2 \pm 3.3 \text{ kJ mol}^{-1}$ , in reasonable agreement with their theoretical value of  $59.3 \text{ kJ mol}^{-1}$  obtained using density functional theory (DFT) at the B3LYP/ECP level, and also in good agreement a theoretical value of  $50.7 \text{ kJ mol}^{-1}$  reported by Lazarou et al. (1997) based on calculations at the MP2/3-21++G(2d,2p) level of theory.

Several additional studies of the  $\text{Cl} + \text{CH}_3\text{I}$  reaction are reported in the literature. Kambanis et al. (1997) conducted low pressure studies ( $P \sim 2 \text{ mTorr}$ ) over the temperature range 273–363 K and reported the Arrhenius expression  $k_{4.1} = 1.3 \times 10^{-11} \exp(-689/T) \text{ cm}^3 \text{ molecule}^{-1} \text{ s}^{-1}$ . Evidence for a kinetic isotope effect was not observed ( $k_{\text{H}}/k_{\text{D}} = 1.09 \pm 0.04$ ) leading these investigators to conclude that reaction (R4.1) proceeds via a weakly bound  $\text{CH}_3\text{I}-\text{Cl}$  adduct. Product studies of reaction (R4.1) have been reported by Goliff and Rowland (1997) who report a 9% yield of  $\text{CH}_3\text{Cl}$  at 295 K and pressures in the range of 760 – 4000 Torr  $\text{CClF}_3$ , as well as by Bilde and Wallington (1998) who report an upper limit  $\text{CH}_3\text{Cl}$  yield of 20% at  $T = 295 \text{ K}$  and  $P = 1 \text{ Torr N}_2$ , and a 50% increase in reactivity upon raising the pressure to 700 Torr  $\text{N}_2$ , air, or  $\text{O}_2$ , suggesting the occurrence of adduct loss processes other than reaction (R4.1c):



In contrast to the findings of Kambanis et al. (1997), Bilde and Wallington, (1998) observed a large kinetic isotopic effect ( $k_{\text{H}}/k_{\text{D}} = 6$  at 295 K and 1 Torr  $\text{N}_2$ ), thereby concluding that reaction (R4.1a) is the dominant channel under their low-pressure

experimental conditions; they report the rate coefficient  $k_{4.1a}(295\text{ K}) = 9.0 \times 10^{-13} \text{ cm}^3 \text{ molecule}^{-1} \text{ s}^{-1}$ , in good agreement with the rate coefficient obtained by extrapolation of the high-temperature results of Ayhens et al. (1997) to 295 K assuming Arrhenius behavior. Cotter et al. (2001a) report a rate coefficient  $k_1 = 1.5 \times 10^{-12} \text{ cm}^3 \text{ molecule}^{-1} \text{ s}^{-1}$  at 298 K and over the pressure range 1.5-12 Torr He which, under their experimental conditions, they attribute primarily to pathway (R4.1a). Cotter and coworkers also have conducted end product analysis studies of reactions 1 and 4 in air at atmospheric pressure and room temperature, (Cotter et al., 2001b) and conclude that both reactions proceed via two channels, one yielding HCl and an iodinated alkyl radical, consistent with reaction (R4.1a), for CH<sub>3</sub>I, or reactions (R4.4a) and (R4.4b), for C<sub>2</sub>H<sub>5</sub>I, and the other yielding I atoms, an alkyl chloride and a carbonyl species, consistent with reactions (R4.1b), (R4.1c), and (R4.3), for CH<sub>3</sub>I, or reactions (R4.4c), (R4.4d) and (R4.5), for C<sub>2</sub>H<sub>5</sub>I:



A combined laser flash photolysis (LFP), competitive kinetics, end product analysis, and theoretical study of reaction (4) has been reported by Orlando et al. (2005). These investigators report Arrhenius expressions for Cl reactions with C<sub>2</sub>H<sub>5</sub>I and C<sub>2</sub>D<sub>5</sub>I applicable over the temperature range 334–434 K, where H-transfer pathways are found to dominate. In units of cm<sup>3</sup> molecule<sup>-1</sup> s<sup>-1</sup>, the reported Arrhenius expressions are  $k_{4.4a}^{\text{H}} + k_{4.4b}^{\text{H}} = 6.5 \times 10^{-11} \exp(-428/T)$  and  $k_{4.4a}^{\text{D}} + k_{4.4b}^{\text{D}} = 2.2 \times 10^{-11} \exp(-317/T)$ . Also,

Orlando et al. (2005) report branching ratios for abstraction pathways at 298 K of 63% and 37% for channels (R4.4a) and (R4.4b), respectively. Equilibration kinetics for reactions (R4.4c) and (R4.4d) were investigated at sub-ambient temperatures yielding a 0 K bond energy for CD<sub>3</sub>CD<sub>2</sub>I–Cl of 57 ± 10 kJ/mol; published theoretical values for the CH<sub>3</sub>CH<sub>2</sub>I–Cl bond strength (Orlando et al., 2005; Enami et al., 2005a) are consistent with the experimental value. Using product studies in conjunction with competitive kinetics techniques, Orlando et al. estimate that  $k_{4,5}(298\text{ K}) \sim (2\text{--}5) \times 10^{-13} \text{ cm}^3 \text{ molecule}^{-1} \text{ s}^{-1}$ . By coupling laser flash photolysis with cavity ring down spectroscopy, Enami et al. (2005a, b) have directly observed the adducts CH<sub>3</sub>I–Cl and C<sub>2</sub>H<sub>5</sub>I–Cl for the first time. Their studies, which were carried out at  $T = 250\text{ K}$  and  $P = 25\text{--}125\text{ Torr}$  of N<sub>2</sub>, provide wavelength-dependent absorption cross sections at  $\lambda \geq 405\text{ nm}$ , a wavelength range that appears to represent only the red tail of the absorption spectra. Recently, laser-induced fluorescence from CH<sub>3</sub>I–Cl excited in the near UV spectral region has been reported (Gravestock, 2006; Gravestock et al., 2008).

In this study we report the results of an experimental study of the gas phase Cl + CH<sub>3</sub>I and Cl + C<sub>2</sub>H<sub>5</sub>I reactions that couples LFP production of Cl with product detection by time-resolved UV-visible absorption spectroscopy (TRUVVAS). The gas phase absorption spectra of the CH<sub>3</sub>I–Cl and C<sub>2</sub>H<sub>5</sub>I–Cl adducts at wavelengths shorter than 405 nm are reported for the first time, and wavelength-dependent absorption cross sections are reported that are in rather poor agreement with literature values (Enami et al., 2005a, b) over the overlapping wavelength regime of the studies (405–500 nm). In addition, the TRUVVAS technique is used as a probe to investigate the kinetics of adduct radical-radical reactions and adduct reactions with RI, O<sub>2</sub>, NO, and NO<sub>2</sub>. Although CH<sub>3</sub>I–Cl

and  $C_2H_5I-Cl$  appear to be of only minor importance in atmospheric chemistry, the results reported in this study are useful for developing an understanding of the kinetics and spectroscopy of gas-phase adducts of radicals with iodine compounds and, more generally, radical-molecule adducts that involve the formation of two-center – 3-electron (2c-3e) bonds; a number of such adducts do play important roles in atmospheric chemistry.

### Experimental Method

The LFP-TRUVVAS apparatus was employed in all studies of the  $RI-Cl$  ( $R = CH_3, C_2H_5$ ) adducts and is discussed in detail in Chapter 2. Only aspects of the apparatus not discussed in Chapter 2 are covered in the current section. All experiments were carried out at temperatures in the range 250 – 261 K. The reaction cell and pre-mixing cell were surrounded by an insulated Pyrex jacket through which an ethanol/methanol mixture was flowed from a temperature-controlled reservoir, enabling the cell temperature to be controlled. The temperatures of the gas mixture at the two exits from the reaction cell were measured with thermocouples. The temperature gradient between the ends of the cell was less than  $2^\circ C$ , and the average of the temperatures measured at the two ends was taken to be the cell temperature. Dry nitrogen gas was sprayed on the exterior of the quartz cell windows to prevent condensation of water vapor when the cell was cooled. Monochromator entrance and exit slits were set at 1.5 mm, providing a spectral resolution of 5.5 nm full width at half maximum (FWHM).

For all kinetic measurements as well as for some spectroscopic studies at wavelengths longer than 350 nm, the  $RI-Cl$  adducts were generated by 308 nm laser

flash photolysis of  $\text{Cl}_2$  in the presence of RI ( $\text{R} = \text{CH}_3, \text{C}_2\text{H}_5$ ). The absorption cross section for  $\text{Cl}_2$  at 308 nm is  $1.72 \times 10^{-19} \text{ cm}^2 \text{ molecule}^{-1}$  (Sander et al., 2006), a typical photolysis fluence was  $\sim 20 \text{ mJ cm}^{-2} \text{ pulse}^{-1}$ , and the pulse duration was  $\sim 25 \text{ ns}$ . For additional spectroscopic studies over the wavelength range 310 – 500 nm, RI–Cl adducts were generated by 248 nm laser flash photolysis of RI in the presence of  $\text{Cl}_2$ . Absorption cross sections for  $\text{CH}_3\text{I}$  and  $\text{C}_2\text{H}_5\text{I}$  at 248 nm are  $8.4 \times 10^{-19}$  and  $8.7 \times 10^{-19} \text{ cm}^2 \text{ molecule}^{-1}$ , respectively (Sander et al., 2006), a typical photolysis fluence was  $28 \text{ mJ cm}^{-2} \text{ pulse}^{-1}$  and, as was the case for 308 nm photolysis, the pulse duration was  $\sim 25 \text{ ns}$ .

Concentrations of both RI and  $\text{Cl}_2$  were measured *in situ* in the slow flow system by UV photometry as well as by mass flow measurements. The *in situ* photometry measurements of  $\text{CH}_3\text{I}$  and  $\text{C}_2\text{H}_5\text{I}$  employed 254 nm as the monitoring wavelength (Hg penray lamp light source). The cross-sections used to convert 254 nm absorbances to concentrations were  $1.16 \times 10^{-18} \text{ cm}^2 \text{ molecule}^{-1}$  and  $1.28 \times 10^{-18} \text{ cm}^2 \text{ molecule}^{-1}$  for  $\text{CH}_3\text{I}$  and  $\text{C}_2\text{H}_5\text{I}$ , respectively (Sander et al., 2006). The *in situ* photometry measurements of  $\text{Cl}_2$  employed 326 nm as the monitoring wavelength (Cd penray lamp light source). The cross-section used to convert the 326 nm absorbance to concentration was  $2.48 \times 10^{-19} \text{ cm}^2 \text{ molecule}^{-1}$  (Sander et al., 2006).

## Results and Discussion

When  $\text{Cl}_2$  was photolyzed at 308 nm in the presence of RI, absorption of the UV-visible probe beam was observed throughout the 350 to 500 nm spectral region. Similarly, when RI was photolyzed at 248 nm in the presence of  $\text{Cl}_2$ , absorption of the UV-visible probe beam was observed throughout the 310 to 500 nm spectral region. In

both cases, absorption was observed only when both RI and Cl<sub>2</sub> were present in the photolyzed gas mixture.

### Identification of the Absorbing Species

Evidence verifying the identity of the absorbing species was obtained by measuring its appearance rate. Absorbance temporal profiles were recorded and analyzed using a nonlinear least squares fit to equation Eq. 4.1, which describes the time evolution of the intermediate in consecutive first-order reactions (Atkins, 2006):

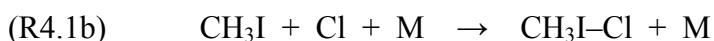
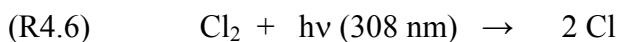
$$\text{(Eq. 4.1)} \quad A_t = \{k_a/(k_d - k_a)\}X\{\exp(-k_a t) - \exp(-k_d t)\}$$

In the above equation,  $A_t$  is the absorbance at time  $t$ ,  $k_a$  is the first-order absorbance appearance rate,  $k_d$  is the first-order absorbance decay rate, and  $X$  is the peak adduct absorbance that would be observed in the absence of a decay. A typical absorbance temporal profile is shown in Figure 1. In this set of experiments, absorbance disappearance resulted primarily from radical-radical reactions and was not a first-order process. The first-order absorbance disappearance rate,  $k_d$ , is thus a parameterized rate coefficient rather than the sum of actual loss processes that are quantitatively attributable to specific first order processes. However, because (i) the observed absorbance loss rates are slow compared to the rates of absorbance appearance, and (ii) the data that were fit were limited to times where the fractional decay of absorbance was small, the parameterization of the absorbance disappearance as a first order process does not seriously impact the reliability of the analysis to determine the pseudo-first order rate coefficient for absorbance appearance. As typified by the data shown in Figure 4.1, the quality of the double exponential fits is quite good. Pseudo-first-order appearance rate

coefficients ( $k_a$ ) were measured at 350 nm in 100 Torr N<sub>2</sub> buffer gas and at 365 nm in 260 Torr N<sub>2</sub> buffer gas for CH<sub>3</sub>I–Cl and C<sub>2</sub>H<sub>5</sub>I–Cl, respectively. As shown in Figure 4.2, plots of  $k_a$  vs. [RI] are linear over the range of RI concentrations employed. The linearity of the  $k_a$  vs. [RI] plots up to the fastest appearance rates measured (ca. 60,000 s<sup>-1</sup> and 40,000 s<sup>-1</sup> for Cl + CH<sub>3</sub>I and Cl + C<sub>2</sub>H<sub>5</sub>I, respectively) demonstrates that the rate-limiting step in production of the absorbing species is the Cl + RI reaction under the conditions investigated. The slopes of the  $k_a$  vs. [RI] plots yield the second order rate coefficients  $k_{4.1} = (1.0 \pm 0.2) \times 10^{-11} \text{ cm}^3 \text{ molecule}^{-1} \text{ s}^{-1}$  at  $T = 261 \text{ K}$  and  $P = 100 \text{ Torr N}_2$  and  $k_{4.4} = (1.1 \pm 0.1) \times 10^{-10} \text{ cm}^3 \text{ molecule}^{-1} \text{ s}^{-1}$  at  $T = 258 \text{ K}$  and  $P = 260 \text{ Torr N}_2$ , where  $k_1 \equiv k_{1a} + k_{1b}$ ,  $k_4 \equiv k_{4a} + k_{4b} + k_{4c}$ , and the uncertainties are  $2\sigma$  and represent precision only. The values for  $k_{4.1}$  and  $k_{4.4}$  evaluated from the absorbance appearance rates agree within experimental uncertainty with Cl + RI rate coefficients obtained at the same temperatures and pressures by monitoring the decay of Cl using atomic resonance fluorescence spectroscopy (Ahyens et al., 1997; Orlando et al., 2005). The data in Figures 4.1 and 4.2 provide strong evidence that the species being observed are indeed the RI–Cl adducts formed as primary products of the reactions of Cl with RI.

#### Adduct Absorption Spectra

The absorption spectrum of CH<sub>3</sub>I–Cl was measured at 300 Torr total pressure (N<sub>2</sub> bath gas) and 250 K using two different methods of Cl generation. The first method involved 308 nm photolysis of Cl<sub>2</sub>:



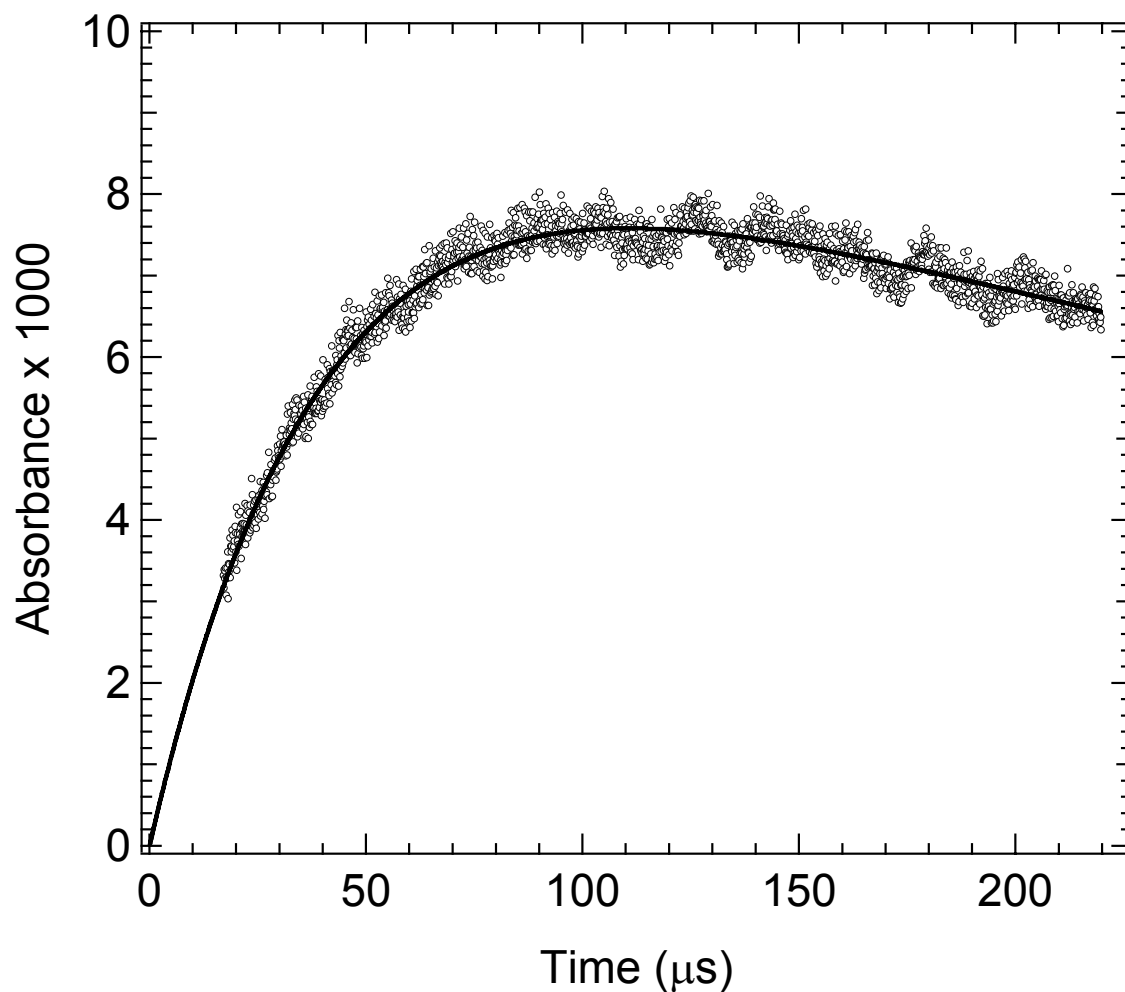


**Figure 4.1** Typical absorbance (base e) temporal profile observed following laser flash photolysis of RI/Cl<sub>2</sub>/N<sub>2</sub> mixtures at 308 nm. Experimental conditions:  $T = 258$  K;  $P = 263$  Torr; R = C<sub>2</sub>H<sub>5</sub>; monitoring wavelength = 365 nm; concentrations in units of  $10^{14}$  molecules cm<sup>-3</sup> are [Cl<sub>2</sub>] = 13.7, [C<sub>2</sub>H<sub>5</sub>I] = 2.04, and [Cl]<sub>0</sub> ≈ 0.07. The solid line is obtained from a nonlinear least squares fit of the data to the sum of an exponential rise and an exponential decay. Best fit appearance ( $k_a$ ) and disappearance ( $k_d$ ) rate coefficients in units of s<sup>-1</sup> are  $k_a = 23810$  and  $k_d = 2120$ .

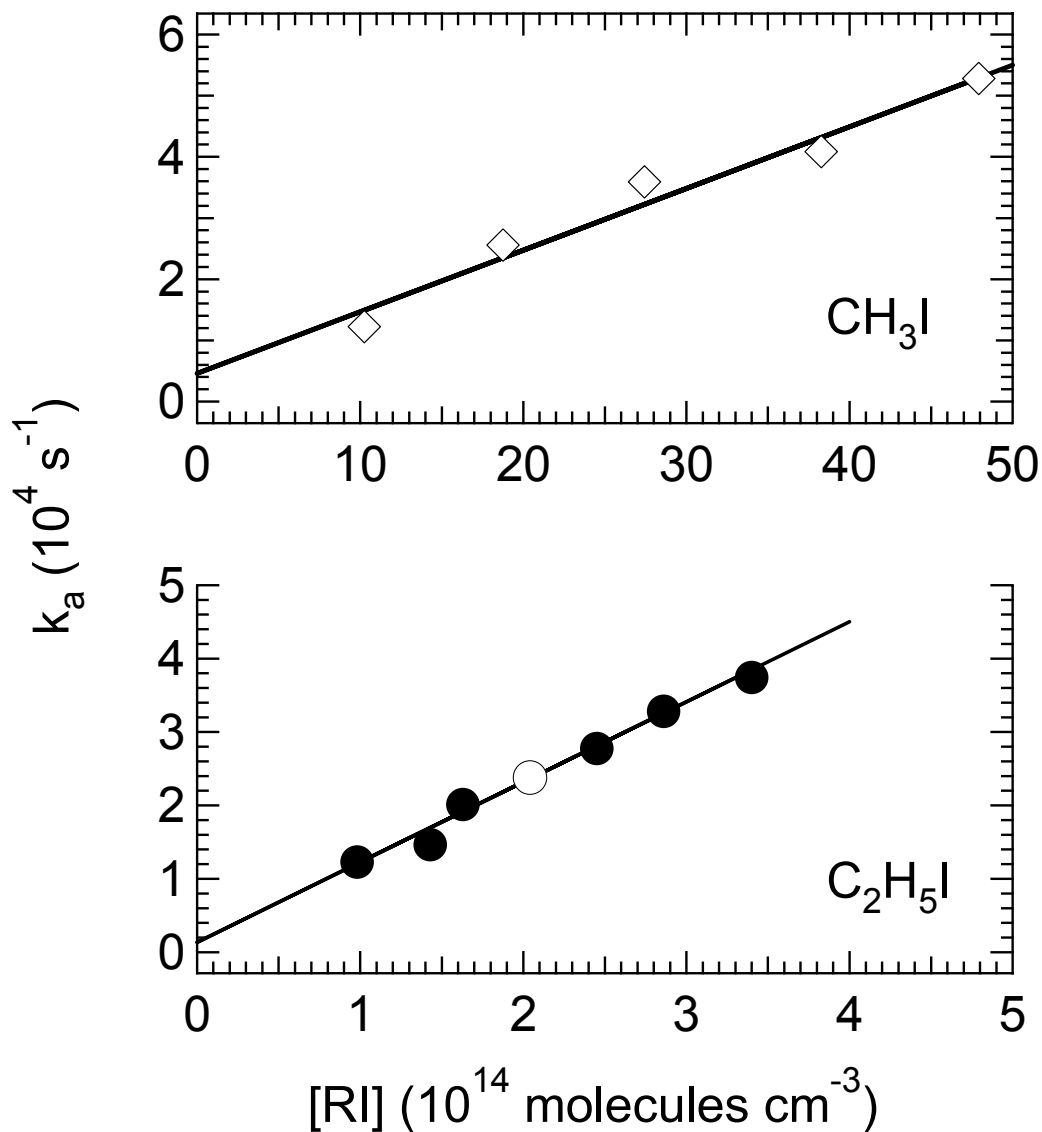
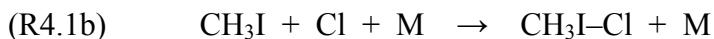
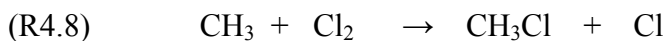


**Figure 4.2** Plots of  $k_a$  versus  $[\text{CH}_3\text{I}]$  for data obtained at  $T = 261 \text{ K}$  and  $P = 100 \text{ Torr N}_2$  and  $k_a$  versus  $[\text{C}_2\text{H}_5\text{I}]$  for data obtained at  $T = 258 \text{ K}$  and  $P = 263 \text{ Torr N}_2$ . The solid lines are obtained from linear least squares analyses; their slopes give the following second order rate coefficients in units of  $10^{-11} \text{ cm}^3 \text{ molecule}^{-1} \text{ s}^{-1}$ :  $k_{4.1} = 1.01 \pm 0.21$  and  $k_{4.4} = 10.9 \pm 0.48$ . The open data point is the one obtained from the data shown in Figure 4.1.

The second method employed 248 nm photolysis of CH<sub>3</sub>I:



Using the first method, absorption measurements were made over the wavelength range 350–500 nm, while the second method facilitated absorption measurements over the wider wavelength range 310–500 nm. A reference wavelength of 350 nm was selected for the CH<sub>3</sub>I–Cl spectral measurements. Absorption measurements were made at this reference wavelength after every 5 measurements at other wavelengths. This was done in order to account for systematic drifts in experimental parameters such as laser power, [Cl<sub>2</sub>], optical alignment, etc. over time. Absorbance measurements at wavelengths other than 350 nm were normalized to the average of the “before” and “after” 350 nm absorbances. The adduct absorption cross section was carefully measured at 350 nm and all cross-sections were then determined by applying the normalization factor to the carefully measured reference cross-section. The absorption spectrum of C<sub>2</sub>H<sub>5</sub>I–Cl was also measured at 300 Torr total pressure (N<sub>2</sub> bath gas) and 250 K using the same methods of producing radicals as for CH<sub>3</sub>I–Cl. The reference wavelength used for the C<sub>2</sub>H<sub>5</sub>I–Cl spectral measurements was 365 nm.

The absolute absorption cross-section measurements at 350 nm for CH<sub>3</sub>I–Cl and at 365 nm for C<sub>2</sub>H<sub>5</sub>I–Cl all employed 308 nm photolysis of Cl<sub>2</sub> as the radical source.

Typical concentrations employed in these measurements in units of  $10^{13}$  molecules  $\text{cm}^{-3}$  were as follows:  $[\text{CH}_3\text{I}] \approx 520$ ;  $[\text{Cl}_2] \approx 58\text{--}400$ ;  $[\text{Cl}]_0 \approx 0.53\text{--}3.7$  for the  $\text{CH}_3\text{I}\text{--Cl}$  experiments and  $[\text{C}_2\text{H}_5\text{I}] \approx 190$ ;  $[\text{Cl}_2] \approx 130\text{--}440$ ;  $[\text{Cl}]_0 \approx 1.4\text{--}4.4$  for the  $\text{C}_2\text{H}_5\text{I}\text{--Cl}$  experiments. High RI concentrations were employed in order to obtain  $\sim 99\%$  conversion of Cl to RI-Cl at equilibrium (based on the equilibrium constants reported by Ayhens et al., 1997 and Orlando et al., 2005). Each cross-section measurement involved averaging 20 photolysis laser pulses. The  $\text{CH}_3\text{I}\text{--Cl}$  cross-section at 350 nm,  $\sigma(\text{CH}_3\text{I})_{350}$  and the  $\text{C}_2\text{H}_5\text{I}\text{--Cl}$  cross-section at 365 nm,  $\sigma(\text{C}_2\text{H}_5\text{I})_{365}$ , were determined from the data using the following relationship:

$$\text{(Eq. 4.2)} \quad \sigma(\text{RI})_\lambda = X / (l [\text{Cl}]_0 F).$$

In Eq. 4.2 X is defined as in Eq. 4.1 (see above),  $l$  is the absorption path length (100 cm),  $[\text{Cl}]_0$  is the concentration of chlorine atoms produced via laser flash photolysis of  $\text{Cl}_2$ , and F is the fraction of Cl atoms converted to adduct. As is typical for gas phase spectroscopic data, the absorbance is defined as  $A = \ln(I_0/I_t)$  where  $I_0$  is the transmitted light intensity before the laser fires and  $I_t$  is the transmitted light intensity at some time  $t$  after the laser fires, i.e., A is a base e absorbance.

The parameter F in Eq. 4.2 can be evaluated using the following relationship:

$$\text{(Eq. 4.3)} \quad F = (1 - F_1) (1 - F_2) (1 - F_3)$$

In Eq. 4.3  $F_1$  is the fraction of Cl atoms that are lost by diffusion from the detection volume and/or reaction with background impurities,  $F_2$  is the fraction of Cl atoms that react with RI by H-abstraction rather than by addition, and  $F_3$  is the fraction of RI-Cl  $\leftrightarrow$  Cl that exists as Cl when the two species are in equilibrium. Employing high

concentrations of RI helps to keep  $F_1$  and  $F_3$  small, while employing relatively high total pressure minimizes  $F_2$ . Based on kinetic and thermodynamic data reported by Ayhens et al. (1997) and Orlando et al. (2005) we estimate that  $F_2 = 0.02$  and  $F_3 = 0.005$  for  $\text{CH}_3\text{I}$  while  $F_2 = 0.09$  and  $F_3 = 0.001$  for  $\text{C}_2\text{H}_5\text{I}$  under the experimental conditions employed. The background loss rate of Cl atoms (typically found to be  $50\text{--}100\text{ s}^{-1}$  in LFP studies of Cl kinetics that employ resonance fluorescence detection) is probably negligible compared to the pseudo-first-order rate coefficient for  $\text{Cl} + \text{RI}$ , which is  $(1.5\text{--}2.5) \times 10^5\text{ s}^{-1}$  under the above experimental conditions. Hence, we conservatively assign  $F_1$  a value of 0.01. The above considerations lead to the results  $F = 0.96 \pm 0.02$  for  $\text{CH}_3\text{I}\text{--Cl}$  and  $F = 0.89 \pm 0.07$  for  $\text{C}_2\text{H}_5\text{I}\text{--Cl}$ ; the reported uncertainties are estimates of accuracy at the 95% confidence level.

Cross-sections obtained from Eq. 4.2 were found to be independent of  $[\text{Cl}]_0$  over the ranges specified above, i.e., Beer's law was obeyed. Evaluation of  $[\text{Cl}]_0$  required (i) careful measurements of  $[\text{Cl}_2]$  and laser power, (ii) careful measurements of  $[\text{RI}]$  since both  $\text{CH}_3\text{I}$  and  $\text{C}_2\text{H}_5\text{I}$  absorb at 308 nm with cross-sections in units of  $\text{cm}^2\text{ molecule}^{-1}$  of  $8.1 \times 10^{-21}$  and  $1.04 \times 10^{-20}$ , respectively (Sander et al., 2006), to generate concentrations of alkyl radicals that are a few percent of  $[\text{Cl}]_0$ , and (iii) careful measurements of the photolysis laser beam cross-sectional area and its divergence down the length of the cell (the laser beam area increased by a factor of 1.5 between the cell entrance and exit, and was assumed to be the average of the entrance and exit areas for purposes of evaluating  $[\text{Cl}]_0$ ).

**Table 4.1** Absorption cross sections for the RI–Cl adducts as a function of wavelength at  $T = 250$  K and a spectral resolution of 5.5 nm (FWHM).

$\lambda^a$	$\sigma(\text{CH}_3\text{I-Cl})^b$	$\sigma(\text{C}_2\text{H}_5\text{I-Cl})^b$	$\lambda^a$	$\sigma(\text{CH}_3\text{I-Cl})^b$	$\sigma(\text{C}_2\text{H}_5\text{I-Cl})^b$
310	3.29	2.66	410	0.57	0.50
315	3.49	2.69	415	0.54	0.50
320	2.97	2.66	420	0.54	0.50
325	2.36	2.12	425	0.55	0.48
330	1.97	1.86	430	0.52	0.48
335	1.92	1.66	435	0.54	0.47
340	1.84	1.50	440	0.52	0.46
345	1.91	1.56	445	0.46	0.43
350	1.95	1.56	450	0.42	0.42
355	1.90	1.56	455	0.38	0.37
360	1.78	1.49	460	0.34	0.34
365	1.60	1.38	465	0.28	0.30
370	1.33	1.20	470	0.23	0.29
375	1.04	0.99	475	0.19	0.28
380	0.86	0.88	480	0.14	0.24
385	0.68	0.71	485	0.12	0.20
390	0.59	0.64	490	0.10	0.17
395	0.54	0.56	495	0.06	0.16
400	0.58	0.55	500	0.04	0.17
405	0.55	0.51			

<sup>a</sup>Units of  $\lambda$  in nm; <sup>b</sup>units of  $\sigma$  in  $10^{-17}$  cm<sup>2</sup> molecule<sup>-1</sup>.

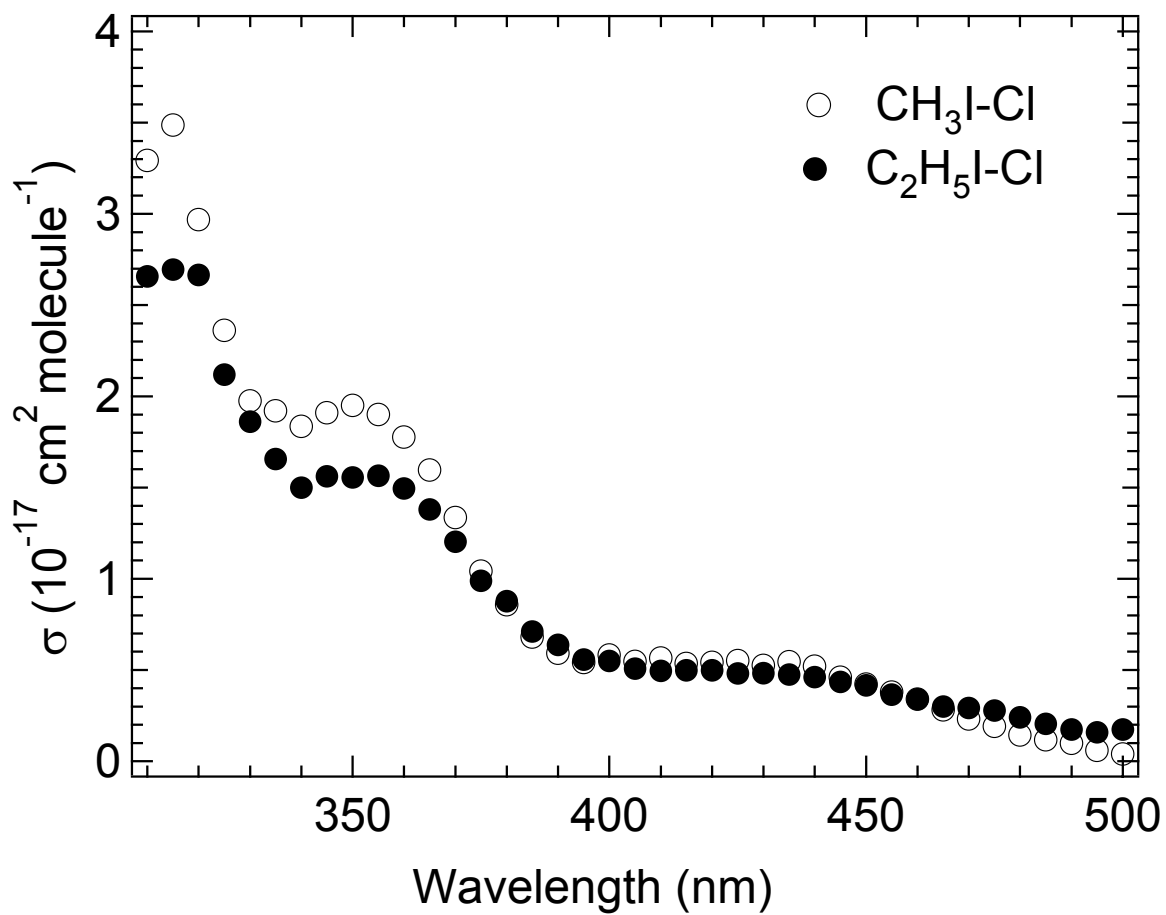


Figure 4.3 Absorption spectra of  $\text{CH}_3\text{I-Cl}$  (open circles) and  $\text{C}_2\text{H}_5\text{I-Cl}$  (filled circles) at a spectral resolution of 5.5 nm (FWHM)

The adduct spectra measured in this study at  $T = 250$  K and  $P = 300$  Torr  $N_2$  are shown in Figure 4.3, and are given in digitized form in Table 4.1. The RI-Cl absorption spectra were measured on several days verifying reproducibility of data and also measured by using two methods of radical generation as discussed above.

In the 350–500 nm spectral region, where measurements were performed using both methods of radical production, the results obtained were essentially identical, again verifying data reproducibility. Consideration of uncertainties in the parameters that must be known to obtain the adduct cross-section (see above), leads to an estimate of  $\pm 35\%$  for the accuracy of the measured values for absolute absorption cross-sections (95% confidence level). We report these cross-sections in units of  $\text{cm}^2 \text{ molecule}^{-1}$  (base e) to be  $\sigma(\text{CH}_3\text{I})_{350} = (1.95 \pm 0.68) \times 10^{-17}$  and  $\sigma(\text{C}_2\text{H}_5\text{I})_{365} = (1.35 \pm 0.47) \times 10^{-17}$ .

The shape of the spectra reported in this study suggests that three different electronic states of RI-Cl are excited by photon absorption in the 310–500 nm wavelength range. Electronic excitation energies and oscillator strengths for  $\text{CH}_3\text{I-Cl}$  and  $\text{C}_2\text{H}_5\text{I-Cl}$  have been evaluated theoretically by Enami et al. (2005a). For both RI-Cl species, two strong absorption bands with similar oscillator strengths are predicted, one at  $\lambda \sim 340$  nm and one at  $\lambda \sim 310$  nm. Our spectra at  $\lambda < 400$  nm are consistent with the theoretical results. However, we also observe evidence for a relatively weak transition at  $\lambda \sim 420$  nm that is not predicted theoretically. The calculations do predict electronic transitions at  $\lambda \sim 550$  nm, 960 nm, and 1080 nm that have little or no oscillator strength. Gravestock et al. (2008) have recently reported observation of laser induced fluorescence from  $\text{CH}_3\text{I-Cl}$  over the excitation wavelength range 345–375 nm. This interesting result

establishes that at least one and possibly both of the electronic states excited by near UV photons is/are bound.

The absorption cross sections reported in this study can be directly compared with those reported by Enami et al. (2005a, b) at the fixed wavelengths 405 nm, 435 nm, and 488 nm and over the range 440–500 nm. While the wavelength dependences of the cross-sections agree reasonably well, the cross-sections reported in this study are smaller than those reported by Enami et al. (2001a) by about a factor of four. Reasons for this discrepancy are not readily ascertainable at this time.

Enami et al. (2005a) attribute the absorption they observe at  $\lambda > 405$  nm to the red tail of short wavelength transitions at  $\sim 310$  nm and  $\sim 340$  nm that they predict theoretically. However, Gravestock et al. (2008) point out that the Enami et al. interpretation of the  $\text{CH}_3\text{I}-\text{Cl}$  absorption at  $\lambda > 405$  nm is almost certainly incorrect because (i) a 500 nm transition between two states with an energy separation of  $hc/\lambda$  with  $\lambda = 340$  nm requires  $9400\text{ cm}^{-1}$  of ground state excitation where an infinitesimal Boltzmann population would be present and (ii) even if the adduct ground state distribution were non-thermal, the required internal excitation is significantly larger than the well-established  $\text{CH}_3\text{I}-\text{Cl}$  bond strength (Ahyens et al., 1997; Lazarou et al., 1997). The above analysis further supports the existence of an electronic state at  $\lambda > 400$  nm that is not predicted in the theoretical analysis of Enami et al., 2005a.

Based on ab initio calculations at the Becke 3LYP/ECP level, structures for  $\text{CH}_3\text{I}$ ,  $\text{CH}_3\text{I}-\text{Cl}$ ,  $\text{C}_2\text{H}_5\text{I}$ , and  $\text{C}_2\text{H}_5\text{I}-\text{Cl}$  were derived (Ahyens et al., 1997; Orlando et al., 2005) and are shown in Figures 4.4 and 4.5.

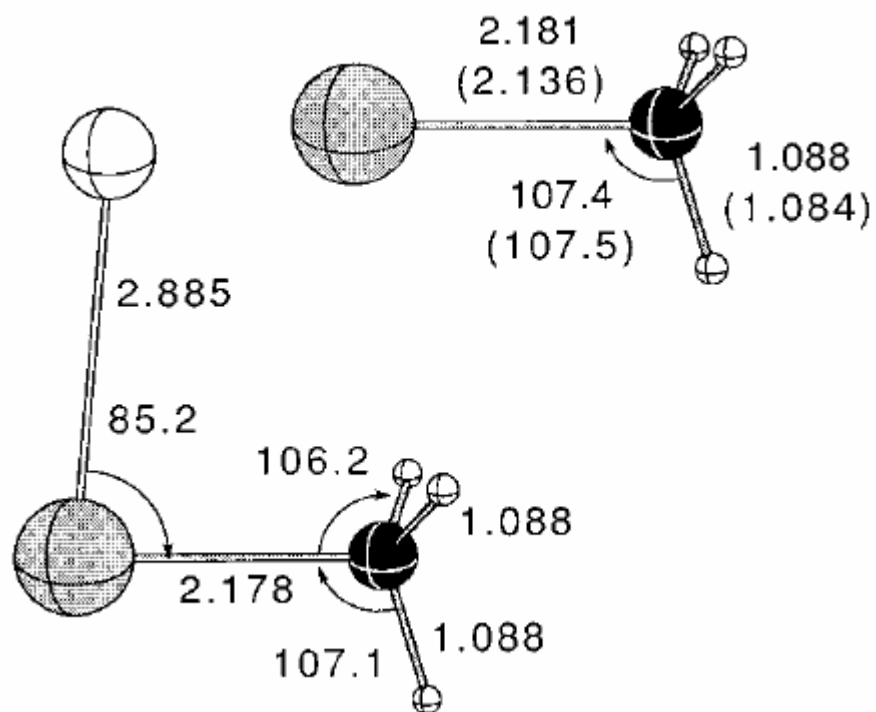
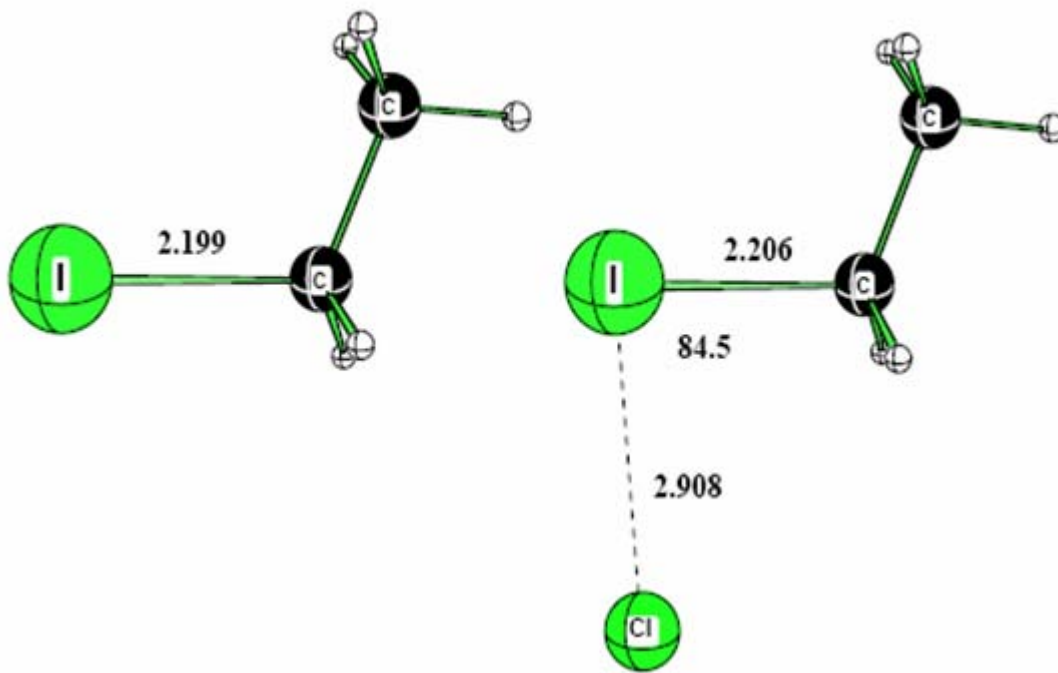


Figure 4.4 Structures for  $\text{CH}_3\text{I}$  and  $\text{CH}_3\text{I-Cl}$  derived from *ab initio* calculations at the B3LYP/ECP level (Ahyens et al., 1997). Bond lengths given in Å units.

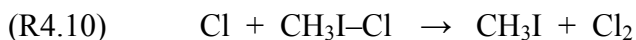


**Figure 4.5** Structures for  $C_2H_5I$  and  $C_2H_5I-Cl$  derived from *ab initio* calculations at the B3LYP/ECP level (Orlando et al., 2005). Bond lengths given in Å units.

In both of these alkyl iodides, bonding of Cl to I results in (i) a slight contraction of the I–Cl bond and (ii) a staggering of the methyl group in the Cl–I–R combination with a pronounced tilt towards chlorine. This tilt along with the findings of an electron population density inspection around the Cl lone pair orbital and the empty  $\pi^*$  combination on CH<sub>3</sub> provides evidence of a stabilizing hyperconjugative interaction (Radom, 1982).

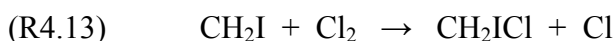
#### Radical-Radical Reaction Kinetics

When reaction mixtures containing only Cl<sub>2</sub>, CH<sub>3</sub>I, and N<sub>2</sub> are subjected to 308 nm laser flash photolysis and detectable levels of CH<sub>3</sub>I–Cl are generated, we expect that CH<sub>3</sub>I–Cl loss will be controlled by the following radical-radical reactions:



The products identified in reactions (R4.9–R4.12) above are the probable dominant products but not necessarily the only products that are energetically feasible. The Cl self-reaction is very slow and, therefore, is not listed above. If experimental conditions are adopted where  $T = 250 \text{ K}$ ,  $P = 300 \text{ Torr N}_2$ ,  $[\text{Cl}_2] = (1\text{--}3) \times 10^{15} \text{ molecules cm}^{-3}$ , and  $[\text{CH}_3\text{I}] > 1 \times 10^{15} \text{ molecules cm}^{-3}$ , then Cl reacts rapidly with CH<sub>3</sub>I to form ~98% CH<sub>3</sub>I–Cl and ~2% CH<sub>2</sub>I (Ahyens et al., 1997), the equilibrium concentration ratio [CH<sub>3</sub>I–

$\text{Cl}]/[\text{Cl}]$  is  $> 140$  (Ahyens et al., 1997), and the concentration of  $\text{CH}_3$  produced from  $\text{CH}_3\text{I}$  photolysis is typically only a few percent of the concentration of  $\text{Cl}$  produced from  $\text{Cl}_2$  photolysis. Under such conditions, loss of  $\text{CH}_3\text{I}-\text{Cl}$  is expected to be controlled by reaction (R4.9). Minor secondary production of  $\text{Cl}$  is expected via reactions (R4.8) and (R4.13), but the impact of these reactions on the derived value for  $k_{4.9}$  is expected to be an insignificant source of uncertainty compared to the uncertainty in  $[\text{CH}_3\text{I}-\text{Cl}]$ .



Values for  $k_{4.8}(250 \text{ K})$  and  $k_{4.13}(250 \text{ K})$  in units of  $10^{-13} \text{ cm}^3 \text{ molecule}^{-1} \text{ s}^{-1}$  are estimated based on literature data at  $T \geq 298 \text{ K}$ , (Timonen and Gutman, 1986; Seetula et al., 1991) to be 17 and 8, respectively.

To experimentally determine  $k_{4.9}$  at  $T = 250 \text{ K}$  and  $P = 300 \text{ Torr}$ , experiments were carried out using (in units of  $10^{15} \text{ molecules cm}^{-3}$ )  $[\text{CH}_3\text{I}] = (1.0-5.4)$  and  $[\text{Cl}_2] = (1.0-3.5)$ . Shown in Figure 4.6 is a typical  $\text{CH}_3\text{I}-\text{Cl}$  temporal profile observed at a monitoring wavelength of 380 nm. The data are plotted as  $[\text{CH}_3\text{I}-\text{Cl}]^{-1}$  vs. time. The linearity of the plot is consistent with the hypothesis that adduct loss is dominated by reaction (R4.9), and the self-reaction rate coefficient,  $2k_{4.9}$ , is obtained from the slope of the plot. Second order rate coefficients obtained from several experiments over the ranges of  $[\text{Cl}_2]$  and  $[\text{CH}_3\text{I}]$  specified above, but at constant laser power, are in good agreement, and give the following mean value for the self-reaction rate coefficient:  $2k_{4.9} = (3.49 \pm 0.24) \times 10^{-10} \text{ cm}^3 \text{ molecule}^{-1} \text{ s}^{-1}$ , where the uncertainty is  $2\sigma$  and represents precision only.

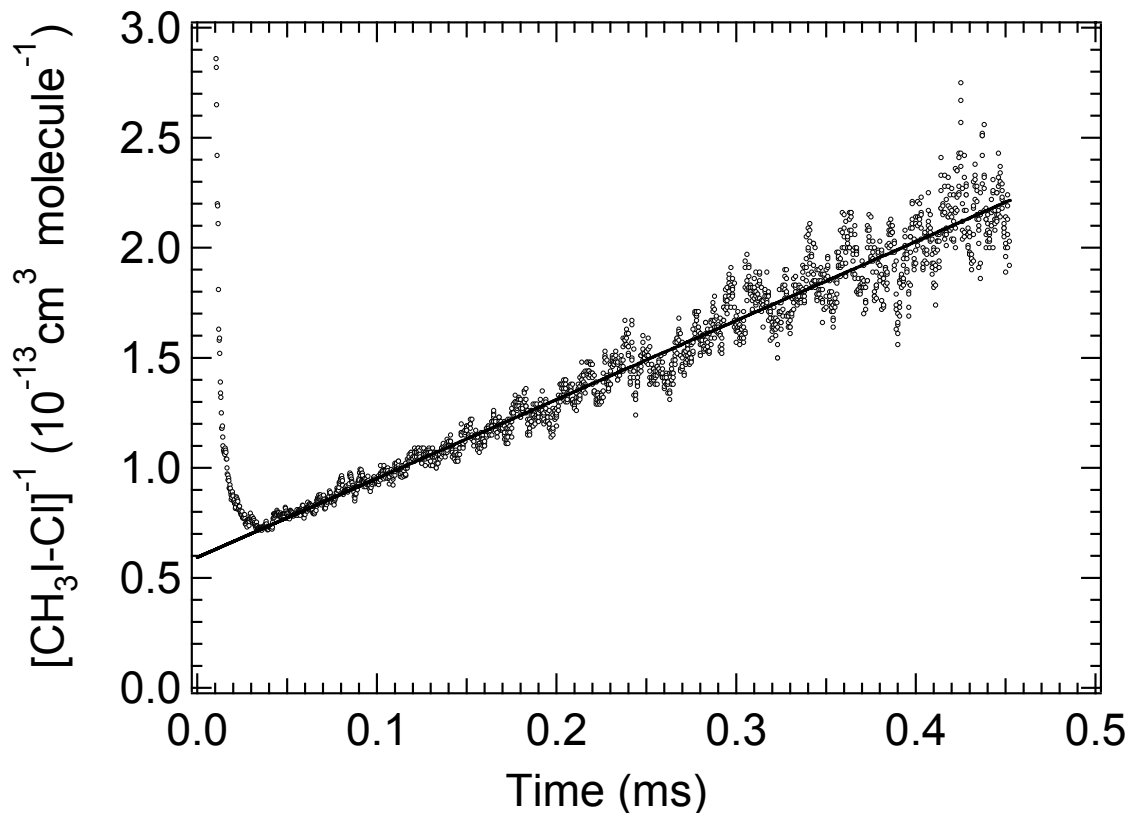
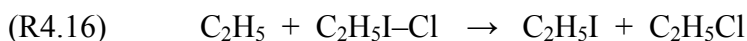
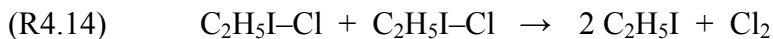


**Figure 4.6** Typical RI-Cl absorbance temporal profile plotted as  $[\text{RI-Cl}]^{-1}$  vs. time. Experimental conditions:  $T = 250 \text{ K}$ ;  $P = 300 \text{ Torr N}_2$ ;  $R = \text{CH}_3$ ; concentrations in units of  $10^{15} \text{ molecules cm}^{-3} = 5.43 \text{ CH}_3\text{I}$  and  $1.34 \text{ Cl}_2$ . The solid line is obtained from a linear least squares analysis; its slope gives  $2k_{4.9} = (3.44 \pm 0.02) \times 10^{-10} \text{ cm}^3 \text{ molecule}^{-1} \text{ s}^{-1}$  where the uncertainty is  $2\sigma$  and represents precision only.

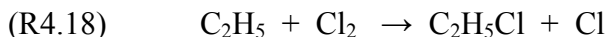
The accuracy of the derived value for  $2k_{4,9}$  is limited by the accuracy of  $[\text{CH}_3\text{I}-\text{Cl}]$ , which in turn is limited by the accuracy of the  $\text{CH}_3\text{I}-\text{Cl}$  absorption cross section at the monitoring wavelength (380 nm), i.e.,  $\pm 35\%$  (see above). Taking the  $\text{CH}_3\text{I}-\text{Cl}$  absorption cross section and imprecision to be the two main sources of uncertainty, we report  $2k_{4,9} = (3.5 \pm 1.2) \times 10^{-10} \text{ cm}^3 \text{ molecule}^{-1} \text{ s}^{-1}$ , where the uncertainty represents estimated accuracy at the 95% confidence level.

When reaction mixtures containing only  $\text{Cl}_2$ ,  $\text{C}_2\text{H}_5\text{I}$ , and  $\text{N}_2$  are subjected to 308 nm laser flash photolysis and detectable levels of  $\text{C}_2\text{H}_5\text{I}-\text{Cl}$  are generated, we expect that  $\text{C}_2\text{H}_5\text{I}-\text{Cl}$  loss will be controlled by the following radical-radical reactions:



If experimental conditions are adopted where  $T = 250 \text{ K}$ ,  $P = 300 \text{ Torr N}_2$ ,  $[\text{Cl}_2] = (1-3) \times 10^{15} \text{ molecules cm}^{-3}$ , and  $[\text{C}_2\text{H}_5\text{I}] > 5 \times 10^{14} \text{ molecules cm}^{-3}$ , then Cl reacts rapidly with  $\text{C}_2\text{H}_5\text{I}$  to form  $\sim 90\%$   $\text{C}_2\text{H}_5\text{I}-\text{Cl}$ ,  $\sim 7\%$   $\text{CH}_3\text{CHI}$  and  $\sim 3\%$   $\text{CH}_2\text{CH}_2\text{I}$ , (Orlando et al., 2005), the equilibrium concentration ratio  $[\text{C}_2\text{H}_5\text{I}-\text{Cl}]/[\text{Cl}]$  is  $> 260$ , (Orlando et al., 2005), and the concentration of  $\text{C}_2\text{H}_5$  produced from  $\text{C}_2\text{H}_5\text{I}$  photolysis is very small compared to the concentration of Cl produced from  $\text{Cl}_2$  photolysis. Under such conditions, loss of  $\text{C}_2\text{H}_5\text{I}-\text{Cl}$  is expected to be controlled predominantly by reaction (R4.14). Minor secondary production of Cl is expected via reactions (R4.18) and (R4.19), but the impact of these

reactions on the derived value for  $k_{4.14}$  is expected to be a small source of uncertainty compared to the uncertainty in  $[\text{C}_2\text{H}_5\text{I}-\text{Cl}]$ .



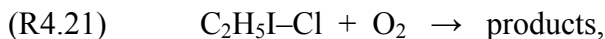
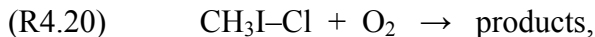
Based on literature data at  $T \geq 298$  K,  $k_{4.18}(250 \text{ K})$  is estimated to be  $2.3 \times 10^{-11} \text{ cm}^3 \text{ molecule}^{-1} \text{ s}^{-1}$  (Timonen and Gutman, 1986). To our knowledge, no kinetic data for reaction (R4.19) are reported in the literature. No Cl is regenerated from secondary chemistry involving the second H-transfer product,  $\text{CH}_2\text{CH}_2\text{I}$ , because this species rapidly decomposes to  $\text{I} + \text{C}_2\text{H}_4$  (Orlando et al., 2005).

To experimentally determine  $k_{4.14}$  at  $T = 250$  K and  $P = 300$  Torr, experiments were carried out using (in units of  $10^{15} \text{ molecules cm}^{-3}$ )  $[\text{C}_2\text{H}_5\text{I}] = (0.64 - 2.17)$  and  $[\text{Cl}_2] = (0.95 - 4.01)$ . As was observed for loss of  $\text{CH}_3\text{I}-\text{Cl}$ , (Figure 4.6), plots of  $[\text{C}_2\text{H}_5\text{I}-\text{Cl}]^{-1}$  vs. time were linear over 2–3 half-lives of decay, i.e., second order kinetics were obeyed. Values for  $k_{4.14}$  were obtained under the assumption that only reaction (R4.14) contributes to the observed decay of absorbance; as discussed above this assumption is likely to be pretty good, although small contributions from reactions (R4.15–R4.17) cannot be completely ruled out. Second order rate coefficients were obtained from the slopes of the  $[\text{C}_2\text{H}_5\text{I}-\text{Cl}]^{-1}$  vs. time plots for several experiments at constant laser power, but over the ranges of  $[\text{Cl}_2]$  and  $[\text{C}_2\text{H}_5\text{I}]$  specified above. The results are quite reproducible, and give the following mean value for the self reaction rate coefficient:  $2k_{4.14} = (3.97 \pm 0.40) \times 10^{-10} \text{ cm}^3 \text{ molecule}^{-1} \text{ s}^{-1}$ , where the uncertainty is  $2\sigma$  and represents precision only. The accuracy of the derived value for  $2k_{4.14}$  is limited by the

accuracy of  $[\text{C}_2\text{H}_5\text{I-Cl}]$ , which in turn is limited by the accuracy of the  $\text{C}_2\text{H}_5\text{I-Cl}$  absorption cross-section at the monitoring wavelength (365 nm or 380 nm), i.e.,  $\pm 35\%$  (see above). Taking the  $\text{C}_2\text{H}_5\text{I-Cl}$  absorption cross-section and imprecision to be the two main sources of uncertainty, leads to the result  $2k_{4.14} = (3.97 \pm 1.39) \times 10^{-10} \text{ cm}^3 \text{ molecule}^{-1} \text{ s}^{-1}$ . In this case a small but non-negligible additional uncertainty arises from the potential impacts of secondary chemistry on the derived value for  $k_{4.14}$ . Hence, we report the rate coefficient  $2k_{4.14} = (4.0 \pm 1.6) \times 10^{-10} \text{ cm}^3 \text{ molecule}^{-1} \text{ s}^{-1}$ , where the uncertainty represents an estimate of accuracy at the 95% confidence level.

#### Kinetics of RI-Cl Reactions with $\text{O}_2$ and RI

To investigate the kinetics of the reaction of RI-Cl with  $\text{O}_2$ , RI-Cl absorbance temporal profiles were measured in 300 Torr of  $\text{O}_2$  with experimental conditions adjusted to high  $[\text{RI}]$  and low  $[\text{Cl}]_0$  in order to minimize the contribution of radical-radical reactions to RI-Cl removal.



Little or no reaction of RI-Cl with  $\text{O}_2$  was observed at  $T \sim 250 \text{ K}$ . In order to establish upper limits for  $k_{4.20}$  and  $k_{4.21}$ , back-to-back experiments were carried out where experimental conditions were held constant except that  $\text{N}_2$  and  $\text{O}_2$  were interchanged as the bath gas. Plots of  $\ln A$  vs time for one set of back-to-back experiments aimed at evaluating  $k_{4.20}$  are shown in Figure 4.7. Plots of  $\ln A$  vs. time are nonlinear in both  $\text{N}_2$  and  $\text{O}_2$  in a manner that suggests the dominance of radical-radical reactions controlling  $\text{CH}_3\text{I-Cl}$  removal, particularly at short times after the laser flash when the adduct

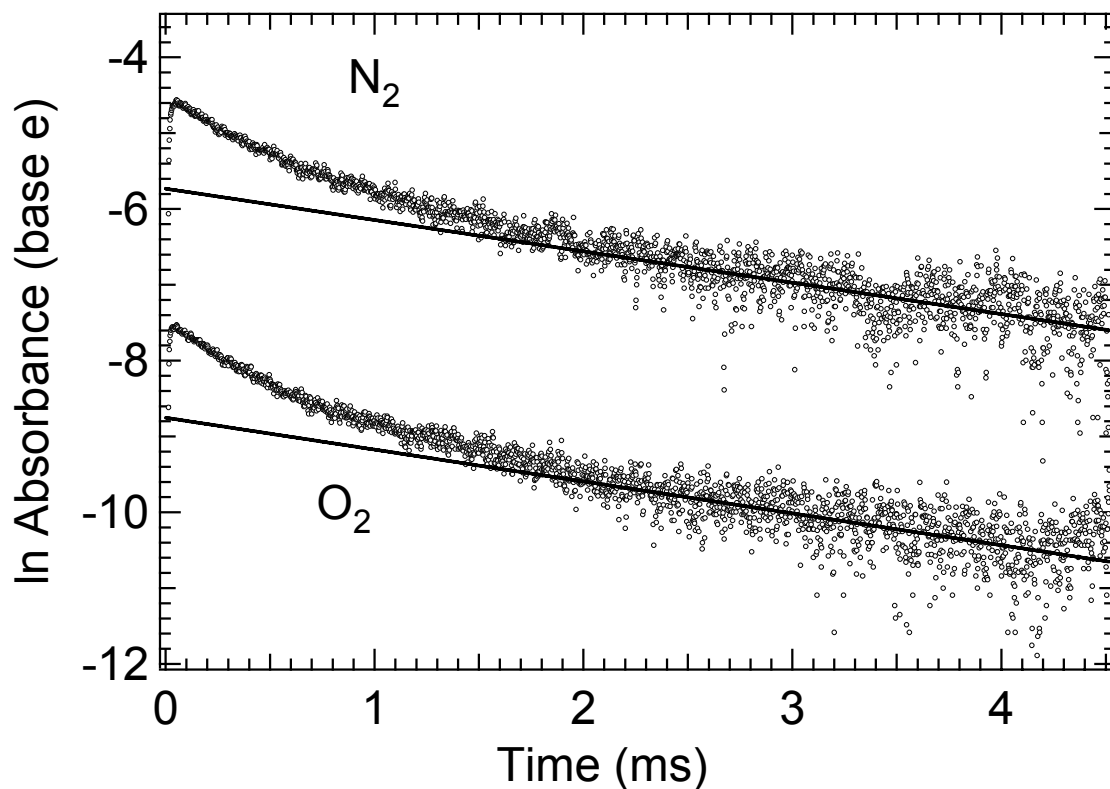


**Figure 4.7 Comparison of CH<sub>3</sub>I absorbance temporal profiles observed at T = 250 K and P = 300 Torr in N<sub>2</sub> vs. O<sub>2</sub> bath gas.** The CH<sub>3</sub>I concentration was  $4.4 \times 10^{15}$  molecules cm<sup>-3</sup> in both experiments. Best fit slopes in units of s<sup>-1</sup> are  $413 \pm 15$  and  $420 \pm 16$  s<sup>-1</sup> for the data obtained in N<sub>2</sub> and O<sub>2</sub>, respectively, within the time intervals 2.0–4.5 ms after the laser flash (uncertainties are  $2\sigma$  and represent precision only). For the sake of clarity, the data obtained in O<sub>2</sub> has been offset downward by 3 units of  $\ln$  concentration.

concentration is relatively high. Linear least-squares analyses of the CH<sub>3</sub>I–Cl temporal profiles at 2 – 4.5 ms after the laser flash (Figure 4.7) give pseudo-first order decay rates ( $k_d$ ) of 413±17 s<sup>-1</sup> in 300 Torr N<sub>2</sub> and 420±17 s<sup>-1</sup> in 300 Torr O<sub>2</sub> (uncertainties are 2σ, precision only). Data analysis was restricted to times less than 4.5 ms after the laser flash because there was so little absorption at later times that quantitative kinetic analysis was precluded. Reactions (R4.9–R4.12), diffusion of RI–Cl out of the detection volume, and reaction of RI–Cl with background impurities in the bath gases may all contribute to the time evolution of absorbance for the data shown in Figure 4.7. However, temporal profiles observed in 300 Torr O<sub>2</sub> were indistinguishable from those observed in 300 Torr N<sub>2</sub> bath gas. Similar behavior was observed in analogous experiments where C<sub>2</sub>H<sub>5</sub>I–Cl temporal profiles were monitored. In order to put reasonable upper limits on  $k_{4.20}$  and  $k_{4.21}$ , it is necessary to consider the fact that secondary chemistry is not identical in N<sub>2</sub> and O<sub>2</sub> bath gases. In O<sub>2</sub>, the H-abstraction products CH<sub>2</sub>I and CH<sub>3</sub>CHI as well as the alkyl radicals CH<sub>3</sub> and C<sub>2</sub>H<sub>5</sub> (produced from 308 nm photolysis of CH<sub>3</sub>I and C<sub>2</sub>H<sub>5</sub>I, respectively) react with O<sub>2</sub> to produce species that are less reactive than their radical precursors. The alkyl radicals CH<sub>3</sub> and C<sub>2</sub>H<sub>5</sub> are converted to peroxy radicals. It is reported in the literature that the dominant channel for the reaction of CH<sub>2</sub>I with O<sub>2</sub> is production of IO + H<sub>2</sub>CO (Enami et al., 2004), although recent (currently unpublished) new results bring this conclusion into question (Gravestock, 2006). At present, there appears to be insufficient information to establish yields of CH<sub>3</sub>CHIOO and IO + CH<sub>3</sub>CHO from the CH<sub>3</sub>CHI + O<sub>2</sub> reaction (Orlando et al., 2005). It is possible (though unlikely) that, in the presence of O<sub>2</sub>, some reduction in the rates of loss of CH<sub>3</sub>I–Cl via

reactions (R4.10–R4.12) and C<sub>2</sub>H<sub>5</sub>I–Cl via reactions (R4.15–R4.17) is compensated for by very slow but non-zero rates of reaction of RI–Cl with O<sub>2</sub>. Taking this potential complication into account, the results of 12 back-to-back experiments like the ones shown in Figure 4.7 for CH<sub>3</sub>I–Cl and 25 analogous back-to-back experiments for C<sub>2</sub>H<sub>5</sub>I–Cl lead to the following conservative upper limits for  $k_{4.20}$  and  $k_{4.21}$  at  $P = 300$  Torr and  $T = 250$  K in units of  $10^{-17}$  cm<sup>3</sup> molecule<sup>-1</sup> s<sup>-1</sup>:  $k_{4.20} < 1.0$  and  $k_{4.21} < 2.5$ .

Product studies conducted by Bilde and Wallington (1998) and by Orlando et al. (2005) provide evidence for the occurrence of reactions (R4.3) and (R4.5). Orlando et al. (2005) have modeled the kinetics in the two experiments (Ahyens et al., 1997; Orlando et al., 2005) based on reasonable assumed reaction mechanisms, and obtain the estimates  $k_{4.3}(298 \text{ K}) = (5\text{--}10) \times 10^{-13}$  cm<sup>3</sup> molecule<sup>-1</sup> s<sup>-1</sup> and  $k_{4.5}(298 \text{ K}) = (2\text{--}5) \times 10^{-13}$  cm<sup>3</sup> molecule<sup>-1</sup> s<sup>-1</sup>.

We were unable to observe strong evidence for the occurrence of RI + RI–Cl reactions, but our data do allow upper limits for  $k_{4.3}$  and  $k_{4.5}$  at 250 K to be deduced. Our approach involves kinetic simulations of the data in N<sub>2</sub> bath gas that were employed to evaluate RI + O<sub>2</sub> rate coefficients; as mentioned above, these data were obtained under experimental conditions where radical concentrations were lower than in the experiments aimed at investigating radical-radical reaction kinetics. The simulations employ simple two reaction schemes: Reactions (R4.3) and (R4.9) for the methyl iodide data and reactions (R4.5) and (R4.14) for the ethyl iodide data. A typical result for the methyl iodide case is shown in Figure 4.8, where the data are plotted as [CH<sub>3</sub>I–Cl]<sup>-1</sup> vs. time. Even at the relatively low radical concentrations employed to obtain the data in Figure 4.8, the data are well simulated assuming the value for  $2k_{4.9}$  obtained as described above

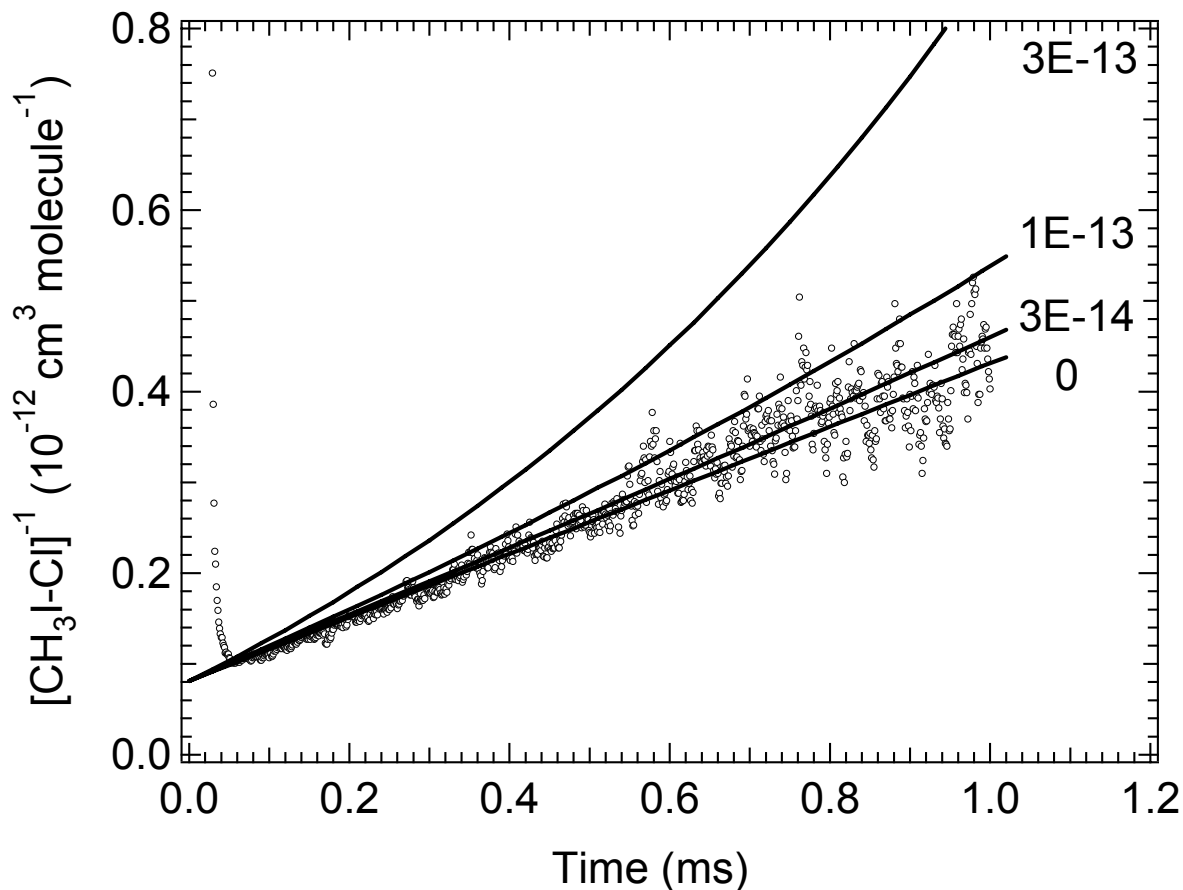
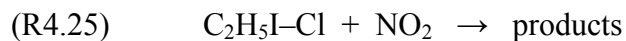
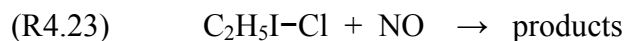


**Figure 4.8**  $\text{CH}_3\text{I-Cl}$  absorbance temporal profile plotted as  $[\text{CH}_3\text{I-Cl}]^{-1}$  vs. time. Experimental conditions:  $T = 250$  K;  $P = 300$  Torr  $\text{N}_2$ ; concentrations in units of  $10^{14}$  molecules  $\text{cm}^{-3} = 36.6$   $[\text{CH}_3\text{I}]$ ,  $9.81$   $[\text{Cl}_2]$ , and  $\sim 0.10$   $[\text{Cl}]_0$ . The straight line represents simulation of the  $[\text{CH}_3\text{I-Cl}]^{-1}$  vs. time plot expected for  $2k_{4,9} = 3.5 \times 10^{-10}$   $\text{cm}^3$  molecule $^{-1}$   $\text{s}^{-1}$  and  $k_{4,3} = 0$ . The curved lines are simulations of the  $[\text{CH}_3\text{I-Cl}]^{-1}$  vs. time plots expected if  $k_{4,3}$  had the values shown in the figure (in units of  $\text{cm}^3$  molecule $^{-1}$   $\text{s}^{-1}$ ).

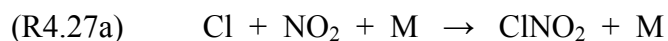
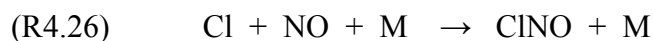
and assuming that  $k_{4,3} = 0$ . The simulations suggest that upward curvature in the  $[\text{CH}_3\text{I}-\text{Cl}]^{-1}$  vs. time plot would be readily observable if  $k_{4,3} \geq 1.5 \times 10^{-13} \text{ cm}^3 \text{ molecule}^{-1} \text{ s}^{-1}$ , so we adopt this value as a conservative upper limit. A similar analysis of the ethyl iodide data suggests that  $k_{4,5} \leq 5 \times 10^{-13} \text{ cm}^3 \text{ molecule}^{-1} \text{ s}^{-1}$ . Direct comparison of our results with literature values is hampered by the fact that our data were obtained at 250 K whereas most previous results (Ahyens et al., 1997; Orlando et al., 2005) were obtained at 298 K. At 250 K, the upper limit value for  $k_3$  obtained in this study is lower than the suggested range of values for  $k_{4,3}$  at 298 K that are consistent with Orlando et al. (2005) analysis of the results of Bilde and Wallington (1998). In their studies at 216 K and 296 K using LIF detection of  $\text{CH}_3\text{I}-\text{Cl}$ , Gravestock et al. (2008) conclude that  $\text{CH}_3\text{I}-\text{Cl}$  decay can be completely attributed to radical-radical reactions, i.e., in agreement with our findings, they obtain no compelling evidence for the occurrence of the  $\text{CH}_3\text{I}-\text{Cl} + \text{CH}_3\text{I}$  reaction.

#### Kinetics of RI-Cl Reactions with NO and NO<sub>2</sub>

The reactions of RI-Cl with NO and NO<sub>2</sub> were studied at  $T = 250 \text{ K}$  and  $P = 300 \text{ Torr}$  (N<sub>2</sub> bath gas) under pseudo-first order conditions with  $[\text{NO}_x] \gg [\text{RI}-\text{Cl}]$ .



The reagent concentrations (units are  $10^{14}$  molecules  $\text{cm}^{-3}$ ) used in experiments investigating reactions (R4.22) and (R4.24) were as follows:  $[\text{Cl}_2] = (5.4\text{--}10.0)$ ;  $[\text{Cl}]_0 = (0.05\text{--}0.07)$ ;  $[\text{CH}_3\text{I}] = (48\text{--}56)$ ;  $[\text{NO}] = (1.13\text{--}11.0)$ ;  $[\text{NO}_2] = (0.866\text{--}7.42)$ . For studies of reactions (R4.23) and (R4.25), the following concentrations were employed (units are  $10^{14}$  molecules  $\text{cm}^{-3}$ ):  $[\text{Cl}_2] = (9.0\text{--}10.1)$ ;  $[\text{Cl}]_0 = (0.08\text{--}0.28)$ ;  $[\text{C}_2\text{H}_5\text{I}] = (15\text{--}16)$ ;  $[\text{NO}] = (0.612\text{--}10.8)$ ;  $[\text{NO}_2] = (2.33\text{--}6.69)$ . Relatively low radical concentrations were employed in order to minimize the effect of radical-radical side reactions on the observed absorbance temporal profiles. Experimental conditions of high  $[\text{RI}] (> 10^{15}$  molecules  $\text{cm}^{-3})$  and low temperature (250 K) minimized the contribution of Cl reactions with NO and  $\text{NO}_2$  to observed RI–Cl kinetics by driving the  $\text{RI–Cl} \leftrightarrow \text{Cl}$  equilibria to over 99% adduct (Ahyens et al., 1997; Orlando et al., 2005).



As typified by the data shown in Figure 4.9, absorbance decays were exponential, i.e., plots of  $\ln A$  vs. time were linear, as would be expected under the experimental conditions employed (see above). Measured pseudo-first order decay rates ( $k_d$ ), obtained from the slopes of plots like the one shown in Figure 4.9, are plotted as a function of  $[\text{RI}]$  in Figures 4.10 and 4.11. The slopes of the  $k_d$  vs.  $[\text{RI}]$  plots give the following second order rate coefficients in units of  $10^{-11}$   $\text{cm}^3$  molecule $^{-1}$  s $^{-1}$  (uncertainties are  $2\sigma$  and represent precision only):  $k_{4.22} = 1.81 \pm 0.28$ ,  $k_{4.24} = 3.26 \pm 0.48$ ,  $k_{4.23} = 1.78 \pm 0.14$ , and  $k_{4.25} = 4.02 \pm 0.93$ .

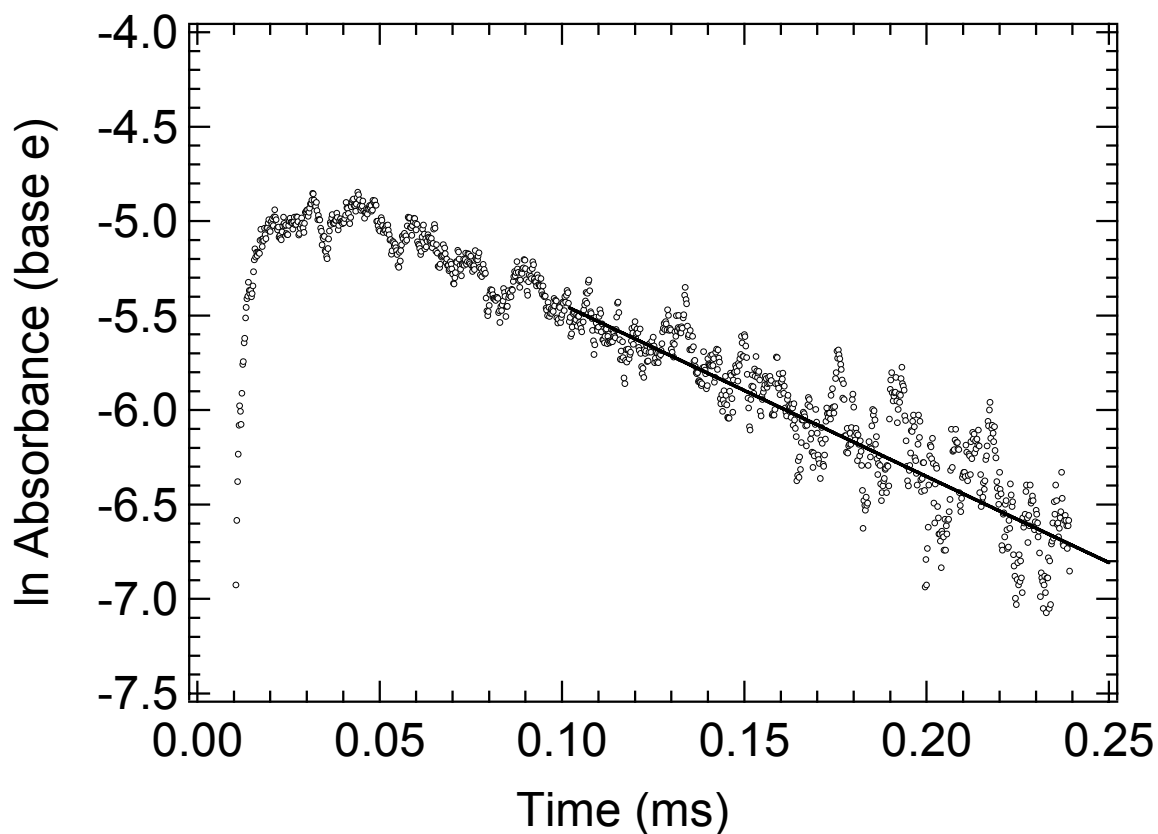


**Figure 4.9** Typical absorbance temporal profile observed following 308 nm laser flash photolysis of  $\text{Cl}_2/\text{RI}/\text{NO}_x/\text{N}_2$  mixtures at  $T = 250 \text{ K}$  and  $P = 300 \text{ Torr}$ . The data shown were obtained with  $\text{NO}_x = \text{NO}$  and  $\text{R} = \text{CH}_3$ . Concentrations in units of  $10^{14}$  molecules  $\text{cm}^{-3}$  are  $[\text{CH}_3\text{I}] = 56.2$ ,  $[\text{NO}] = 3.92$ ,  $[\text{Cl}_2] = 5.19$ , and  $[\text{Cl}]_0 \approx 0.05$ . The solid line is obtained from a linear least squares analysis of the  $\ln$  absorbance vs. time ( $t$ ) data at  $t > 100 \mu\text{s}$  after the laser flash; its slope gives the pseudo-first order decay rate  $9020 \text{ s}^{-1}$ .

For  $[Cl]_0 \sim 1 \times 10^{13}$  per  $cm^3$  (see above), reactions (R4.9) and (R4.14) make small but significant contributions to RI-Cl adduct removal. As a result, pseudo-first order decay rates were obtained from the slopes of plots like the one shown in Figure 4.9 using only data obtained at times where  $A < 0.004$  (i.e.,  $[RI-Cl] < 2 \times 10^{12}$  molecules per  $cm^3$ ). Based on the above discussion of radical-radical reaction kinetics, we consider the contribution of reactions (R4.9) and (R4.14) insignificant when  $[RI-Cl] < 2 \times 10^{12}$  molecules per  $cm^3$ . Since side reactions have little or no impact on the accuracy of the reported rate coefficients, it appears that accuracy is limited by precision and by the accuracy with which the concentrations of NO and NO<sub>2</sub> were known (estimated to be  $\pm 5\%$  for each). Hence, we report the following rate coefficients in units of  $10^{-11} \text{ cm}^3 \text{ molecule}^{-1} \text{ s}^{-1}$ :  $k_{4.22} = 1.8 \pm 0.4$ ,  $k_{4.24} = 3.3 \pm 0.6$ ,  $k_{4.23} = 1.8 \pm 0.3$  and  $k_{4.25} = 4.0 \pm 0.9$ ; the uncertainties are estimates of accuracy at the 95% confidence level.

Although there are no other reported measurements of  $k_{4.22} - k_{4.25}$  with which to compare our results, it is of interest to note that the rate coefficients reported in this study are very similar in magnitude to rate coefficients for the reactions of  $(CH_3)_2S-Cl$  (Urbanski and Wine, 1999),  $SCS-Cl$ , (Dookwah-Roberts et al., 2005 and Chapter 3 of this dissertation), and  $CH_3(O)S(Cl)CH_3$  (Kleissas et al., 2007), with NO and NO<sub>2</sub>, all of which were measured using an analogous technique to the one employed in this study. All  $X-Cl + NO_x$  ( $X = (CH_3)_2S, SCS, (CH_3)_2SO, CH_3I, C_2H_5I$ ) rate coefficients are within the range  $(1-4) \times 10^{-11} \text{ cm}^3 \text{ molecule}^{-1} \text{ s}^{-1}$  and reactivity of these adducts with O<sub>2</sub> is not observed.

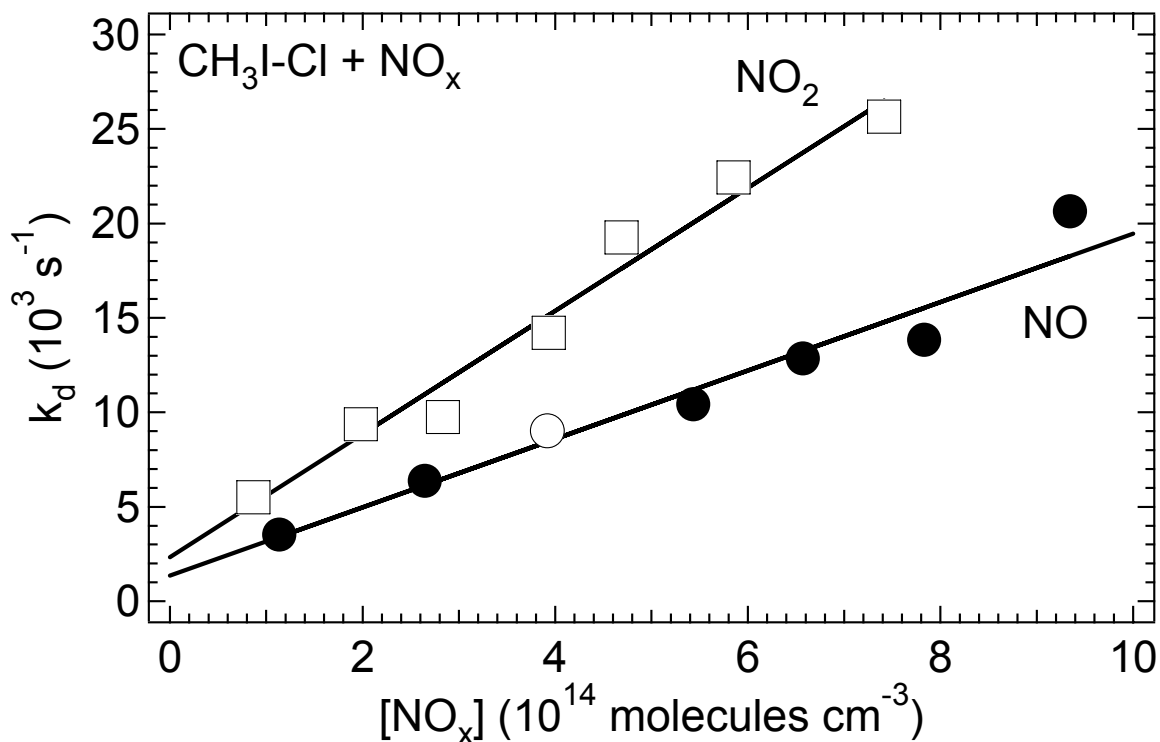


**Figure 4.10** Plots of pseudo-first-order  $\text{CH}_3\text{I-Cl}$  decay rates ( $k_d$ ) versus  $[\text{NO}_x]$  for data obtained at  $T = 250 \text{ K}$  and  $P = 300 \text{ Torr N}_2$ . The solid lines are obtained from linear least-squares analyses; their slopes give the following rate coefficients in units of  $10^{-11} \text{ cm}^3 \text{ molecule}^{-1} \text{ s}^{-1}$  (uncertainties are  $2\sigma$  and represent precision only):  $k_{4,22} = 1.81 \pm 0.28$  and  $k_{4,24} = 3.26 \pm 0.48$ . The open data point is the one obtained from the data shown in Figure 4.7.

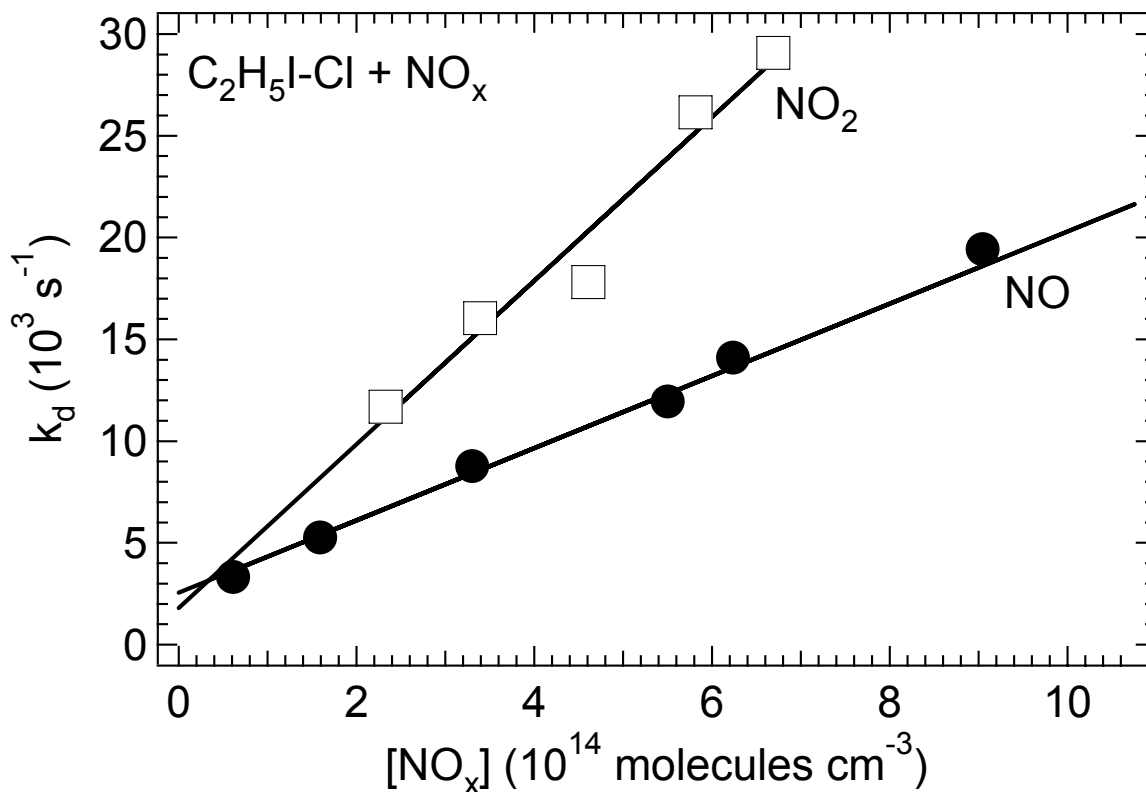


**Figure 4.11** Plots of pseudo-first-order  $\text{C}_2\text{H}_5\text{I-Cl}$  decay rates ( $k_d$ ) versus  $[\text{NO}_x]$  for data obtained at  $T = 256 \text{ K}$  and  $P = 300 \text{ Torr N}_2$ . The solid lines are obtained from linear least-squares analyses; their slopes give the following rate coefficients in units of  $10^{-11} \text{ cm}^3 \text{ molecule}^{-1} \text{ s}^{-1}$  (uncertainties are  $2\sigma$  and represent precision only):  $k_{4.23} = 1.78 \pm 0.14$  and  $k_{4.25} = 4.02 \pm 0.93$ .

It appears that Cl adducts react rapidly with compounds like NO and NO<sub>2</sub>, where transfer of the chlorine atom to generate ClNO, ClNO<sub>2</sub>, or ClONO is energetically favorable. Because Cl–OO is bound by only 19 kJ mol<sup>-1</sup> (Nicovich et al., 1990), the chlorine transfer reaction between the above-mentioned adducts and O<sub>2</sub> cannot occur at a significant rate at T < 300 K.

### Atmospheric Implications

Alkyl iodides are removed from the atmosphere predominantly by photolysis, reaction with OH radicals, and reaction with Cl atoms. Table 4.2 lists 298 K rate coefficients for reactions of CH<sub>3</sub>I and C<sub>2</sub>H<sub>5</sub>I with Cl and OH. Based on these rate coefficients, loss rates via these three routes for CH<sub>3</sub>I and C<sub>2</sub>H<sub>5</sub>I are given in Table 4.3. Wingenter et al. (2005) estimated that Cl atom concentrations vary from 5 – 500 x 10<sup>3</sup> atoms cm<sup>-3</sup>, with an average MBL concentration of ~ 4 x 10<sup>4</sup> atoms cm<sup>-3</sup>. Using the lower limit and average MBL concentrations, two loss rate scenarios have been derived in Table 4.3 in order to demonstrate the sensitivity of this oxidation pathway to Cl atom concentration. As shown in Table 4.3 and as mentioned previously, photolysis dominates atmospheric removal of these alkyl iodides, followed by reaction with OH radicals. However, using average MBL Cl atom concentrations we see that the Cl oxidation pathway of CH<sub>3</sub>I is equally as important as loss via OH oxidation. In the case of C<sub>2</sub>H<sub>5</sub>I, Cl oxidation is greater than OH oxidation by a factor of 2.5 – 21, depending on the Cl concentration used and can account for as much as 23% of C<sub>2</sub>H<sub>5</sub>I loss in the MBL *if* loss of C<sub>2</sub>H<sub>5</sub>I-Cl is dominated by processes that do not regenerate C<sub>2</sub>H<sub>5</sub>I. The results obtained in this study taken in conjunction with the kinetic and thermodynamic results reported by

**Table 4.2** Rate coefficients for the reactions of Cl and OH with CH<sub>3</sub>I and C<sub>2</sub>H<sub>5</sub>I used in construction of Table 4.3

<b>RI</b>	<b><i>k</i><sub>Cl</sub></b>	<b><i>k</i><sub>OH</sub></b>
CH <sub>3</sub> I	1.51 <sup>a</sup>	0.07 <sup>b</sup>
C <sub>2</sub> H <sub>5</sub> I	16 <sup>a</sup>	0.03 <sup>a</sup>

<sup>a</sup>Cotter et al. (2001); <sup>b</sup>Brown et al. (1990); *k*<sub>Cl</sub> and *k*<sub>OH</sub> (10<sup>-12</sup> cm<sup>3</sup> molecule<sup>-1</sup> s<sup>-1</sup>)

**Table 4.3 Rate of loss of CH<sub>3</sub>I and C<sub>2</sub>H<sub>5</sub>I under typical surface MBL conditions, with respect to photolysis and reaction with OH and Cl, using (a) concentrations of [OH] = 9 x 10<sup>5</sup> (Prinn et al., 2001); (b) [Cl] = 5 x 10<sup>3</sup>; and (c) [Cl] = 4 x 10<sup>4</sup> molecules cm<sup>-3</sup> (Wingenter et al., 2005)**

<b>RI</b>	<b>Photolysis<sup>a,b</sup></b>	<b>OH<sup>a</sup></b>	<b>Cl<sup>a</sup> scenario(a)</b>	<b>Cl<sup>a</sup> scenario (b)</b>
CH <sub>3</sub> I	1.7	0.06	0.008	0.06
C <sub>2</sub> H <sub>5</sub> I	2.1	0.03	0.08	0.64

<sup>a</sup>Loss rates units are: 1 x 10<sup>-6</sup> s<sup>-1</sup>; <sup>b</sup>Ref. Cotter et al. (2001)

Ahyens et al. (1997) and Orlando et al. (2005) allow us to examine the potential importance of the most likely tropospheric CH<sub>3</sub>I-Cl and C<sub>2</sub>H<sub>5</sub>I-Cl degradation pathways; these include photolysis, thermal dissociation, reaction with O<sub>2</sub>, and reaction with NO<sub>x</sub>.

The absorption cross sections reported in this study have been used along with tabulated actinic flux (F) data at the Earth's surface for best estimate of surface albedo supplied by Finlayson-Pitts and Pitts (2000), and an assumed quantum yield of unity for CH<sub>3</sub>I-Cl and C<sub>2</sub>H<sub>5</sub>I-Cl destruction (the maximum possible value) to obtain a maximum first order photolysis rate, J<sub>max</sub> for these adducts:

$$(Eq. 4.4) \quad J_{\max}(\theta) = \int \sigma(\lambda) F(\lambda, \theta) d\lambda$$

The parameter  $\theta$  in Eq. 4.4 is the solar zenith angle. We obtain  $J_{\max} = 2.73$  and  $1.74 \text{ s}^{-1}$  at  $\theta = 0^\circ$  and  $\theta = 60^\circ$  respectively for CH<sub>3</sub>I-Cl and  $J_{\max} = 2.69$  and  $1.74 \text{ s}^{-1}$  at  $\theta = 0^\circ$  and  $60^\circ$  respectively for C<sub>2</sub>H<sub>5</sub>I-Cl.

Temperature dependent rate coefficients for thermal dissociation of CH<sub>3</sub>I-Cl and C<sub>2</sub>H<sub>5</sub>I-Cl at atmospheric pressure have been estimated based on kinetic and thermodynamic results reported by Ahyens et al. (1997) and Orlando et al. (2005). At 298 K, the thermal dissociation rate coefficients for these adducts are  $\sim 8,000$  and  $10,000 \text{ s}^{-1}$  for CH<sub>3</sub>I-Cl and C<sub>2</sub>H<sub>5</sub>I-Cl respectively, whereas, at 250 K (average polar temperature in January is  $\sim 246 \text{ K}$ ), their thermal dissociation loss rates are  $73$  and  $1 \text{ s}^{-1}$ , respectively.

Mixing ratios of NO<sub>x</sub> in the remote MBL are only a few parts per trillion. Hence, reactions of CH<sub>3</sub>I-Cl and C<sub>2</sub>H<sub>5</sub>I-Cl with NO and NO<sub>2</sub> are potentially important only in relatively polluted coastal regions where NO<sub>x</sub> mixing ratios can be in the parts per billion

(ppb) range. For example, if one assumes 1 ppb  $\text{NO}_x$  ( $\sim 2.5 \times 10^{10}$  molecules  $\text{cm}^{-3}$  at atmospheric pressure and typical lower atmospheric temperatures) and a rate coefficient of  $2.7 \times 10^{-11}$   $\text{cm}^3$  molecule $^{-1}$  s $^{-1}$  for  $\text{RI-Cl} + \text{NO}_x$  (based on this work), a first order rate coefficient of 0.7 s $^{-1}$  is obtained for these adducts removal by  $\text{NO}_x$ . Using the upper limit rate coefficients of 1 and  $2.5 \times 10^{-17}$   $\text{cm}^3$  molecule $^{-1}$  s $^{-1}$  determined in this study for the  $\text{CH}_3\text{I-Cl} + \text{O}_2$  and  $\text{C}_2\text{H}_5\text{I-Cl} + \text{O}_2$  reactions respectively, leads to upper limit first order rate coefficients of 59 and 147 s $^{-1}$  for these adducts removal by  $\text{O}_2$  at atmospheric pressure and 250 K.

The analysis discussed above suggests that thermal dissociation of the  $\text{CH}_3\text{I-Cl}$  adduct dominates removal of this species even at low temperatures (250 K), however, in the case of  $\text{C}_2\text{H}_5\text{I-Cl}$  adduct, using the upper limit reaction rate with  $\text{O}_2$ , reaction (R4.21) can dominate removal of this species at 250 K. However, the actual rate coefficient,  $k_{4,21}$ , is probably significantly smaller than the upper limit value reported here and thermal dissociation is the likely dominant removal process for this species even at lower temperatures.

**CHAPTER 5**  
**SPECTROSCOPIC AND KINETIC STUDY OF THE GAS PHASE**  
**(CH<sub>3</sub>)<sub>2</sub>S–Br ADDUCT**

**Effect of Bromine on the Sulfur Cycle**

In the clean marine boundary layer (MBL), dimethylsulfide (DMS) emissions dominate as the source of atmospheric sulfur. As mentioned previously, OH, Cl, BrO and NO<sub>3</sub> are assumed to be the main oxidants for DMS and reaction with these oxidants can proceed by abstraction and/or addition. The importance of these oxidation pathways is based on the final products generated; H<sub>2</sub>SO<sub>4</sub>, produced mainly via the abstraction pathway, can lead to the production of new aerosols (von Glasow and Crutzen, 2004), whereas all other DMS products can only grow existing particles. The reaction of BrO with DMS can be a significant DMS sink (Toumi, 1994; von Glasow et al., 2004) and leads to the addition of oxygen to DMS. In the cloudy marine boundary layer (MBL) an increase in DMS oxidation by BrO can lead to the production of DMSO which is rapidly taken up by clouds. This reduces the DMS to SO<sub>2</sub> conversion efficiency, which is indicative of the potential for formation of new cloud condensation nuclei (CCN), but increases the size of already present CCN by the formation of particulate sulfur (methane sulfonic acid and sulfate) (von Glasow et al., 2002; von Glasow and Crutzen, 2004). This and other feedbacks like increased drizzle formation due to larger CCN would lead

to a reduction in cloud albedo. Boucher et al. (2003) performed a sensitivity study with a global model assuming a constant daytime BrO mixing ratio of 1 pmol mol<sup>-1</sup> in the MBL and found a reduction of tropospheric DMS burden by ~ 30%. In a model study using 24 hour average MBL “high latitude” and “tropics” BrO mixing ratios of 0.1 – 0.3 and 0.05 pmol mol<sup>-1</sup> respectively, performed by von Glasow et al. (2004), the tropospheric DMS burden is reduced due to the reaction of DMS + BrO by 26% and 6% in their scenarios of “high latitude” and “tropics” respectively.

Observations of very high BrO mixing ratios during ozone depletion events (ODEs) imply that this reaction probably dominates under such conditions, especially when OH and NO<sub>3</sub> concentrations are low (Saiz-Lopez et al., 2007).

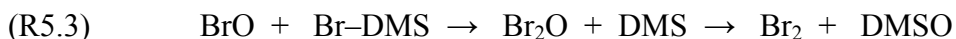


This reaction leads to Br production which, in the presence of DMS and under low temperature conditions, reacts rapidly with DMS:



For example, at 274 K and 600 Torr of N<sub>2</sub>, Wine et al. (1993) reported a rate constant,  $k_{5.12}$ , of  $1.2 \times 10^{-10} \text{ cm}^3 \text{ molecule}^{-1} \text{ s}^{-1}$  and extrapolation of their kinetic data to conditions typical of the springtime Arctic boundary layer (790 Torr, 230 – 270 K) suggests a rate constant for  $k_{5.2}$  of  $(1.3 \pm 0.2) \times 10^{-10} \text{ cm}^3 \text{ molecule}^{-1} \text{ s}^{-1}$ . The short lifetime of (CH<sub>3</sub>)<sub>2</sub>S–Br (Br–DMS) toward unimolecular decomposition and the very slow upper limit rate

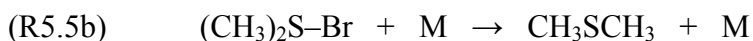
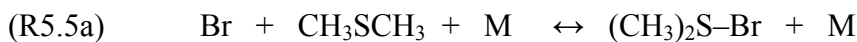
constant for the reaction of Br–DMS with O<sub>2</sub> (Wine et al., 1993) suggest that this species is of likely minor atmospheric importance. However, the reaction of Br atoms with DMS plays a significant role in conjunction with reaction (R5.1), and is believed to occur in two ways (Ingham et al., 1999):



Reaction (R5.2) also represents a major interference in any laboratory investigation of the very important reaction (R5.1). This laboratory coupling between Br–DMS adduct formation and BrO reaction with DMS led to our spectroscopic and kinetic study of the Br–DMS adduct.

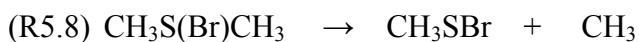
### **The Reaction of Bromine atoms with DMS**

It is well established that under atmospheric conditions, reaction of Br with DMS proceeds via reaction (R5.5), i.e., addition to the sulfur atom (Wine et al. 1993; Ingham et al., 1999; Nakano et al. 2001). Above 375 K, reactions (R5.6a) and (R5.6b), hydrogen abstraction has been shown to be the operative reaction pathway (Jefferson et al., 1994):



The first study of reactions (R5.5a) and (R5.5b) was conducted in our lab, using laser flash photolysis coupled with resonance fluorescence detection of Br atoms (LFP/RF) (Wine et al., 1993); equilibration kinetics for these reactions were investigated in the temperature regime 260 – 310 K and over the pressure range 25 – 600 Torr. A 298 K bond strength of  $14.5 \pm 1.2$  kcal/mol was obtained for  $(\text{CH}_3)_2\text{S}-\text{Br}$  and under typical springtime Arctic boundary layer conditions of 760 Torr, 230 – 270 K, a rate coefficient for reaction (R5.5) of  $1.3 \times 10^{-10} \text{ cm}^3 \text{ molecule}^{-1} \text{ s}^{-1}$  was reported. An upper limit for reaction (R5.7) of  $k_{5.7} < 3 \times 10^{-16} \text{ cm}^3 \text{ molecule}^{-1} \text{ s}^{-1}$  was also obtained. By employing the same technique (LFP/RF), Jefferson et al. (1994) determined the C–H bond strength in DMS, the temperature dependence of reactions (R5.6a) and (R5.6b) over the temperature range 386 – 604 K and pressure range 20 – 200 Torr  $\text{N}_2$ , and reported the Arrhenius expressions:  $k_{5.6a} = 9.0 \times 10^{-11} \exp(-2386/T)$  and  $k_{5.6b} = 8.6 \times 10^{-13} \exp(836/T)$ . Ingham et al. (1999), using pulsed laser photolysis (PLP) coupled with RF, and under conditions of 100 Torr  $\text{N}_2$  and 295 K, obtained the rate coefficients:  $k_{5.5a} = 6.36 \times 10^{-11} \text{ cm}^3 \text{ s}^{-1}$  and  $k_{5.5b} = 1.02 \times 10^4 \text{ s}^{-1}$  and equilibrium rate constant  $K_{5.5} = 6.24 \times 10^{-15} \text{ cm}^3$ , in good agreement with that obtained by Wine et al. (1993). Absorption of  $(\text{CH}_3)_2\text{S}-\text{Br}$  was first observed by Wine et al. (1993) but no spectrum was reported. The first  $(\text{CH}_3)_2\text{S}-\text{Br}$  UV absorption spectrum was reported by Ingham et al. (1999), which, over the wavelength range 300 – 450 nm, possessed a strong absorption band at  $\lambda_{\text{max}} = 365$  nm with  $\sigma_{\text{max}} = 2.74 \times 10^{-17} \text{ cm}^2 \text{ molecule}^{-1}$ . A combined FT-IR kinetic and product study of reaction (R5.5), at 298 K and 1000 mbar  $\text{N}_2 + \text{O}_2$ , has been reported by Maurer et al. (1999). An “overall” rate constant of  $k_{\text{Br}+\text{DMS}} \leq 1 \times 10^{-13} \text{ cm}^3 \text{ molecule}^{-1} \text{ s}^{-1}$  was reported with

“overall” referring to equilibrium reactions (R5.5a) and (R5.5b) followed by reaction (R5.8):



The major sulfur products observed in their study were SO<sub>2</sub>, CH<sub>3</sub>SBr, and DMSO. Nakano et al. (2001), using cavity ring down spectroscopy (CRDS), also investigated the equilibrium kinetics and UV spectroscopy of (CH<sub>3</sub>)<sub>2</sub>S–Br. The reported adduct cross-section at λ = 338.3 nm differs from that reported by Ingham et al. (1999) by ~ 35%.

In this study we report the results of an experimental study of the gas phase Br + (CH<sub>3</sub>)<sub>2</sub>S reaction that couples LFP production of Br with product detection by time-resolved UV-visible absorption spectroscopy (TRUVVAS). The gas phase absorption spectrum of the (CH<sub>3</sub>)<sub>2</sub>S–Br adduct over the wavelength range 310 – 450 nm is reported and compared with that previously reported in the literature. In addition, the TRUVVAS technique is used as a probe to investigate the kinetics of adduct radical-radical reactions and adduct reactions with O<sub>2</sub>, NO, and NO<sub>2</sub>. The results reported in this study are useful for resolving spectral data discrepancy in the literature, for understanding the likely atmospheric fate of the (CH<sub>3</sub>)<sub>2</sub>S–Br adduct, and for characterizing interferences in laboratory studies of BrO + DMS.

## Experimental Method

The experimental apparatus is described in Chapter 2. Experimental details that are specific to this study are discussed below.

All experiments were carried out at a temperature of 265 K and pressure of 200 Torr. The reaction cell and pre-mixing cell were surrounded by an insulated Pyrex jacket

through which an ethanol/methanol mixture was flowed from a temperature-controlled reservoir, enabling the cell temperature to be controlled. The temperatures of the gas mixture at the two exits from the reaction cell were measured with thermocouples. The temperature gradient between the ends of the cell was less than 2°C, and the average of the temperatures measured at the two ends was taken to be the cell temperature. Dry nitrogen gas was sprayed on the exterior of the quartz cell windows to prevent condensation of water vapor when the cell was cooled. Monochromator entrance and exit slits were set at 1.5 mm, providing a spectral resolution of 5.5 nm full width at half maximum (FWHM).

Atomic bromine was generated by 248 nm laser flash photolysis (LFP) of CF<sub>2</sub>Br<sub>2</sub>. The absorption cross section for CF<sub>2</sub>Br<sub>2</sub> at 248 nm is  $7.20 \times 10^{-19} \text{ cm}^2 \text{ molecule}^{-1}$  (Sander et al., 2006), and the quantum yield for production of Br is close to unity (Talukdar et al., 1996). A typical photolysis fluence was  $\sim 20 \text{ mJ cm}^{-2} \text{ pulse}^{-1}$ , and the pulse duration was  $\sim 25 \text{ ns}$ . The absorption cross section for DMS at 248 nm is  $1.28 \times 10^{-20} \text{ cm}^2 \text{ molecule}^{-1}$ , (Hearn et al., 1990). Dimethyl sulfide (DMS) concentrations employed in these experiments were  $\leq 3 \times 10^{15} \text{ molecules cm}^{-3}$ , which, using typical laser fluence as mentioned above, implies that laser light attenuation from DMS absorption is  $\sim 0.4\%$ . Since laser power measurements were within  $\pm 5\%$  accuracy, a 0.4% reduction in light level is below our detection limit and is well accounted for in our  $\pm 35\%$  experimental error, hence, this was not considered to be consequential to our experiments. The quantum yields of CH<sub>3</sub>S and H from DMS photolysis at 248 nm are 0.93 and zero respectively (Barone et al., 1994), thus, under typical experimental conditions employed

in this work,  $[\text{CH}_3\text{S}] \equiv [\text{CH}_3]$  radicals produced from DMS photolysis is  $\leq 3 \times 10^{11}$  molecules  $\text{cm}^{-3}$ .

Concentrations of DMS were measured *in situ* in the slow flow system by UV photometry as well as by mass flow measurements. The *in situ* photometry measurements of DMS employed 213.9 nm as the monitoring wavelength (Zn penray lamp light source). The cross-section used to convert 213.9 nm DMS absorbances to concentrations was  $1.70 \times 10^{-18} \text{ cm}^2 \text{ molecule}^{-1}$  (Hearn et al., 1990). Concentrations of  $\text{CF}_2\text{Br}_2$  were measured *in situ* in the slow flow system by mass flow measurements. Bulb fraction measurements of  $\text{CF}_2\text{Br}_2$  and DMS were performed using photometry and employed 228.8 nm as the monitoring wavelength (Cd penray light source). The cross-sections used to convert 228.8 nm absorbances to concentrations were  $2.45 \times 10^{-18} \text{ cm}^2 \text{ molecule}^{-1}$  and  $1.16 \times 10^{-18} \text{ cm}^2 \text{ molecule}^{-1}$  for  $\text{CF}_2\text{Br}_2$  and DMS, respectively (Sander et al., 2006; Wine et al., 1981). In the kinetics experiments, the concentrations of NO and  $\text{NO}_2$  were determined from mass flow measurements of  $\text{NO}_2/\text{N}_2$  or  $\text{NO}_2/\text{N}_2/\text{O}_2$  mixtures combined with photometric measurements of the  $\text{NO}_2$  mole fraction in the  $\text{NO}_2/\text{N}_2/\text{O}_2$  mixtures as discussed in Chapter 2. The pure gases used in this work were obtained from Air Products ( $\text{O}_2$ ,  $\text{N}_2$ ) and Spectra Gases (NO), and had the following stated minimum purities:  $\text{N}_2$ , 99.999%;  $\text{O}_2$ , 99.994%; NO, 99.0%. The  $\text{N}_2$  and  $\text{O}_2$  were used as supplied. Nitric oxide (NO) was degassed at 77 K prior to use. The liquids used in this work, DMS and  $\text{CF}_2\text{Br}_2$ , were supplied by Sigma-Aldrich and had stated minimum purities of 99.0% and 97%, respectively. These liquids were transferred under  $\text{N}_2$  into vials fitted with high-vacuum stopcocks. After repeated degassing at 77 K, appropriate amounts were transferred into 12-L Pyrex bulbs and diluted with  $\text{N}_2$ .

## Results and Discussion

When  $\text{CF}_2\text{Br}_2$  was photolyzed at 248 nm in the presence of DMS, absorption of the UV-visible probe beam was observed throughout the 310 to 450 nm spectral region. Absorption was observed only when both  $\text{CF}_2\text{Br}_2$  and DMS were present in the photolyzed gas mixture.

### Identification of the Absorbing Species

Evidence verifying the identity of the absorbing species was obtained by measuring its appearance rate. Absorbance temporal profiles were recorded and analyzed using a nonlinear least squares fit to equation (4.1), which describes the time evolution of the intermediate in consecutive first-order reactions (Atkins, 2006):

$$\text{(Eq. 4.1)} \quad A_t = \{k_a/(k_d - k_a)\}X\{\exp(-k_a t) - \exp(-k_d t)\}$$

In the above equation,  $A_t$  is the absorbance at time  $t$ ,  $k_a$  is the first-order absorbance appearance rate,  $k_d$  is the first-order absorbance decay rate, and  $X$  is the peak adduct absorbance that would be observed in the absence of a decay. A typical absorbance temporal profile is shown in Figure 5.1. In this set of experiments, absorbance disappearance resulted primarily from radical-radical reactions and was not a first-order process. The first-order absorbance disappearance rate,  $k_d$ , is thus a parameterized rate coefficient rather than the sum of actual loss processes that are quantitatively attributable to specific first order processes.

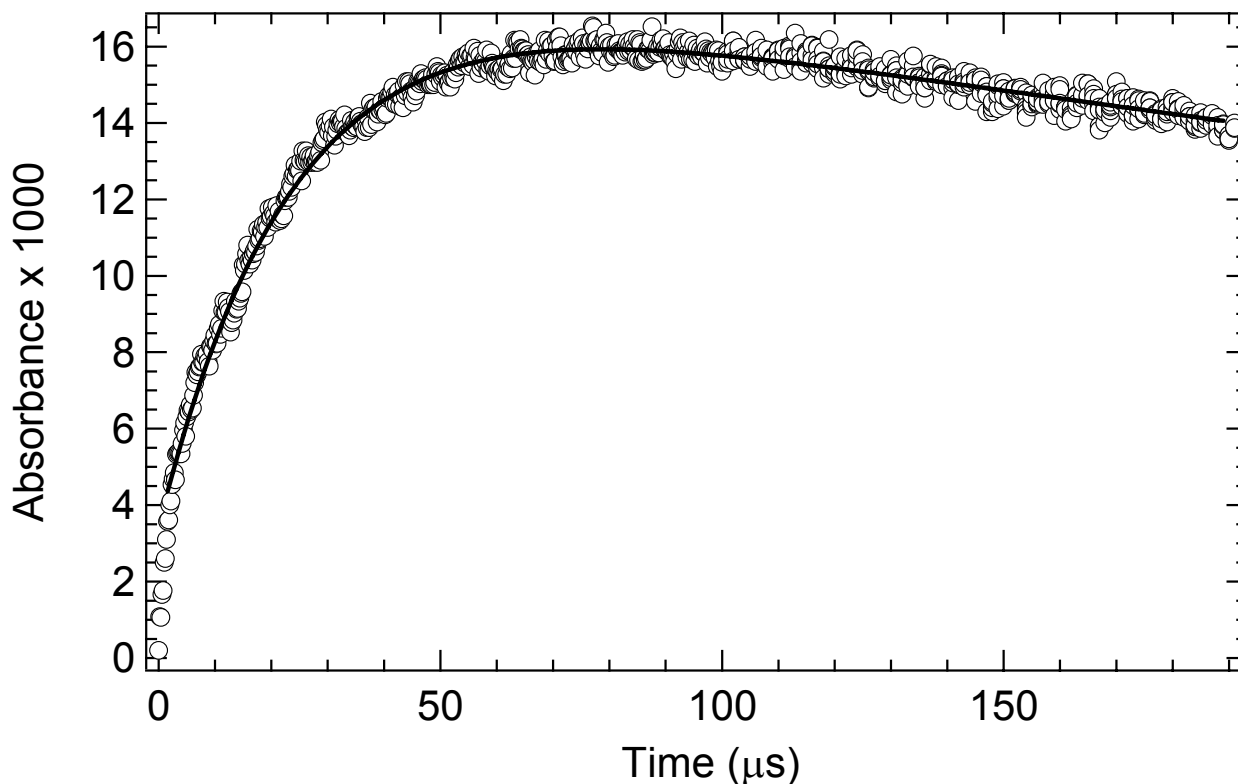


**Figure 5.1** Typical absorbance (base e) temporal profile observed following laser flash photolysis of DMS/CF<sub>2</sub>Br<sub>2</sub>/N<sub>2</sub> mixtures at 248 nm. Experimental conditions:  $T = 265$  K;  $P = 200$  Torr; monitoring wavelength = 365 nm; concentrations in units of  $10^{14}$  molecules  $\text{cm}^{-3}$  are  $[\text{CF}_2\text{Br}_2] = 1.45$ ,  $[\text{DMS}] = 3.69$ , and  $[\text{Br}]_0 \approx 0.05$ . The solid line is obtained from a nonlinear least squares fit of the data to the sum of an exponential rise and an exponential decay. Best fit appearance ( $k_a$ ) and disappearance ( $k_d$ ) rate coefficients in units of  $\text{s}^{-1}$  are  $k_a = 40,290$  and  $k_d = 1500$ .

However, because (i) the observed absorbance loss rates are slow compared to the rates of absorbance appearance, and (ii) the data that were fit were limited to times where the fractional decay of absorbance was small, the parameterization of the absorbance disappearance as a first order process does not seriously impact the reliability of the analysis to determine the pseudo-first order rate coefficient for absorbance appearance. As typified by the data shown in Figure 5.1, the quality of the double exponential fits is quite good. Pseudo-first-order appearance rate coefficients ( $k_a$ ) were measured at 365 nm in 200 Torr N<sub>2</sub> buffer. As shown in Figure 5.2, plots of  $k_a$  vs. [DMS] are linear over the range of DMS concentrations employed. The linearity of the  $k_a$  vs. [DMS] plots up to the fastest appearance rates measured (ca. 65,000 s<sup>-1</sup>) demonstrates that the rate-limiting step in production of the absorbing species is the Br + DMS reaction under the conditions investigated. The slope of the  $k_a$  vs. [DMS] plot yields the second order rate coefficient  $k_{5.5} = (8.97 \pm 1.32) \times 10^{-11} \text{ cm}^3 \text{ molecule}^{-1} \text{ s}^{-1}$  at  $T = 265 \text{ K}$  and  $P = 200 \text{ Torr N}_2$ , where  $k_{5.5} \equiv k_{5.5a} + k_{5.5b}$ , and the uncertainties are  $2\sigma$  and represent precision only. The value for  $k_{5.5}$  evaluated from the absorbance appearance rate agrees, within experimental uncertainty, with the Br + DMS rate coefficient obtained at the same temperature and pressure by monitoring the decay of Br using atomic resonance fluorescence spectroscopy (Wine et al., 1993). The data in Figures 5.1 and 5.2 provide strong evidence that the species being observed is indeed the Br–DMS adduct formed as a primary product of the reaction of Br with DMS.

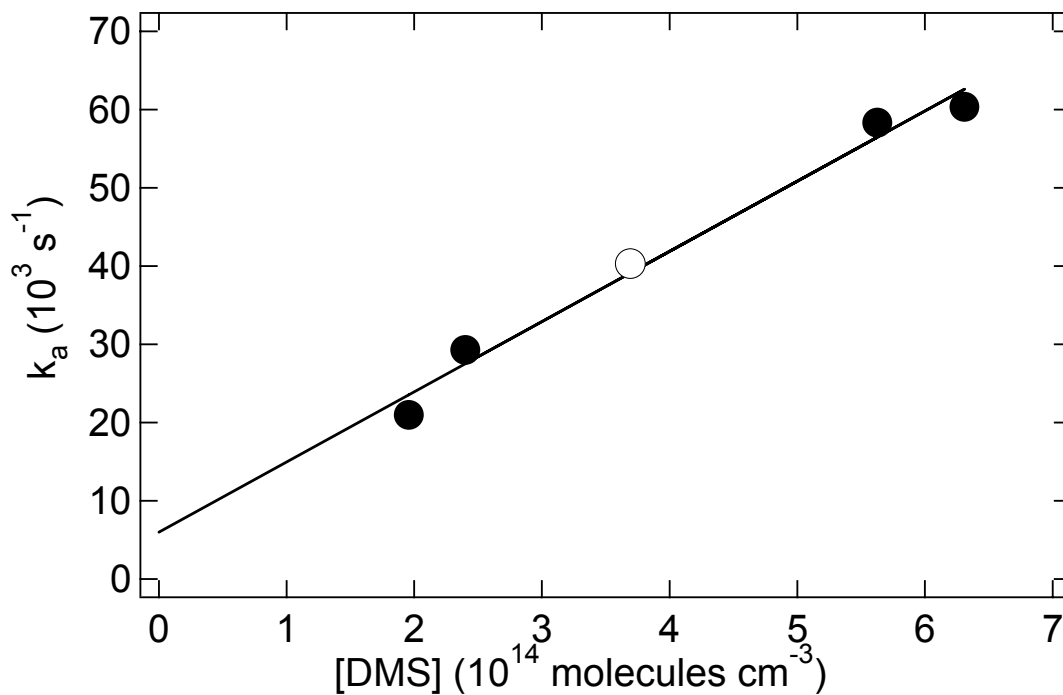
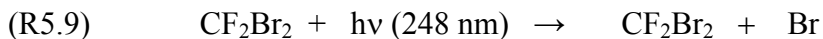


**Figure 5.2** Plots of  $k_a$  versus [DMS] for data obtained at  $T = 265 \text{ K}$  and  $P = 200 \text{ Torr N}_2$ . The solid line is obtained from linear least squares analysis; its slope gives the following second order rate coefficient in units of  $10^{-11} \text{ cm}^3 \text{ molecule}^{-1} \text{ s}^{-1}$ :  $k_{5,5} = 8.97 \pm 1.32$ . The open data point is the one obtained from the data shown in Figure 5.1.

### Adduct Absorption Spectrum

The absorption spectrum of Br–DMS was measured at 200 Torr total pressure (N<sub>2</sub> bath gas) and 265 K using 248 nm photolysis of CF<sub>2</sub>Br<sub>2</sub> to generate Br atoms:



Absorption measurements were made over the wavelength range 310–450 nm, and a reference wavelength of 365 nm was selected. Absorption measurements were made at this reference wavelength after every 5 measurements at other wavelengths. This was done in order to account for systematic drifts in experimental parameters such as laser power, [CF<sub>2</sub>Br<sub>2</sub>], optical alignment, etc. over time. Absorbance measurements at wavelengths other than 365 nm were normalized to the average of the “before” and “after” 365 nm absorbances. The adduct absorption cross section was carefully measured at 365 nm and all cross-sections were then determined by applying the normalization factor to the carefully measured reference cross-section.

The absolute absorption cross-section measurement at 365 nm for Br–DMS employed 248 nm photolysis of CF<sub>2</sub>Br<sub>2</sub> as the radical source. Typical reagent concentrations employed in these measurements in units of 10<sup>13</sup> molecules cm<sup>-3</sup> were as follows: [DMS] ≈ 110; [CF<sub>2</sub>Br<sub>2</sub>] ≈ 4.7–20; [Br]<sub>0</sub> ≈ 0.2–1.0. High DMS concentrations were employed in order to obtain ~ 99% conversion of Br to Br–DMS at equilibrium (based on the equilibrium constants reported by Wine et al., 1993). Each cross-section measurement involved averaging temporal profiles obtained from 20 photolysis laser

pulses. The Br–DMS cross-section at 365 nm ( $\sigma_{365}$ ) was determined from the data using the following relationship:

$$\text{(Eq. 5.1)} \quad \sigma_{365} = X / (l [\text{Br}]_0 F)$$

In Eq. 5.1, X is defined as in Eq. 4.1 (see above),  $l$  is the absorption path length (100 cm),  $[\text{Br}]_0$  is the concentration of bromine atoms produced via laser flash photolysis of  $\text{CF}_2\text{Br}_2$ , and F is the fraction of Br atoms converted to adduct. As is typical for gas phase spectroscopic data, the absorbance is defined as  $A = \ln(I_0/I_t)$  where  $I_0$  is the transmitted light intensity before the laser fires and  $I_t$  is the transmitted light intensity at some time  $t$  after the laser fires, i.e., A is a base e absorbance. The parameter F in Eq. 5.1 can be evaluated using the following relationship:

$$\text{(Eq. 5.2)} \quad F = (1 - F_1) (1 - F_2) (1 - F_3)$$

In Eq. 5.2,  $F_1$  is the fraction of Br atoms that are lost by diffusion from the detection volume and/or reaction with background impurities,  $F_2$  is the fraction of Br atoms that react with DMS by H-abstraction rather than by addition, and  $F_3$  is the fraction of Br–DMS + Br that exists as Br when the two species are in equilibrium. Employing high concentrations of DMS helps to keep  $F_1$  and  $F_3$  small, while employing relatively high total pressure minimizes  $F_2$ . Based on kinetic and thermodynamic data reported by Wine et al. (1993) and Jefferson et al. (1994) we estimate that  $F_2 = 0.0001$  and  $F_3 = 0.009$  under the experimental conditions employed. The background loss rate of Br atoms (typically found to be 20–50  $\text{s}^{-1}$  in LFP studies of Br kinetics that employ resonance

fluorescence detection) is probably negligible compared to the pseudo-first-order rate coefficient for Br + DMS, which is approximately  $1 \times 10^5 \text{ s}^{-1}$  under the above experimental conditions. The intercept of the plot ( $\sim 6,000 \pm 5,800 \text{ s}^{-1}$ ) shown in Figure 5.2 is, within experimental uncertainty, approximately what we expect based on the known Br–DMS unimolecular decomposition rate, i.e.,  $1,350 \text{ s}^{-1}$  (Wine et al., 1993), however, an unusually fast Br loss by impurity reactions cannot be completely ruled out. Hence, we conservatively assign  $F_1$  a value of  $0.05 \pm 0.05$  to account for all possibilities. The above considerations lead to the results  $F = 0.94 \pm 0.06$  where the reported uncertainties are estimates of accuracy at the 95% confidence level.

Cross-sections obtained from Eq. 5.1 were found to be independent of  $[\text{Br}]_0$  over the ranges specified above, i.e., Beer's law was obeyed. Evaluation of  $[\text{Br}]_0$  required (i) careful measurements of  $[\text{CF}_2\text{Br}_2]$  and laser power, (ii) careful measurements of  $[\text{DMS}]$ , and (iii) careful measurements of the photolysis laser beam cross-sectional area and its divergence down the length of the cell (the laser beam area increased by a factor of 1.5 between the cell entrance and exit, and was assumed to be the average of the entrance and exit areas for purposes of evaluating  $[\text{Br}]_0$ ).

The adduct spectra measured in this study at  $T = 265 \text{ K}$  and  $P = 200 \text{ Torr N}_2$  are shown in Figure 5.3. The Br–DMS absorption spectrum was measured on several days verifying reproducibility of data. The quarter-meter monochromator used for the measurements had a spectral dispersion of 3.7 nm per mm and slit widths were set at 1.5 mm for all spectral measurements. The expected spectral resolution of 5.5 nm FWHM (full width at half maximum) was confirmed through measurement of atomic penray lamp emission lines at several wavelengths within the spectral range of interest.

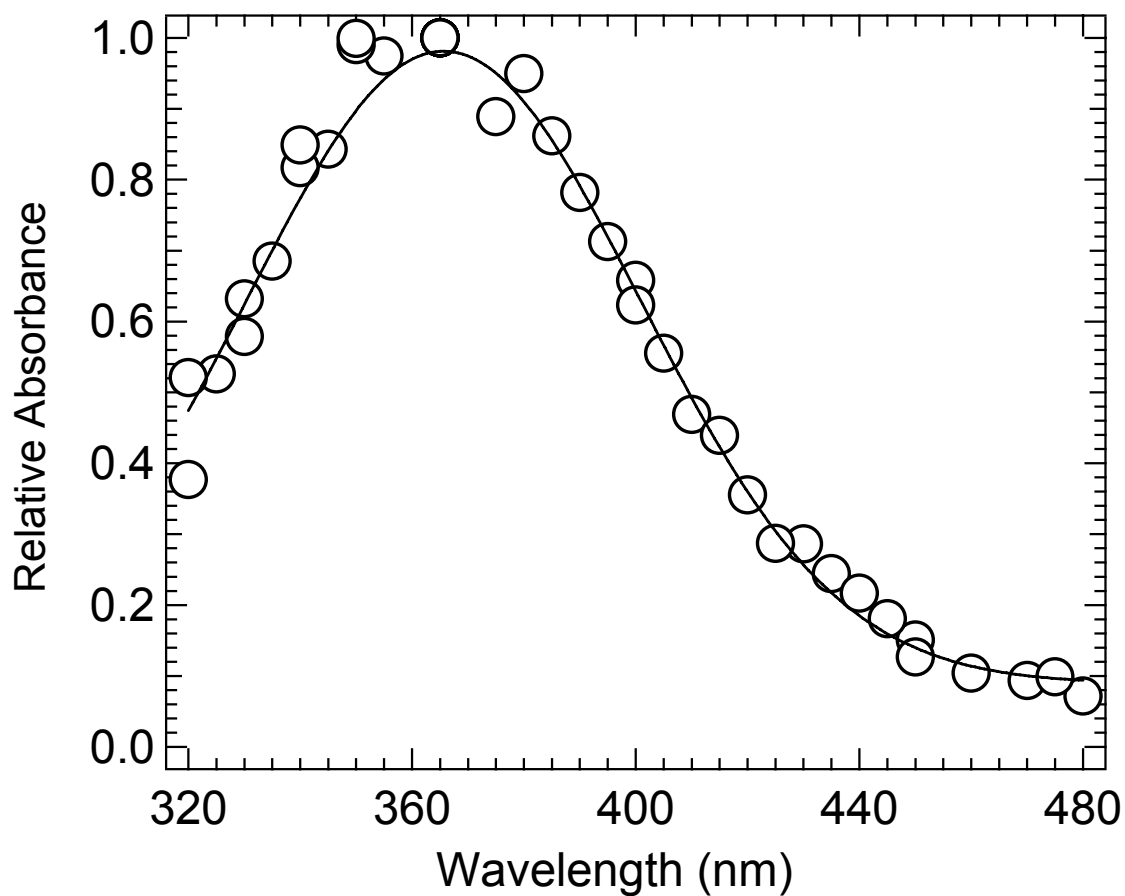


**Figure 5.3 Absorption spectrum of Br-DMS at a spectral resolution of 5.5 nm.** The solid line is obtained by fitting absorbance vs. wavelength data to a Gaussian function (Eq 5.3). The best fit parameters are  $\sigma_{\max} = 2.70 \times 10^{-17} \text{ cm}^2$ ,  $\lambda_{\max} = 365.63 \text{ nm}$ , and  $\text{FW} = 49.78$ .

The solid line in Figure 5.3 is obtained by fitting absorbance vs. wavelength data to a Gaussian functional form. The data are well described by a single Gaussian function, suggesting that the observed absorption spectrum is attributable to a single electronic transition. The similarity between the gas phase absorption spectrum reported in this study and that reported in the literature (Ingham et al., 1999) lends further support to our conclusion that the species being observed in this study is the Br–DMS adduct.

Consideration of uncertainties in the parameters that must be known to obtain the adduct cross-section (see above), leads to an estimate of  $\pm 35\%$  for the accuracy of the measured cross-section (95% confidence level). The best fit Gaussian function suggests that maximum absorbance occurs at  $\sim 365$  nm with  $\sigma_{\max} = 0.999 \sigma_{365}$ . The absorption cross section at any desired wavelength over the range 320 – 500 nm in units of  $\text{cm}^2 \text{ molecule}^{-1}$  can be obtained with good accuracy using the best fit function:

$$\text{(Eq 5.3)} \quad \sigma(\lambda) = \sigma_{\max} \exp \{-FW [\ln(\lambda_{\max}/\lambda)]^2\}$$

where  $\sigma(\lambda)$  is the cross section at wavelength  $\lambda$ ,  $\sigma_{\max} = 2.70 \times 10^{-17} \text{ cm}^2$ , and  $\lambda_{\max} = 365.63$  nm are the cross section and wavelength at maximum absorption, and  $FW = 49.78$  is a width parameter.

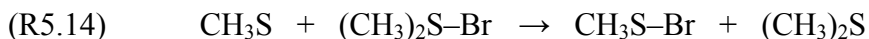
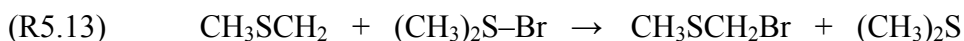
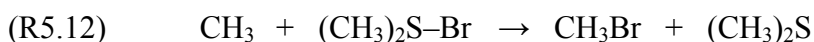
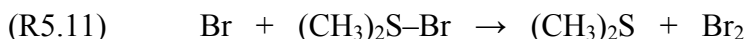
We report our measured 365 nm cross section to be  $\sigma_{365} = (2.69 \pm 0.94) \times 10^{-17} \text{ cm}^2 \text{ molecule}^{-1}$ . The absorption cross sections reported in this study can be directly compared with those reported by Ingham et al. (1999) and Nakano et al. (2001). The wavelength dependences of the cross-sections as well  $\lambda_{\max} = 365$  nm are in excellent agreement with the spectrum reported by Ingham et al. (1999). However, the cross-

section we obtain at 338.3 nm is 40% larger than that reported at this wavelength by Nakano et al. (2001), although our results can be considered to agree with those of Nakano et al. (2001) within the combined experimental uncertainties.

Figure 5.4, courtesy of Dr. M. McKee of Auburn University, shows a schematic of the most probable structure for the  $(\text{CH}_3)_2\text{S}-\text{Br}$  adduct obtained using the B3LYP/6-311+G(2d,p)/ECP(I/SDD) level of theory.

### Radical-Radical Reaction Kinetics

When reaction mixtures containing only  $\text{CF}_2\text{Br}_2$ , DMS, and  $\text{N}_2$  are subjected to 248 nm laser flash photolysis and detectable levels of  $\text{Br}-\text{DMS}$  are generated, we expect that  $(\text{CH}_3)_2\text{S}-\text{Br}$  loss will be controlled by the following radical-radical reactions:



The products identified in reactions (R5.10–R5.14) above are the probable dominant products but not necessarily the only products that are energetically feasible. The Br self-reaction is very slow and, therefore, is not listed above. If experimental conditions are adopted where  $T = 265$  K,  $P = 200$  Torr  $\text{N}_2$ ,  $[\text{Br}]_0 = (1-3) \times 10^{13}$  molecules  $\text{cm}^{-3}$ , and  $[\text{DMS}] > 1 \times 10^{15}$  molecules  $\text{cm}^{-3}$ , then Br reacts rapidly with DMS to form  $\sim 99.99\%$   $(\text{CH}_3)_2\text{S}-\text{Br}$  and  $\sim 0.01\%$   $\text{CH}_3\text{SCH}_2$ , (Wine et al., 1993; Jefferson et al., 1994),

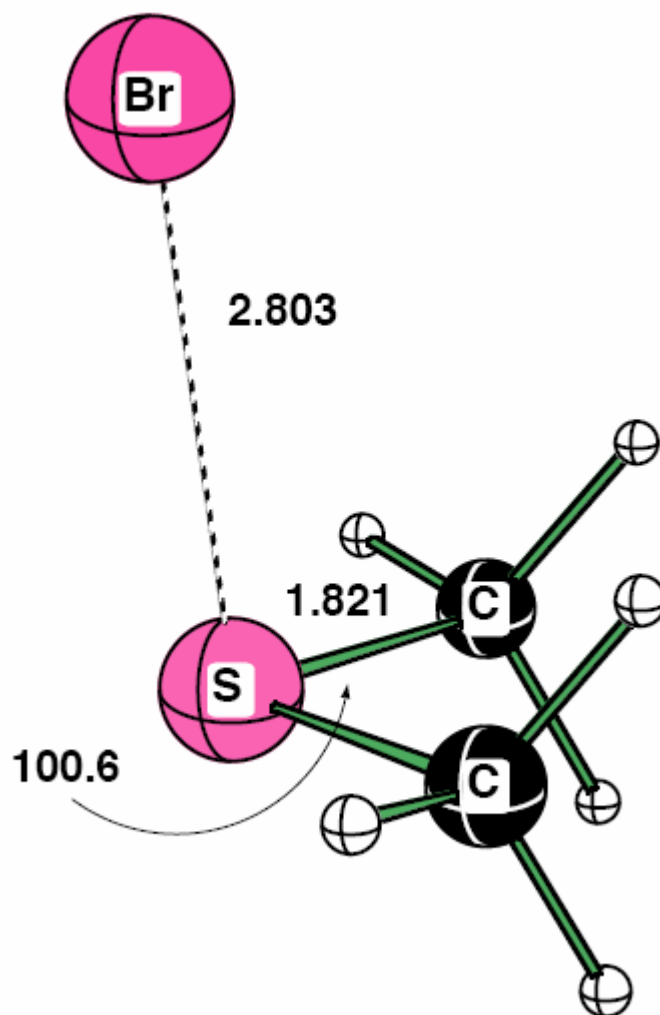


**Figure 5.4** Structure for (CH<sub>3</sub>)<sub>2</sub>S-Br derived from *ab initio* calculations at the B3LYP/ECP level courtesy of Dr. M. McKee of Auburn University. Bond lengths are in Å units.

the equilibrium concentration ratio  $[\text{Br-DMS}]/[\text{Br}]$  is  $> 247$  (Wine et al., 1993), and the concentration of  $\text{CH}_3$  and  $\text{CH}_3\text{S}$  produced from DMS photolysis are typically only a few percent of the concentration of Br produced from  $\text{CF}_2\text{Br}_2$  photolysis. Under such conditions, loss of Br-DMS is expected to be controlled by reaction (R5.10).

Shown in Figure 5.5 is a typical Br-DMS temporal profile observed at a monitoring wavelength of 365 nm following 248 nm laser flash photolysis of reaction mixtures containing  $(0.75\text{--}1.5) \times 10^{15} \text{ CF}_2\text{Br}_2 \text{ cm}^{-3}$ ,  $\sim 1.8 \times 10^{15} \text{ DMS cm}^{-3}$ , and 200 Torr  $\text{N}_2$ . The data are plotted as  $[\text{Br-DMS}]^{-1}$  vs. time. The linearity of the plot is consistent with the hypothesis that adduct loss is dominated by reaction (R5.10), and the self-reaction rate coefficient  $2k_{5.10}$ , is obtained from the slope of the plot. Second order rate coefficients obtained from several experiments over the ranges of  $[\text{CF}_2\text{Br}_2]$  and  $[\text{DMS}]$  specified above, but at constant laser power, are in good agreement, and give the following mean value for the self-reaction rate coefficient:  $2k_{5.10} = (2.91 \pm 0.20) \times 10^{-10} \text{ cm}^3 \text{ molecule}^{-1}\text{s}^{-1}$ , where the uncertainty is  $2\sigma$  and represents precision only. The accuracy of the derived value for  $2k_{5.10}$  is limited by the accuracy of  $[\text{Br-DMS}]$ , which in turn is limited by the accuracy of the Br-DMS absorption cross section at the monitoring wavelength (365 nm), i.e.,  $\pm 35\%$  (see above). Taking the Br-DMS absorption cross section and imprecision to be the two main sources of uncertainty, we report  $2k_{5.10} = (2.9 \pm 1.0) \times 10^{-10} \text{ cm}^3 \text{ molecule}^{-1} \text{ s}^{-1}$ , where the uncertainty represents estimated accuracy at the 95% confidence level.

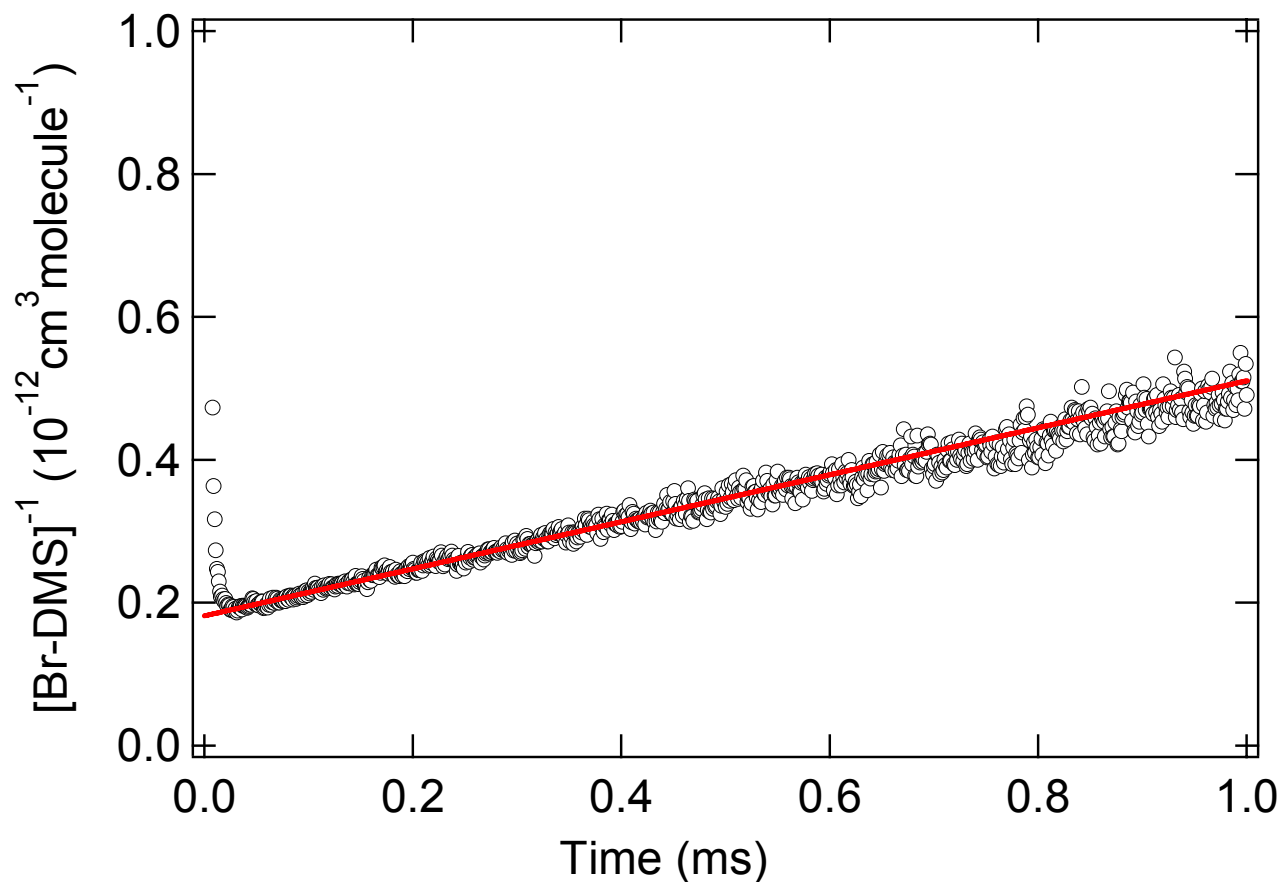


**Figure 5.5** Typical Br–DMS absorbance temporal profile plotted as  $[\text{Br-DMS}]^{-1}$  vs. time. Experimental conditions:  $T = 265 \text{ K}$ ;  $P = 200 \text{ Torr N}_2$ ; concentrations in units of  $10^{15} \text{ molecules cm}^{-3} = 1.75 \text{ DMS}$  and  $0.75 \text{ CF}_2\text{Br}_2$ . The solid line is obtained from a linear least squares analysis; its slope gives  $2k_{5.18} = (3.24 \pm 0.03) \times 10^{-10} \text{ cm}^3 \text{ molecule}^{-1} \text{ s}^{-1}$  where the uncertainty is  $2\sigma$  and represents precision only.

Ingham et al. (1999) reported the radical-radical rate constants (in units of  $10^{-10}$   $\text{cm}^3 \text{ molecule}^{-1} \text{ s}^{-1}$ ) to be:  $k_{5.10} = 0.2$  and  $k_{5.11} = 4.2$ . Under their experimental conditions:  $T = 295 \text{ K}$ ,  $P = 100 \text{ Torr N}_2$ ,  $[\text{DMS}] = (0.7 - 7) \times 10^{14} \text{ molecules cm}^{-3}$ , the temporal evolution of Br atom decay was followed and a kinetic simulation, which included reactions R5.5a, R5.5b, and R5.11, was performed to deduce  $k_{5.11}$ . Another kinetic simulation was performed, which consisted of reactions (R5.5a), (R5.5b), and (R5.10), in order to determine  $k_{5.10}$ . However, the value obtained for  $k_{5.10}$  was anti-correlated with  $[\text{DMS}]$  and varied by a factor of 10 over their employed experimental conditions. Since the derived rate coefficient,  $k_{5.11}$ , reproduced the observed Br decay profiles over the range of experimental conditions, these investigators concluded that  $k_{5.10} < 2 \times 10^{-11} \text{ cm}^3 \text{ s}^{-1}$ .

Based on the kinetic data reported by Ingham et al. (1999) along with their adopted experimental conditions listed above, the  $[\text{Br-DMS}]/[\text{Br}]$  ratio varied over the range 0.3 – 0.8 which can lead to contributions from both reactions (R5.10) and (R5.11), whereas, in our experiments, we adopted experimental conditions that would minimize contributions from reaction (R5.11) in order to “isolate” and study reaction (R5.10), i.e., the  $[\text{Br-DMS}]/[\text{Br}]$  ratio was consistently  $> 99\%$ .

#### Kinetics of Br–DMS Reaction with O<sub>2</sub>

To investigate the kinetics of the reaction of Br–DMS with O<sub>2</sub>, Br–DMS absorbance temporal profiles were measured in 200 Torr of O<sub>2</sub> with experimental conditions adjusted to high  $[\text{DMS}]$  and low  $[\text{Br}]_0$  in order to minimize the contribution of radical-radical reactions to Br–DMS removal.



In order to establish upper limits for  $k_{5.7}$ , back-to-back experiments were carried out where experimental conditions were held constant except that  $\text{N}_2$  and  $\text{O}_2$  were interchanged as the bath gas. Plots of  $\ln A$  vs time for one set of back-to-back experiments aimed at evaluating  $k_{5.7}$  are shown in Figure 5.6. Plots of  $\ln A$  vs. time are nonlinear in both  $\text{N}_2$  and  $\text{O}_2$  in a manner that suggests the dominance of radical-radical reactions controlling Br-DMS removal, particularly at short times after the laser flash when the adduct concentration is relatively high. Linear least-squares analyses of the Br-DMS temporal profiles at 3 – 9 ms after the laser flash (Figure 5.6) give pseudo-first order decay rates ( $k_d$ ) of  $31 \pm 7 \text{ s}^{-1}$  in 200 Torr  $\text{N}_2$  and  $66 \pm 9 \text{ s}^{-1}$  in 200 Torr  $\text{O}_2$  (uncertainties are  $2\sigma$ , precision only). This apparent increase in observed Br-DMS decay suggests a rate coefficient of  $k_{5.7} = 8.0 \times 10^{-18} \text{ cm}^3 \text{ molecule}^{-1} \text{ s}^{-1}$ . Data analysis was restricted to times less than 9 ms after the laser flash because there was so little absorption at later times that quantitative kinetic analysis was precluded. Reaction (R5.12), diffusion of Br-DMS out of the detection volume, and reaction of Br-DMS with background impurities in the bath gases may all contribute to the time evolution of absorbance for the data shown in Figure 5.6. In order to put reasonable upper limits on  $k_{5.7}$ , it is necessary to consider the fact that secondary chemistry is not identical in  $\text{N}_2$  and  $\text{O}_2$  bath gases. In  $\text{O}_2$ , the radicals  $\text{CH}_3$  and  $\text{CH}_3\text{S}$  (produced from 248 nm photolysis of DMS) react with  $\text{O}_2$  to produce ROO species ( $\text{R} = \text{CH}_3, \text{CH}_3\text{S}$ ) that are less reactive than the radical precursor.

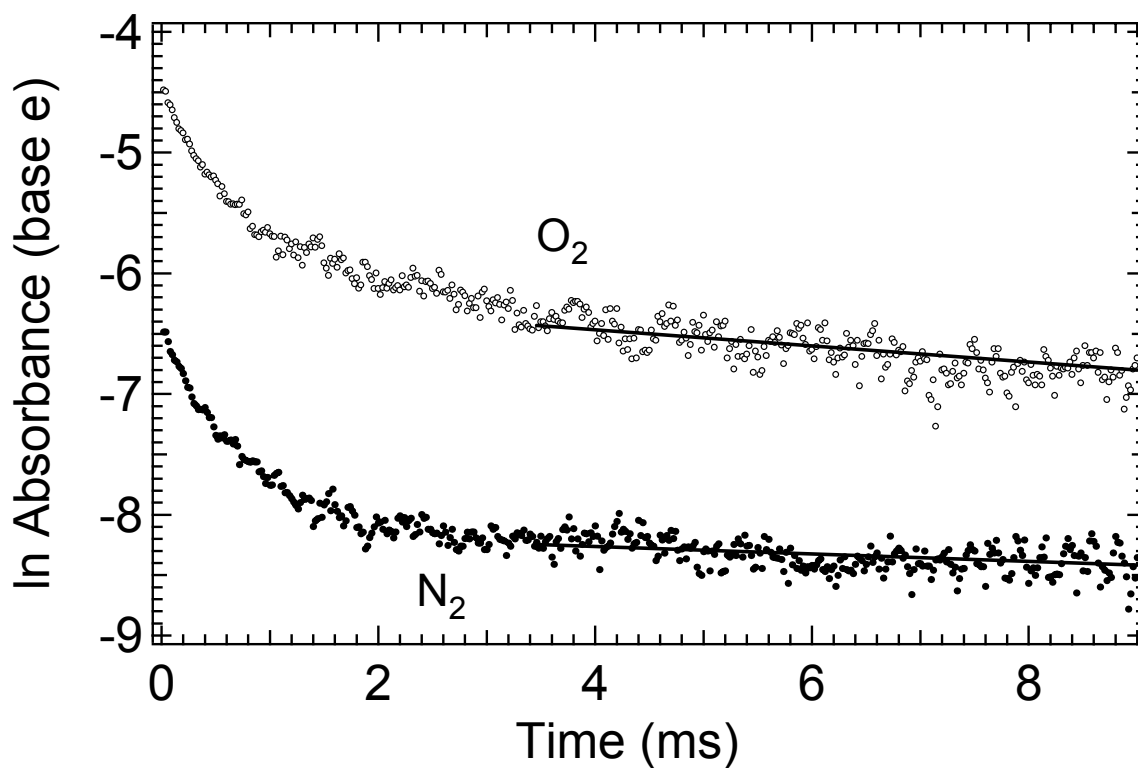


**Figure 5.6** Comparison of Br-DMS absorbance temporal profiles observed at  $T = 265$  K and  $P = 200$  Torr in  $N_2$  vs.  $O_2$  bath gas. The DMS concentration was  $1.2 \times 10^{15}$  molecules  $cm^{-3}$  in both experiments. Best fit slopes in units of  $s^{-1}$  are  $31 \pm 7$  and  $67 \pm 10$  for the data obtained in  $N_2$  and  $O_2$ , respectively, within the time intervals 3–9 ms after the laser flash (uncertainties are  $2\sigma$  and represent precision only). For the sake of clarity, the data obtained in  $O_2$  has been offset downward by 2 units of  $\ln$  concentration.

It is possible (though unlikely) that, in the presence of O<sub>2</sub>, some reduction in the rate of loss of Br–DMS via radical–radical reactions is compensated for by very slow but non-zero rate of reaction of Br–DMS with O<sub>2</sub>.

Using LFP/RF detection of Br atoms, and a total pressure of 50 Torr O<sub>2</sub>, Wine et al. (1993) reported an upper limit of  $k_{5.7} < 3.0 \times 10^{-16} \text{ cm}^3 \text{ molecule}^{-1} \text{ s}^{-1}$ . Nakano et al. (2001), using CRDS conducted experiments using 100 Torr of O<sub>2</sub> at ambient temperature and based on their inability to detect BrO as a possible product of reaction R5.7, reported an upper limit for the reaction of  $k_{5.7} < 1.0 \times 10^{-18} \text{ cm}^3 \text{ molecule}^{-1} \text{ s}^{-1}$ . The implications of these rate coefficients are discussed later on in this chapter.

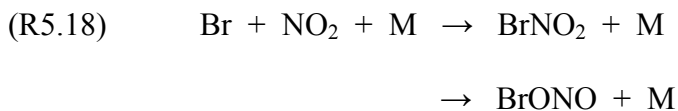
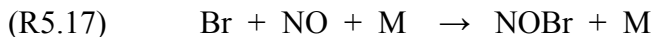
#### Kinetics of Br–DMS Reactions with NO and NO<sub>2</sub>

The reactions of RI–Cl with NO and NO<sub>2</sub> were studied at  $T = 265 \text{ K}$  and  $P = 200$  Torr (N<sub>2</sub> bath gas) under pseudo-first order conditions with  $[\text{NO}_x] \gg [\text{Br–DMS}]$ .



The reagent concentrations (units are 10<sup>14</sup> molecules cm<sup>-3</sup>) used in experiments investigating reactions (R5.15) and (R5.16) were as follows:  $[\text{CF}_2\text{Br}_2] = (1.8\text{--}4.5)$ ;  $[\text{Br}]_0 = (0.05\text{--}0.09)$ ;  $[\text{DMS}] = (12\text{--}20)$ ;  $[\text{NO}] = (4.19\text{--}19.2)$ ;  $[\text{NO}_2] = (0.429\text{--}8.16)$ . Relatively low radical concentrations were employed in order to minimize the effect of radical–radical side reactions on the observed absorbance temporal profiles. Experimental conditions of high  $[\text{DMS}] (> 10^{15} \text{ molecules cm}^{-3})$  and low temperature (265 K) minimized the contribution of Br reactions with NO and NO<sub>2</sub> such as shown in possible

reactions (R5.17 and R5.18) to observed Br–DMS kinetics by driving the Br–DMS  $\leftrightarrow$  Br equilibria to over 99% adduct (Wine et al., 1993).



As typified by the data shown in Figure 5.6, absorbance decays were exponential, i.e., plots of  $\ln A$  vs. time were linear, as would be expected under the experimental conditions employed (see above). Measured pseudo-first order decay rates ( $k_d$ ), obtained from the slopes of plots like the one shown in Figure 5.7, are plotted as a function of [DMS] in Figure 5.8. The slopes of the  $k_d$  vs. [DMS] plots give the following second order rate coefficients in units of  $10^{-11} \text{ cm}^3 \text{ molecule}^{-1} \text{ s}^{-1}$  (uncertainties are  $2\sigma$  and represent precision only):  $k_{5.15} = 1.25 \pm 0.18$ , and  $k_{5.16} = 2.56 \pm 0.02$ . Since most measured decay rates exceeded  $10,000 \text{ s}^{-1}$  as shown in Figure 5.8, we conclude that the occurrence of radical-radical side reactions does not compromise the accuracy of the reported values for  $k_{5.15}$  and  $k_{5.16}$ . At  $T = 298 \text{ K}$  and  $P = 30 \text{ Torr Ar}$ ,  $k_{5.17} \sim 5.8 \times 10^{-13} \text{ cm}^3 \text{ molecule}^{-1} \text{ s}^{-1}$  (Dolson and Klingshirn, 1993) and  $k_{5.18} \sim 4.1 \times 10^{-12} \text{ cm}^3 \text{ molecule}^{-1} \text{ s}^{-1}$  (Atkinson et al., 2006). It is clear that the values for  $k_{5.15}$  and  $k_{5.16}$  reported in this study are faster than the known values for  $k_{5.17}$  and  $k_{5.18}$ ; this observation, along with the establishment of experimental conditions where the equilibrium concentration of Br–DMS was much greater than the equilibrium concentration of Br, leads to the conclusion that reactions (R5.17) and (R5.18) made negligible contributions to Br–DMS kinetics in this study.

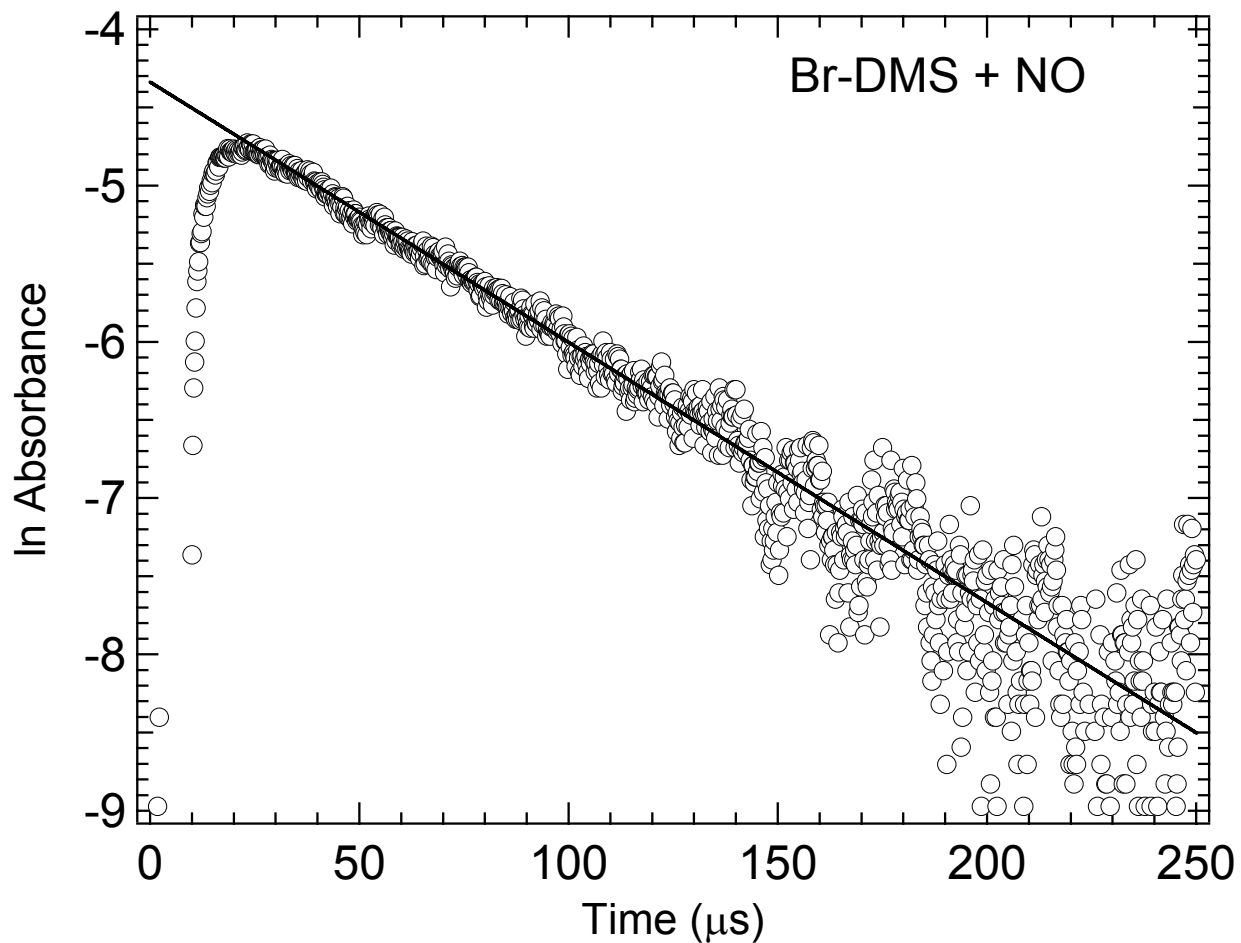


**Figure 5.7** Typical absorbance temporal profile observed following 248 nm laser flash photolysis of  $\text{CF}_2\text{Br}_2/\text{DMS}/\text{NO}_x/\text{N}_2$  mixtures at  $T = 265 \text{ K}$  and  $P = 200 \text{ Torr}$ . The data shown were obtained with  $\text{NO}_x = \text{NO}$ . Concentrations in units of  $10^{14}$  molecules  $\text{cm}^{-3}$  are  $[\text{DMS}] = 18.8$ ,  $[\text{NO}] = 9.72$ ,  $[\text{CF}_2\text{Br}_2] = 4.57$ , and  $[\text{Br}]_0 \approx 0.05$ . The solid line is obtained from a linear least squares analysis of the  $\ln$  absorbance vs. time ( $t$ ) data; its slope gives the pseudo-first order decay rate  $16,700 \text{ s}^{-1}$ .

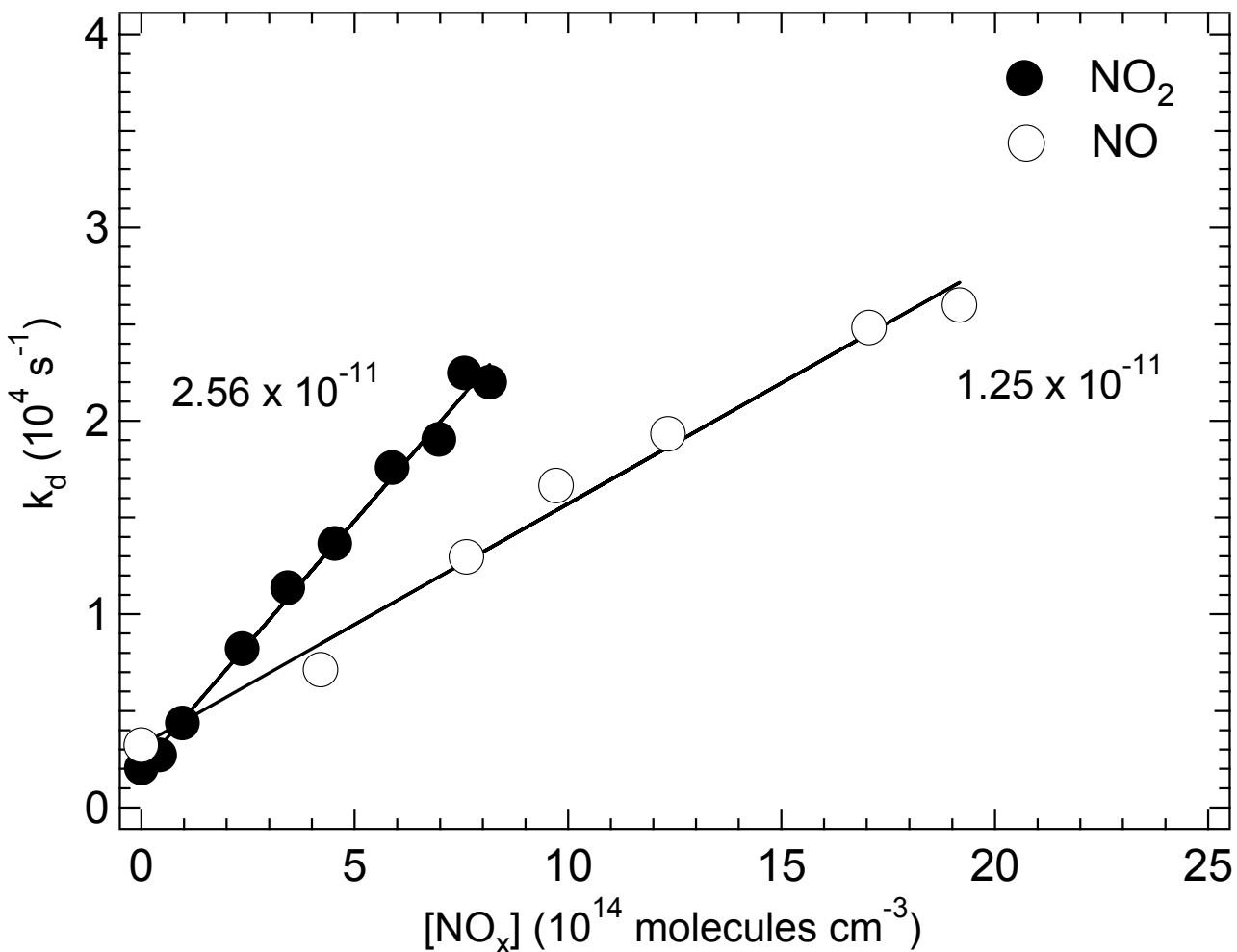


**Figure 5.8** Plots of pseudo-first-order Br–DMS decay rates ( $k_d$ ) versus  $[\text{NO}_x]$  for data obtained at  $T = 265 \text{ K}$  and  $P = 200 \text{ Torr N}_2$ . The solid lines are obtained from linear least-squares analyses; their slopes give the following rate coefficients in units of  $10^{-11} \text{ cm}^3 \text{ molecule}^{-1} \text{ s}^{-1}$  (uncertainties are  $2\sigma$  and represent precision only):  $k_{5.15} = 1.25 \pm 0.18$  and  $k_{5.16} = 2.56 \pm 0.02$ .

To our knowledge, no kinetic data are reported in the literature for the reaction of Br atoms with N<sub>2</sub>O<sub>4</sub>. However, given that (i) a relatively small fraction of NO<sub>2</sub> existed in the dimer form under the experimental conditions employed (0 – 0.4% of [NO<sub>2</sub>]<sub>0</sub>); and (ii) Br is almost certainly much more reactive with NO<sub>2</sub> than with N<sub>2</sub>O<sub>4</sub>, it seems safe to assume that the Br + N<sub>2</sub>O<sub>4</sub> reaction had a negligible influence on Br–DMS kinetics in this study.

Since side reactions such as (R5.17 and R.18) have little or no impact on the accuracy of the reported rate coefficients, it appears that accuracy is limited by precision and by the accuracy with which the concentrations of NO and NO<sub>2</sub> were known (estimated to be ± 5% for each). Hence, we report the following rate coefficients in units of 10<sup>-11</sup> cm<sup>3</sup> molecule<sup>-1</sup> s<sup>-1</sup>:  $k_{5,15} = 1.3 \pm 0.3$  and  $k_{5,16} = 2.6 \pm 0.5$ ; the uncertainties are estimates of accuracy at the 95% confidence level.

Although there are no other reported measurements of  $k_{5,15}$  and  $k_{5,16}$  with which to compare our results, it is of interest to note that the rate coefficients reported in this study are very similar in magnitude to rate coefficients for the reactions of (CH<sub>3</sub>)<sub>2</sub>S–Cl (Urbanski and Wine, 1999), SCS–Cl, (Dookwah-Roberts et al., 2005; Chapter 3 of this dissertation), CH<sub>3</sub>(O)S(Cl)CH<sub>3</sub> (Kleissas et al., 2007), and RI–Cl (R = CH<sub>3</sub>, C<sub>2</sub>H<sub>5</sub>) (Dookwah-Roberts et al., 2008; Chapter 4 of this dissertation) with NO and NO<sub>2</sub>, all of which were measured using an analogous technique to the one employed in this study. All X–Cl + NO<sub>x</sub> (X = (CH<sub>3</sub>)<sub>2</sub>S, SCS, (CH<sub>3</sub>)<sub>2</sub>SO, CH<sub>3</sub>I, C<sub>2</sub>H<sub>5</sub>I) rate coefficients are within the range (1–4) × 10<sup>-11</sup> cm<sup>3</sup> molecule<sup>-1</sup> s<sup>-1</sup> and reactivity of these adducts with O<sub>2</sub> is not observed. It appears that Br adducts, like Cl adducts, react rapidly with compounds like

NO and NO<sub>2</sub>, where transfer of the halogen atom to generate NOBr, BrNO<sub>2</sub>, BrONO or the Cl analogues (ClNO etc.) is energetically favorable.

### Atmospheric Fate of Br–DMS

The results obtained in this study taken in conjunction with the kinetic and thermodynamic results reported by Wine et al. (1993) allow us to examine the potential importance of the most likely tropospheric Br–DMS degradation pathways; these include photolysis, thermal dissociation, reaction with O<sub>2</sub>, and reaction with NO<sub>x</sub>.

The absorption cross sections reported in this study have been used along with tabulated actinic flux (F) data at the Earth's surface for best estimate of surface albedo supplied by Finlayson-Pitts and Pitts (2000), and an assumed quantum yield of unity for Br–DMS destruction (the maximum and most probable value) to obtain a maximum first order photolysis rate, J<sub>max</sub>:

$$\text{(Eq. 5.4)} \quad J_{\max}(\theta) = \int \sigma(\lambda) F(\lambda, \theta) d\lambda$$

The parameter  $\theta$  in Eq. 5.4 is the solar zenith angle. We obtain  $J_{\max} = 0.58 \text{ s}^{-1}$  and  $0.36 \text{ s}^{-1}$  at  $\theta = 0^\circ$  and  $60^\circ$  respectively.

Temperature dependent rate coefficients for thermal dissociation of Br–DMS at atmospheric pressure have been estimated based on kinetic and thermodynamic results reported by Wine et al. (1993). The thermal dissociation rate coefficients are  $\sim 10,000 \text{ s}^{-1}$  and  $1,000 \text{ s}^{-1}$  at 298 K and 265 K respectively.

Mixing ratios of NO<sub>x</sub> in the remote MBL are only a few parts per trillion (ppt) but in the polar boundary layer hundreds of ppt have been observed with an average of 225 ppt (Davis et al., 2001). Hence, reactions of Br–DMS with NO and NO<sub>2</sub> are potentially important in polar boundary layer chemistry and relatively polluted coastal regions where NO<sub>x</sub> mixing ratios can be in the parts per billion (ppb) range. For example, if one assumes 1 ppb NO<sub>x</sub> ( $\sim 2.5 \times 10^{10}$  molecules cm<sup>-3</sup> at atmospheric pressure and typical lower atmospheric temperatures) and a rate coefficient of  $2 \times 10^{-11}$  cm<sup>3</sup> molecule<sup>-1</sup> s<sup>-1</sup> for Br–DMS + NO<sub>x</sub> (based on this work), a first order rate coefficient of 0.5 s<sup>-1</sup> is obtained for these adducts removal by NO<sub>x</sub>. Using the Br–DMS + O<sub>2</sub> upper limit rate coefficients in units of 10<sup>-18</sup> cm<sup>3</sup> molecule<sup>-1</sup> s<sup>-1</sup>: 300 (Wine et al., 1993), 30 (this work), and 1 (Nakano et al., 2001), lead to upper limit first order rate coefficients of 1661, 166 and 5.5 s<sup>-1</sup> respectively, for Br–DMS removal by O<sub>2</sub> at atmospheric pressure and 265 K.

The analysis discussed above suggests that thermal dissociation of the Br–DMS adduct dominates removal of this species even at low temperatures (265 K), however, product studies (Maurer et al., 1999; Ballesteros et al., 2002) have observed CH<sub>3</sub>SBr as one of the main primary products formed from Br oxidation of DMS in air, and the potential pathway suggested for this product formation is:



To the best of this author's knowledge, no kinetic data are available for CH<sub>3</sub>SBr. One possible atmospheric fate of CH<sub>3</sub>SBr is photolysis to yield CH<sub>3</sub>S and Br. The net effect of this speculation is that the initial reactants are not reformed, i.e., DMS is not regenerated and formation of the Br–DMS adduct represents a net loss of atmospheric DMS. In order to ascertain the significance of this unimolecular decomposition pathway

of Br–DMS, more investigations are needed to elucidate the exact reaction pathway for CH<sub>3</sub>SBr production as well as kinetic behavior and products formed from reactions involving CH<sub>3</sub>SBr.

**CHAPTER 6**  
**SPECTROSCOPIC AND KINETIC STUDY OF THE GAS PHASE**  
**(CH<sub>3</sub>)<sub>2</sub>S–I ADDUCT**

**Effect of Iodine on the Sulfur Cycle**

An understanding of the oxidation pathways of DMS is essential in order to understand and quantify the effects of sulfur oxidation on aerosol and cloud condensation nuclei formation, radiative balance in the MBL, and the Earth's climate. Hydroxyl radicals (OH) and NO<sub>3</sub> have been assumed to be the main gas phase oxidizers of DMS (Barnes et al., 2006 and references therein), although studies have shown that BrO, for example, Toumi, 1994; Finlayson-Pitts and Pitts, 2000, and Cl, for example, Stickel et al., 1992; Arsene et al., 2005 are also major oxidants of DMS. Almost three decades ago, it was proposed (Chameides and Davis, 1980) that IO radicals may play a role in DMS oxidation and several laboratory and computational studies have been conducted since then to investigate the kinetics and products of this potentially important reaction:



As shown in Table 6.1, rate coefficients obtained for this reaction,  $k_{6.1}$ , vary by over three orders of magnitude, that is,  $(0.88 - 3000) \times 10^{-14} \text{ cm}^3 \text{ molecule}^{-1} \text{ s}^{-1}$ .

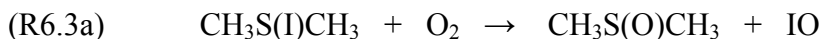
**Table 6.1 Literature Rate Coefficients at 298 K for the Reaction of IO Radicals with DMS**

<sup>a</sup> $k_{6.15}$	<i>P</i> (Torr)/bath gas	Method	Reference
1500	1/He	DF/MS	Martin et al., 1987
3000	760/ N <sub>2</sub>	FTIR	Barnes et al., 1987
<3.5	40-300/N <sub>2</sub> +O <sub>2</sub>	LFP–UV-vis	Daykin and Wine, (1990)
(1.5±0.2)	1.1–1.8/He	DF-MS	Maguin et al. (1991)
(0.88±0.27)	0–5.1/He	DF-MS	Barnes et al. (1991)
(1.6±0.3)	2.5–2.7/He	DF-MS	Knight and Crowley, (2001)
(1.0±0.3)	5/ N <sub>2</sub>	CRDS	Nakano et al. (2003)
(25±2)	200/ N <sub>2</sub>	CRDS	Nakano et al. (2003)
(2.0±0.5)	5–300/He	PLP-LIF	Gravestock et al. (2005)
(1.44±0.15)	50–300/ N <sub>2</sub> or air	PLP-LIF	Dillon et al. (2006)

<sup>a</sup>Units are x 10<sup>-14</sup> cm<sup>3</sup> molecule<sup>-1</sup> s<sup>-1</sup>

Studies conducted earlier than Daykin and Wine, (1990) such as Martin et al. (1987) and Barnes et al. (1987) which reported high rate constants ( $1.5$  and  $3.0 \times 10^{-11} \text{ cm}^3 \text{ molecule}^{-1} \text{ s}^{-1}$  respectively), were found to be erroneous due to heterogeneous chemistry that was unaccounted for in the derivation of  $k_{6,1}$ . The current IUPAC recommendation of  $k_{6,1}$  (298 K) is  $(1.5 \pm 0.2) \times 10^{-14} \text{ cm}^3 \text{ molecule}^{-1} \text{ s}^{-1}$ , leading to the conclusion that IO does not play an important role in DMS oxidation and the iodine and sulfur cycles remain uncoupled.

In this study we investigate another possible iodine and sulfur coupling through the reactions:



### **The Reaction of Iodine atoms with DMS**

There is one investigation of the I + DMS reaction reported in the literature, which was conducted by Shum and Benson (1985) at low pressures  $< 10$  Torr and high temperatures 630 – 650 K. These researchers employed very low pressure pyrolysis (VLPP) and reported an Arrhenius expression for reaction (R6.4),  $k_{6,4} = 2.62 \times 10^{-10} \exp(-13436/T) \text{ cm}^3 \text{ molecule}^{-1} \text{ s}^{-1}$ , which gives a 298 K rate constant of  $6.9 \times 10^{-30} \text{ cm}^3 \text{ molecule}^{-1} \text{ s}^{-1}$ , implying that at temperatures  $\leq 298$  K, if an I + DMS reaction occurs at all, the mechanism must involve adduct formation.



In this work we report the results of an experimental study of the gas phase I + DMS reaction that couples LFP production of I with product detection by TRUVVAS. The gas phase absorption spectrum of the I-DMS adduct in the wavelength range 350–550 nm is reported for the first time, as well as the kinetics of adduct reactions with O<sub>2</sub>, NO, and NO<sub>2</sub>. In parallel with this TRUVVAS study, a resonance fluorescence (RF) study was also being conducted in our lab to determine the equilibrium kinetics of the I-DMS adduct. It is worth mentioning that the recent work in our lab represents the only available information on the I-DMS adduct.

Additional motivation for this study was derived from the work of Enami et al., 2004. These investigators reported IO production via the reaction: CH<sub>2</sub>I + O<sub>2</sub> → HCHO + IO, which led to the consideration that reaction (R6.3a) may be possible. However, a detailed mechanistic study of this reaction (Gravestock, 2006) provides evidence that IO is not formed by direct reaction of CH<sub>2</sub>I + O<sub>2</sub>.

### **Experimental Method**

The kinetics and spectroscopy of the I–DMS adduct were studied by monitoring the absorbance temporal profile generated by 248 nm photolysis of the reaction mixture CH<sub>3</sub>I/DMS/N<sub>2</sub>/O<sub>2</sub>. The absorption cross section for CH<sub>3</sub>I at 248 nm is 8.4 x 10<sup>-19</sup> cm<sup>2</sup>. Iodomethane (CH<sub>3</sub>I) has an I + I\* quantum yield (Φ) of unity and Φ(I\*) in the range 0.72 – 0.81 (Sander et al., 2006 and references therein); a typical photolysis fluence was ~20

mJ cm<sup>-2</sup> and the pulse duration was ~25 ns. A high pressure Xe arc lamp was used as the UV-VIS probe source and a 0.22 m grating monochromator and photomultiplier tube were used for probe beam detection. In spectrum mapping experiments, the monochromator entrance and exit slits were set to 1.5 mm and gave a resolution of 5.5 nm (full width half maximum), while in experiments where attempts were made to observe IO absorption, slit widths of 0.2 mm were used which gave a resolution of 0.72 nm and an effective IO absorption cross section of  $(1.8 \pm 0.3) \times 10^{-17}$  cm<sup>2</sup> (Daykin and Wine, 1990).

Concentrations of both CH<sub>3</sub>I and DMS were measured *in situ* in the slow flow system by UV photometry and by mass flow measurements. The *in situ* photometry measurements were conducted using two separate absorption cells. A 1 m absorption cell, Zn pen ray lamp, 214 nm band-pass filter, and side-on PMT were used for CH<sub>3</sub>I monitoring, and a 40.6 cm absorption cell, Hg pen ray lamp, 254 nm band-pass filter and side-on PMT were used for DMS monitoring. The cross-sections used to convert 214 nm and 254 nm absorbances to concentrations were  $1.69 \times 10^{-18}$  cm<sup>2</sup> molecule<sup>-1</sup> (Sander et al., 2006) and  $5.2 \times 10^{-21}$  cm<sup>2</sup> molecule<sup>-1</sup> (Hearn et al., 1990) for CH<sub>3</sub>I and DMS, respectively. The absorption cross section for DMS at 248 nm is  $1.28 \times 10^{-20}$  cm<sup>2</sup> molecule<sup>-1</sup> (Hearn et al., 1990); DMS concentrations employed in these experiments were  $\leq 3 \times 10^{16}$  molecules cm<sup>-3</sup> which, using the typical laser fluence mentioned above, implies that laser light attenuation from DMS absorption is ~ 4% at high [DMS]. The quantum yields of CH<sub>3</sub>S and H from DMS photolysis at 248 nm are 0.93 and zero respectively (Barone et al., 1994), thus, [CH<sub>3</sub>S]  $\equiv$  [CH<sub>3</sub>] radicals produced from DMS photolysis is  $\leq 2.4 \times 10^{13}$  cm<sup>-3</sup> each. All experiments were carried out under “slow flow” conditions, i.e.,

the linear flow rate of the reaction mixture through the reaction cell (typically  $10 \text{ cm s}^{-1}$ ) was fast enough to replenish the entire volume of the reaction cell between photolysis laser pulses (laser repetition rate was 0.1 Hz and the cell length was 100 cm), but slow enough that kinetic observations could be analyzed assuming static conditions.

The concentrations of NO and NO<sub>2</sub> were determined from mass flow measurements of NO<sub>2</sub>/N<sub>2</sub> or NO<sub>2</sub>/N<sub>2</sub>/O<sub>2</sub> mixtures combined with photometric measurements of the NO<sub>2</sub> mole fraction in the NO<sub>2</sub>/N<sub>2</sub>/O<sub>2</sub> mixtures as described in Chapter 2.

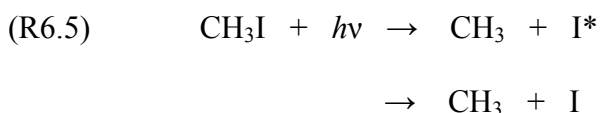
Experiments were carried out over a temperature range of 205 – 235 K and a pressure range of 20 – 250 Torr of 2% O<sub>2</sub> in N<sub>2</sub>. The reaction cell and pre-mixing cell were surrounded by an insulated Pyrex jacket through which an ethanol/methanol mixture was flowed from a temperature-controlled reservoir, enabling the cell temperature to be controlled. The temperature of the gas mixture was determined by inserting a thermocouple at various points inside the reaction cell. The average of the temperatures measured, which ranged from 203 K – 205 K, was taken to be the cell temperature. Dry nitrogen gas was sprayed on the exterior of the quartz cell windows to prevent condensation of water vapor when the cell was cooled.

The pure gases used in this work were obtained from Air Products (2% O<sub>2</sub> in N<sub>2</sub>, O<sub>2</sub>, N<sub>2</sub>) and Spectra Gases (NO), and had the following stated minimum purities: 2%O<sub>2</sub> in N<sub>2</sub>, >99.9%; N<sub>2</sub>, 99.999%; O<sub>2</sub>, 99.994%; NO, 99.0%. The 2%O<sub>2</sub> in N<sub>2</sub>, N<sub>2</sub>, and O<sub>2</sub> were used as supplied. Nitric oxide (NO) was degassed at 77 K prior to use. The liquids used in this work, DMS, CH<sub>3</sub>OH and CH<sub>3</sub>I, were supplied by Sigma-Aldrich and had stated minimum purities of 99.0%, 99.8% and 99.9% respectively. Dimethyl sulfide and

methanol were transferred under N<sub>2</sub> into Pyrex reservoirs which were then submerged into thermostat-regulated baths. Iodomethane was transferred under N<sub>2</sub> into a vial fitted with a high-vacuum stopcock. After repeated degassing at 77 K, appropriate amounts were transferred into a 12-L Pyrex bulb and diluted with N<sub>2</sub>.

## Results and Discussion

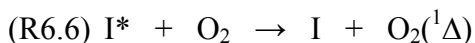
When CH<sub>3</sub>I was photolyzed at 248 nm in the presence of DMS, absorption of the UV-visible probe beam was observed throughout the 340 to 550 nm spectral region. Absorption was observed only when both CH<sub>3</sub>I and DMS were present in the photolyzed gas mixture. The likely products formed following 248 nm photolysis of CH<sub>3</sub>I are:



where I\* is the <sup>2</sup>P<sub>1/2</sub> spin-orbit excited state atom and I is the <sup>2</sup>P<sub>3/2</sub> ground state atom.

The yield of I\* formed is ~ 0.8 (Pence et al., 1981; Baughcum and Leone, 1980) and, in the presence of a quenching gas such as O<sub>2</sub>, deactivation of I\* occurs mainly via reaction

(R6.6) (Derwent and Thrush, 1971):



The excited O<sub>2</sub>(<sup>1</sup>Δ) formed in reaction (R6.6) is quite unreactive with nitrogen and oxygen in the bath gas and is likely unreactive with DMS or CH<sub>3</sub>I (Sander et al., 2006).

The rate constants for O<sub>2</sub> and CH<sub>3</sub>OH quenching of I\* are, (in units of 10<sup>-12</sup> cm<sup>3</sup> molecule<sup>-1</sup> s<sup>-1</sup>), ~ 15 and 5.5 respectively (Chichinin, 2006 and references therein). Back to back experiments were conducted alternating between methanol (1.6 x 10<sup>16</sup> molecules cm<sup>-3</sup>) and O<sub>2</sub> (4.3 x 10<sup>16</sup> molecules cm<sup>-3</sup>) as the quenching gas with the monochromator setting tuned to 427.2 nm with 0.22 mm slits. The peak absorbance was found to be equally small in both cases, indicating that IO was not being produced. The monochromator setting was then switched to 390 nm (approximately the  $\sigma_{\max}$  of the absorbing species) and the appearance rate,  $k_a$ , as well as the maximum observed absorbance ( $A$ ) were determined under four sets of conditions. The data obtained suggested that no apparent experimental advantage was achieved by using methanol as the quenching gas and, given the difficulty of introducing methanol to the reaction mixture at low temperatures, we henceforth employed 2% O<sub>2</sub> in N<sub>2</sub> as our bath gas. Under the experimental conditions employed, the appearance of absorbance was very fast (~300,000 s<sup>-1</sup>) compared to the decay of absorbance (~6,000 s<sup>-1</sup>). Absorbance temporal profiles were recorded and analyzed using a nonlinear least squares fit to Eq. 4.1, which describes the time evolution of the intermediate in consecutive first-order reactions (Atkins, 2006):

$$\text{(Eq. 4.1)} \quad A_t = \{k_a/(k_d - k_a)\}X\{\exp(-k_a t) - \exp(-k_d t)\}$$

In the above equation,  $A_t$  is the absorbance at time  $t$ ,  $k_a$  is the rate at which the adduct equilibrates, i.e., the rate of the forward reaction plus the rate of adduct decomposition,  $k_d$  is the first-order absorbance decay rate, and  $X$  is the peak adduct absorbance that would be observed in the absence of a decay. A typical absorbance temporal profile is

shown in Figure 6.1. In these experiments our measured appearance rates range from 250,000 – 300,000 s<sup>-1</sup>, which can be attributed to the sum of the adduct formation rate ~ 108,000 and the adduct decomposition rate of ~ 1.5 times its formation rate. The adduct formation rate was estimated based on a rate coefficient for  $k_{6,2a} = 3.1 \times 10^{-12} \text{ cm}^3 \text{ molecule}^{-1} \text{ s}^{-1}$  obtained in He bath gas at  $T = 190 \text{ K}$  and  $P = 40 \text{ Torr}$ , and  $[\text{DMS}] = 1.8 \times 10^{16} \text{ molecules cm}^{-3}$ . This appearance rate was not resolvable since our electronic response rate was ~ 690,000 and precluded our determination of  $k_{6,2a}$  due to the fast decomposition rate.

Prior to conducting experiments to study the I–DMS adduct, IO was produced in our reaction cell by 308 nm photolysis of I<sub>2</sub>/NO<sub>2</sub>/N<sub>2</sub> gas mixtures. Iodine monoxide (IO) absorbance temporal profiles were observed by tuning the monochromator wavelength to 427.2 nm (the peak of the strong, diffuse 4-0 band of the IO A<sup>2</sup>π - X<sup>2</sup>π system [Coleman et al., 1948; Durie and Ramsay, 1958]) and by using slit widths of 0.2 mm. Possible contribution to observed absorbance temporal profiles due to IO were sought by tuning our monitoring wavelength on and off of 427.2 nm and employing narrow slit widths of 0.2 mm. However, there was no increase in absorption, suggesting that this species was not contributing to the observed absorption. Shown in Figures 6.2 and 6.3 are the spectra obtained in this study and that of I<sub>2</sub> respectively. Observed in Figure 6.2, in the region 360 – 450 nm, there exists a strong band suggesting the presence of an absorbing species other than I<sub>2</sub>, which may be formed as a reaction product, for example, via reaction (R6.7).

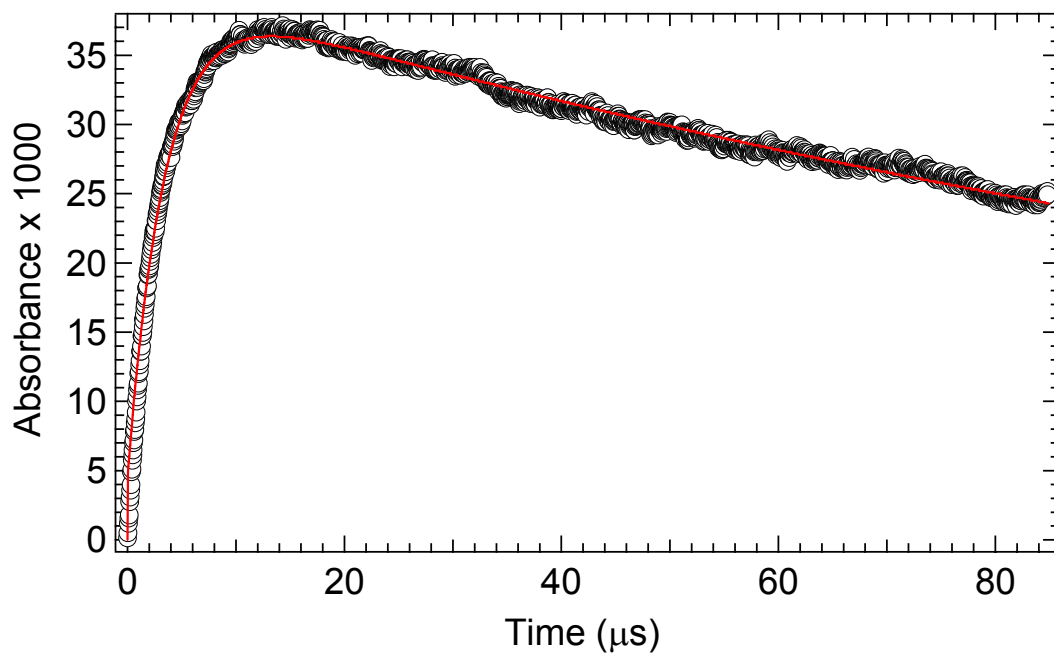


**Figure 6.1** Typical absorbance (base e) temporal profile observed following laser flash photolysis of DMS/CH<sub>3</sub>I/2% O<sub>2</sub> in N<sub>2</sub> mixtures at 248 nm. Experimental conditions:  $T = 205$  K;  $P = 50$  Torr; monitoring wavelength = 390 nm; concentrations in units of  $10^{14}$  molecules  $\text{cm}^{-3}$  are  $[\text{CH}_3\text{I}] = 7.88$ ,  $[\text{DMS}] = 180$ , and  $[\text{I}]_0 \approx 0.22$ . The solid line is obtained from a nonlinear least squares fit of the data to the sum of an exponential rise and an exponential decay. Best fit appearance ( $k_a$ ) and disappearance ( $k_d$ ) rate coefficients in units of  $\text{s}^{-1}$  are  $k_a = 253,000$  and  $k_d = 6800$ .

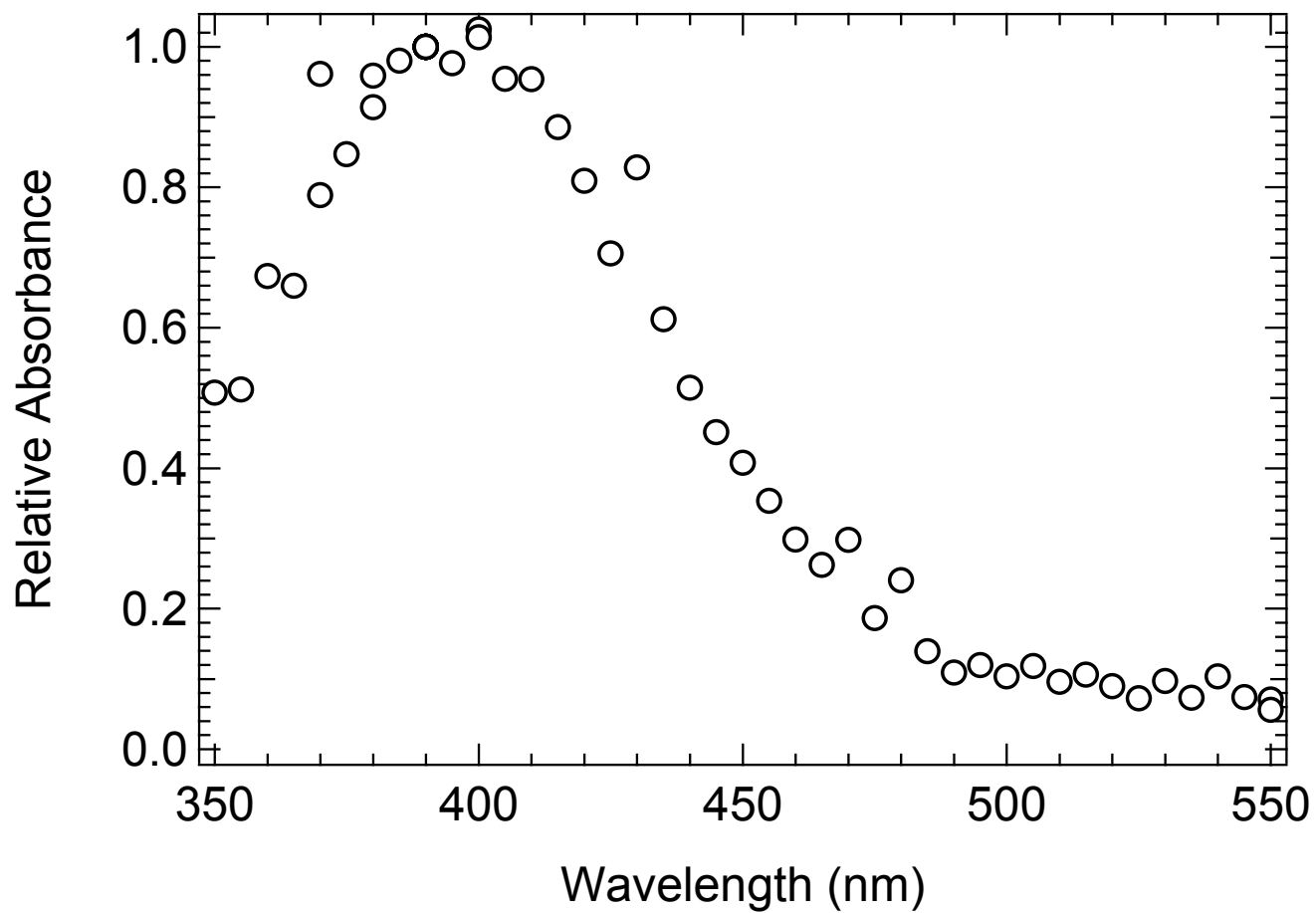


Figure 6.2 I-DMS absorption spectrum at a spectral resolution of 5.5 nm.

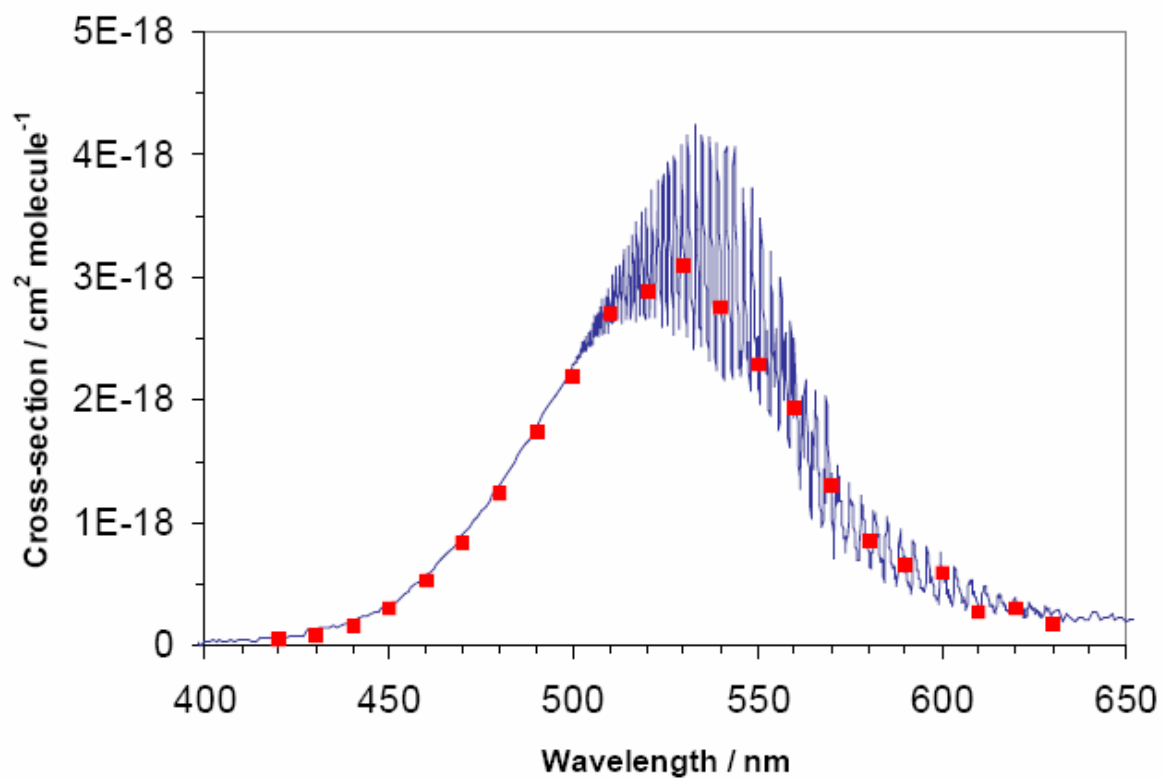


Figure 6.3 Absorption spectrum of I<sub>2</sub> (Tellinghuisen, 1973 – spectral resolution of 2.6 nm; Saiz-Lopez et al., 2004 – spectral resolution of 0.1 nm)

In the absence of comparable data such as appearance rate coefficients and other gas or liquid phase spectra for the I–DMS adduct coupled with the fact that transient absorption is only observable at very low temperatures (205 K), our data suggest that the observed spectrum shown in Figure 6.2 is most likely that of the I–DMS adduct.

The tail of the I–DMS spectrum is probably due to I<sub>2</sub> absorption in the region 500 – 550 nm, coinciding with the peak of the I<sub>2</sub> absorption spectrum as shown in Figure 6.3.

### Adduct Absorption Spectrum

The absorption spectrum of I–DMS was measured on several days to verify reproducibility, and under conditions of 50 Torr total pressure (N<sub>2</sub> bath gas containing 2% O<sub>2</sub>) and 205 K using 248 nm photolysis of CH<sub>3</sub>I to generate I\* atoms which are quenched as discussed above. Absorption measurements were made over the wavelength range 350–550 nm, and a reference wavelength of 390 nm was selected. Absorption measurements were made at this reference wavelength after every 5 measurements at other wavelengths. This was done in order to account for systematic drifts in experimental parameters such as laser power, [CH<sub>3</sub>I], optical alignment, etc. over time. Absorbance measurements at wavelengths other than 390 nm were normalized to the average of the “before” and “after” 390 nm absorbances. The adduct absorption cross section was carefully measured at 390 nm and all cross-sections were then determined by applying the normalization factor to the carefully measured reference cross-section. Typical reagent concentrations employed in these measurements in units of 10<sup>14</sup> molecules cm<sup>-3</sup> were as follows: [DMS] ≈ 260; [CH<sub>3</sub>I] ≈ 0.81–7.4; [I]<sub>0</sub> ≈ 0.02–0.23; a

typical absorbance temporal profile under these conditions is shown in Figure 6.1. In the absence of equilibrium data for the I–DMS adduct, experiments were conducted to determine the optimum DMS concentration to be employed in our experiments by holding  $[I]_0$  constant ( $\sim 7.3 \times 10^{13}$  molecules  $\text{cm}^{-3}$ ) and varying  $[\text{DMS}]$  concentrations until no change in adduct absorbance was observed ( $\sim 3 \times 10^{16}$  molecules  $\text{cm}^{-3}$ ) under conditions of  $P = 50$  Torr of 2%  $\text{O}_2$  and  $T = 205$  K. Subsequent to completion of these TRUVVAS experiments, some experiments employing resonance fluorescence detection of I atom decay which were performed at  $P = 10 - 40$  Torr  $\text{O}_2$  and  $T = 190$  K, permitted  $\Delta H_{190}$  determination. Based on ab initio data supplied by Dr. M. McKee of Auburn University (see Table 6.2),  $\Delta S_{190}$  for reaction (R6.2a) was calculated to be  $-88.3 \text{ J K}^{-1} \text{ mol}^{-1}$  and  $K_c$  at 205 K was derived. The I–DMS cross-section at 390 nm ( $\sigma_{390}$ ) was, therefore, determined from the data using the following relationship:

$$\text{(Eq. 6.1)} \quad \sigma_{390} = X / (l [I]_0 F).$$

In Eq. 6.1,  $X$  is defined as in Eq. 4.1 (see above),  $l$  is the absorption path length (100 cm),  $[I]_0$  is the concentration of iodine atoms produced via laser flash photolysis of  $\text{CH}_3\text{I}$ , and  $F$  is the fraction of I atoms converted to adduct. As is typical for gas phase spectroscopic data, the absorbance is defined as  $A = \ln(I_0/I_t)$  where  $I_0$  is the transmitted light intensity before the laser fires and  $I_t$  is the transmitted light intensity at some time  $t$  after the laser fires, i.e.,  $A$  is a base  $e$  absorbance.

The parameter  $F$  in Eq. 6.1 can be evaluated using the following relationship:

$$\text{(Eq. 6.2)} \quad F = (1 - F_1) (1 - F_2) (1 - F_3)$$

**Table 6.2 Structural parameters used in the evaluation of absolute entropies for DMS, I atoms, and I–DMS adduct**

<b>DMS</b>	
Vibrational frequencies <sup>a</sup>	178.1, 178.4, 258.3, 674.3, 726.7, 912.8, 950.5, 985.3, 1050.5, 1340.4, 1364.2, 1463.1, 1471.9, 1478.5, 1486.6, 3028.4, 3031.3, 3098.7, 3106.3, 3122.9, 3123.9
Rotational constants <sup>a</sup>	0.6; 0.2; 0.2
Methyl rotational barrier	1.87 kcal/mol

<b>I–DMS</b>	
Vibrational frequencies <sup>a</sup>	74.6, 91.1, 146.2, 164.5, 182.5, 263.4, 668.6, 720.4, 920.5, 945.2, 975.9, 1055.5, 1340.3, 1361.4, 1457.2, 1463.9, 1469.2, 1474.5, 3043.4, 3045.3, 3128.1, 3131.7, 3145.1, 3145.9
Rotational constants <sup>a</sup>	0.2; 0.0; 0.0
Methyl rotational barrier	1.64 kcal/mol

**Calculations at the B3LYP/6-311+G(2D,P)/ECP(I/SDD) level and were kindly supplied by Dr. M. McKee.**

<sup>a</sup>Units in cm<sup>-1</sup>.

In Eq. 6.2,  $F_1$  is the fraction of I atoms that are lost by diffusion from the detection volume and/or reaction with background impurities,  $F_2$  is the fraction of I atoms that react with DMS by H-abstraction rather than by addition, and  $F_3$  is the fraction of I–DMS + I that exists as I when the two species are in equilibrium.

The background loss rate of I atoms observed in RF experiments was found to be  $\sim 30 \text{ s}^{-1}$ , hence we conservatively assign  $F_1$  the value  $0.05 \pm 0.05$ ,  $F_2$  is too small to be considered (Shum and Benson, 1985), and based on calculations of  $K_c$  noted above,  $F_2 \sim 0.60 \pm 0.09$ . The above considerations lead to the results  $F = 0.38 \pm 0.14$  where the reported uncertainties are estimates of accuracy at the 95% confidence level.

Cross-sections obtained from Eq. 6.1 were found to be independent of  $[I]_0$  over the ranges specified above, i.e., Beer's law was obeyed. Evaluation of  $[I]_0$  required (i) careful measurements of  $[CH_3I]$  and laser power, (ii) careful measurements of  $[DMS]$ , and (iii) careful measurements of the photolysis laser beam cross-sectional area and its divergence down the length of the cell (the laser beam area increased by a factor of 1.5 between the cell entrance and exit, and was assumed to be the average of the entrance and exit areas for purposes of evaluating  $[I]_0$ ).

The adduct spectrum measured in this study at  $T = 205 \text{ K}$  and  $P = 50 \text{ Torr}$  2%  $O_2$  is shown in Figure 6.2 and is given in digitized form in Table 6.3. As mentioned previously, the I–DMS absorption spectrum was measured on several days verifying reproducibility of data. The 1.5 mm monochromator slit widths used for these measurements had a spectral dispersion of 5.5 nm FWHM (full width half maximum).

**Table 6.3** Absorption cross sections for the I–DMS adduct as a function of wavelength at  $T = 205$  K and a spectral resolution of 5.5 nm (FWHM).

$\lambda^a$	$\sigma^b$	$\lambda^a$	$\sigma^b$	$\lambda^a$	$\sigma^b$
350	2.08	425	2.89	500	0.42
355	2.09	430	3.39	505	0.48
360	2.75	435	2.50	510	0.39
365	2.70	440	2.10	515	0.43
370	3.58	445	1.85	520	0.37
375	3.46	450	1.67	525	0.30
380	3.83	455	1.44	530	0.40
385	4.01	460	1.22	535	0.30
390	4.09	465	1.07	540	0.42
395	3.99	470	1.22	545	0.30
400	4.17	475	0.76	550	0.26
405	3.90	480	0.98		
410	3.90	485	0.57		
415	3.62	490	0.45		
420	3.31	495	0.49		

<sup>a</sup>Units of  $\lambda$  in nm; <sup>b</sup>units of  $\sigma$  in  $10^{-17}$  cm<sup>2</sup> molecule<sup>-1</sup>.

Consideration of uncertainties in the parameters that must be known to obtain the adduct cross section (see above), leads to an estimate of  $\pm 40\%$  for the accuracy of the measured cross section at 390 nm (95% confidence level). We report this cross-section to be  $\sigma_{395} \approx \sigma_{\max} = (4.1 \pm 1.6) \times 10^{-17} \text{ cm}^2 \text{ molecule}^{-1}$ .

As mentioned previously, there are no other measurements with which to compare the absorption cross sections and wavelength dependencies reported in this study, however, by comparison with other halogen sulfur adducts studied such as  $(\text{CH}_3)_2\text{S}-\text{Cl}$  (Urbanski and Wine, 1999),  $\text{SCS}-\text{Cl}$ , (Dookwah-Roberts et al., 2005, Chapter 3 of this dissertation),  $\text{CH}_3(\text{O})\text{S}(\text{Cl})\text{CH}_3$  (Kleissas et al., 2007), and  $(\text{CH}_3)_2\text{S}-\text{Br}$  (Chapter 5 of this dissertation), the  $\sigma_{\max}$  obtained for I-DMS is almost exactly equal to that reported for  $\text{CH}_3(\text{O})\text{S}(\text{Cl})\text{CH}_3$  ( $4.0 \times 10^{-17} \text{ cm}^2 \text{ molecule}^{-1}$ ) and slightly larger than reported cross sections for  $(\text{CH}_3)_2\text{S}-\text{Cl}$  and  $(\text{CH}_3)_2\text{S}-\text{Br}$ ,  $3.48$  and  $2.7 \times 10^{-17} \text{ cm}^2 \text{ molecule}^{-1}$  respectively. Also, the I-DMS spectrum is red-shifted from the Br-DMS spectrum which is red-shifted from the Cl-DMS spectrum, consistent with the trend observed for numerous halogenated species.

Figure 6.4, courtesy of Dr. M. McKee of Auburn University, shows a schematic of the most probable structure for the  $(\text{CH}_3)_2\text{S}-\text{I}$  adduct obtained using the B3LYP/6-311+G(2d,p)/ECP(I/SDD) level of theory.

### Radical-Radical Reaction Kinetics

When reaction mixtures containing only  $\text{CH}_3\text{I}$ , DMS,  $\text{N}_2$  and  $\text{O}_2$  are subjected to 248 nm laser flash photolysis and detectable levels of I-DMS are generated, we expect that  $(\text{CH}_3)_2\text{S}-\text{I}$  loss will be controlled by the following radical-radical reactions:

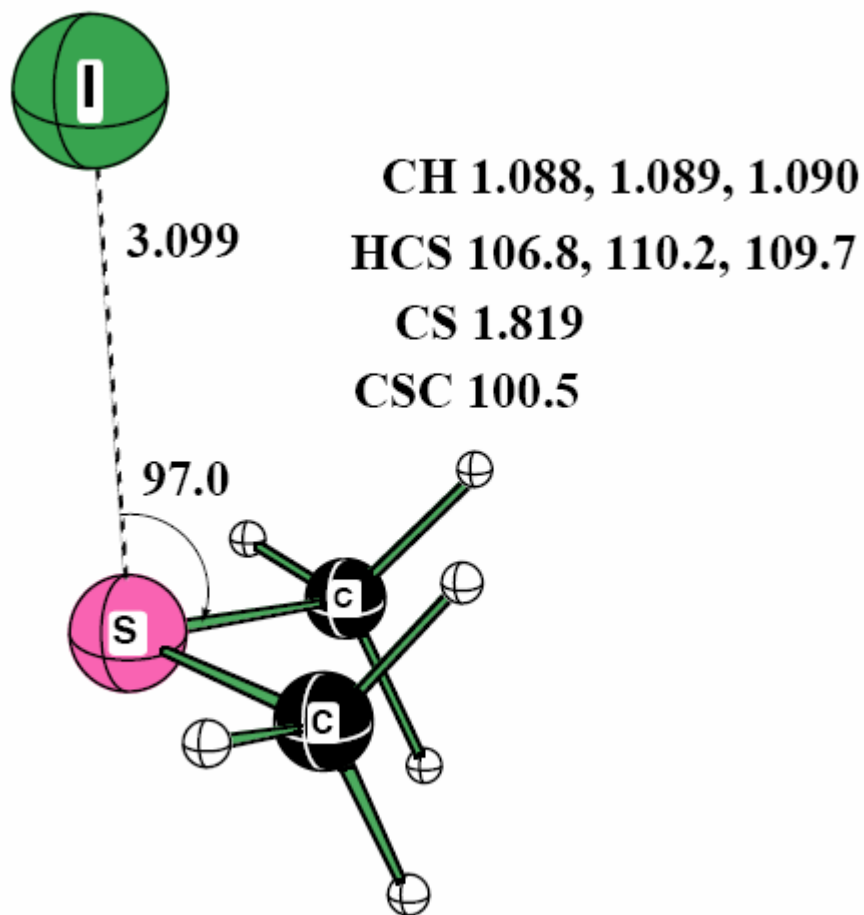
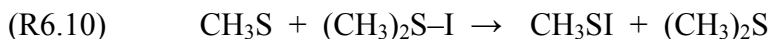
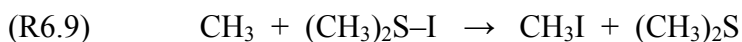
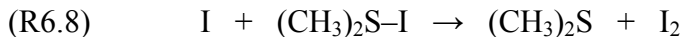
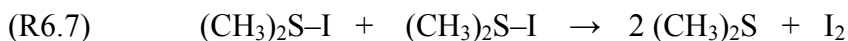
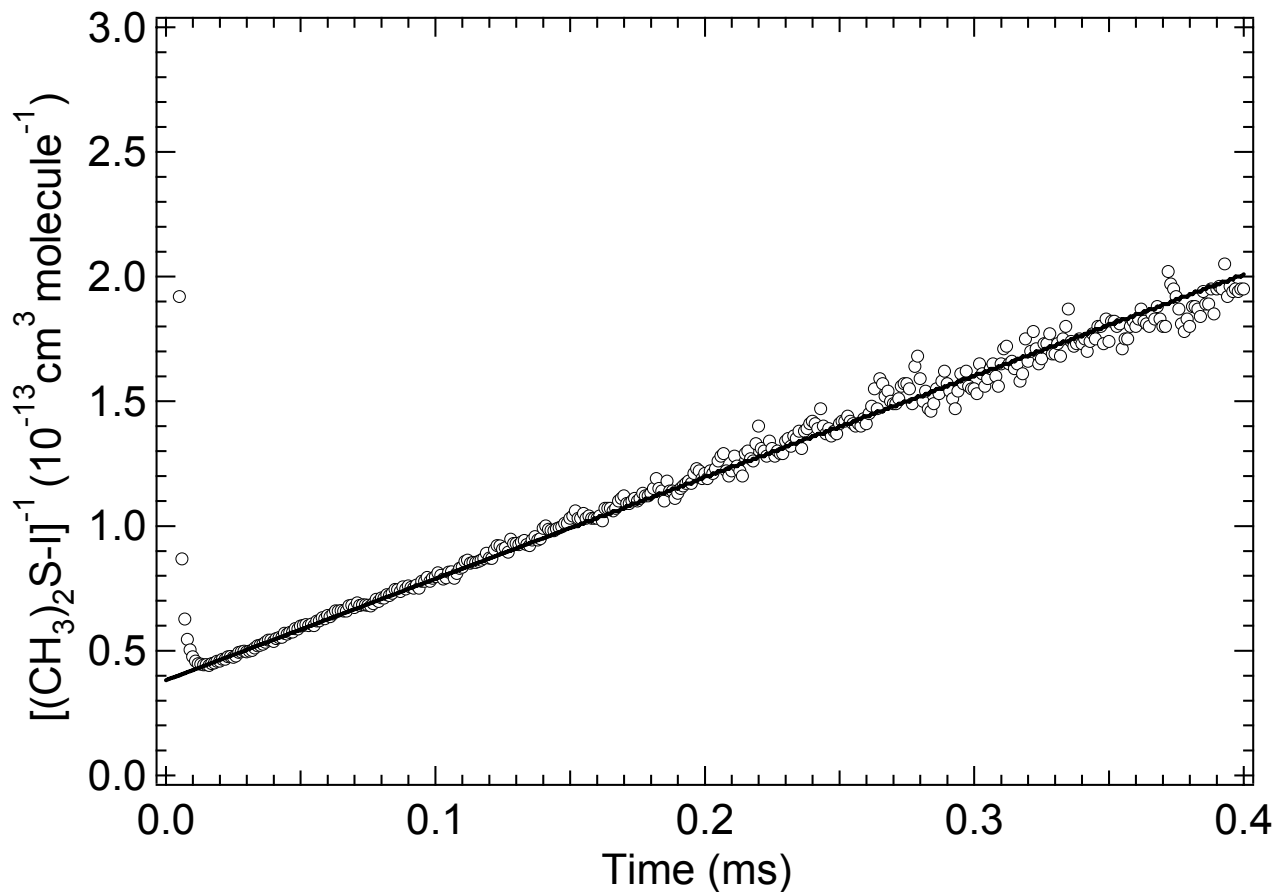


Figure 6.4 Structure for  $(\text{CH}_3)_2\text{S-I}$  derived from ab initio calculations at the B3LYP/ECP level courtesy Dr. M. McKee.



Because  $[(CH_3)_2S-I]$  is not in large excess over  $[I]$ , other reactions may also be important. The products identified in reactions (R6.7–R6.10) above are the probable dominant products but not necessarily the only products that are energetically feasible. The I self-reaction is very slow and, therefore, is not listed above. For experimental conditions adopted where  $T = 205$  K,  $P = 50$  Torr 2%  $O_2$  in  $N_2$ ,  $[I]_0 = (0.3-3.2) \times 10^{13}$  molecules  $cm^{-3}$ , and  $[DMS] = 2.6 \times 10^{16}$  molecules  $cm^{-3}$ , I reacts rapidly with DMS to form ~40%  $(CH_3)_2S-I$  as derived from  $K_c$  above, thus implying that contributions from reaction (R6.8) are likely; radical reaction contributions from reactions (R6.8) and (R6.10) are also likely due to high  $[DMS]$  employed. The concentration of  $CH_3$  produced from DMS photolysis plus  $CH_3I$  photolysis was in the range  $(1.7 - 4.1) \times [I]_0$  and  $[CH_3S]$  produced from DMS photolysis was  $\sim 2.3 \times 10^{13}$  molecules  $cm^{-3}$ .

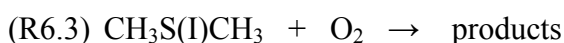
Based on our experimental limitations of temperature and  $[DMS]$  we were unable to drive the equilibrium of reaction (R6.2) further than to 40% adduct conversion. As a result, high radical concentrations were unavoidable leading to numerous possibilities for radical-radical reactions occurring simultaneously in our reaction cell. This precluded our determination of  $k_{6.7}$ . A typical absorbance temporal profile, plotted as  $[I-DMS]^{-1}$  versus time, is shown in Figure 6.5.



**Figure 6.5** Typical I-DMS absorbance temporal profile plotted as  $[I-DMS]^{-1}$  vs. time. Experimental conditions:  $T = 205$  K;  $P = 50$  Torr 2%  $O_2$  in  $N_2$ ; concentrations in units of  $10^{14}$  molecules  $cm^{-3} = 5.24$   $CH_3I$  and 265 DMS. The solid line is obtained from a linear least squares analysis; its slope gives  $k = (4.14 \pm 0.02) \times 10^{-10}$   $cm^3$  molecule $^{-1}$  s $^{-1}$  where the uncertainty is  $2\sigma$  and represents precision only.

### Kinetics of I–DMS Reaction with O<sub>2</sub>

To investigate the kinetics of the reaction of I–DMS with O<sub>2</sub>, I–DMS absorbance temporal profiles were measured in 250 Torr of O<sub>2</sub> with experimental conditions adjusted to high [DMS] and low [I]<sub>0</sub> in order to accentuate the importance of any pseudo-first order component in the decay in the presence of O<sub>2</sub>.



Temporal profiles observed in 250 Torr of 100% O<sub>2</sub> were indistinguishable from those observed in 2% O<sub>2</sub> in N<sub>2</sub> bath gas; a plot of [I–DMS]<sup>-1</sup> versus time for a typical experiment is shown in Figure 6.5. Little or no reaction of I–DMS with O<sub>2</sub> was observed at  $T \sim 205$  K. In order to put a reasonable upper limit on  $k_{6.3}$ , kinetic simulations were carried out for a simple two-reaction scheme, i.e., radical-radical reactions and (R6.3), with the radical-radical reaction rate fixed at an average gas kinetic limit of  $5.0 \times 10^{-10} \text{ cm}^3 \text{ molecule}^{-1} \text{ s}^{-1}$  (typical of radical-radical reaction rate coefficients measured in previous studies). Shown in Figure 6.6 are plots of simulated temporal profiles for  $k_{6.3} = 0, 3.0, \text{ and } 5.0 \times 10^{-17} \text{ cm}^3 \text{ molecule}^{-1} \text{ s}^{-1}$ . We conclude that upward curvature in [I–DMS]<sup>-1</sup> versus time plot would have been observed if  $k_{6.3} > 3.0 \times 10^{-17} \text{ cm}^3 \text{ molecule}^{-1} \text{ s}^{-1}$ , and we adopt this value as the upper limit for  $k_{6.3}$  that is consistent with our data.

### Kinetics of I–DMS Reactions with NO and NO<sub>2</sub>

The reactions of I–DMS with NO and NO<sub>2</sub> were studied at  $T = 205$  K and  $P = 50$  Torr (2% O<sub>2</sub> bath gas) under pseudo-first order conditions with  $[\text{NO}_x] \gg [\text{I–DMS}]$ .

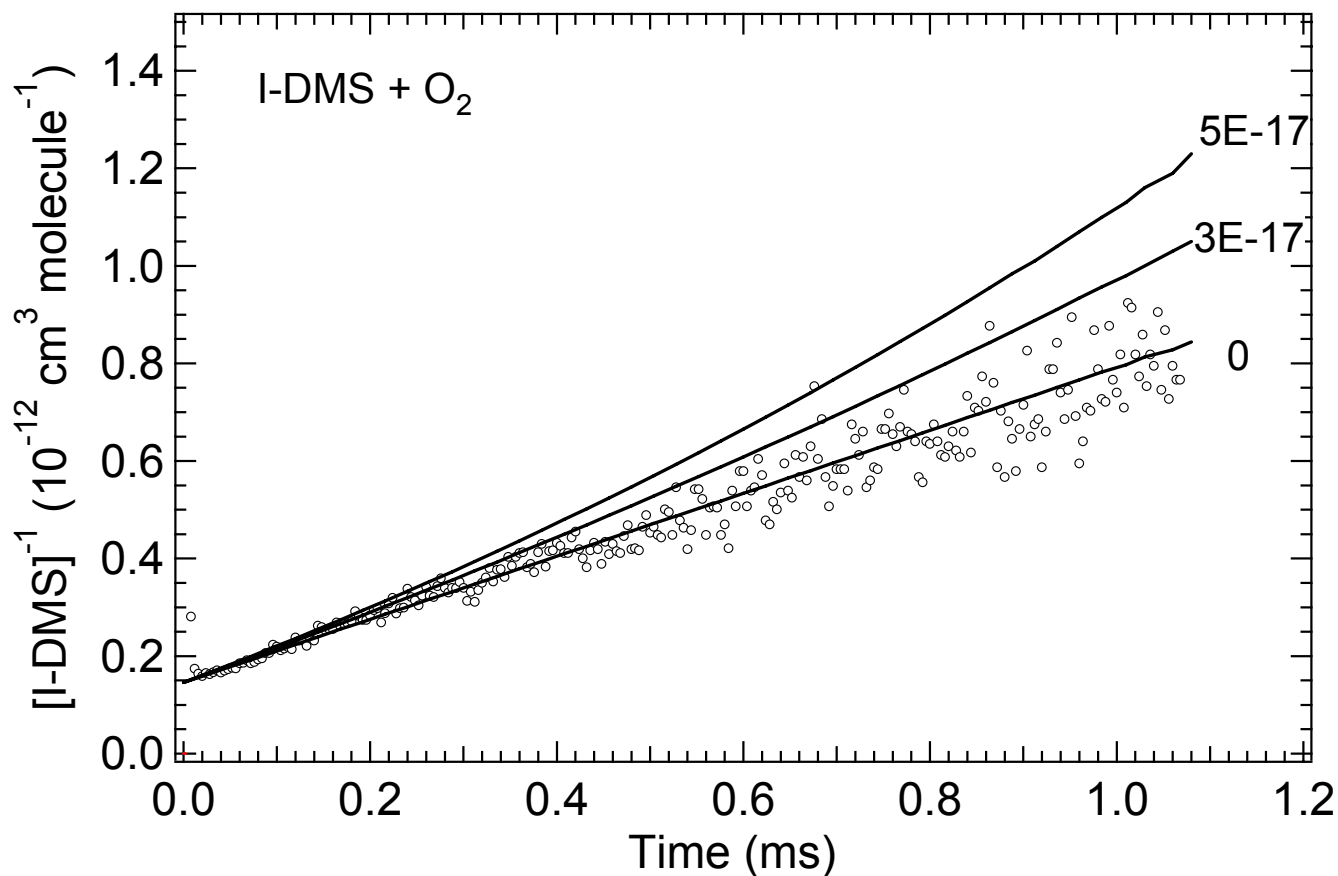
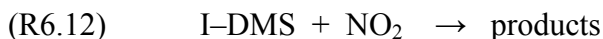
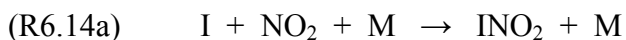
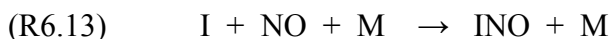


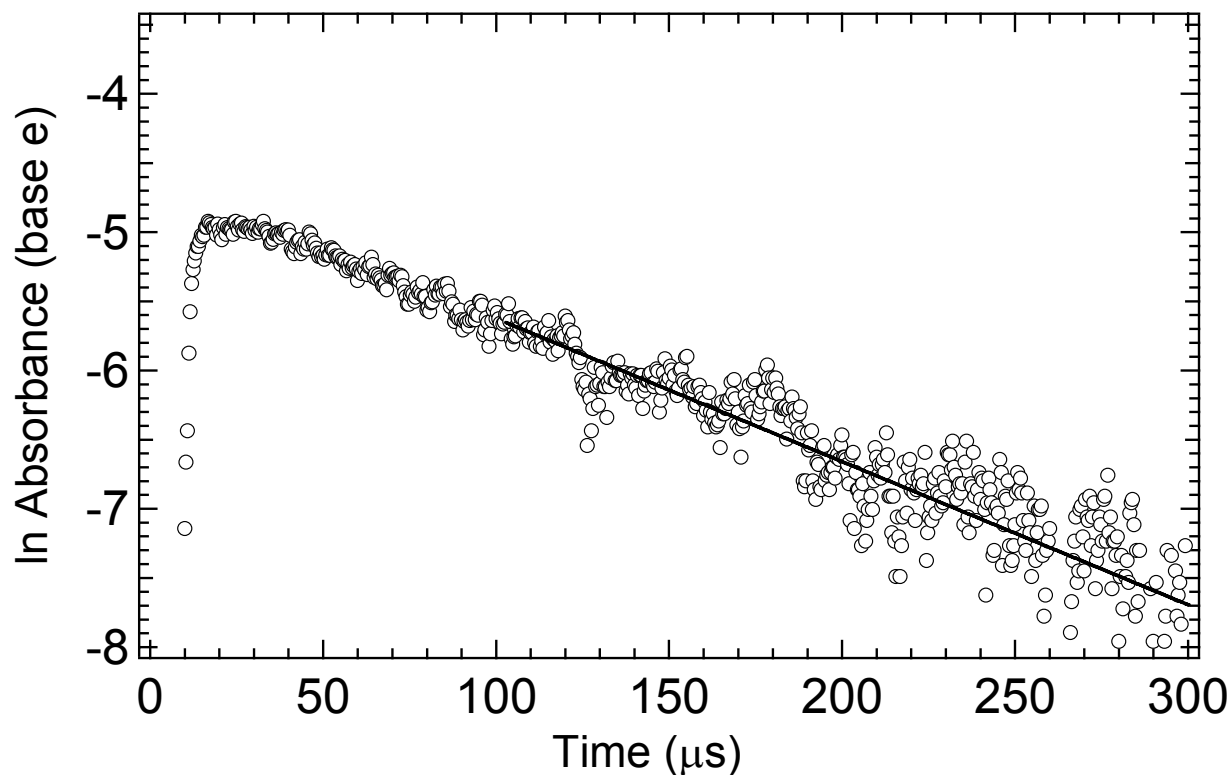
**Figure 6.6** I-DMS absorbance temporal profile plotted as  $[I-DMS]^{-1}$  vs. time. Experimental conditions:  $T = 205$  K;  $P = 258$  Torr 2%  $O_2$  in  $N_2$ ; concentrations in units of  $10^{14}$  molecules  $cm^{-3} = 4.49$   $[CH_3I]$ , 448  $[DMS]$ , and  $\sim 0.11$   $[I]_0$ . The straight line represents simulation of the  $[I-DMS]^{-1}$  vs. time plot expected for a radical-radical rate coefficient of  $5 \times 10^{-10}$   $cm^3$  molecule $^{-1}$  s $^{-1}$  and  $k_{6,3} = 0$ . The curved lines are simulations of the  $[I-DMS]^{-1}$  vs. time plots expected if  $k_{6,3}$  had the values shown in the figure (in units of  $cm^3$  molecule $^{-1}$  s $^{-1}$ ).



The reagent concentrations (units are  $10^{14}$  molecules  $\text{cm}^{-3}$ ) used in experiments investigating reactions (R6.11) and (R6.12) were as follows:  $[\text{CH}_3\text{I}] = (1.8\text{--}3.9)$ ;  $[\text{I}]_0 = (0.04\text{--}0.08)$ ;  $[\text{DMS}] = (270\text{--}353)$ ;  $[\text{NO}] = (1.14\text{--}6.84)$ ;  $[\text{NO}_2] = (1.02\text{--}8.22)$ . Concentrations of  $\text{NO}_2$  were corrected for dimer formation assuming a 205 K equilibrium constant of  $7.0 \times 10^{-15} \text{ cm}^3 \text{ molecule}^{-1}$  for  $\text{NO}_2 + \text{NO}_2 \leftrightarrow \text{N}_2\text{O}_4$  (Sander et al., 2006); the magnitude of the correction ranged from 24% to 43% for the range of  $\text{NO}_2$  concentrations employed to measure  $k_{6,12}$ . Temperatures below 205 K could not be achieved with our experimental apparatus and higher  $[\text{DMS}]$  would lead to attenuation of the laser light as discussed earlier in this chapter. Given these limitations, contributions from reactions (R6.13) and (R6.14) must be accounted for:



As typified by the data shown in Figure 6.7, absorbance decays were exponential, i.e., plots of  $\ln A$  vs. time were linear, indicating pseudo first order conditions were employed. However, the peak concentration of I-DMS for the temporal profile shown in



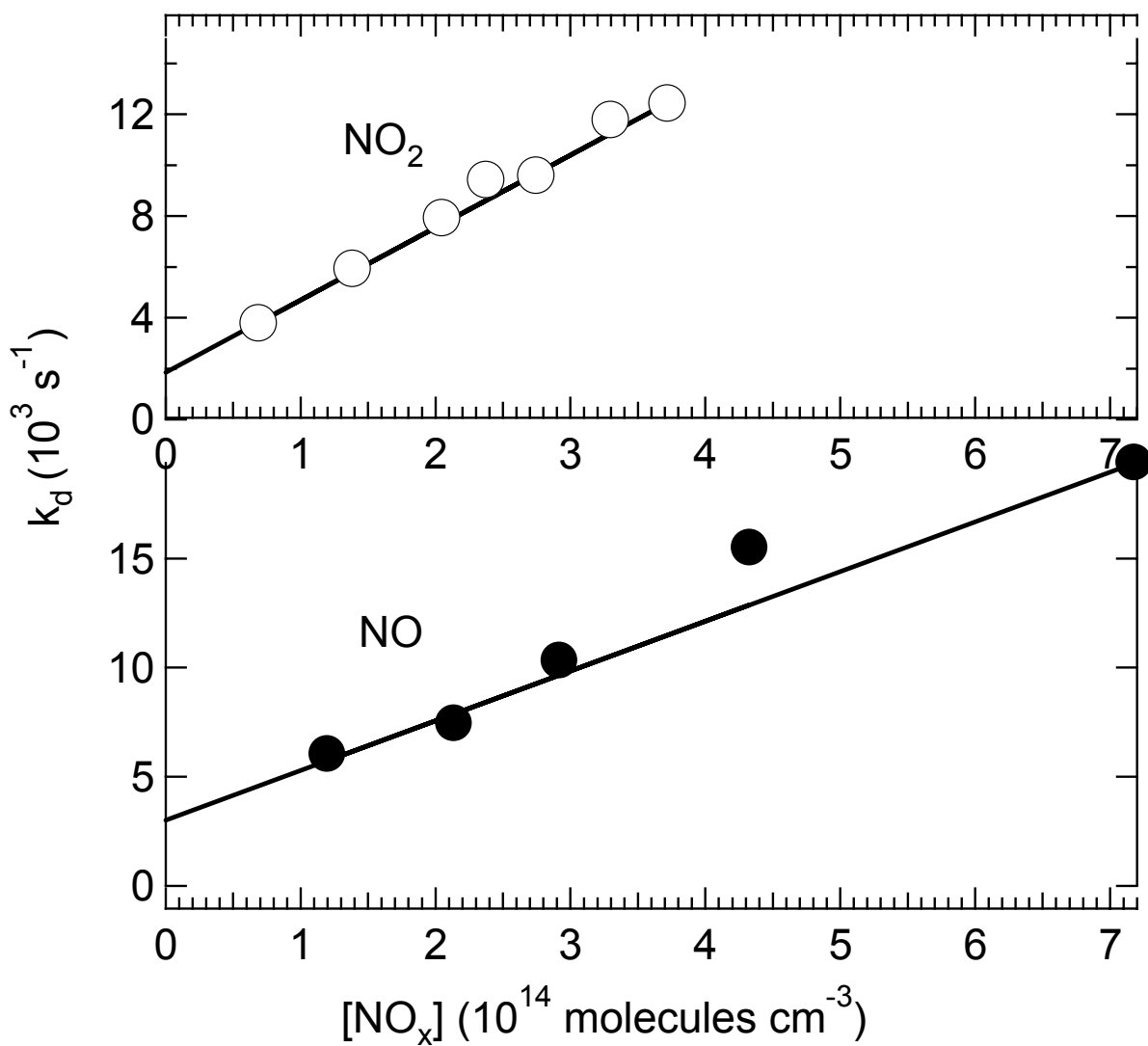
**Figure 6.7** Typical absorbance temporal profile observed following 248 nm laser flash photolysis of  $\text{CH}_3\text{I}/\text{DMS}/\text{NO}_x/2\%\text{O}_2$  in  $\text{N}_2$  mixtures at  $T = 205 \text{ K}$  and  $P = 50 \text{ Torr}$ . The data shown were obtained with  $\text{NO}_x = \text{NO}$ . Concentrations in units of  $10^{14}$  molecules  $\text{cm}^{-3}$  are  $[\text{CH}_3\text{I}] = 1.94$ ,  $[\text{NO}] = 2.91$ ,  $[\text{DMS}] = 369$ , and  $[\text{I}]_0 \approx 0.05$ . The solid line is obtained from a linear least squares analysis of the  $\ln$  absorbance vs. time ( $t$ ) data at  $t > 100 \mu\text{s}$  after the laser flash; its slope gives the pseudo-first order decay rate  $10,800 \text{ s}^{-1}$ .

Figure 6.7, as well as for most other temporal profiles measured, is large enough for reaction (R6.7) to make small but significant contributions to I-DMS removal. As a result, pseudo first order decay rates were obtained from the slopes of plots like the one shown in Figure 6.7 using only data obtained at times where  $A < 0.003$  (i.e.,  $[I-DMS] < 7 \times 10^{11}$  per  $\text{cm}^3$ ). At  $T = 205$  K and  $P = 50$  Torr,  $k_{6.13} \sim 6.3 \times 10^{-14}$  and  $k_{6.14} \sim 1.1 \times 10^{-12}$   $\text{cm}^3 \text{ molecule}^{-1} \text{ s}^{-1}$  (Sander et al., 2006) and no distinction was made between  $k_{6.14a}$  and  $k_{6.14b}$  in the literature.

The measured pseudo-first order decay rates ( $k_d$ ), obtained from the slopes of plots like the one shown in Figure 6.7, are plotted as a function of [DMS] in Figure 6.8. Based on the discussion of radical-radical reaction kinetics above, the slopes of the  $k'$  vs. [DMS] plots (Figure 6.8) represent weighted averages of rate constants as follows:

$$\text{(Eq 6.3)} \quad k' = k_{(I+NO_x)}[NO_x]f_I + k_{(I-DMS+NO_x)}[NO_x]f_{I-DMS} + k_{\text{bkgd}}$$

$k'$  represents the decay rates obtained from the slopes of plots like the one shown in Figure 6.7;  $k_{(I+NO_x)}$  represents rate coefficients  $k_{6.13}$  and  $k_{6.14}$ ;  $k_{(I-DMS+NO_x)}$  represents rate coefficients  $k_{6.11}$  and  $k_{6.12}$ ;  $f_I$  and  $f_{I-DMS}$  represent the equilibrium fractions of I atoms and I-DMS radicals, respectively and  $k_{\text{bkgd}}$  represents adduct loss due to diffusion, reaction with impurities, and reaction with radicals. The slopes of the plots in Figure 6.8 give the following second order rate coefficients in units of  $10^{-11} \text{ cm}^3 \text{ molecule}^{-1} \text{ s}^{-1}$  (uncertainties are  $2\sigma$  and represent precision only):  $k'(NO) = 2.28 \pm 0.60$ , and  $k'(NO_2) = 2.85 \pm 0.28$ .



**Figure 6.8** Plots of pseudo-first-order I-DMS decay rates ( $k_d$ ) versus  $[\text{NO}_x]$  for data obtained at  $T = 205 \text{ K}$  and  $P = 50 \text{ Torr}$  2%  $\text{O}_2$  in  $\text{N}_2$ . The solid lines are obtained from linear least-squares analyses; their slopes give the following rate coefficients in units of  $10^{-11} \text{ cm}^3 \text{ molecule}^{-1} \text{ s}^{-1}$  (uncertainties are  $2\sigma$  and represent precision only):  $k'(\text{NO}) = 2.28 \pm 0.60$  and  $k'(\text{NO}_2) = 2.85 \pm 0.28$ .

Corrections based on kinetic data reported by DeMore et al., 1997, and using Eq 6.3 give corrected second order rate coefficients in units of  $10^{-11} \text{ cm}^3 \text{ molecule}^{-1} \text{ s}^{-1}$  (uncertainties are  $2\sigma$  and represent precision only):  $k_{6,11} = 5.69 \pm 1.70$ , and  $k_{6,12} = 6.96 \pm 0.70$ .

Loss of adduct due to diffusion is generally small and reaction with impurities are also likely minimal since I atoms are relatively unreactive, therefore, it appears that the majority of  $k_{\text{bkgd}}$  is probably accounted for by radical-radical reactions. Assuming a gas kinetic limit rate coefficient for possible radical-radical reactions of  $5 \times 10^{-10} \text{ cm}^3 \text{ molecule}^{-1} \text{ s}^{-1}$  and our employed radical concentration range of  $4 - 8 \times 10^{12} \text{ molecules cm}^{-3}$ , allows us to account for the observed intercepts shown in Figure 6.8. However, in order to put error bars on our reported rate coefficients, it is necessary to point out that radical-radical interference will be more pronounced at low  $[\text{NO}_x]$  and less pronounced at high  $[\text{NO}_x]$  resulting in a decreased slope and high intercept. To account for the above-mentioned effects, we report the following rate coefficients in units of  $10^{-11} \text{ cm}^3 \text{ molecule}^{-1} \text{ s}^{-1}$ :  $k_{6,11} = 5.69 \pm 2.0$  and  $k_{6,12} = 6.96 \pm 0.8$ ; the uncertainties are estimates of accuracy at the 95% confidence level.

Although there are no other reported measurements of  $k_{6,11}$  and  $k_{6,12}$  with which to compare our results, it is of interest to note that the rate coefficients reported in this study are larger than rate coefficients for the reactions of NO and NO<sub>2</sub> with (CH<sub>3</sub>)<sub>2</sub>S-Cl (Urbanski and Wine, 1999), SCS-Cl, (Dookwah-Roberts et al., 2005; Chapter 3 of this dissertation), CH<sub>3</sub>(O)S(Cl)CH<sub>3</sub> (Kleissas et al., 2007), RI-Cl (R = CH<sub>3</sub>, C<sub>2</sub>H<sub>5</sub>) (Dookwah-Roberts et al., accepted 2008; Chapter 4 of this dissertation) and (CH<sub>3</sub>)<sub>2</sub>S-Br (Chapter 5 of this dissertation), all of which were measured using an analogous technique

to the one employed in this study. All X-Cl + NO<sub>x</sub> (X = (CH<sub>3</sub>)<sub>2</sub>S, SCS, (CH<sub>3</sub>)<sub>2</sub>SO, CH<sub>3</sub>I, C<sub>2</sub>H<sub>5</sub>I, (CH<sub>3</sub>)<sub>2</sub>S-Br) rate coefficients are within the range (1-4) x 10<sup>-11</sup> cm<sup>3</sup> molecule<sup>-1</sup> s<sup>-1</sup> and reactivity of these adducts with O<sub>2</sub> is not observed. It appears that I adducts, like Cl and Br adducts, react rapidly with compounds like NO and NO<sub>2</sub>, where transfer of the halogen atom to generate INO, INO<sub>2</sub>, or IONO is energetically favorable. The faster rates of reactions R6.11 and R6.12 are probably due to the weaker, longer S-I bond in (CH<sub>3</sub>)<sub>2</sub>S-I (3.099 Å) as compared to the S-Br bond in (CH<sub>3</sub>)<sub>2</sub>S-Br (2.803 Å) as seen in Figures 6.4 and 5.4 respectively.

### **Atmospheric Fate of I-DMS**

The results obtained in this study taken in conjunction with the kinetic and thermodynamic results from RF experiments (as yet unpublished) and ab initio data (see Table 6.2) supplied by Dr. M. McKee of Auburn University allow us to examine the potential importance of the most likely tropospheric I-DMS degradation pathways; these include photolysis, thermal dissociation, reaction with O<sub>2</sub>, and reaction with NO<sub>x</sub>.

As expected, the thermal decomposition rate of I-DMS at 190 K is very fast, that is, ~ 23,000 s<sup>-1</sup>. This loss rate far surpasses any other I-DMS loss pathway, while the loss rate due to reaction with O<sub>2</sub> occurs at ≤ 220 s<sup>-1</sup> based on the upper limit rate coefficient, *k*<sub>6.3</sub>, reported in this study. Since essentially no adduct + O<sub>2</sub> reaction was observed as well as no IO production was detected, we conclude that the iodine and sulfur cycles remain decoupled and the I-DMS adduct does not play a significant role in DMS oxidation.

# CHAPTER 7

## SUMMARY OF ADDUCT SPECTROSCOPIC AND KINETIC STUDIES

### Observed Trends in Adduct Spectroscopic Data

In this work the kinetics and spectroscopy of five adducts have been investigated using Time Resolved UV-Visible Absorption Spectroscopy (TRUVVAS). Upon examination of the X-DMS spectra as shown in Figure 7.1, where X = Cl, Br, or I, we observe a trend in  $\lambda_{\text{max}}$  reflecting a red shift in peak wavelength from 340 to 395 nm as we move from Cl to I. This data is tabulated in Table 7.1. Within an experimental error of  $\sim 30\%$ , the  $\sigma_{\text{max}}$  of all adducts studied in this work are  $\sim 3 \times 10^{-17} \text{ cm}^2 \text{ molecule}^{-1}$ . Spectroscopy data presented in this thesis also allows for comparison between RI-Cl adducts, where R = CH<sub>3</sub> or C<sub>2</sub>H<sub>5</sub>. In both cases three absorption bands were detected, occurring at 315, 350, and 420 nm while  $\sigma_{\text{max}}$  observed at 315 nm was  $\sim 30\%$  higher for R = CH<sub>3</sub>. The gas phase SCS-Cl spectrum was blue shifted when compared to the liquid phase SCS-Cl adduct spectra but in both cases two absorption bands were observed, a strong band at  $\sim 365$  nm and a weak band at  $\sim 480$  nm.

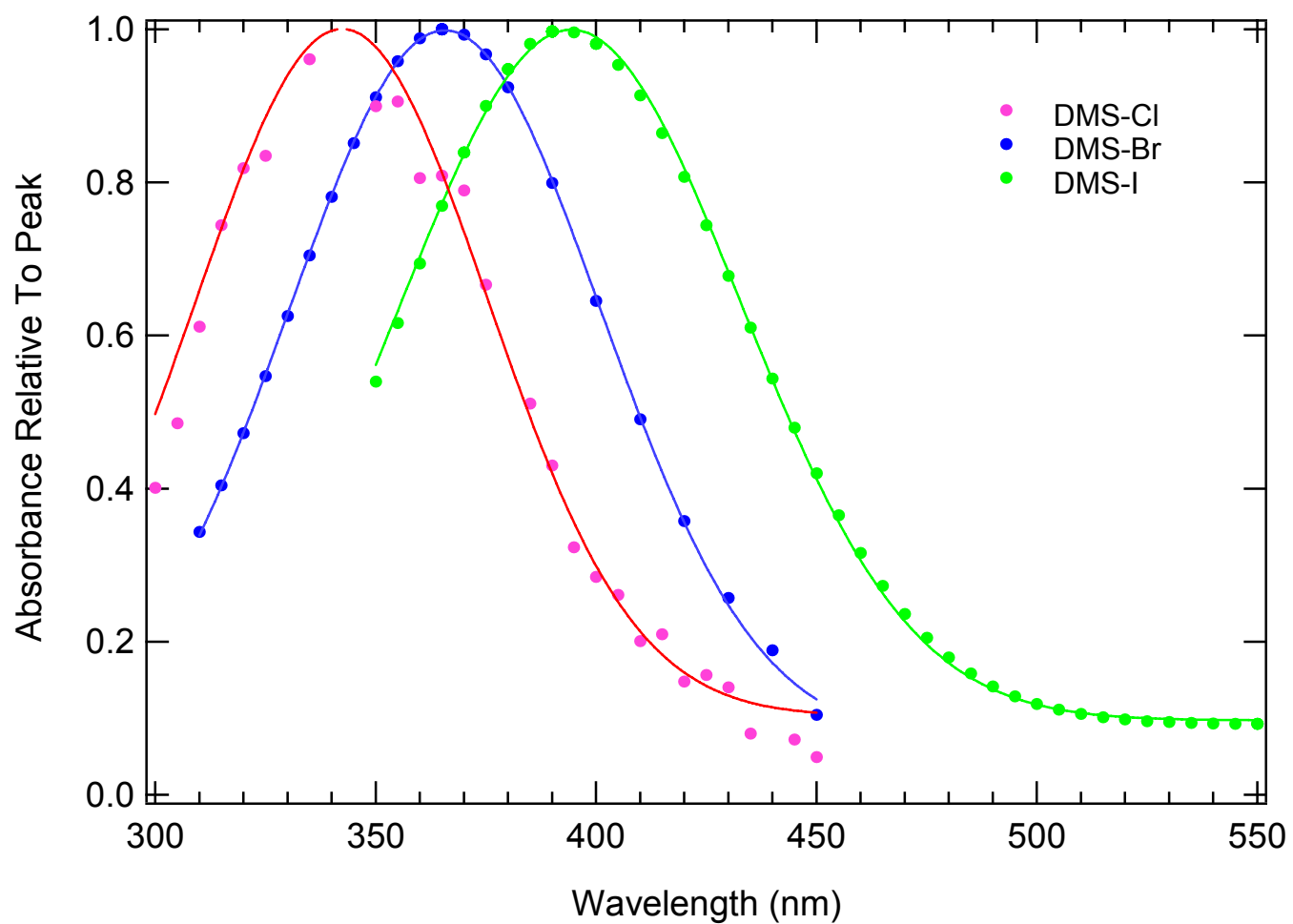


**Figure 7.1 Comparison of X-DMS adduct absorption spectra.** The solid lines are Gaussian fits of the data points.

**Table 7.1 Comparison of adduct  $\lambda_{\max}$ ,  $\sigma_{\max}$ , molecular ionization potential, and radical electron affinity**

<b>Adduct</b>	$\lambda_{\max}$	$\sigma_{\max}$ <sup>a</sup>	<b>IP<sub>molec</sub> (eV)<sup>g</sup></b>	<b>EA<sub>rad</sub> (eV)<sup>g</sup></b>
I-DMS	395	4.09	8.69	2.52
Br-DMS	366	2.70	8.69	3.36
Cl-DMS <sup>b</sup>	340	3.48	8.69	3.62
CH <sub>3</sub> I-Cl	315	3.50	9.54	3.62
C <sub>2</sub> H <sub>5</sub> I-Cl	315	2.70	9.35	3.62
SCS-Cl(g)	365	2.30	10.07	3.62
SCS-Cl (liq) <sup>c,d</sup>	370	none reported		
Cl-DMSO(g) <sup>e</sup>	394	4.00	9.10	3.62
Cl-DMSO(aq) <sup>f</sup>	390	2.22		

<sup>a</sup>Units are in  $10^{-17}$  cm<sup>2</sup> molecule<sup>-1</sup>; <sup>b</sup>Urbanski and Wine, 1999; <sup>c</sup>Chateauneuf, 1993; <sup>d</sup>non-polar solvent; <sup>e</sup>Kleissas et al., 2007; <sup>f</sup>Lei Zhu dissertation, 2004; <sup>g</sup>NIST webbook and references therein.

Figure 7.2 is a graph showing the correlation observed between adduct bond strengths and the difference between the ionization potential of DMS and the respective halogen electron affinity. A correlation coefficient ( $R^2$ ) of 0.98 indicates a strong relationship exists between these two variables which is consistent with the findings of Clark (1988). In a systematic theoretical study of a series of three-electron bonded radical cations, Clark showed that the three-electron bond energy of  $[X \cdot \cdot Y]^+$  decreases exponentially with  $\Delta IP$ , the difference between the ionization potentials (IP) of X and Y. This observation was explained in terms of the high energy of the anti-bonding orbital resulting from overlap of the donor HOMO (highest occupied molecular orbital) and radical SOMO (singly occupied molecular orbital).

A review of the theoretical data present in the literature for the adducts studied in this work reveals a lack of information on the orbitals and transitions involved in the 2 center – 3 electron bonds formed between DMS and halogen radicals, however, an analogous theoretical study conducted by Pathak et al. (2005) provides some insight into the likely possibilities. Pathak et al. (2005), using ab initio and DFT methods, investigated the spectra, structure and bonding of adducts formed with the thiocyanate anion ( $SCN^-$ ) and Cl, Br, I and SCN radicals. These researchers concluded that (i)  $SCNX^-$  adducts ( $X = Cl, Br, I$ ) show the presence of 2c-3e  $\sigma$  bonds, (ii) the binding energy of the 2c-3e bonded systems decrease from Cl to I systems, (iii)  $(NCS \cdots X)^-$  systems are more stable than  $(SCN \cdots X)^-$  systems, and (iv) excited state calculations show that the strong optical absorption exhibited by these species is due to  $\sigma - \sigma^*$  electronic transition.

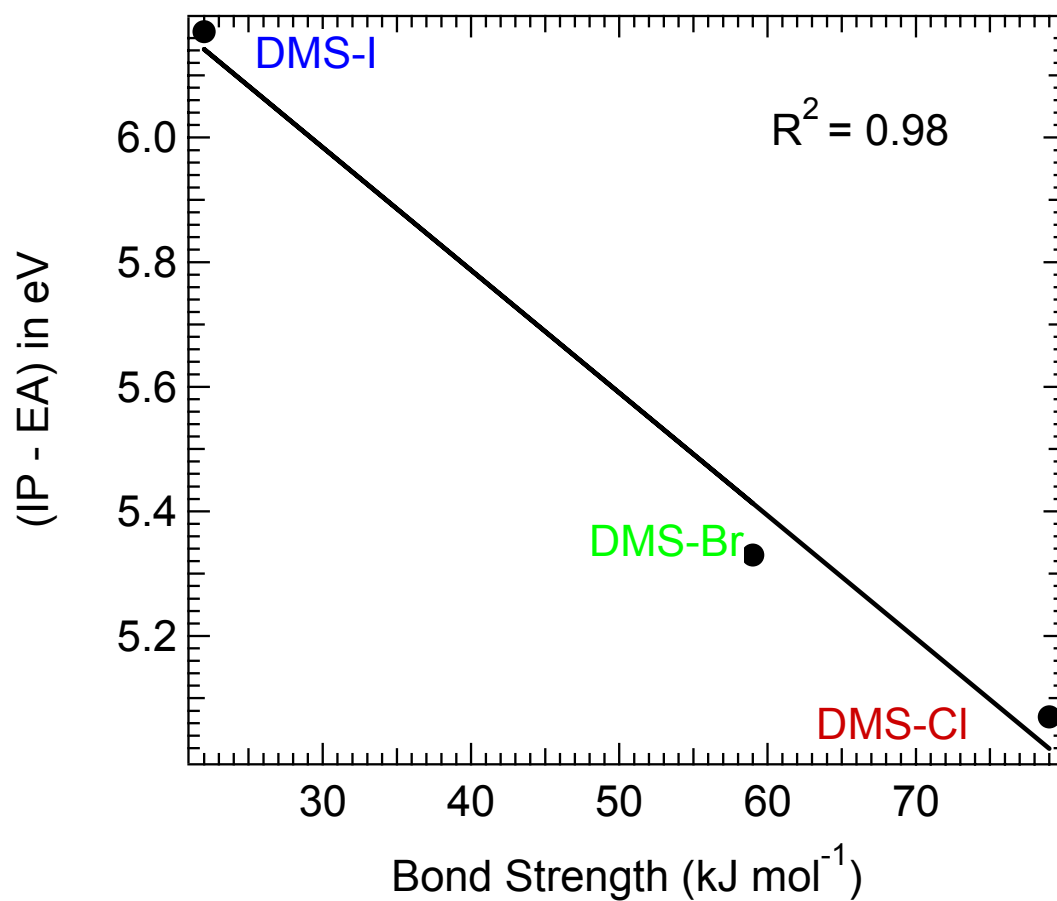


**Figure 7.2** Plot of  $[\text{IP}(\text{DMS}) - \text{EA}(\text{X})]$  ( $\text{X} = \text{I}, \text{Br}, \text{Cl}$ ) vs. adduct bond strength. The straight line is a linear least squares fit of the data points and the derived correlation coefficient ( $R^2$ ) of 0.98 shows a strong relationship between the adduct bond strength and the difference between DMS ionization potential and halogen electron affinity.

Aqueous phase spectra for the  $\text{CNSX}^{\cdot-}$  adducts ( $X = \text{Cl, Br, I}$ ) are reported in the literature and exhibit the following trend in  $\lambda_{\text{max}}$ :  $\text{CNCl}^{\cdot-} = 390 \text{ nm}$  (Schoeneshoefer, 1969);  $\text{CNBr}^{\cdot-} = 400 \text{ nm}$  (Schoeneshoefer and Henglein, 1969);  $\text{CNI}^{\cdot-} = 420 \text{ nm}$  (Schoeneshoefer and Henglein, 1970). Based on the above discussion we can speculate that the observed strong absorption band observed in the DMS-X spectra is likely due to  $\sigma - \sigma^*$  electronic transition. The three band spectra obtained for  $\text{CH}_3\text{I-Cl}$  and  $\text{C}_2\text{H}_5\text{I-Cl}$  adducts suggest the possible occurrence of multiple transitions and the absence of a shift in  $\lambda_{\text{max}}$  between these two adducts indicates that adduct bond strength is more sensitive to differences in the electron affinity of the halogen radical rather than differences in the ionization potential of the molecular moiety.

## Adduct Kinetics Comparisons and Future Research Recommendations

Kinetic data for radical-radical reactions and reactions of adducts with atmospherically relevant species such as O<sub>2</sub>, NO, and NO<sub>2</sub> are reported for the first time in all cases except for SCS-Cl and Br-DMS where upper limits for their reactions with O<sub>2</sub> have been reinvestigated. These data are tabulated in Table 7.2. All adduct + NO<sub>x</sub> rate coefficients were found to be within the range (1–4) × 10<sup>-11</sup> cm<sup>3</sup> molecule<sup>-1</sup> s<sup>-1</sup>, except for the DMS–I adduct where rates of ~ 6.5 × 10<sup>-11</sup> cm<sup>3</sup> molecule<sup>-1</sup> s<sup>-1</sup> were obtained, and reactivity of these adducts with O<sub>2</sub> was not observed. It appears that these halogen adducts react rapidly with compounds like NO and NO<sub>2</sub>, where transfer of the halogen atom to generate XNO, XNO<sub>2</sub>, or XONO, where X = Cl, Br, or I, is energetically favorable. The atmospheric importance of the adduct, DMS–OH is as a result of its higher rate of reaction with O<sub>2</sub> than its rate of thermal decomposition to reform DMS and OH (Hynes et al., 1986; Hynes et al., 1995; Barone et al., 1996); important products of the reaction of DMS–OH with O<sub>2</sub> are DMSO and HO<sub>2</sub>. The lack of reactivity of the halogen-DMS adducts with O<sub>2</sub> reduces their potential importance in the atmosphere, however there are two notable exceptions: (i) the upper limit reported in the study of C<sub>2</sub>H<sub>5</sub>I–Cl with O<sub>2</sub> ( $k_{4.21} \sim 2.5 \times 10^{-17}$  cm<sup>3</sup> molecule<sup>-1</sup>s<sup>-1</sup>) makes this reaction comparable to the thermal decomposition of this adduct. No product studies of reaction (R4.21) have been conducted, however, major products identified from reaction (R4.4) at 298 K and 1 atmosphere of air include CO<sub>2</sub>, CH<sub>2</sub>O, CO, acetic acid, peracetic acid, CH<sub>3</sub>OH, and acetaldehyde (Orlando et al., 2005).

**Table 7.2 Comparison of adduct kinetics**

<b>Adduct</b>	<b><sup>a</sup>k<sub>O2</sub></b>	<b><sup>a</sup>k<sub>NO</sub></b>	<b><sup>a</sup>k<sub>NO2</sub></b>
I-DMS	< 3 x 10 <sup>-4</sup>	570	700
Br-DMS	< 8 x 10 <sup>-5</sup>	130	260
Cl-DMS <sup>b</sup>	< 4 x 10 <sup>-5</sup>	120	270
CH <sub>3</sub> I-Cl	< 3 x 10 <sup>-4</sup>	200	350
C <sub>2</sub> H <sub>5</sub> I-Cl	< 1 x 10 <sup>-4</sup>	200	390
DMSO-Cl <sup>c</sup> (g)	< 3 x 10 <sup>-5</sup>	120	210
SCS-Cl	< 5 x 10 <sup>-5</sup>	220	130

<sup>a</sup>Units are in 10<sup>-13</sup> cm<sup>3</sup> molecule<sup>-1</sup> s<sup>-1</sup>; <sup>b</sup>Urbanski and Wine, 1999; <sup>c</sup>Kleissas et al., 2007

Further experiments at low temperatures and higher pressures are required in order to (i) conclusively establish or rule out the atmospheric importance of reaction (R4.21); (ii) determine whether thermal decomposition of Br–DMS can lead to products other than Br and DMS as indicated in product studies (Maurer et al., 1999; Ballesteros et al., 2002) where CH<sub>3</sub>SBr has been identified as one of the main primary products formed from Br oxidation of DMS in air, and the potential pathway suggested for this product formation is:



To the best of this author's knowledge, no kinetic data are available for CH<sub>3</sub>SBr. One possible atmospheric fate of CH<sub>3</sub>SBr is photolysis to yield CH<sub>3</sub>S and Br. The net effect of this speculation is that the initial reactants are not reformed, i.e., DMS is not regenerated and formation of the Br–DMS adduct represents a net loss of atmospheric DMS. In order to ascertain the significance of this unimolecular decomposition pathway of Br–DMS, more investigations are needed to elucidate the exact reaction pathway for CH<sub>3</sub>SBr production as well as kinetic behavior and products formed from reactions involving CH<sub>3</sub>SBr.

## REFERENCES

- Adams, J. W., & Cox, R. A. (2002). Halogen chemistry of the marine boundary layer. [Article]. *Journal De Physique Iv*, 12(PR10), 105-124.
- Albrecht, B. A. (1989). AEROSOLS, CLOUD MICROPHYSICS, AND FRACTIONAL CLOUDINESS. [Article]. *Science*, 245(4923), 1227-1230.
- Allan, B. J., & Plane, J. M. C. (2002). A study of the recombination of IO with NO<sub>2</sub> and the stability of INO<sub>3</sub>: Implications for the atmospheric chemistry of iodine. [Article]. *Journal of Physical Chemistry A*, 106(37), 8634-8641.
- Aloisio, S. (2006). Theoretical study of adducts of dimethyl sulfide with hydroperoxyl and hydroxyl radicals. *Chemical Physics*, 326(2-3), 335-343.
- Amels, P., Elias, H., & Wannowius, K. J. (1997). Kinetics and mechanism of the oxidation of dimethyl sulfide by hydroperoxides in aqueous medium - Study on the potential contribution of liquid-phase oxidation of dimethyl sulfide in the atmosphere. *Journal of the Chemical Society-Faraday Transactions*, 93(15), 2537-2544.
- Andreae, M. O. (1990). Ocean-atmosphere interactions in the global biogeochemical sulfur cycle. *Marine Chemistry*, 30(1-3), 1-29.
- Andreae, M. O., Atlas, E., Harris, G. W., Helas, G., deKock, A., Koppmann, R., et al. (1996). Methyl halide emissions from savanna fires in southern Africa. [Article]. *Journal of Geophysical Research-Atmospheres*, 101(D19), 23603-23613.
- Ariya, P. A., Catoire, V., Sander, R., Niki, H., & Harris, G. W. (1997). Trichloroethene and tetrachloroethene: Tropospheric probes for Cl- and Br-atom reactions during polar sunrise. [Article]. *Tellus Series B-Chemical and Physical Meteorology*, 49(5), 583-591.
- Ariya, P. A., Sander, R., & Crutzen, P. J. (2000). Significance of HO<sub>x</sub> and peroxides production due to alkene ozonolysis during fall and winter: A modeling study. [Article]. *Journal of Geophysical Research-Atmospheres*, 105(D14), 17721-17738.
- Arsene, C., Barnes, I., & Becker, K. H. (1999). FT-IR product study of the photo-oxidation of dimethyl sulfide: Temperature and O<sub>2</sub> partial pressure dependence. *Physical Chemistry Chemical Physics*, 1(24), 5463-5470.

- Arsene, C., Barnes, I., Becker, K. H., & Benter, T. (2005). Gas-phase reaction of Cl with dimethyl sulfide: Temperature and oxygen partial pressure dependence of the rate coefficient. *International Journal of Chemical Kinetics*, 37(2), 66-73.
- Arsene, C., Barnes, I., Becker, K. H., & Mocanu, R. (2001). FT-IR product study on the photo-oxidation of dimethyl sulphide in the presence of NO<sub>x</sub> - temperature dependence. *Atmospheric Environment*, 35(22), 3769-3780.
- Arsene, C., Barnes, I., Becker, K. H., Schneider, W. F., Wallington, T. T., Mihalopoulos, N., et al. (2002). Formation of methane sulfinic acid in the gas-phase OH-radical initiated oxidation of dimethyl sulfoxide. [Article]. *Environmental Science & Technology*, 36(23), 5155-5163.
- Ashworth, S. H., Allan, B. J., & Plane, J. M. C. (2002). High resolution spectroscopy of the OIO radical: Implications for the ozone-depleting potential of iodine. [Article]. *Geophysical Research Letters*, 29(10), 4.
- Atkinson, R. (2000). Atmospheric chemistry of VOCs and NO<sub>x</sub>. [Review]. *Atmospheric Environment*, 34(12-14), 2063-2101.
- Atkinson, R., Baulch, D. L., Cox, R. A., Hampson, R. F., Kerr, J. A., Rossi, M. J., et al. (1997). Evaluated kinetic and photochemical data for atmospheric chemistry: Supplement VI - IUPAC subcommittee on gas kinetic data evaluation for atmospheric chemistry. *Journal of Physical and Chemical Reference Data*, 26(6), 1329-1499.
- Atkinson, R., Baulch, D. L., Cox, R. A., Hampson, R. F., Kerr, J. A., & Troe, J. (1989). Evaluated kinetic and photochemical data for atmospheric chemistry .3. IUPAC subcommittee on gas kinetic data evaluation for atmospheric chemistry. [Article]. *Journal of Physical and Chemical Reference Data*, 18(2), 881-1097.
- Atkinson, R., Perry, R. A., & Pitts, J. N. (1978). Rate constants for reaction of OH radicals with COS, CS<sub>2</sub> AND CH<sub>3</sub>SCH<sub>3</sub> over temperature range 299-K 430-K. [Article]. *Chemical Physics Letters*, 54(1), 14-18.
- Ayers, G. P., & Cainey, J. M. (2007). The CLAW hypothesis: a review of the major developments. *Environmental Chemistry*, 4(6), 366-374.
- Ayhens, Y. V., Nicovich, J. M., McKee, M. L., & Wine, P. H. (1997). Kinetic and mechanistic study of the reaction of atomic chlorine with methyl iodide over the temperature range 218-694 K. [Article]. *Journal of Physical Chemistry A*, 101(49), 9382-9390.

- Babbs, C. F., & Griffin, D. W. (1989). Scatchard analysis of methane sulfinic acid production from dimethyl-sulfoxide – A method to quantify hydroxyl radical formation in physiologic systems. *Free Radical Biology and Medicine*, 6(5), 493-503.
- Ballesteros, B., Jensen, N. R., & Hjorth, J. (2002). FT-IR study of the kinetics and products of the reactions of dimethylsulphide, dimethylsulphoxide and dimethylsulphone with Br and BrO. [Article]. *Journal of Atmospheric Chemistry*, 43(2), 135-150.
- Bandy, A. R., Maroulis, P. J., Shalaby, L., & Wilner, L. A. (1981). Evidence for a short tropospheric residence time for carbon-disulfide. [Article]. *Geophysical Research Letters*, 8(11), 1180-1183.
- Bandy, A. R., Tucker, B. J., & Maroulis, P. J. (1985). Determination of part-per-trillion by volume levels of atmospheric carbon-disulfide by gas-chromatography mass-spectrometry. [Article]. *Analytical Chemistry*, 57(7), 1310-1314.
- Bardouki, H., Berresheim, H., Vrekoussis, M., Sciare, J., Kouvarakis, G., Oikonomou, K., et al. (2003). Gaseous (DMS, MSA, SO<sub>2</sub>, H<sub>2</sub>SO<sub>4</sub> and DMSO) and particulate (sulfate and methanesulfonate) sulfur species over the northeastern coast of Crete. *Atmospheric Chemistry and Physics*, 3, 1871-1886.
- Bardouki, H., da Rosa, M. B., Mihalopoulos, N., Palm, W. U., & Zetzsch, C. (2002). Kinetics and mechanism of the oxidation of dimethylsulfoxide (DMSO) and methanesulfinate (MSI-) by OH radicals in aqueous medium. *Atmospheric Environment*, 36(29), 4627-4634.
- Barnes, I., Bastian, V., & Becker, K. H. (1988). Kinetics and mechanisms of the reaction of OH radicals with dimethyl sulfide. [Article]. *International Journal of Chemical Kinetics*, 20(6), 415-431.
- Barnes, I., Bastian, V., Becker, K. H., & Martin, D. (1989). Fourier-Transform IR studies of the reactions of dimethyl-sulfoxide with OH, NO<sub>3</sub>, and Cl radicals. [Review]. *Acs Symposium Series*, 393, 476-488.
- Barnes, I., Bastian, V., Becker, K. H., & Overath, R. D. (1991). Kinetic-studies of the reactions of IO, BRO, and CLO with dimethyl sulfide. [Article]. *International Journal of Chemical Kinetics*, 23(7), 579-591.
- Barnes, I., Becker, K. H., Carlier, P., & Mouvier, G. (1987). FTIR study of the DMS/NO<sub>2</sub>/I<sub>2</sub>/N<sub>2</sub> photolysis system – The reaction of IO radicals with DMS. [Article]. *International Journal of Chemical Kinetics*, 19(6), 489-501.

- Barnes, I., Becker, K. H., Fink, E. H., Reimer, A., Zabel, F., & Niki, H. (1983). Rate-constant and products of the reaction  $\text{CS}_2 + \text{OH}$  on the presence of  $\text{O}_2$ . [Article]. *International Journal of Chemical Kinetics*, 15(7), 631-645.
- Barnes, I., Becker, K. H., Martin, D., Carlier, P., Mouvier, G., Jourdain, J. L., et al. (1989). Impact of halogen oxides on dimethyl sulfide oxidation in the marine atmosphere. [Review]. *Acs Symposium Series*, 393, 464-475.
- Barnes, I., Becker, K. H., & Patroescu, I. (1994). The tropospheric oxidation of dimethyl sulfide - A new source of carbonyl sulfide. *Geophysical Research Letters*, 21(22), 2389-2392.
- Barnes, I., Becker, K. H., & Patroescu, I. (1996). FTIR product study of the OH initiated oxidation of dimethyl sulphide: Observation of carbonyl sulphide and dimethyl sulphoxide. *Atmospheric Environment*, 30(10-11), 1805-1814.
- Barnes, I., Hjorth, J., & Mihalopoulos, N. (2006). Dimethyl sulfide and dimethyl sulfoxide and their oxidation in the atmosphere. *Chemical Reviews*, 106(3), 940-975.
- Barone, S. B., Turnipseed, A. A., & Ravishankara, A. R. (1996). Reaction of OH with dimethyl sulfide (DMS) .1. Equilibrium constant for  $\text{OH} + \text{DMS}$  reaction and the kinetics of the  $\text{OH} + \text{DMS} + \text{O}_2$  reaction. [Article]. *Journal of Physical Chemistry*, 100(35), 14694-14702.
- Barrie, L. A., Bottenheim, J. W., Schnell, R. C., Crutzen, P. J., & Rasmussen, R. A. (1988). Ozone destruction and photochemical-reactions at polar sunrise in the lower arctic atmosphere. [Article]. *Nature*, 334(6178), 138-141.
- Bates, T. S., Charlson, R. J., & Gammon, R. H. (1987). Evidence for the climatic role of marine biogenic sulfur. [Article]. *Nature*, 329(6137), 319-321.
- Baughcum, S. L., & Leone, S. R. (1980). Photofragmentation infrared-emission studies of vibrationally excited free-radicals  $\text{CH}_3$  AND  $\text{CH}_2$ . [Article]. *Journal of Chemical Physics*, 72(12), 6531-6545.
- Becker, K. H., Nelsen, W., Su, Y. H., & Wirtz, K. (1990). A new mechanism for the reaction  $\text{CS}_2 + \text{OH}$ . [Article]. *Chemical Physics Letters*, 168(6), 559-563.
- Bedjanian, Y., Poulet, G., & LeBras, G. (1996). Kinetic study of the reaction of BrO radicals with dimethylsulfide. [Article]. *International Journal of Chemical Kinetics*, 28(5), 383-389.

- Bell, N., Hsu, L., Jacob, D. J., Schultz, M. G., Blake, D. R., Butler, J. H., et al. (2002). Methyl iodide: Atmospheric budget and use as a tracer of marine convection in global models. [Article]. *Journal of Geophysical Research-Atmospheres*, 107(D17), 12.
- Berresheim, H., & Jaeschke, W. (1983). The contribution of volcanoes to the global atmospheric sulfur budget. [Article]. *Journal of Geophysical Research-Oceans and Atmospheres*, 88(NC6), 3732-3740.
- Bilde, M., & Wallington, T. J. (1998). Atmospheric chemistry of CH<sub>3</sub>I: Reaction with atomic chlorine at 1-700 torr total pressure and 295 K. [Article]. *Journal of Physical Chemistry A*, 102(9), 1550-1555.
- Blake, N. J., Blake, D. R., Sive, B. C., Chen, T. Y., Rowland, F. S., Collins, J. E., et al. (1996). Biomass burning emissions and vertical distribution of atmospheric methyl halides and other reduced carbon gases in the South Atlantic region. [Article]. *Journal of Geophysical Research-Atmospheres*, 101(D19), 24151-24164.
- Bosch, H., Camy-Peyret, C., Chipperfield, M. P., Fitzenberger, R., Harder, H., Platt, U., et al. (2003). Upper limits of stratospheric IO and OIO inferred from center-to-limb-darkening-corrected balloon-borne solar occultation visible spectra: Implications for total gaseous iodine and stratospheric ozone. [Article]. *Journal of Geophysical Research-Atmospheres*, 108(D15), 24.
- Boucher, O., Moulin, C., Belviso, S., Aumont, O., Bopp, L., Cosme, E., et al. (2003). DMS atmospheric concentrations and sulphate aerosol indirect radiative forcing: a sensitivity study to the DMS source representation and oxidation. [Article]. *Atmospheric Chemistry and Physics*, 3, 49-65.
- Brown, A. C., Canosamas, C. E., & Wayne, R. P. (1990). A kinetic-study of the reactions of OH with CH<sub>3</sub>I and CF<sub>3</sub>I. [Article]. *Atmospheric Environment Part a-General Topics*, 24(2), 361-367.
- Bulatov, V. P., Cheskis, S. G., Iogansen, A. A., Kulakov, P. V., Sarkisov, O. M., & Hassinen, E. (1988). Reaction of OH radicals with CS<sub>2</sub>. [Article]. *Chemical Physics Letters*, 153(2-3), 258-262.
- Burkholder, J. B., Curtius, J., Ravishankara, A. R., & Lovejoy, E. R. (2004). Laboratory studies of the homogeneous nucleation of iodine oxides. [Article]. *Atmospheric Chemistry and Physics*, 4, 19-34.
- Calvert, J. G., & Lindberg, S. E. (2003). A modeling study of the mechanism of the halogen-ozone-mercury homogeneous reactions in the troposphere during the polar spring. [Article]. *Atmospheric Environment*, 37(32), 4467-4481.

- Campos, M., Nightingale, P. D., & Jickells, T. D. (1996). A comparison of methyl iodide emissions from seawater and wet depositional fluxes of iodine over the southern North Sea. [Article]. *Tellus Series B-Chemical and Physical Meteorology*, 48(1), 106-114.
- Carl, S. A., & Crowley, J. N. (2001). 298 K rate coefficients for the reaction of OH with i-C<sub>3</sub>H<sub>7</sub>I, n-C<sub>3</sub>H<sub>7</sub>I and C<sub>3</sub>H<sub>8</sub>. [Article]. *Atmospheric Chemistry and Physics*, 1, 1-7.
- Carpenter, L. J. (2003). Iodine in the marine boundary layer. [Review]. *Chemical Reviews*, 103(12), 4953-4962.
- Carpenter, L. J., & Liss, P. S. (2000). On temperate sources of bromoform and other reactive organic bromine gases. [Article]. *Journal of Geophysical Research-Atmospheres*, 105(D16), 20539-20547.
- Carpenter, L. J., Liss, P. S., & Penkett, S. A. (2003). Marine organohalogens in the atmosphere over the Atlantic and Southern Oceans. [Article]. *Journal of Geophysical Research-Atmospheres*, 108(D9), 13.
- Carpenter, L. J., Malin, G., Liss, P. S., & Kupper, F. C. (2000). Novel biogenic iodine-containing trihalomethanes and other short-lived halocarbons in the coastal East Atlantic. [Article]. *Global Biogeochemical Cycles*, 14(4), 1191-1204.
- Carpenter, L. J., Sturges, W. T., Penkett, S. A., Liss, P. S., Alicke, B., Hebestreit, K., et al. (1999). Short-lived alkyl iodides and bromides at Mace Head, Ireland: Links to biogenic sources and halogen oxide production. [Article]. *Journal of Geophysical Research-Atmospheres*, 104(D1), 1679-1689.
- Chameides, W. L., & Davis, D. D. (1980). Iodine – It's possible role in tropospheric photochemistry. [Article]. *Journal of Geophysical Research-Oceans and Atmospheres*, 85(NC12), 7383-7398.
- Chang, S. Y., & Allen, D. T. (2006). Atmospheric chlorine chemistry in southeast Texas: Impacts on ozone formation and control. [Article]. *Environmental Science & Technology*, 40(1), 251-262.
- Charlson, R. J., Lovelock, J. E., Andreae, M. O., & Warren, S. G. (1987). Oceanic phytoplankton, atmospheric sulfur, cloud albedo and climate. [Review]. *Nature*, 326(6114), 655-661.
- Charlson, R. J., Schwartz, S. E., Hales, J. M., Cess, R. D., Coakley, J. A., Hansen, J. E., et al. (1992a). Aerosols and global warming – Response. [Letter]. *Science*, 256(5057), 598-599.

- Charlson, R. J., Schwartz, S. E., Hales, J. M., Cess, R. D., Coakley, J. A., Hansen, J. E., et al. (1992b). Climate forcing by anthropogenic aerosols. [Article]. *Science*, 255(5043), 423-430.
- Chateaufneuf, J. E. (1993). Spectroscopic detection and reactivity of the chlorine atom carbon-disulfide molecular-complex. [Article]. *Journal of the American Chemical Society*, 115(5), 1915-1921.
- Chin, M., & Davis, D. D. (1993). Global sources and sinks of OCS and CS<sub>2</sub> and their distributions. [Article]. *Global Biogeochemical Cycles*, 7(2), 321-337.
- Chin, M., Rood, R. B., Allen, D. J., Andreae, M. O., Thompson, A. M., Lin, S. J., et al. (1998). Processes controlling dimethylsulfide over the ocean: Case studies using a 3-D model driven by assimilated meteorological fields. *Journal of Geophysical Research-Atmospheres*, 103(D7), 8341-8353.
- Clark, T. (1988). Odd-electron delta-bonds. *Journal of the American Chemical Society*, 110(6), 1672-1678.
- Coleman, E. H., Gaydon, A. G., & Vaidya, W. M. (1948). Spectrum of iodine oxide (IO) in flames. [Letter]. *Nature*, 162(4107), 108-109.
- Cooper, D. J., & Saltzman, E. S. (1993). Measurements of atmospheric dimethyl sulfide, hydrogen sulfide and carbon-disulfide during GTE CITE-3. [Article]. *Journal of Geophysical Research-Atmospheres*, 98(D12), 23397-23409.
- Cotter, E. S. N., Booth, N. J., Canosa-Mas, C. E., Gray, D. J., Shallcross, D. E., & Wayne, R. P. (2001). Reactions of Cl atoms with CH<sub>3</sub>I, C<sub>2</sub>H<sub>5</sub>I, 1-C<sub>3</sub>H<sub>7</sub>I, 2-C<sub>3</sub>H<sub>7</sub>I and CF<sub>3</sub>I: kinetics and atmospheric relevance. [Article]. *Physical Chemistry Chemical Physics*, 3(3), 402-408.
- Cotter, E. S. N., Booth, N. J., Canosa-Mas, C. E., & Wayne, R. P. (2001). Release of iodine in the atmospheric oxidation of alkyl iodides and the fates of iodinated alkoxy radicals. [Article]. *Atmospheric Environment*, 35(12), 2169-2178.
- Cotter, E. S. N., Canosa-Mas, C. E., Manners, C. R., Wayne, R. P., & Shallcross, D. E. (2003). Kinetic study of the reactions of OH with the simple alkyl iodides: CH<sub>3</sub>I, C<sub>2</sub>H<sub>5</sub>I, 1-C<sub>3</sub>H<sub>7</sub>I and 2-C<sub>3</sub>H<sub>7</sub>I. [Article]. *Atmospheric Environment*, 37(8), 1125-1133.
- Cox, R. A., Bloss, W. J., Jones, R. L., & Rowley, D. M. (1999). OIO and the atmospheric cycle of iodine. [Article]. *Geophysical Research Letters*, 26(13), 1857-1860.
- Cox, R. A., & Sheppard, D. (1980). Reactions of OH radicals with gaseous sulfur-compounds. [Article]. *Nature*, 284(5754), 330-331.

- Criegee, R., & Wenner, G. (1949). \*Die ozonisierung des 9,10-oktalin. [Article]. *Annalen Der Chemie-Justus Liebig*, 564(1), 9-15.
- Cronkhite, J. M., Stickel, R. E., Nicovich, J. M., & Wine, P. H. (1999). Laser flash photolysis studies of radical-radical reaction kinetics: The HO<sub>2</sub>+IO reaction. [Article]. *Journal of Physical Chemistry A*, 103(17), 3228-3236.
- Crutzen, P. J. (1976). Possible importance of CSO for sulfate layer of stratosphere. [Article]. *Geophysical Research Letters*, 3(2), 73-76.
- Davis, D., Crawford, J., Liu, S., McKeen, S., Bandy, A., Thornton, D., et al. (1996). Potential impact of iodine on tropospheric levels of ozone and other critical oxidants. [Article]. *Journal of Geophysical Research-Atmospheres*, 101(D1), 2135-2147.
- Davis, D., Nowak, J. B., Chen, G., Buhr, M., Arimoto, R., Hogan, A., et al. (2001). Unexpected high levels of NO observed at South Pole. [Article]. *Geophysical Research Letters*, 28(19), 3625-3628.
- Daykin, E. P., & Wine, P. H. (1990). Rate of reaction of IO radicals with dimethylsulfide. [Article]. *Journal of Geophysical Research-Atmospheres*, 95(D11), 18547-18553.
- Derwent, R. G., & Thrush, B. A. (1971a). Measurements on O<sub>2</sub>1DELTA and O<sub>2</sub>1SIGMA+G in discharge flow systems. [Article]. *Transactions of the Faraday Society*, 67(583), 2036-&.
- Derwent, R. G., & Thrush, B. A. (1971b). Radiative lifetime of metastable iodine atom I(52P<sub>1-2</sub>). [Article]. *Chemical Physics Letters*, 9(6), 591-&.
- Diau, E. W. G., & Lee, Y. P. (1991a). Kinetics of the reactions of CS<sub>2</sub>OH with O<sub>2</sub>, NO, and NO<sub>2</sub>. [Article]. *Journal of Physical Chemistry*, 95(20), 7726-7732.
- Diau, E. W. G., & Lee, Y. P. (1991b). Termolecular rate coefficients and the standard enthalpy of the reaction OH+CS<sub>2</sub>+M-]HOCS<sub>2</sub>+M. [Article]. *Journal of Physical Chemistry*, 95(1), 379-386.
- Dillon, T. J., Karunanandan, R., & Crowley, J. N. (2006). The reaction of IO with CH<sub>3</sub>SCH<sub>3</sub>: products and temperature dependent rate coefficients by laser induced fluorescence. *Physical Chemistry Chemical Physics*, 8(7), 847-855.
- Dimmer, C. H., Simmonds, P. G., Nickless, G., & Bassford, M. R. (2001). Biogenic fluxes of halomethanes from Irish peatland ecosystems. [Article]. *Atmospheric Environment*, 35(2), 321-330.

- Dookwah-Roberts, V., Nicovich, J. M., & Wine, P. H. (2006). Spectroscopy and kinetics of weakly-bound adducts of Cl atoms with CH<sub>3</sub>I and C<sub>2</sub>H<sub>5</sub>I. *Abstracts of Papers of the American Chemical Society*, 231.
- Dookwah-Roberts, V., Soller, R., Nicovich, J. M., & Wine, P. H. (2005). Spectroscopic and kinetic study of the gas-phase CS<sub>2</sub>-Cl adduct. [Article]. *Journal of Photochemistry and Photobiology a-Chemistry*, 176(1-3), 114-123.
- Durie, R. A., & Ramsay, D. A. (1958). Absorption spectra of the halogen monoxides. [Article]. *Canadian Journal of Physics*, 36(1), 35-&.
- Enami, S., Hashimoto, S., Kawasaki, M., Nakano, Y., Ishiwata, T., Tonokura, K., et al. (2005). Observation of adducts in the reaction of Cl atoms with XCH<sub>2</sub>I (X = H, CH<sub>3</sub>, Cl, Br, I) using cavity ring-down spectroscopy. [Article]. *Journal of Physical Chemistry A*, 109(8), 1587-1593.
- Enami, S., Nakano, Y., Hashimoto, S., Kawasaki, M., Aloisio, S., & Francisco, J. S. (2004). Reactions of Cl atoms with dimethyl sulfide: A theoretical calculation and an experimental study with cavity ring-down spectroscopy. [Article]. *Journal of Physical Chemistry A*, 108(39), 7785-7789.
- Enami, S., Ueda, J., Goto, M., Nakano, Y., Aloisio, S., Hashimoto, S., et al. (2004). Formation of iodine monoxide radical from the reaction of CH<sub>2</sub>I with O-2. [Article]. *Journal of Physical Chemistry A*, 108(30), 6347-6350.
- Enami, S., Yamanaka, T., Hashimoto, S., Kawasaki, M., & Tonokura, K. (2005). Direct observation of adduct formation of alkyl and aromatic iodides with Cl atoms using cavity ring-down spectroscopy. [Article]. *Journal of Physical Chemistry A*, 109(27), 6066-6070.
- Estupinan, E. G., Nicovich, J. M., & Wine, P. H. (2001). A temperature-dependent kinetics study of the important stratospheric reaction O(P-3)+NO<sub>2</sub> -> O-2+NO. [Article]. *Journal of Physical Chemistry A*, 105(42), 9697-9703.
- Fan, S. M., & Jacob, D. J. (1992). Surface ozone depletion in Arctic spring sustained by bromine reactions on aerosols. [Article]. *Nature*, 359(6395), 522-524.
- Finlaysonpitts, B. J., Livingston, F. E., & Berko, H. N. (1990). Ozone destruction and bromine photochemistry at ground-level in the Arctic spring. [Article]. *Nature*, 343(6259), 622-625.
- Flyunt, R., Makogon, O., Schuchmann, M. N., Asmus, K. D., & von Sonntag, C. (2001). OH-Radical-induced oxidation of methanesulfinic acid. The reactions of the methanesulfonyl radical in the absence and presence of dioxygen. *Journal of the Chemical Society-Perkin Transactions 2*(5), 787-792.

- Gab, S., Hellpointner, E., Turner, W. V., & Korte, F. (1985). Hydroxymethyl hydroperoxide and bis(hydroxymethyl) peroxide from gas-phase ozonolysis of naturally-occurring alkenes. [Article]. *Nature*, 316(6028), 535-536.
- Gabler, H. E., & Heumann, K. G. (1993). Trace analysis of chlorine in high-purity refractory metals with isotope-dilution-mass-spectrometry [Article]. *Fresenius Journal of Analytical Chemistry*, 346(4), 426-428.
- Galbally, I. E., Bentley, S. T., & Meyer, C. P. (2000). Mid-latitude marine boundary-layer ozone destruction at visible sunrise observed at Cape Grim, Tasmania, 41 degrees 5. [Article]. *Geophysical Research Letters*, 27(23), 3841-3844.
- Garcia, R. R., & Solomon, S. (1994). A new numerical-model of the middle atmosphere 2. Ozone and related species. [Article]. *Journal of Geophysical Research-Atmospheres*, 99(D6), 12937-12951.
- Goliff, W. S., & Rowland, F. S. (1997). Methyl chloride formation by gas phase thermal chlorine atom reaction with methyl iodide and methyl bromide. [Article]. *Geophysical Research Letters*, 24(23), 3029-3032.
- Golombek, A., & Prinn, R. G. (1993). A global 3-Dimensional model of the stratospheric sulfuric-acid layer. *Journal of Atmospheric Chemistry*, 16(2), 179-199.
- Gonzalez-Garcia, N., Gonzalez-Lafont, A., & Lluch, J. M. (2007). Methanesulfinic acid reaction with OH: Mechanism, rate constants, and atmospheric implications. *Journal of Physical Chemistry A*, 111(32), 7825-7832.
- Goodsite, M. E., Plane, J. M. C., & Skov, H. (2004). A theoretical study of the oxidation of Hg-0 to HgBr<sub>2</sub> in the troposphere. [Article]. *Environmental Science & Technology*, 38(6), 1772-1776.
- Gravestock, T., Blitz, M. A., & Heard, D. E. (2005). Kinetics study of the reaction of iodine monoxide radicals with dimethyl sulfide. [Article]. *Physical Chemistry Chemical Physics*, 7(10), 2173-2181.
- Gravestock, T. J. (2006). A kinetic and spectroscopic study of chemistry relating to the atmospheric role of iodine species. [PhD. Dissertation]. The University of Leeds.
- Gross, A., Barnes, I., Sorensen, R. M., Kongsted, J., & Mikkelsen, K. V. (2004). A theoretical study of the reaction between CH<sub>3</sub>S(OH)CH<sub>3</sub> and O-2. [Article]. *Journal of Physical Chemistry A*, 108(41), 8659-8671.
- Gu, M., & Turecek, F. (1992). The elusive dimethylhydroxysulfuranyl radical – An intermediate or a transition-state. [Article]. *Journal of the American Chemical Society*, 114(18), 7146-7151.

- Halmer, M. M., Schmincke, H. U., & Graf, H. F. (2002). The annual volcanic gas input into the atmosphere, in particular into the stratosphere: a global data set for the past 100 years. [Article]. *Journal of Volcanology and Geothermal Research*, 115(3-4), 511-528.
- Happell, J. D., & Wallace, D. W. R. (1996). Methyl iodide in the Greenland/Norwegian Seas and the tropical Atlantic Ocean: Evidence for photochemical production. [Article]. *Geophysical Research Letters*, 23(16), 2105-2108.
- Hausmann, M., & Platt, U. (1994). Spectroscopic measurement of bromine oxide and ozone in the high arctic during polar sunrise experiment 1992. [Article]. *Journal of Geophysical Research-Atmospheres*, 99(D12), 25399-25413.
- Hearn, C. H., Turcu, E., & Joens, J. A. (1990). The near UV absorption spectra of dimethyl sulfide, diethyl sulfide and dimethyl disulfide at T = 300-K. [Article]. *Atmospheric Environment Part a-General Topics*, 24(7), 1939-1944.
- Hebestreit, K., Stutz, J., Rosen, D., Matveiv, V., Peleg, M., Luria, M., et al. (1999). DOAS measurements of tropospheric bromine oxide in mid-latitudes. *Science*, 283(5398), 55-57.
- Hewitt, A. D., Brahan, K. M., Boone, G. D., & Hewitt, S. A. (1996). Kinetics and mechanism of the Cl+CO reaction in air. [Article]. *International Journal of Chemical Kinetics*, 28(10), 763-771.
- Hoffmann, S. M. A., Smith, D. J., Urena, A. G., & Grice, R. (1984). Breakdown of long-lived collision dynamics in the reactions of chlorine atoms with alkyl iodides. [Article]. *Chemical Physics Letters*, 107(1), 99-102.
- Hoffmann, S. M. A., Smith, D. J., Urena, A. G., Steele, T. A., & Grice, R. (1984). Reactive scattering of a supersonic chlorine atom beam - Cl + CH<sub>3</sub>I. [Article]. *Molecular Physics*, 53(5), 1067-1079.
- Hofmann, D. J. (1990). Increase in the stratospheric background sulfuric-acid aerosol mass in the past 10 years. [Article]. *Science*, 248(4958), 996-1000.
- Honninger, G., Bobrowski, N., Palenque, E. R., Torrez, R., & Platt, U. (2004). Reactive bromine and sulfur emissions at Salar de Uyuni, Bolivia. *Geophysical Research Letters*, 31(4).
- Honninger, G., & Platt, U. (2002). Observations of BrO and its vertical distribution during surface ozone depletion at Alert. [Article]. *Atmospheric Environment*, 36(15-16), 2481-2489.

- Huebert, B. J., Howell, S., Laj, P., Johnson, J. E., Bates, T. S., Quinn, P. K., et al. (1993). Observations of the atmospheric sulfur cycle on SAGA-3. [Article]. *Journal of Geophysical Research-Atmospheres*, 98(D9), 16985-16995.
- Hynes, A. J., Stoker, R. B., Pounds, A. J., McKay, T., Bradshaw, J. D., Nicovich, J. M., et al. (1995). A mechanistic study of the reaction of OH with dimethyl-D(6) sulfide – direct observation of adduct formation and the kinetics of the adduct reaction with O-2. [Article]. *Journal of Physical Chemistry*, 99(46), 16967-16975.
- Hynes, A. J., & Wine, P. H. (1986). Direct kinetic and mechanistic study of the OH+ dimethylsulfide reaction under atmospheric conditions. [Meeting Abstract]. *Abstracts of Papers of the American Chemical Society*, 191, 134-PETR.
- Hynes, A. J., Wine, P. H., & Nicovich, J. M. (1988). Kinetics and mechanism of the reaction of OH with CS<sub>2</sub> under atmospheric conditions. [Article]. *Journal of Physical Chemistry*, 92(13), 3846-3852.
- Hynes, A. J., Wine, P. H., & Semmes, D. H. (1986). Kinetics and mechanism of OH reactions with organic sulfides. [Article]. *Journal of Physical Chemistry*, 90(17), 4148-4156.
- Ingham, T., Bauer, D., Sander, R., Crutzen, P. J., & Crowley, J. N. (1999). Kinetics and products of the reactions BrO+DMS and Br+DMS at 298 K. [Article]. *Journal of Physical Chemistry A*, 103(36), 7199-7209.
- Inomata, Y., Matsunaga, K., Murai, Y., Osada, K., & Iwasaka, Y. (1999). Simultaneous measurement of volatile sulfur compounds using ascorbic acid for oxidant removal and gas chromatography-flame photometric detection. [Article]. *Journal of Chromatography A*, 864(1), 111-119.
- James, J. D., Harrison, R. M., Savage, N. H., Allen, A. G., Grenfell, J. L., Allan, B. J., et al. (2000). Quasi-Lagrangian investigation into dimethyl sulfide oxidation in maritime air using a combination of measurements and model. [Article]. *Journal of Geophysical Research-Atmospheres*, 105(D21), 26379-26392.
- Jefferson, A., Nicovich, J. M., & Wine, P. H. (1994). Temperature-dependent kinetic studies of the reactions BR(P-2(3/2))+CH<sub>3</sub>SCH<sub>3</sub>[--]CH<sub>3</sub>SCH<sub>2</sub>+HBR – Heat of formation of the CH<sub>3</sub>SCH<sub>2</sub> radical. [Article]. *Journal of Physical Chemistry*, 98(29), 7128-7135.
- Jenkin, M. E., Cox, R. A., & Candeland, D. E. (1985). Photochemical aspects of tropospheric iodine behavior. [Article]. *Journal of Atmospheric Chemistry*, 2(4), 359-375.

- Jimenez, J. L., Bahreini, R., Cocker, D. R., Zhuang, H., Varutbangkul, V., Flagan, R. C., et al. (2003a). New particle formation from photooxidation of diiodomethane (CH<sub>2</sub>I<sub>2</sub>). [Article]. *Journal of Geophysical Research-Atmospheres*, 108(D10), 25.
- Jimenez, J. L., Bahreini, R., Cocker, D. R., Zhuang, H., Varutbangkul, V., Flagan, R. C., et al. (2003b). New particle formation from photooxidation of diiodomethane (CH<sub>2</sub>I<sub>2</sub>) (vol 108, Art no 4318, 2003). [Correction]. *Journal of Geophysical Research-Atmospheres*, 108(D23), 1.
- Johnson, J. E., & Bates, T. S. (1993). Atmospheric measurements of carbonyl sulfide, dimethyl sulfide, and carbon-disulfide using the electron-capture sulfur detector. [Article]. *Journal of Geophysical Research-Atmospheres*, 98(D12), 23411-23421.
- Jones, B. M. R., Burrows, J. P., Cox, R. A., & Penkett, S. A. (1982). OCS formation in the reaction of OH with CS<sub>2</sub>. [Article]. *Chemical Physics Letters*, 88(4), 372-376.
- Jones, B. M. R., Cox, R. A., & Penkett, S. A. (1983). Atmospheric chemistry of carbon-disulfide. [Article]. *Journal of Atmospheric Chemistry*, 1(1), 65-86.
- Junge, C. E., Chagnon, C. W., & Manson, J. E. (1961a). Stratospheric aerosols. [Article]. *Journal of Meteorology*, 18(1), 81-108.
- Junge, C. E., Chagnon, C. W., & Manson, J. E. (1961b). World-wide stratospheric aerosol layer. [Meeting Abstract]. *Journal of Geophysical Research*, 66(8), 2540-&.
- Junge, C. E., Manson, J. E., & Chagnon, C. W. (1961). A world-wide stratospheric aerosol layer. [Article]. *Science*, 133(346), 1478-&.
- Kambanis, K. G., Lazarou, Y. G., & Papagiannakopoulos, P. (1997). Absolute reaction rate of chlorine atoms with iodomethane. [Article]. *Chemical Physics Letters*, 268(5-6), 498-504.
- Keene, W. C., Khalil, M. A. K., Erickson, D. J., McCulloch, A., Graedel, T. E., Lobert, J. M., et al. (1999). Composite global emissions of reactive chlorine from anthropogenic and natural sources: Reactive Chlorine Emissions Inventory. *Journal of Geophysical Research-Atmospheres*, 104(D7), 8429-8440.
- Kiehl, J. T., Schneider, T. L., Rasch, P. J., Barth, M. C., & Wong, J. (2000). Radiative forcing due to sulfate aerosols from simulations with the National Center for Atmospheric Research Community Climate Model, Version 3. [Article]. *Journal of Geophysical Research-Atmospheres*, 105(D1), 1441-1457.

- Kleissas, K. M., Nicovich, J. M., & Wine, P. H. (2007). Spectroscopy and kinetics of the gas phase addition complex of atomic chlorine with dimethyl sulfoxide. [Article]. *Journal of Photochemistry and Photobiology a-Chemistry*, 187(1), 1-9.
- Klick, S., & Abrahamsson, K. (1992). Biogenic volatile iodated hydrocarbons in the ocean. [Article]. *Journal of Geophysical Research-Oceans*, 97(C8), 12683-12687.
- Knight, G. P., & Crowley, J. N. (2001). The reactions of IO with HO<sub>2</sub>, NO and CH<sub>3</sub>SCH<sub>3</sub>: Flow tube studies of kinetics and product formation. [Article]. *Physical Chemistry Chemical Physics*, 3(3), 393-401.
- Knispel, R., Koch, R., Siese, M., & Zetzsch, C. (1990). Adduct formation of OH radicals with benzene, toluene, and phenol and consecutive reactions of the adducts with NO<sub>x</sub> and O<sub>2</sub>. [Article]. *Berichte Der Bunsen-Gesellschaft-Physical Chemistry Chemical Physics*, 94(11), 1375-1379.
- Kreidenweis, S. M., Walcek, C. J., Feingold, G., Gong, W. M., Jacobson, M. Z., Kim, C. H., et al. (2003). Modification of aerosol mass and size distribution due to aqueous-phase SO<sub>2</sub> oxidation in clouds: Comparisons of several models. *Journal of Geophysical Research-Atmospheres*, 108(D7).
- Kukui, A., Borissenko, D., Laverdet, G., & Le Bras, G. (2003). Gas-phase reactions of OH radicals with dimethyl sulfoxide and methane sulfinic acid using turbulent flow reactor and chemical ionization mass spectrometry. *Journal of Physical Chemistry A*, 107(30), 5732-5742.
- Kurylo, M. J. (1978a). Flash-photolysis resonance fluorescence investigation of reaction of OH radicals with dimethyl sulfide. [Article]. *Chemical Physics Letters*, 58(2), 233-237.
- Kurylo, M. J. (1978b). Flash-photolysis resonance fluorescence investigation of reactions of OH radicals with OCS and CS<sub>2</sub>. [Article]. *Chemical Physics Letters*, 58(2), 238-242.
- Lazarou, Y. G., Kambanis, K. G., & Papagiannakopoulos, P. (1997). Ab initio computational study of the interaction of Cl atoms with HI, CH<sub>3</sub>I and CH<sub>3</sub>OCH<sub>2</sub>I. [Article]. *Chemical Physics Letters*, 271(4-6), 280-286.
- Lebras, G., & Platt, U. (1995). A possible mechanism for combined chlorine and bromine catalyzed destruction of tropospheric ozone in the arctic. [Article]. *Geophysical Research Letters*, 22(5), 599-602.
- Lee, J. H., Michael, J. V., Payne, W. A., & Stief, L. J. (1978). Temperature dependence of rate constant for Cl+NO+N<sub>2</sub>→NOCl+N<sub>2</sub>. [Article]. *Journal of Chemical*

*Physics*, 68(12), 5410-5413.

- Lindberg, S. E., Brooks, S., Lin, J., Scott, K., Goodsite, M., Tilden, M. S., et al. (2001). Dynamic oxidation of mercury in the arctic troposphere: Mercury speciation in air, deposition, and accumulation in snow from the Barrow, Alaska arctic mercury study. [Meeting Abstract]. *Abstracts of Papers of the American Chemical Society*, 222, U429-U429.
- Liss, P. S., & Slater, P. G. (1974). Flux of gases across air-sea interface. [Article]. *Nature*, 247(5438), 181-184.
- Lovejoy, E. R., Kroeger, K. S., & Ravishankara, A. R. (1990). The kinetics of the CS<sub>2</sub>OD+O<sub>2</sub> reaction. [Article]. *Chemical Physics Letters*, 167(3), 183-187.
- Lovejoy, E. R., Murrells, T. P., Ravishankara, A. R., & Howard, C. J. (1990). Oxidation of CS<sub>2</sub> by reaction with OH .2. YIELDS OF HO<sub>2</sub> AND SO<sub>2</sub> IN OXYGEN. [Article]. *Journal of Physical Chemistry*, 94(6), 2386-2393.
- Lovejoy, E. R., Ravishankara, A. R., & Howard, C. J. (1994). Yield of (OSO)-O-16-O-18 from the (OH)-O-18 initiated oxidation of CS<sub>2</sub> in O-16(2). [Article]. *International Journal of Chemical Kinetics*, 26(5), 551-560.
- Lovelock, J. E. (1975). Natural halocarbons in air and in sea. [Article]. *Nature*, 256(5514), 193-194.
- Lovelock, J. E., & Maggs, R. J. (1973). Halogenated hydrocarbons in and over Atlantic. [Article]. *Nature*, 241(5386), 194-196.
- Lunell, S., Huang, M. B., Sahetchian, K. A., Chachaty, C., & Zabel, F. (1990). Reaction of CS<sub>2</sub> with OH - A quantum chemical study. [Article]. *Journal of the Chemical Society-Chemical Communications*(14), 949-951.
- Maguin, F., Mellouki, A., Laverdet, G., Poulet, G., & Lebras, G. (1991). Kinetics of the reactions of the IO radical with dimethyl sulfide, methanethiol, ethylene, and propylene. [Article]. *International Journal of Chemical Kinetics*, 23(3), 237-245.
- Makela, J. M., Hoffmann, T., Holzke, C., Vakeva, M., Suni, T., Mattila, T., et al. (2002). Biogenic iodine emissions and identification of end-products in coastal ultrafine particles during nucleation bursts. [Article]. *Journal of Geophysical Research-Atmospheres*, 107(D19), 14.
- Manley, S. L., & Dastoor, M. N. (1987). Methyl halide (CH<sub>3</sub>X) production from the giant-kelp, macrocystis, and estimates of global CH<sub>3</sub>X production by kelp. [Note]. *Limnology and Oceanography*, 32(3), 709-715.
- Manley, S. L., & Dastoor, M. N. (1988). Methyl-iodide (CH<sub>3</sub>I) production by kelp and

- associated microbes. [Article]. *Marine Biology*, 98(4), 477-482.
- Mano, S., & Andreae, M. O. (1994). Emission of methyl-bromide from biomass burning. [Article]. *Science*, 263(5151), 1255-1257.
- Maroulis, P. J., & Bandy, A. R. (1980). Measurements of atmospheric concentrations of CS<sub>2</sub> in the eastern-United-States. [Article]. *Geophysical Research Letters*, 7(9), 681-684.
- Marshall, P. (1991). A computational study of adducts between atomic chlorine and carbon-dioxide, carbonyl sulfide and carbon-disulfide. [Article]. *Theochem-Journal of Molecular Structure*, 82(3-4), 309-319.
- Martin, D., Barnes, I., & Becker, K. H. (1987). Rate-constant and products of the reaction Cl+CS<sub>2</sub> in air. [Article]. *Chemical Physics Letters*, 140(2), 195-199.
- Martin, D., Jourdain, J. L., Laverdet, G., & Lebras, G. (1987). Kinetic study of the reaction of IO with CH<sub>3</sub>SCH<sub>3</sub>. [Article]. *International Journal of Chemical Kinetics*, 19(6), 503-512.
- Martinez, M., Arnold, T., & Perner, D. (1999). The role of bromine and chlorine chemistry for arctic ozone depletion events in Ny-Alesund and comparison with model calculations. [Article]. *Annales Geophysicae-Atmospheres Hydrospheres and Space Sciences*, 17(7), 941-956.
- Martinez, R. I., Herron, J. T., & Huie, R. E. (1981). The mechanism of ozone-alkene reactions in the gas-phase - A mass-spectrometric study of the reactions of 8 linear and branched-chain alkenes. [Article]. *Journal of the American Chemical Society*, 103(13), 3807-3820.
- Maul, C., Haas, T., Gericke, K. H., & Comes, F. J. (1995). Spin selectivity in the ultraviolet photodissociation of phosgene. [Article]. *Journal of Chemical Physics*, 102(8), 3238-3247.
- Maurer, T., Barnes, I., & Becker, K. H. (1999). FT-IR kinetic and product study of the Br-initiated oxidation of dimethyl sulfide. [Article]. *International Journal of Chemical Kinetics*, 31(12), 883-893.
- McConnell, J. C., Henderson, G. S., Barrie, L., Bottenheim, J., Niki, H., Langford, C. H., et al. (1992). Photochemical bromine production implicated in Arctic boundary-layer ozone depletion. [Article]. *Nature*, 355(6356), 150-152.
- McElroy, M. B., Salawitch, R. J., Wofsy, S. C., & Logan, J. A. (1986). Reductions of Antarctic ozone due to synergistic interactions of chlorine and bromine. [Article]. *Nature*, 321(6072), 759-762.

- McFiggans, G., Coe, H., Burgess, R., Allan, J., Cubison, M., Alfarra, M. R., et al. (2004). Direct evidence for coastal iodine particles from *Laminaria* macroalgae - linkage to emissions of molecular iodine. [Article]. *Atmospheric Chemistry and Physics*, 4, 701-713.
- McFiggans, G., Cox, R. A., Mossinger, J. C., Allan, B. J., & Plane, J. M. C. (2002). Active chlorine release from marine aerosols: Roles for reactive iodine and nitrogen species. [Article]. *Journal of Geophysical Research-Atmospheres*, 107(D15), 15.
- McFiggans, G., Plane, J. M. C., Allan, B. J., Carpenter, L. J., Coe, H., & O'Dowd, C. (2000). A modeling study of iodine chemistry in the marine boundary layer. [Article]. *Journal of Geophysical Research-Atmospheres*, 105(D11), 14371-14385.
- McKee, M. L. (1993a). Computational study of addition and abstraction reactions between OH radical and dimethyl sulfide - A difficult case. [Article]. *Journal of Physical Chemistry*, 97(42), 10971-10976.
- McKee, M. L. (1993b). Computational study of the addition of OH radical to S=C=S. [Article]. *Chemical Physics Letters*, 201(1-4), 41-46.
- McKee, M. L. (1993c). Theoretical study of the CH<sub>3</sub>SOO radical. [Article]. *Chemical Physics Letters*, 211(6), 643-648.
- McKee, M. L. (1993d). Theoretical-study of the ClCS<sub>2</sub> adduct. [Article]. *Chemical Physics Letters*, 209(3), 195-200.
- McKee, M. L. (2003). Comparison of gas-phase and solution-phase reactions of dimethyl sulfide and 2-(methylthio)ethanol with hydroxyl radical. [Article]. *Journal of Physical Chemistry A*, 107(35), 6819-6827.
- McKee, M. L., & Wine, P. H. (2001). Ab initio study of the atmospheric oxidation of CS<sub>2</sub>. [Article]. *Journal of the American Chemical Society*, 123(10), 2344-2353.
- Molina, M. J., Molina, L. T., & Kolb, C. E. (1996). Gas-phase and heterogeneous chemical kinetics of the troposphere and stratosphere. [Review]. *Annual Review of Physical Chemistry*, 47, 327-367.
- Montzka, S. A., Butler, J. H., Hall, B. D., Mondeel, D. J., & Elkins, J. W. (2003). A decline in tropospheric organic bromine. [Article]. *Geophysical Research Letters*, 30(15), 4.

- Moore, R. M., & Groszko, W. (1999). Methyl iodide distribution in the ocean and fluxes to the atmosphere. [Article]. *Journal of Geophysical Research-Oceans*, 104(C5), 11163-11171.
- Moore, R. M., & Tokarczyk, R. (1992). Chloro-iodomethane in north-Atlantic waters - A potentially significant source of atmospheric iodine. [Article]. *Geophysical Research Letters*, 19(17), 1779-1782.
- Mouri, H., Nagao, I., Okada, K., Koga, S., & Tanaka, H. (1999). Individual-particle analyses of coastal Antarctic aerosols. [Article]. *Tellus Series B-Chemical and Physical Meteorology*, 51(3), 603-611.
- Muramatsu, Y., & Yoshida, S. (1995). Volatilization of methyl-iodide from the soil-plant system. [Article]. *Atmospheric Environment*, 29(1), 21-25.
- Murrells, T. P., Lovejoy, E. R., & Ravishankara, A. R. (1990). Oxidation of CS<sub>2</sub> by reaction with OH .1. Equilibrium-constant for the reaction OH+CS<sub>2</sub> reversible CS<sub>2</sub>OH and the kinetics of the CS<sub>2</sub>OH+O<sub>2</sub> reaction. [Article]. *Journal of Physical Chemistry*, 94(6), 2381-2386.
- Nagao, I., Matsumoto, K., & Tanaka, H. (1999a). Characteristics of dimethylsulfide, ozone, aerosols, and cloud condensation nuclei in air masses over the northwestern Pacific Ocean. [Review]. *Journal of Geophysical Research-Atmospheres*, 104(D9), 11675-11693.
- Nagao, I., Matsumoto, K., & Tanaka, H. (1999b). Sunrise ozone destruction found in the sub-tropical marine boundary layer. [Article]. *Geophysical Research Letters*, 26(22), 3377-3380.
- Nakano, Y., Enami, S., Nakamichi, S., Aloisio, S., Hashimoto, S., & Kawasaki, M. (2003). Temperature and pressure dependence study of the reaction of IO radicals with dimethyl sulfide by cavity ring-down laser spectroscopy. [Article]. *Journal of Physical Chemistry A*, 107(33), 6381-6387.
- Nakano, Y., Goto, M., Hashimoto, S., Kawasaki, M., & Wallington, T. J. (2001). Cavity ring-down spectroscopic study of the reactions of Br atoms and BrO radicals with dimethyl sulfide. [Article]. *Journal of Physical Chemistry A*, 105(49), 11045-11050.
- Nguyen, B. C., Bonsang, B., & Gaudry, A. (1983). The role of the ocean in the global atmospheric sulfur cycle. [Article]. *Journal of Geophysical Research-Oceans and Atmospheres*, 88(NC15), 903-914.

- Nguyen, B. C., Mihalopoulos, N., & Belviso, S. (1990). Seasonal variation of atmospheric dimethylsulfide at Amsterdam Island in the southern Indian-Ocean. [Article]. *Journal of Atmospheric Chemistry*, 11(1-2), 123-141.
- Nicovich, J. M., Shackelford, C. J., & Wine, P. H. (1990a). Kinetics and thermochemistry of reversible adduct formation in the reaction of Cl(P-2J) with CS<sub>2</sub>. [Article]. *Journal of Physical Chemistry*, 94(7), 2896-2903.
- Nicovich, J. M., Kreutter, K. D., & Wine, P. H. (1990b). Kinetics of the reactions of Cl(2PJ) and Br(2P3/2) with O-3. [Article]. *International Journal of Chemical Kinetics*, 22(4), 399-414.
- Nicovich, J. M., McKee, M. L., Piety, C. A., Ayhens, Y. V., & Wine, P. H. (1996). Adduct formation in the reactions of chlorine atoms with halomethanes. [Meeting Abstract]. *Abstracts of Papers of the American Chemical Society*, 211, 82-PHYS.
- Nicovich, J. M., Parthasarathy, S., Pope, F. D., Pegus, A. T., McKee, M. L., & Wine, P. H. (2006). Kinetics, mechanism, and thermochemistry of the gas phase reaction of atomic chlorine with dimethyl sulfoxide. *Journal of Physical Chemistry A*, 110(21), 6874-6885.
- Nicovich, J. M., Wang, S., & Wine, P. H. (1995). Kinetics of the reactions of atomic chlorine with H<sub>2</sub>S, D<sub>2</sub>S, CH<sub>3</sub>SH, and CD<sub>3</sub>SD. [Article]. *International Journal of Chemical Kinetics*, 27(4), 359-368.
- O'Dowd, C. D., Hameri, K., Makela, J. M., Pirjola, L., Kulmala, M., Jennings, S. G., et al. (2002). A dedicated study of New Particle Formation and Fate in the Coastal Environment (PARFORCE): Overview of objectives and achievements. [Article]. *Journal of Geophysical Research-Atmospheres*, 107(D19), 16.
- O'Dowd, C. D., Jimenez, J. L., Bahreini, R., Flagan, R. C., Seinfeld, J. H., Hameri, K., et al. (2002). Marine aerosol formation from biogenic iodine emissions. [Article]. *Nature*, 417(6889), 632-636.
- Oram, D. E., & Penkett, S. A. (1994). Observations in eastern England of elevated methyl-iodide concentrations in air of Atlantic origin. [Article]. *Atmospheric Environment*, 28(6), 1159-1174.
- Orlando, J. J., Piety, C. A., Nicovich, J. M., McKee, M. L., & Wine, P. H. (2005). Rates and mechanisms for the reactions of chlorine atoms with iodoethane and 2-iodopropane. [Article]. *Journal of Physical Chemistry A*, 109(30), 6659-6675.
- Osborne, D. W., Doescher, R. N., & Yost, D. M. (1942). The heat capacity, heats of fusion and vaporization, vapor pressure and entropy of dimethyl sulfide. [Article].

*Journal of the American Chemical Society*, 64, 169-172.

- Patroescu, I. V., Barnes, I., Becker, K. H., & Mihalopoulos, N. (1999). FT-IR product study of the OH-initiated oxidation of DMS in the presence of NO<sub>x</sub>. *Atmospheric Environment*, 33(1), 25-35.
- Paulson, S. E., Chung, M. Y., & Hasson, A. S. (1999). OH radical formation from the gas-phase reaction of ozone with terminal alkenes and the relationship between structure and mechanism. [Article]. *Journal of Physical Chemistry A*, 103(41), 8125-8138.
- Pence, W. H., Baughcum, S. L., & Leone, S. R. (1981). Laser UV photofragmentation of halogenated molecules – selective bond-dissociation and wavelength-specific quantum yields for excited I(P-2(1/2) and BR(P-2(1/2) atoms. [Article]. *Journal of Physical Chemistry*, 85(25), 3844-3851.
- Pernice, H., Garcia, P., Willner, H., Francisco, J. S., Mills, F. P., Allen, M., et al. (2004). Laboratory evidence for a key intermediate in the Venus atmosphere: Peroxychloroformyl radical. [Article]. *Proceedings of the National Academy of Sciences of the United States of America*, 101(39), 14007-14010.
- Pham, M., Muller, J. F., Brasseur, G. P., Granier, C., & Megie, G. (1995). A three-dimensional study of the tropospheric sulfur cycle. [Review]. *Journal of Geophysical Research-Atmospheres*, 100(D12), 26061-26092.
- Piety, C. A., Nicovich, J. M., Ayhens, Y. V., Soller, R., & Wine, P. H. (1996). Kinetics of non-adduct-forming channels in the reactions of chlorine atoms with halomethanes. [Meeting Abstract]. *Abstracts of Papers of the American Chemical Society*, 211, 87-PHYS.
- Piety, C. A., Soller, R., Nicovich, J. M., McKee, M. L., & Wine, P. H. (1998). Kinetic and mechanistic study of the reaction of atomic chlorine with methyl bromide over an extended temperature range. [Article]. *Chemical Physics*, 231(2-3), 155-169.
- Plane, J. M. C., Joseph, D. M., Allan, B. J., Ashworth, S. H., & Francisco, J. S. (2006). An experimental and theoretical study of the reactions OIO plus NO and OH plus OH. *Journal of Physical Chemistry A*, 110(1), 93-100.
- Platt, U., & Hausmann, M. (1994). Spectroscopic measurement of the free-radicals NO<sub>3</sub>, BRO, IO, and OH in the troposphere. [Review]. *Research on Chemical Intermediates*, 20(3-5), 557-578.
- Platt, U., & Janssen, C. (1995). Observation and role of the free radicals NO<sub>3</sub>, ClO, BrO and IO in the troposphere. [Article]. *Faraday Discussions*, 175-198.

- Prinn, R. G., Huang, J., Weiss, R. F., Cunnold, D. M., Fraser, P. J., Simmonds, P. G., et al. (2001). Evidence for substantial variations of atmospheric hydroxyl radicals in the past two decades. [Article]. *Science*, 292(5523), 1882-1888.
- Quack, B., & Wallace, D. W. R. (2003). Air-sea flux of bromoform: Controls, rates, and implications. [Review]. *Global Biogeochemical Cycles*, 17(1), 27.
- Radom L., Structural consequences of hyperconjugation in molecular structure and conformation; Czismadia, I. G., Ed.; Elsevier: New York, 1982; pp 1-64.
- Rasch, P. J., Barth, M. C., Kiehl, J. T., Schwartz, S. E., & Benkovitz, C. M. (2000a). A description of the global sulfur cycle and its controlling processes in the National Center for Atmospheric Research Community Climate Model, Version 3. [Article]. *Journal of Geophysical Research-Atmospheres*, 105(D1), 1367-1385.
- Rasch, P. J., Barth, M. C., Kiehl, J. T., Schwartz, S. E., & Benkovitz, C. M. (2000b). A description of the global sulfur cycle and its controlling processes in the National Center for Atmospheric Research Community Climate Model, Version 3 (vol 105, pg 1367, 2000). [Correction]. *Journal of Geophysical Research-Atmospheres*, 105(D5), 6783-6783.
- Rasmussen, R. A., Khalil, M. A. K., Gunawardena, R., & Hoyt, S. D. (1982). Atmospheric methyl-iodide (CH<sub>3</sub>I). [Article]. *Journal of Geophysical Research-Oceans and Atmospheres*, 87(NC4), 3086-3090.
- Rattigan, O. V., Shallcross, D. E., & Cox, R. A. (1997). UV absorption cross-sections and atmospheric photolysis rates of CF<sub>3</sub>I, CH<sub>3</sub>I, C<sub>2</sub>H<sub>5</sub>I and CH<sub>2</sub>Cl. [Article]. *Journal of the Chemical Society-Faraday Transactions*, 93(16), 2839-2846.
- Ravishankara, A. R., Smith, G. J., & Davis, D. D. (1988). A kinetics study of the reaction of Cl with NO<sub>2</sub>. [Article]. *International Journal of Chemical Kinetics*, 20(10), 811-814.
- Redeker, K. R., Wang, N. Y., Low, J. C., McMillan, A., Tyler, S. C., & Cicerone, R. J. (2000). Emissions of methyl halides and methane from rice paddies. [Article]. *Science*, 290(5493), 966-969.
- Reifenhauser, W., & Heumann, K. G. (1992). Determinations of methyl-iodide in the Antarctic atmosphere and the south Polar Sea. [Article]. *Atmospheric Environment Part a-General Topics*, 26(16), 2905-2912.
- Roehl, C. M., Burkholder, J. B., Moortgat, G. K., Ravishankara, A. R., & Crutzen, P. J. (1997). Temperature dependence of UV absorption cross sections and atmospheric implications of several alkyl iodides. [Article]. *Journal of*

*Geophysical Research-Atmospheres*, 102(11D), 12819-12829.

- Russell, G. A. (1958a). Directive effects in aliphatic substitutions .11. Solvent effects in the reactions of free radicals and atoms effects of solvents on the position of attack of chlorine atoms upon 2,3-dimethylbutane, isobutene and 2-deuterio-2-methylpropane. [Article]. *Journal of the American Chemical Society*, 80(18), 4987-4996.
- Russell, G. A. (1958b). Directive effects in aliphatic substitutions .12. Solvent effects in the reactions of free radicals and atoms. Effects of solvents in the competitive photochlorination of hydrocarbons and their derivatives. [Article]. *Journal of the American Chemical Society*, 80(18), 4997-5001.
- Saiz-Lopez, A., Mahajan, A. S., Salmon, R. A., Bauguitte, S. J. B., Jones, A. E., Roscoe, H. K., et al. (2007). Boundary layer halogens in coastal Antarctica. [Article]. *Science*, 317(5836), 348-351.
- Saiz-Lopez, A., Shillito, J. A., Coe, H., & Plane, J. M. C. (2006). Measurements and modelling of I-2, IO, OIO, BrO and NO<sub>3</sub> in the mid-latitude marine boundary layer. *Atmospheric Chemistry and Physics*, 6, 1513-1528.
- Saiz-Lopez, A., & Plane, J. M. C. (2004). Novel iodine chemistry in the marine boundary layer. [Article]. *Geophysical Research Letters*, 31(4), 4.
- Saiz-Lopez, A., Plane, J. M. C., & Shillito, J. A. (2004). Bromine oxide in the mid-latitude marine boundary layer. [Article]. *Geophysical Research Letters*, 31(3), 4.
- Saiz-Lopez, A., Saunders, R. W., Joseph, D. M., Ashworth, S. H., & Plane, J. M. C. (2004). Absolute absorption cross-section and photolysis rate of I-2. [Article]. *Atmospheric Chemistry and Physics*, 4, 1443-1450.
- Sandalls, F. J., & Penkett, S. A. (1977). Measurements of carbonyl sulfide and carbon-disulfide in atmosphere. [Note]. *Atmospheric Environment*, 11(2), 197-199.
- Sander, R., & Crutzen, P. J. (1996). Model study indicating halogen activation and ozone destruction in polluted air masses transported to the sea. [Article]. *Journal of Geophysical Research-Atmospheres*, 101(D4), 9121-9138.
- Sander, R., Vogt, R., Harris, G. W., & Crutzen, P. J. (1997). Modeling the chemistry ozone, halogen compounds, and hydrocarbons in the arctic troposphere during spring. [Article]. *Tellus Series B-Chemical and Physical Meteorology*, 49(5), 522-532.
- Sander, S. P., Finlayson-Pitts, B. J., Friedl, R. R., Golden, D. M., Huie, R. E., Keller-Rudek, H., Kolb, C. E., Kurylo, M. J., Molina, M. J., Moortgat, G. K., Orkin, V. L., Ravishankara, A. R., Wine, P. H., *Chemical kinetics and photochemical data for use in atmospheric studies, Evaluation No. 15*, JPL Publication 06-2, Jet

Propulsion Laboratory, Pasadena, CA, 2006.

- Sayin, H., & McKee, M. L. (2004). Computational study of the reactions between XO (X = Cl, Br, I) and dimethyl sulfide. *Journal of Physical Chemistry A*, 108(37), 7613-7620.
- Scaduto, R. C. (1995). Oxidation of DMSO and methanesulfinic acid by the hydroxyl radical. *Free Radical Biology and Medicine*, 18(2), 271-277.
- Schall, C., & Heumann, K. G. (1993). GC determination of volatile organoiodine and organobromine compounds in Arctic seawater and air samples. [Article]. *Fresenius Journal of Analytical Chemistry*, 346(6-9), 717-722.
- Schonesh.M, & Henglein, A. (1969). Investigation by pulse radiation of dissociation equilibria of mixed radical anion complex BrSCN(-). *Berichte Der Bunsen-Gesellschaft Fur Physikalische Chemie*, 73(3), 289-&.
- Schonesh.M, & Henglein, A. (1970). Pulse radiolytic studies of ISCN- and I2SCN- (iodothiocyanate) complexes. *Berichte Der Bunsen-Gesellschaft Fur Physikalische Chemie*, 74(4), 393-&.
- Seetula, J. A., Gutman, D., Lightfoot, P. D., Rayes, M. T., & Senkan, S. M. (1991). Kinetics of the reactions of partially halogenated methyl radicals (CH<sub>2</sub>Cl, CH<sub>2</sub>Br, CH<sub>2</sub>I, AND CHCl<sub>2</sub>) with molecular chlorine. [Article]. *Journal of Physical Chemistry*, 95(26), 10688-10693.
- Sehested, K., & Holcman, J. (1996). A pulse radiolysis study of the OH radical induced autoxidation of methanesulfinic acid. *Radiation Physics and Chemistry*, 47(3), 357-360.
- Seinfeld, J. H. and S. N. Pandis (1998). Atmospheric Chemistry and Physics: From air pollution to climate change. New York, John Wiley & Sons.
- Shum, L. G. S., & Benson, S. W. (1985a). Iodine catalyzed pyrolysis of dimethyl sulfide – heats of formation of CH<sub>3</sub>SCH<sub>2</sub>I, the CH<sub>3</sub>SCH<sub>2</sub> radical, and the pibond energy in CH<sub>2</sub>S. [Article]. *International Journal of Chemical Kinetics*, 17(3), 277-292.
- Shum, L. G. S., & Benson, S. W. (1985b). The pyrolysis of dimethyl sulfide, kinetics and mechanism. [Article]. *International Journal of Chemical Kinetics*, 17(7), 749-761.
- Simpson, W. R., von Glasow, R., Riedel, K., Anderson, P., Ariya, P., Bottenheim, J., et al. (2007). Halogens and their role in polar boundary-layer ozone depletion. [Review]. *Atmospheric Chemistry and Physics*, 7(16), 4375-4418.

- Singh, H. B., Salas, L. J., & Stiles, R. E. (1983). Methyl halides in and over the eastern Pacific (40-degrees-N-32-degrees-S). [Article]. *Journal of Geophysical Research-Oceans and Atmospheres*, 88(NC6), 3684-3690.
- Sive, B. C., Varner, R. K., Mao, H., Blake, D. R., Wingenter, O. W., & Talbot, R. (2007). A large terrestrial source of methyl iodide. [Article]. *Geophysical Research Letters*, 34(17), 5.
- Skov, H., Christensen, J. H., Goodsite, M. E., Heidam, N. Z., Jensen, B., Wahlin, P., et al. (2004). Fate of elemental mercury in the arctic during atmospheric mercury depletion episodes and the load of atmospheric mercury to the arctic. [Article]. *Environmental Science & Technology*, 38(8), 2373-2382.
- Solomon, S. (1990). Progress towards a quantitative understanding of Antarctic ozone depletion. [Review]. *Nature*, 347(6291), 347-354.
- Solomon, S., Garcia, R. R., & Ravishankara, A. R. (1994). On the role of iodine in ozone depletion. [Article]. *Journal of Geophysical Research-Atmospheres*, 99(D10), 20491-20499.
- Sorensen, S., FalbeHansen, H., Mangoni, M., Hjorth, J., & Jensen, N. R. (1996). Observation of DMSO and CH<sub>3</sub>S(O)OH from the gas phase reaction between DMS and OH. *Journal of Atmospheric Chemistry*, 24(3), 299-315.
- Spicer, C. W., Chapman, E. G., Finlayson-Pitts, B. J., Plastridge, R. A., Hubbe, J. M., Fast, J. D., et al. (1998). Unexpectedly high concentrations of molecular chlorine in coastal air. [Article]. *Nature*, 394(6691), 353-356.
- Steiner, M. G., & Babbs, C. F. (1990). Quantitation of the hydroxyl radical by reaction with dimethyl-sulfoxide. *Archives of Biochemistry and Biophysics*, 278(2), 478-481.
- Stickel, R. E., Chin, M., Daykin, E. P., Hynes, A. J., Wine, P. H., & Wallington, T. J. (1993). Mechanistic studies of the OH-initiated oxidation of CS<sub>2</sub> in the presence of O<sub>2</sub>. [Article]. *Journal of Physical Chemistry*, 97(51), 13653-13661.
- Stickel, R. E., Nicovich, J. M., Wang, S., Zhao, Z., & Wine, P. H. (1992). Kinetic and mechanistic study of the reaction of atomic chlorine with dimethyl sulfide. *Journal of Physical Chemistry*, 96(24), 9875-9883.
- Stickel, R. E., Zhao, Z., & Wine, P. H. (1993a). Branching ratios for hydrogen-transfer in the reactions of OD radicals with CH<sub>3</sub>SCH<sub>3</sub> and CH<sub>3</sub>SC<sub>2</sub>H<sub>5</sub>. [Article]. *Chemical Physics Letters*, 212(3-4), 312-318.

- Stickel, R. E., Zhao, Z., & Wine, P. H. (1993b). Tunable diode-laser studies of atmospheric sulfur oxidation mechanisms. [Meeting Abstract]. *Abstracts of Papers of the American Chemical Society*, 206, 227-PHYS.
- Sturges, W. T., & Barrie, L. A. (1988). Chlorine, bromine and iodine in Arctic aerosols. [Article]. *Atmospheric Environment*, 22(6), 1179-1194.
- Stutz, J., Ackermann, R., Fast, J. D., & Barrie, L. (2002). Atmospheric reactive chlorine and bromine at the Great Salt Lake, Utah. *Geophysical Research Letters*, 29(10).
- Stutz, J., Hebestreit, K., Alicke, B., & Platt, U. (1999). Chemistry of halogen oxides in the troposphere: Comparison of model calculations with recent field data. [Article]. *Journal of Atmospheric Chemistry*, 34(1), 65-85.
- Sze, N. D., & Ko, M. K. W. (1979a). CS<sub>2</sub> and COS in the stratospheric sulfur budget. [Article]. *Nature*, 280(5720), 308-310.
- Sze, N. D., & Ko, M. K. W. (1979b). Is CS<sub>2</sub> a precursor for atmospheric COS. [Article]. *Nature*, 278(5706), 731-732.
- Talukdar, R. K., Hunter, M., Warren, R. F., Burkholder, J. B., & Ravishankara, A. R. (1996). UV laser photodissociation of CF<sub>2</sub>ClBr and CF<sub>2</sub>Br<sub>2</sub> at 298 K: Quantum yields of Cl, Br, and CF<sub>2</sub>. [Article]. *Chemical Physics Letters*, 262(6), 669-674.
- Tan, X. D., Bi, Y. Y., Su, Y. J., Li, Y., He, J., Yi, P. F., et al. (2000). Carbon disulfide at a Chinese viscose factory external and internal exposure assessment. [Article]. *Journal of Environmental Monitoring*, 2(6), 666-669.
- Tang, T., & McConnell, J. C. (1996). Autocatalytic release of bromine from Arctic snow pack during polar sunrise. [Article]. *Geophysical Research Letters*, 23(19), 2633-2636.
- Tellingh, J. (1973). Resolution of Visible-Infrared absorption-spectrum of I<sub>2</sub> into 3 contributing transitions. *Journal of Chemical Physics*, 58(7), 2821-2834.
- Thompson, K. C., Canosa-Mas, C. E., & Wayne, R. P. (2002). Kinetics and mechanism of the reaction between atomic chlorine and dimethyl selenide; comparison with the reaction between atomic chlorine and dimethyl sulfide. [Article]. *Physical Chemistry Chemical Physics*, 4(17), 4133-4139.
- Tian, Y., Tian, Z. M., Wei, W. M., He, T. J., Chen, D. M., & Liu, F. C. (2007). Ab initio study of the reaction of OH radical with methyl sulfinic acid (MSIA). *Chemical Physics*, 335(2-3), 133-140.

- Timonen, R. S., & Gutman, D. (1986). Kinetics of the reactions of methyl, ethyl, isopropyl, and tert butyl radicals with molecular chlorine. [Article]. *Journal of Physical Chemistry*, 90(13), 2987-2991.
- Torres, A. L., Maroulis, P. J., Goldberg, A. B., & Bandy, A. R. (1980). Atmospheric OCS measurements on project GAMETAG. [Article]. *Journal of Geophysical Research-Oceans and Atmospheres*, 85(NC12), 7357-7360.
- Toumi, R. (1994). BrO as a sink for dimethylsulfide in the marine atmosphere. [Article]. *Geophysical Research Letters*, 21(2), 117-120.
- Tucker, B. J., Maroulis, P. J., & Bandy, A. R. (1985). Free tropospheric measurements of CS<sub>2</sub> over a 45-degrees-N to 45-degrees-S latitude range. [Article]. *Geophysical Research Letters*, 12(1), 9-11.
- Tuckermann, M., Ackermann, R., Golz, C., LorenzenSchmidt, H., Senne, T., Stutz, J., et al. (1997). DOAS-observation of halogen radical-catalysed arctic boundary layer ozone destruction during the ARCTOC-campaigns 1995 and 1996 in Ny-Alesund, Spitsbergen. [Article]. *Tellus Series B-Chemical and Physical Meteorology*, 49(5), 533-555.
- Turecek, F. (1994). The dimethylsulfide-hydroxyl radical reaction - An ab-initio study. [Article]. *Journal of Physical Chemistry*, 98(14), 3701-3706.
- Turecek, F. (2000). Franck-Condon dominated chemistry. Formation and dissociations of the dimethylhydroxysulfuranyl radical. [Article]. *Collection of Czechoslovak Chemical Communications*, 65(4), 455-476.
- Turnipseed, A. A., Barone, S. B., & Ravishankara, A. R. (1996). Reaction of OH with dimethyl sulfide .2. Products and mechanisms. *Journal of Physical Chemistry*, 100(35), 14703-14713.
- Twomey, S. (1974). Pollution and planetary albedo. [Article]. *Atmospheric Environment*, 8(12), 1251-1256.
- Uchimaru, T., Tsuzuki, S., Sugie, M., Tokuhashi, K., & Sekiya, A. (2005). A theoretical study on the strength of two-center three-electron bond in (CH<sub>3</sub>)<sub>2</sub>S-OH and H<sub>2</sub>S-OH adducts. [Article]. *Chemical Physics Letters*, 408(4-6), 216-220.
- Urbanski, S. P., Stickel, R. E., & Wine, P. H. (1998). Mechanistic and kinetic study of the gas-phase reaction of hydroxyl radical with dimethyl sulfoxide. *Journal of Physical Chemistry A*, 102(51), 10522-10529.

- Urbanski, S. P., & Wine, P. H. (1999). Spectroscopic and kinetic study of the Cl-S(CH<sub>3</sub>)<sub>2</sub> adduct. [Article]. *Journal of Physical Chemistry A*, 103(50), 10935-10944.
- Vandresen, S., & Resende, S. M. (2004). The atmospheric reaction between DMSO and the chlorine radical. [Article]. *Journal of Physical Chemistry A*, 108(12), 2284-2289.
- Veltwisch, D., Janata, E., & Asmus, K. D. (1980). Primary processes in the reaction of OH-radicals with sulfoxides. *Journal of the Chemical Society-Perkin Transactions 2*(1), 146-153.
- Vogt, R., Crutzen, P. J., & Sander, R. (1996). A mechanism for halogen release from sea-salt aerosol in the remote marine boundary layer. [Article]. *Nature*, 383(6598), 327-330.
- Vogt, R., Sander, R., Von Glasow, R., & Crutzen, P. J. (1999). Iodine chemistry and its role in halogen activation and ozone loss in the marine boundary layer: A model study. [Article]. *Journal of Atmospheric Chemistry*, 32(3), 375-395.
- von Glasow, R., & Crutzen, P. J. (2004). Model study of multiphase DMS oxidation with a focus on halogens. [Article]. *Atmospheric Chemistry and Physics*, 4, 589-608.
- von Glasow, R., von Kuhlmann, R., Lawrence, M. G., Platt, U., & Crutzen, P. J. (2004). Impact of reactive bromine chemistry in the troposphere. [Article]. *Atmospheric Chemistry and Physics*, 4, 2481-2497.
- Waddington, G., Smith, J. C., Williamson, K. D., & Scott, D. W. (1962). Carbon disulfide as a reference substance for vapor-flow calorimetry – chemical, thermodynamic properties. [Article]. *Journal of Physical Chemistry*, 66(6), 1074-&.
- Wagner, T., Leue, C., Wenig, M., Pfeilsticker, K., & Platt, U. (2001). Spatial and temporal distribution of enhanced boundary layer BrO concentrations measured by the GOME instrument aboard ERS-2. *Journal of Geophysical Research-Atmospheres*, 106(D20), 24225-24235.
- Wagner, T., & Platt, U. (1998). Satellite mapping of enhanced BrO concentrations in the troposphere. [Article]. *Nature*, 395(6701), 486-490.
- Walling, C., & Mayahi, M. F. (1959). Some solvent and structural effects in free radical chlorination. [Article]. *Journal of the American Chemical Society*, 81(6), 1485-1488.

- Wallington, T. J., Andino, J. M., Potts, A. R., & Wine, P. H. (1991). A competitive kinetics study of the reaction of Cl with CS<sub>2</sub> in air at 298-K. [Article]. *Chemical Physics Letters*, 176(1), 103-108.
- Wallington, T. J., Atkinson, R., Tuazon, E. C., & Aschmann, S. M. (1986). The reaction of OH radicals with dimethyl sulfide. [Article]. *International Journal of Chemical Kinetics*, 18(8), 837-846.
- Wang, D. Q., Li, Y. L., Ho, W. S., Leung, K. H., & Phillips, D. L. (2002). Transient resonance Raman and density functional theory investigation of the chlorine atom/carbon disulfide molecular complex involved in selective alkane photochlorination reactions. [Article]. *Journal of Organic Chemistry*, 67(3), 747-752.
- Wang, D. Q., & Phillips, D. L. (2002). Density functional theory study of CS<sub>2</sub>/Cl adducts and their isomerization reactions. [Article]. *Chemical Physics Letters*, 362(3-4), 205-209.
- Wang, L., Zhang, F., & Chen, J. M. (2001). Carbonyl sulfide derived from catalytic oxidation of carbon disulfide over atmospheric particles. [Article]. *Environmental Science & Technology*, 35(12), 2543-2547.
- Warneck, P. (1999). *Chemistry of the natural atmosphere*. San Diego, Academic Press.
- Watts, S. F. (2000). The mass budgets of carbonyl sulfide, dimethyl sulfide, carbon disulfide and hydrogen sulfide. [Review]. *Atmospheric Environment*, 34(5), 761-779.
- Watts, S. F., Watson, A., & Brimblecombe, P. (1987). Measurements of the aerosol concentrations of methanesulfonic acid, dimethyl-sulfoxide and dimethyl sulfone in the marine atmosphere of the British-Isles. *Atmospheric Environment*, 21(12), 2667-2672.
- Wayne, R. P., Poulet, G., Biggs, P., Burrows, J. P., Cox, R. A., Crutzen, P. J., et al. (1995). Halogen oxides - radicals, sources and reservoirs in the laboratory and in the atmosphere. [Review]. *Atmospheric Environment*, 29(20), 2677-2881.
- Weiss, P. S., Johnson, J. E., Gammon, R. H., & Bates, T. S. (1995). Reevaluation of the open-ocean source of carbonyl sulfide to the atmosphere. [Article]. *Journal of Geophysical Research-Atmospheres*, 100(D11), 23083-23092.

- Williams, M. B., Campuzano-Jost, P., Cossairt, B. M., Hynes, A. J., & Pounds, A. J. (2007). Experimental and theoretical studies of the reaction of the OH radical with alkyl sulfides: 1. Direct observations of the formation of the OH-DMS adduct-pressure dependence of the forward rate of addition and development of a predictive expression at low temperature. *Journal of Physical Chemistry A*, *111*(1), 89-104.
- Wilson, C., & Hirst, D. M. (1997). Ab initio study of the reaction of chlorine atoms with H<sub>2</sub>S, CH<sub>3</sub>SH, CH<sub>3</sub>SCH<sub>3</sub> and CS<sub>2</sub>. [Article]. *Journal of the Chemical Society-Faraday Transactions*, *93*(16), 2831-2837.
- Wine, P. H., Nicovich, J. M., Stickel, R. E., Zhao, Z., Shackelford, C. J., Kreutter, K. D., Daykin, E. P., Wang, S. NATO ASI Series 1, Global Environmental Change, Niki, H., Becker, K. H., Eds., 1993, 17, 385.
- Wine, P. H., Nicovich, J. M., Stickel, R. E., & Hynes, A. J. (1995). Laboratory studies of weakly bound adducts of atmospheric interest. [Meeting Abstract]. *Abstracts of Papers of the American Chemical Society*, *210*, 19-PHYS.
- Wine, P. H., Nicovich, J. M., Zhu, L., McKee, M. L., Parthasarathy, S., Connelly, S. E., et al. (2002). Laboratory studies of the atmospheric chemistry of organic sulfur species. *Abstracts of Papers of the American Chemical Society*, *223*, U524-U524.
- Wine, P. H., Shah, R. C., & Ravishankara, A. R. (1980). Rate of reaction of OH with CS<sub>2</sub>. [Article]. *Journal of Physical Chemistry*, *84*(20), 2499-2503.
- Wine, P. H., Thompson, R. J., Ravishankara, A. R., Semmes, D. H., Gump, C. A., Torabi, A., et al. (1984). Kinetics of the reaction OH+SO<sub>2</sub>+M-[HOSO<sub>2</sub>+M – Temperature and pressure-dependence in the falloff region. *Journal of Physical Chemistry*, *88*(10), 2095-2104.
- Wingenter, O. W., Blake, D. R., Blake, N. J., Sive, B. C., Rowland, F. S., Atlas, E., et al. (1999). Tropospheric hydroxyl and atomic chlorine concentrations, and mixing timescales determined from hydrocarbon and halocarbon measurements made over the Southern Ocean. [Article]. *Journal of Geophysical Research-Atmospheres*, *104*(D17), 21819-21828.
- Wingenter, O. W., Kubo, M. K., Blake, N. J., Smith, T. W., Blake, D. R., & Rowland, F. S. (1996). Hydrocarbon and halocarbon measurements as photochemical and dynamical indicators of atmospheric hydroxyl, atomic chlorine, and vertical mixing obtained during Lagrangian flights. [Article]. *Journal of Geophysical Research-Atmospheres*, *101*(D2), 4331-4340.

- Wingenter, O. W., Sive, B. C., Blake, N. J., Blake, D. R., & Rowland, F. S. (2005). Atomic chlorine concentrations derived from ethane and hydroxyl measurements over the equatorial Pacific Ocean: Implication for dimethyl sulfide and bromine monoxide. [Article]. *Journal of Geophysical Research-Atmospheres*, 110(D20), 10.
- Xu, H., & Joens, J. A. (1993). CS<sub>2</sub> absorption cross-section measurements from 187 NM to 230 NM. [Article]. *Geophysical Research Letters*, 20(11), 1035-1037.
- Yang, X., Cox, R. A., Warwick, N. J., Pyle, J. A., Carver, G. D., O'Connor, F. M., et al. (2005). Tropospheric bromine chemistry and its impacts on ozone: A model study. [Article]. *Journal of Geophysical Research-Atmospheres*, 110(D23), 18.
- Yokouchi, Y., Mukai, H., Yamamoto, H., Otsuki, A., Saitoh, C., & Nojiri, Y. (1997). Distribution of methyl iodide, ethyl iodide, bromoform, and dibromomethane over the ocean (east and southeast Asian seas and the western Pacific). [Article]. *Journal of Geophysical Research-Atmospheres*, 102(D7), 8805-8809.
- Yokouchi, Y., Nojiri, Y., Barrie, L. A., Toom-Sauntry, D., & Fujinuma, Y. (2001). Atmospheric methyl iodide: High correlation with surface seawater temperature and its implications on the sea-to-air flux. [Article]. *Journal of Geophysical Research-Atmospheres*, 106(D12), 12661-12668.
- Yu, Y., Geyer, A., Xie, P. H., Galle, B., Chen, L. M., & Platt, U. (2004). Observations of carbon disulfide by differential optical absorption spectroscopy in Shanghai. [Article]. *Geophysical Research Letters*, 31(11), 4.
- Yung, Y. L., Pinto, J. P., Watson, R. T., & Sander, S. P. (1980). Atmospheric bromine and ozone perturbations in the lower stratosphere. [Article]. *Journal of the Atmospheric Sciences*, 37(2), 339-353.
- Zhang, L. N., & Qin, Q. Z. (2000). Theoretical studies on CS<sub>2</sub>OH-O<sub>2</sub>: a possible intermediate in the OH initiated oxidation of CS<sub>2</sub> by O<sub>2</sub>. [Article]. *Journal of Molecular Structure-Theochem*, 531, 375-379.
- Zhao, Z., Stickel, R. E., & Wine, P. H. (1996). Branching ratios for methyl elimination in the reactions of OD radicals and Cl atoms with CH<sub>3</sub>SCH<sub>3</sub>. [Article]. *Chemical Physics Letters*, 251(1-2), 59-66.
- Zhu, L., Nicovich, J. M., & Wine, P. H. (2003a). Temperature-dependent kinetics studies of aqueous phase reactions of hydroxyl radicals with dimethylsulfoxide, dimethylsulfone, and methanesulfonate. *Aquatic Sciences*, 65(4), 425-435.

Zhu, L., Nicovich, J. M., & Wine, P. H. (2003b). Temperature-dependent kinetics studies of aqueous phase reactions of SO<sub>4</sub><sup>-</sup> radicals with dimethylsulfoxide, dimethylsulfone, and methanesulfonate. *Journal of Photochemistry and Photobiology a-Chemistry*, 157(2-3), 311-319.